# Sandpiper Marine Phosphate Project

Dredging Sediment Plume Dispersion Modelling

HR Wallingford
*Working with water*

HR Wallingford
*Working with water*
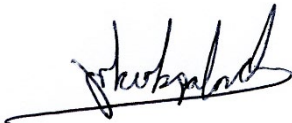
# Document information

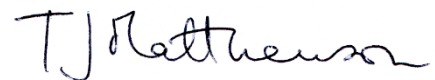| | |
|---|---|
| Document permissions | Confidential - client |
| Project number | DJR6213 |
| Project name | Sandpiper Marine Phosphate Project |
| Report title | Dredging Sediment Plume Dispersion Modelling |
| Report number | RT001 |
| Release number | R05-00 |
| Report date | July 2020 |
| Client | Namibian Marine Phosphate (Pty) Ltd |
| Client representative | Mike Woodborne |
| Project manager | John Kirkpatrick |
| Project director | Tom Matthewson |

# Document authorisation

| Prepared | Approved | Authorised |
|---|---|---|

# Document history

| Date | Release | Prepared | Approved | Authorised | Notes |
|---|---|---|---|---|---|
| 20 Jul 2020 | 05-00 | JKI | JS | TJM | Final (with minor update to Executive Summary) |
| 09 Jul 2020 | 04-00 | JS | JKI | TJM | Final (with minor updates) |
| 17 Apr 2020 | 03-00 | JS | JKI | TJM | Final |
| 13 Jan 2020 | 02-00 | JS | JKI | TJM | Draft report issued for further comment |
| 20 Dec 2019 | 01-00 | JS | JKI | TJM | Draft report issued for comment |

# Executive Summary

## The Sandpiper Project

The Sandpiper marine phosphate project is being developed by Namibian Marine Phosphate (Pty) Ltd (NMP). It is proposed to extract phosphate sediment by dredging from water depths of around 200 m in Mining Licence 170, Namibia. An annual recovery volume of 5.5 million tonnes of phosphate-rich sea bed material would be extracted for a 20 year period of the mine licence within a target area called SP-1. The phosphate sands would be recovered by a trailing suction hopper dredger.

Certain studies need to be completed and submitted for consideration to grant an Environmental Clearance Certificate for Licence Area ML 170. This study presents a comprehensive hydrodynamic model to show the predicted dispersion and settlement of particulate matter from the overspill plume in the vicinity of dredging works.

## Studies undertaken

The purpose of this report is therefore to present the findings of hydrodynamic modelling of the dispersion and settlement of particulate matter from dredging plumes in the vicinity of dredging works in the 20 year plan area within SP-1. Making use of site-specific observations of water currents and other available data, water flows in the mine area have been modelled in three dimensions (3D). The dredger process has been analysed in order to make reasonable estimates of the rates of sediment releases from dredging. These inputs have then been used in the dispersion model to predict the extent of suspended sediments and subsequent deposition from dredging, above background levels. The modelling outputs are dependent on the observational data available, and may be refined as more extensive baseline data become available.

## Zone of influence (ZoI) from dredging

Summary information for the sediment plume is provided in Table ES.1 at the end of this section.

The overall Zone of Influence from this dredging activity for the 20-year period extends over an area of 513 km$^2$ outside of the 20 year mining plan area. The overall (20-year) ZoI intersects with a very small proportion of the areas identified as important for hake and monkfish trawling. Within this overall ZoI, 288 km$^2$ extends into waters with depths shallower than the 200 m water depth representing fish habitat where trawling is prohibited.

It must be emphasised that the overall ZoI represents the area within which non-negligible changes in suspended sediment and/or deposition above background are predicted to occur at any time within the proposed 20 year period of mining. However, at any given moment within the 20 years, the plume represents a much smaller area than the ZoI. For example, the ZoI for a single dredging operation extends up to 5 km$^2$ outside the 20-year mining plan area.

## Sediment deposition

With specific regard to the footprint of sediment deposition over 20-years, the area is similar to (but slightly smaller than) the overall ZoI described above. Whilst the predicted deposition rates appear unlikely to be sufficiently high to cause an ecological smothering effect, the seabed area experiencing greater than 0.1 m of deposition above background rates is likely to change to a predominantly silty substrate. It is predicted that 151 km$^2$ of seabed over the 20-year licence period, outside the 20 year mining plan area may experience a change in substrate. The scale of this predicted effect would need to be verified by field monitoring of the dredging activity.

### Suspended sediments

The extents of predicted increases in peak suspended sediment concentration vary with the position of the dredging but, as a whole, the suspended sediment footprint associated with the 20 year mining plan is predicted to extend up to 23 km north, 8 km east, 12 km south and 4 km west of the 20 year mining plan area. The predicted peak increases in plume concentration outside of the 20 year mining plan area are less than 50 mg/l above background.

Mean increases in suspended sediment concentrations above background are always predicted to be below 5 mg/l, except at the surface within 100 m (horizontally) of the dredging.

Time series analysis at locations sited 2 km from the boundary of the 20 year mining plan area shows that the predicted increase in surface concentrations of suspended sediments above background, outside of the 20 year mining plan area, do not exceed the acute concentration threshold of ecological effects of 7.6 mg/l (defined as the concentration at which no more than 5 % of taxa may be compromised). The mid-depth concentrations and near-bed concentrations increases above background exceed this threshold for 4 % of the time or less.

### Single dredge cycle

During a single dredging cycle, the plume (defined by sediment concentration increases above background of 7.6 mg/l) is present at the surface for up to 3 hours following cessation of dredging, and in the middle of the water column for 25-30 hours following cessation of dredging. The bottom plume is present for 17.5-30 hours but appears 20 or so hours after dredging ceases.

Deposition above background over an individual cycle (58.5 hours) is predicted to be 0.3 mm or less and corresponds to a total volume of about 15,000 $m^3$.

### Walvis Bay

There is no indication of the risk of an effect due to dredging within the 20 year mining plan area upon water quality for the salt refining industry intake in Walvis Bay.

### Potential refinements to modelling undertaken

The modelling and analysis described in this report has used the available data and understanding of physical processes on the Namibian shelf. The modelling undertaken has used advanced techniques to reproduce the hydrodynamics and dispersion of sediment plumes arising from dredging. The assessment and the conclusions presented in this report therefore represent the current understanding of the likely behaviour and consequent effects of dredging plumes.

However, the studies have indicated that there are some aspects of the modelling which could potentially require refinement. These aspects include addressing the nature of the observed high turbidity events, the currently available measurements of near bed currents, the contribution of extreme weather or ocean events to long-term deposition, the settling velocity of dredged material released in the overflow and the overflow sediment discharge.

Collection of additional site data, to specifically address these aspects, would facilitate further refinement of the modelling undertaken to date. It is therefore planned that, following consent, further measurements and analysis will be undertaken. This will provide the additional validation data sets to refine the numerical modelling as necessary and to demonstrate its reliability and accuracy.

## Summary information for the sediment plume

Summary information for the sediment plume is provided below in Table ES.1.

Table ES.1: Summary information for sediment plume

| Aspect of plume | | Outside 20 year mining plan area | | | Outside of ML 170 area | At Walvis Bay intakes |
|---|---|---|---|---|---|---|
| | | Total area | Inside fishery area | Inshore of -200 m contour | | |
| Zone of Influence | | 513 km$^2$ | ~10 km$^2$ (Hake) ~3 km$^2$ (Monkfish) | 288 km$^2$ | 11 km$^2$ | None |
| Peak suspended solids above background (20 years' dredging)  * | | < 48 mg/l | < 25 mg/l | < 30 mg/l | < 18 mg/l | None |
| Mean suspended solids above background (20 years' dredging) | | < 18 mg/l | < 2 mg/l | < 4 mg/l | < 3 mg/l | None |
| Depth of sediment deposition (20 years' dredging) | | ≤ 0.7 m | 0 m (Hake) ≤ 0.02 m (Monkfish) | ≤ 0.5 m | ≤ 0.08 m Mean 0.02-0.03 m | None |
| Area of sediment deposition (20 years' dredging) | > 5 mm depth | 412 km$^2$ | ~3 km$^2$ | 237 km$^2$ | 84.5 km$^2$ | None |
| | > 0.1 m depth | 151 km$^2$ | 0 km$^2$ | 26 km$^2$ | 10 km$^2$ | None |
| Single dredging operation ZoI, typical area of plume (if present) | | 1-5 km$^2$ | | | | None |
| Sediment deposition (single operation) | Thickness | ≤ 0.3 mm | ≤ 0.3 mm | ≤ 0.3 mm | ≤ 0.3 mm | None |
| | Volume | ~15,000 m$^3$ | Dependent on dredging location | | | None |

Note:       *  Not including immediate (near-field) vicinity of dredger

# Contents

## Tables

# 1.  Introduction

## 1.1.  Project background

The Sandpiper marine phosphate project is being developed by Namibian Marine Phosphate (Pty) Ltd (NMP).  It is proposed to extract phosphate sediment by dredging from water depths of around 200 m in Mining Licence 170, Namibia. An annual recovery volume of 5.5 million tonnes of phosphate-rich seabed material would be extracted for a 20 year period of the mine licence. The phosphate sands would be recovered by a trailing suction hopper dredger (TSHD).

## 1.2.  Project location

The Sandpiper marine phosphate project is located on the Namibian continental shelf approximately 120 km south southwest (SSW) of Walvis Bay. The eastern boundary of the Mining Licence (ML) Area is approximately 60 km off the coast (directly west of Conception Bay). The water depths in the licence area range from 180 to 300 m (Figure 1.1). The Mining Licence Area is 25.2 km wide (greatest width) and 115 km long (longest length) and covers an area of 2,233 km$^2$.

NMP has verified to internationally approved standards the existence of a potentially world-class phosphate deposit of 1,832 Mt (at 15% P2O5) in the Mining Licence Area (NMP, 2014a).

The phosphate-enriched sediments and defined mineral resources/reserves are located throughout almost the entire Mining Licence Area (deeper areas at the southeast and southwest of the ML are excluded where P2O5 levels fall below 15%). Within the ML, three target dredging areas have been identified, with the assessment of the target dredge site Sandpiper-1 (SP-1) being the focus for the current environmental approval and 20 year mine plan (Figure 1.2). The other sites (SP-2 and SP-3) may be considered for extraction at a later stage and will be subject then to their own specific environmental evaluations.

## 1.3.  Project status

Following an exploration programme, a mining licence (ML 170) was issued by the Ministry of Mines and Energy (MME) in 2011.  This included a condition requiring the completion of an Environmental Impact Assessment (EIA), submission of an Environmental Management Programme Report (EMPR) and an environmental contract with the Ministry of Environment and Tourism (MET) once the EMPR was approved. Following promulgation of the Environmental Management Act 2007, the environmental contract has been replaced by the requirement to apply for Environmental Clearance Certificate (ECC).

NMP have therefore submitted an application to the Environment Commissioner for an ECC, accompanied by an Environmental Impact Assessment, Environmental Management Plan, and other supporting 'verification' studies (NMP, 2014).

To inform the determination of the ECC application, and as part of a further public consultation process completed during 2018, the Environment Commissioner requested that an independent review be conducted of the EIA and verification programme.  This review (Newell and Muhapi, 2018) concluded that certain studies should be completed and submitted for approval before consideration of whether to grant an ECC for Licence Area ML 170.  These supplementary studies included, *inter alia*, the presentation of a

comprehensive hydrodynamic model to show the predicted dispersion and settlement of particulate matter from the overspill plume in the vicinity of dredging works.
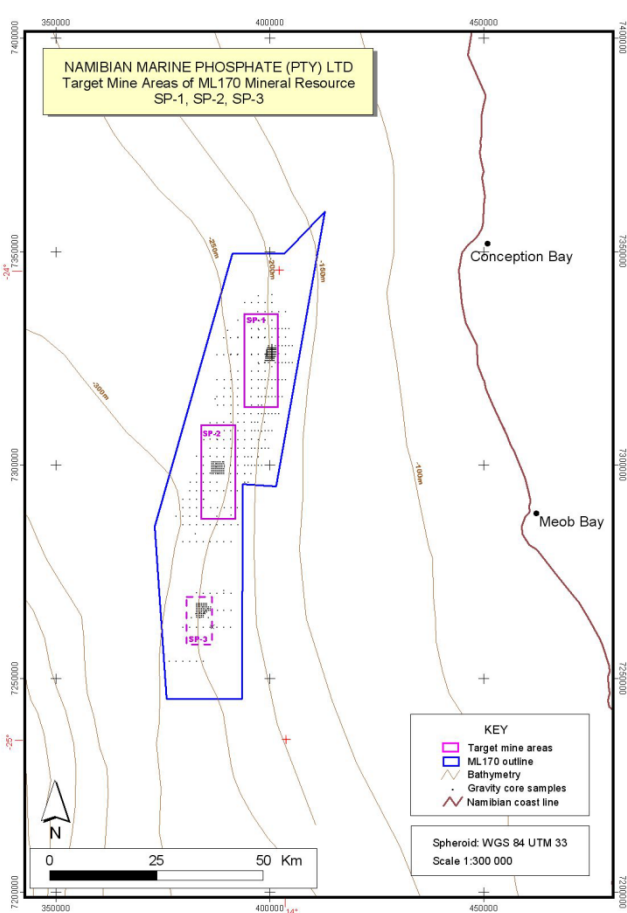


Figure 1.1: General Location of the project of Mining Licence 170

*Source:    NMP (2014)*
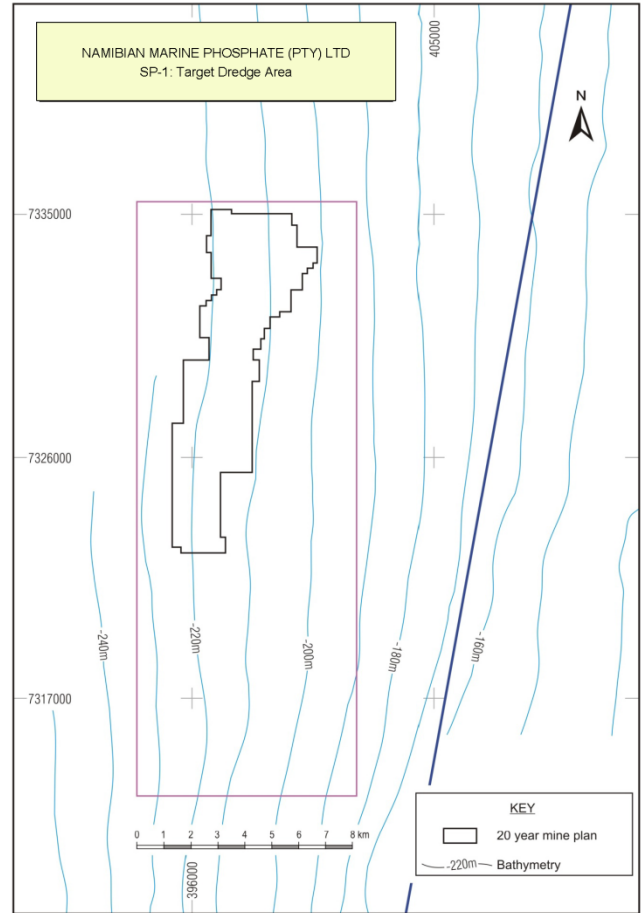


Figure 1.2: 20 year mining plan area, within SP-1 (target dredge area)

*Source:    NMP (2014)*

## 1.4. Purpose of this report

The purpose of this report is to present the findings of hydrodynamic modelling of the dispersion and settlement of particulate matter from the overspill plume in the vicinity of dredging works in SP-1.

Making use of site-specific observations of water currents and other available data, water flows in the mine area have been modelled in three dimensions (3D). The dredger process has also been simulated in order to make reasonable estimates of the rates of sediment releases from dredging. These inputs have then been used in the dispersion model to predict the extent of suspended sediments and subsequent deposition from dredging.

The results of this modelling are presented in this report, overlain on potentially sensitive areas such as fish spawning areas and seawater intakes.

## 1.5. Definitions

In this report the following terms are used:

- **Zone of Influence** (ZoI) – this is the zone or area within which the dredging will lead to changes above background levels in suspended sediment concentrations, or to deposition of sediment on the seabed, which are not negligible and the environmental significance of which requires assessment. As explained later in this report, **the ZoI is defined as the combined area resulting from the suspended sediment footprint and deposition footprint as defined below**. Note that changes within the ZoI are not necessarily environmentally significant, but these changes cannot be immediately dismissed as insignificant. Outside of the ZoI, however, any changes can be considered as insignificant and it can be concluded that there is no environmental impact.

- **Suspended sediment footprint** – this is defined as the area within which *either* peak concentration increases of more than 7.6 mg/l are experienced; *or* mean concentration increases of more than 1 mg/l are experienced over the course of the 20 year dredging period. In both cases, these are increases above background levels.

- **Deposition footprint** – this is defined as the area within which deposition of 5 mm or more above background levels is predicted to occur over the 20 year period of mining.

# 2. Proposed dredging activities

## 2.1. Background information

A critical input to the modelling described in this report is a complete understanding of the relevant aspects of the mining processes to be undertaken. The following key background information has been used to inform the understanding of the dredging equipment and process, which have been modelled in this study:

- NMP Document: Sandpiper Project Environmental Verification Report (2014), Dredging of Marine Phosphate ML 170, Section D, Appendix 6 – Dredging Project Description;

- Bateman Documents:
  - Sandpiper Feasibility Study, Bulk Sample 1797B – Size Analyses (Report 14082-600-BT-PR-RE-001-P0 dated 30/06/11);
  - Testwork Report – Characterisation of Sandpiper High Grade Marine Phosphate Feed and Phosphate Solubility Results (Report 13919/3 dated June 2011).

- Jan De Nul (JDN) Documents:
  - Sandpiper Phosphate Project – Dredging technology (Report PS.NAM-PA-13.002-FJ-A dated 17/04/13);
  - Sandpiper Phosphate Project – Reduction of fines content on board TSHD Cristobal Colon (Report PS.NAM-PA-15.002-FJ-C dated 23/07/15);
  - Extract from Sandpiper Phosphate Project – Dredging Works Cost Breakdown 2012 (Spreadsheet PS-NAM-PA-15.004-FJ-1 dated 25/10/2015).

- 12No. NMP photographs taken on board TSHD Cristobal Colon, illustrating the hopper loading and overflow weir installations.

## 2.2. Dredging location

Dredging operations are planned within a demarcated '20 year mine plan' area, within the 'SP-1' extraction target area, which in turn is inside the ML 170 licensed area – see Figure 2.1.
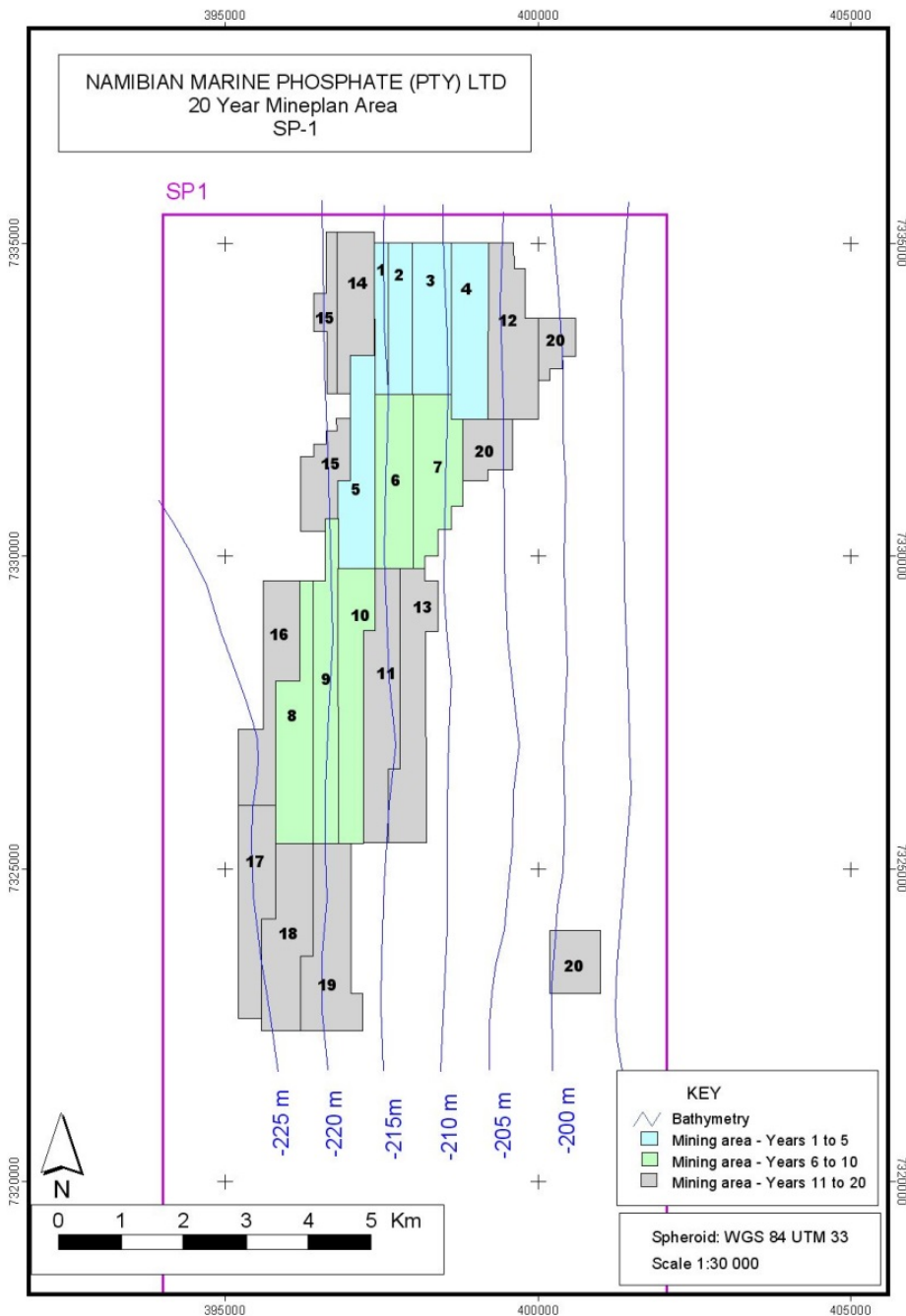


Figure 2.1: Location of '20 year mine plan' target dredge area within area SP-1

*Source:    NMP (2014)*

Whilst the overall mining licensed area covers 2,233km$^2$, the SP-1 target dredge area covers approximately 176 km$^2$ (approximately 8 km wide and 22 km long).

The 20 year mine plan area covers approximately 34 km$^2$ where dredging operations are specifically targeted at this time and sits inside the SP-1 area. The mine plan includes a small area (0.81 km$^2$) to the SW which is separate from the rest of the mining area. This area is a small proportion of the area that is proposed for mining in Year 20. The mining of the small area has not been investigated in this report. However, as it forms part of the proposed mining, figures presented in this report include this area as part of the mining plan.

## 2.3. Dredging equipment

Jan De Nul (JDN) are proposing the use of conventional dredging techniques, with adaptation of existing standard trailer suction dredging equipment to facilitate working in water depths of up to 225 m.

The selected dredging technique is that of the Trailing Suction Hopper Dredger (TSHD), which is a sea-going, self-propelled dredging vessel that uses a trailing pipe/s to use hydraulic suction to lift seabed material to the surface. A schematic drawing is shown in Figure 2.2.

TSHDs typically operate in up to 50 m of water and are deployed for the mining and transporting of sand materials for use as reclamation fill (as capital works) and for the dredging of siltation (as maintenance works). JDN have successfully undertaken dredging in water depths of up to 150 m and so have expertise in the use of TSHDs for dredging deeper depths.
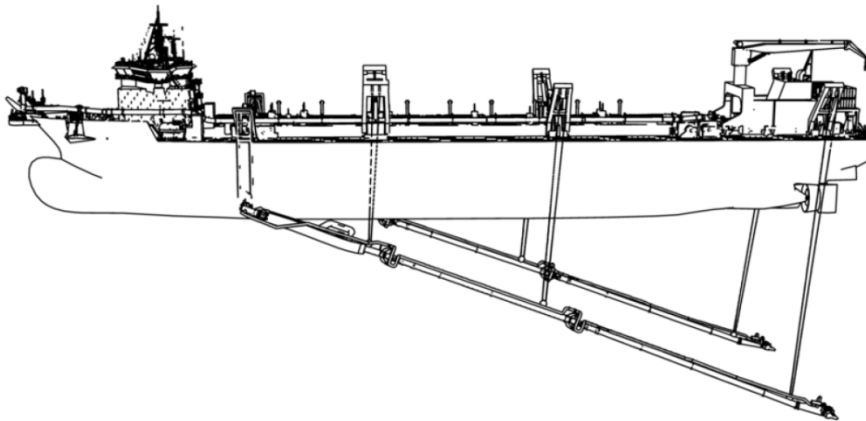


Figure 2.2: Schematic of TSHD

*Source:    JDN (2013)*

One or two suction pipes are lowered to the seabed, trailing behind the TSHD vessel sailing forward at 1-2 knots. Drag head(s) are used to fluidise and then entrain bed materials into the suction pipe(s), which in turn use centrifugal pumps to lift the solids/water slurry mixture into the TSHD's hopper (i.e. hold).

Maximising the density of the slurry (by maximising the proportion of solids and minimising the proportion of transport water) is desirable for most efficient operations. The maximum achievable density of the pumped slurry depends on numerous factors, but will always mostly comprise water. Therefore, in order to maximise the hopper load (and in turn the economic efficiency of the dredging operation), it is necessary to overflow water from the hopper to permit further loading of solids. This overflow water will contain a proportion of

solids that have not settled within the hopper. It is these overflowed solids that form the sediment plume in the waters surrounding the working TSHD.

Once the hopper is economically loaded, the suction pipes are raised back onto the TSHD's deck and the TSHD sails to the discharge location. Material is typically discharged via the hopper bottom doors or, via pipe at the bow, in the form of rainbowing or pipeline to shore (pumpashore). In the case of this project, JDN are proposing that the TSHD sails from the mine area (for approximately 185 km) and discharges the dredged material via pipeline to shore at the Port of Walvis Bay.

## 2.3.1.  Vessel

JDN are proposing the use of the Trailing Suction Hopper Dredger (TSHD) Cristóbal Colón. She has a hopper capacity of 46,000 $m^3$ and is, alongside her sister vessel the Leiv Eiriksson, currently the largest TSHD in the world. The scaling up of the latest generation of mega TSHDs have made dredging challenging soils in deeper waters and transporting them great distances more economically feasible than ever before. As hulls are extended to increase hopper capacity, ever-longer suction pipes can be installed – resulting in increased maximum working depths.

The main particulars of the Cristóbal Colón / Leiv Eiriksson (in standard configuration) are given in Table 2.1.

Table 2.1: JDN proposed TSHD vessel particulars – type Cristóbal Colón / Leiv Eiriksson

| Vessel particulars | Units | Value |
|---|---|---|
| MAIN PARTICULARS | | |
| Length overall | m | 213.5 |
| Length between perpendiculars | m | 196 |
| Breadth moulded | m | 41 |
| Depth moulded | m | 20 |
| Lightweight | tonnes | 26,492 |
| Total installed power | kW | 41,650 |
| Propulsive power free sailing | kW | 38,400 |
| Speed, loaded | kn | 17 |
| Speed, unloaded | kn | 19 |
| Draught, loaded | m | 15.15 |
| Draught, unloaded | m | 10 |
| Hopper capacity (to top overflow) | $m^3$ | 46,000 |
| Maximum hopper load | tonnes | 74,367 |
| Maximum dredging depth | m | 155 |
| DREDGING ARRANGEMENT | | |
| Number of suction pipes | No. | 2 (each with one submerged pump) |
| Diameter of suction pipe(s) | mm | 1,300 |
| Dredge pump power | kW | 13,000 |
| Inboard pump power | kW | 16,000 |

| Vessel particulars | Units | Value |
|---|---|---|
| Jet pump power on draghead | kW | 4,300 |
| Hopper length | m | 111 |
| Hopper width | m | 31 |
| Hopper depth | m | 11 |
| Number of overflow weirs | No. | 2 (fore and aft, only one used at time) |
| Hopper overflow weir stroke | m | 9.21 |

Source:    *JDN (2019)*

### 2.3.2.   Project-specific vessel adaptations

Two main adaptations of the TSHD vessel are proposed to make this mining operation feasible with the proposed vessel, and comprise:

- Funnel-shaped draghead;
- Jack-knife suction pipe.

**Funnel-shaped draghead**

The draghead is mounted at the lower end of the suction pipe. The design promoted by JDN for use on the Sandpiper project is not of typical type. It is funnel shaped and has been designed to optimise material recovery in the top two layers of bed sediments (L1 and L2), which contain the phosphate resource and are therefore to be targeted by the Sandpiper project. The draghead has a width of 3 m and will remove bed sediments to a depth of approximately 0.5-0.75 m per pass.

Bed sediments are fluidised by water which is jetted at high flow rates through a set of jet nozzles at the front of the draghead, before being entrained into the suction pipe. A grid is installed across the suction mouth to prevent larger objects from entering the pumps.

**Jack-knife suction pipe**

The TSHD promoted by JDN has a maximum dredging depth of 155 m with the 'longest configuration' standard design. In order to achieve the dredging depths required on the Sandpiper project, the draghead at the end of the standard suction pipe will be replaced by a double swivel that connects an additional 100 m long pipe (as shown in Figure 2.3). The funnel-shaped draghead is then mounted at the lower end of this additional pipe, extending the maximum dredging depth to 225 m.
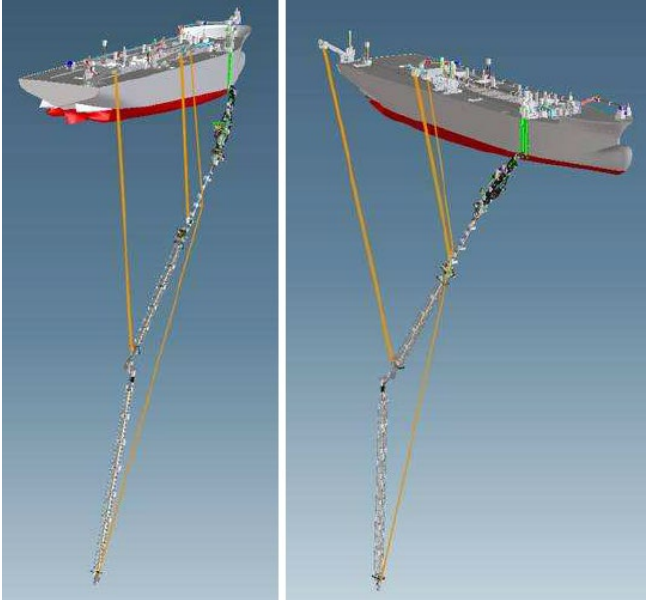
Figure 2.3: Jack-knife suction pipe with additional 100 m lower pipe section

*Source:    JDN (2013)*

## 2.4. Key features of the dredging process

There are numerous specific details to consider in order to correctly define the dredging process (as proposed by JDN) for the purposes of this sediment plume dispersion modelling study.

After discussion with the JDN technical staff (JDN, 2019), the following assumptions about the dredging process have been confirmed as a reasonable representation of the proposed dredging process:

■ General:

- The typical sailing distance between the SP-1 extraction target area and the shore discharge location in Walvis Bay is assumed to be 100 nautical miles (185.2 km), in line with provided JDN calculations;

- The phosphate sands to be dredged are in 200-225 m of water and are attainable with the modified plant proposed by JDN.

■ Dredged sediments:

- There is no overburden to be removed prior to gaining access to the phosphate sands resource material;

- The phosphate sands to be dredged are within the top two layers of bed sediments (i.e. layers L1 and L2);

- These sediment layers will not be targeted individually – instead the dredging will remove bed sediments to a depth of 0.5-0.75 m in each pass, to a point just above the footwall clay (layer L3);

- The footwall clay horizon level varies throughout the extraction target area, but is typically 1-3 m below the original seabed level on the eastern side. The horizon generally deepens moving to the west, where it is more than 6 m below the seabed level in places;

- The intention is not to dredge into the footwall clay, but rather to leave a residual thickness of sediments over the footwall as an uneven 'hummocked' surface (envisaged to be 10-15% of the original volume of targeted sediment layers);

- Therefore, only a minimal proportion of layer L3 material has been accounted for when Bateman developed their composite material PSD;

- The composite material PSD is very similar to that of the layer L2 PSD, but with a slightly increased quantity coarser materials.

■ Hopper loading and overflow operations:

- Only one suction pipe (i.e. trailing arm and draghead) will be used to load the hopper with dredged materials;

- The hopper is not pre-filled with water up to the overflow weir level prior to commencing loading of dredged materials;

- Therefore there is a delay between starting to load the hopper and starting to overflow water (i.e. the pre-overflow period);

- The full hopper load is 37,750 m$^3$. The hopper has only a small rest load (order 750 m$^3$) prior to commencing loading of dredged materials;

- Only one overflow weir will be used to discharge water from the hopper at a time;

- The two overflow weirs are used alternatively, i.e. aft loading box used with fore overflow (as shown in Figure 2.4) and fore loading box used with aft overflow;

- This distributes the dredged material evenly over the hopper and maintains an even keel for sailing back to the discharge location.
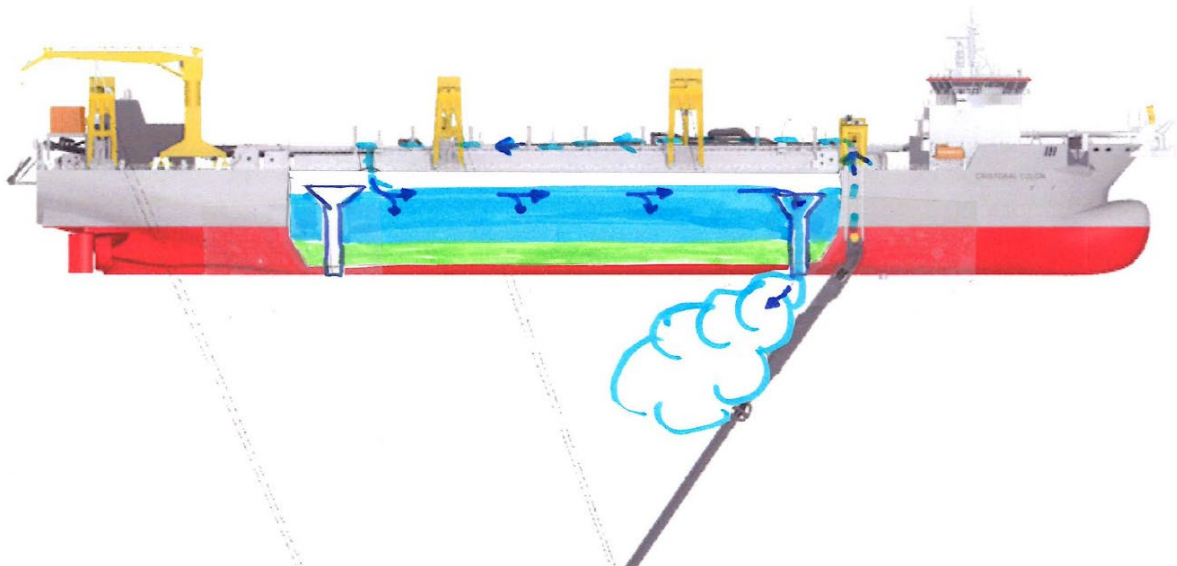


Figure 2.4: TSHD hopper loading (and overflow) process

*Source:    JDN (2015)*

## 2.5. Dredging cycle

An initial analysis of the dredging cycle was calculated by JDN as given below in Table 2.2 on the basis of a dredging path length of 4 km (JDN, 2013). It can be seen that only 38 % of the total operational cycle time is productive dredging time, where bed materials are being mined and loaded into the dredger's hopper (i.e. 798 minutes per each dredge cycle of 2,106 minutes).

Table 2.2: Dredging cycle times calculated by JDN

| Dredging cycle times | Minutes | Hours |
|---|---:|---:|
| Loading | 798 | 13.30 |
| Turning | 199 | 3.32 |
| Sailing time, loaded unrestricted | 353 | 5.88 |
| Sailing time, loaded restricted | 0 | 0.00 |
| Accelerate / slow down | 20 | 0.33 |
| Connect to pipeline | 40 | 0.67 |
| Discharge to shore | 360 | 6.00 |
| Disconnect from pipeline | 20 | 0.33 |
| Sailing time, unloaded unrestricted | 316 | 5.26 |
| Sailing time, loaded restricted | 0 | 0.00 |
| Total cycle time | 2,106 | 35.10 |
| Loading proportion of total dredging cycle | | 38% |

Source:    *modified from JDN (2013)*

The current mining plan presented in Figure 2.1 indicates that, for most of the 20 years of mining, the length of the dredging path between turns of the dredger will be less than 4 km.  A more representative distance is 2.5 km and this means that, to win the same volume of resource, loading will have to continue for a longer period.  JDN's cycle time (based on a dredging path length of 4 km) has therefore been adjusted for a dredging path length of 2.5 km, and is given below in Table 2.3.

It is important to note that the TSHD is not necessarily overflowing fine material for the full duration the hopper is being loaded (i.e. 798 minutes).  Dredging typically commences with only a small residual load in the bottom of the hopper and therefore it takes some time for sufficient dredged slurry to be pumped into the hopper such that the water level rises to the weir level of the hopper overflow installation.  It is at this point that overflow commences.  This is illustrated in Figure 2.4 with the settled material (hopper load) shaded green and the hopper free water shaded blue.  It can be seen that the surface water is being weired off through the fore overflow installation.

Table 2.3: Adjusted dredging cycle times for a 2.5 km dredge path

| Dredging cycle times | Minutes | Hours |
|---|---|---|
| Loading | 798 | 13.30 |
| Turning | 308 | 5.13 |
| Sailing time | 353 | 5.88 |
| Accelerate / slow down | 20 | 0.33 |
| Connect to pipeline | 40 | 0.67 |
| Discharge to shore | 360 | 6.00 |
| Disconnect from pipeline | 20 | 0.33 |
| Sailing time | 316 | 5.27 |
| Total cycle time | 2,215 | 36.92 |
| Loading proportion of total dredging cycle | | 36% |

The graph in Figure 2.5 shows the change in hopper volumes (sand load, water and total volume) throughout the dredge cycle. The period 'DR1' covers the duration of time between dredging commencing and overflow commencing (i.e. the pre-overflow period). This is a period of 142 minutes.

The period 'DR2' covers the duration of time where dredging and overflow continues simultaneously and is a period of 964 minutes (including turning). It is during this period that the sediment plume is being generated by the dredging operations.

It should also be noted that the graph in Figure 2.5 is a generalised representation of the dredging processes and cycle. Detail, such as gaps in the loading of material into the hopper whilst the TSHD is turning, are not shown. On the basis of a 2.5 km dredge path, turning accounts for 29 % of operational dredging time – therefore the actual overflow duration whilst loading is 684 minutes (964 x 71 %).

In addition to the above, it is important to recognise that whilst dredging is a 24 hours per day, 365 days per year operation, it is not 100 % efficient. Operating plant in the marine environment means breaks in between some dredging cycles (e.g. due to weather, breakdown, scheduled repairs, bunkering/victualling, or dredging production exceeding phosphate sales requirement) are inevitable.

JDN have calculated that the average project operating hours are 100 operating hours per week (per 168 hour week period). On the original JDN analysis (Table 2.2) this equates to a project average of 2.87 dredging cycles per week (i.e. one dredging cycle every 58.5 hours). Although a shorter dredge path would reduce the average number of dredging cycles per week (Table 2.3), the allowance for maintenance and downtime tends to be an imprecise estimate. For this reason this study assumes the 58.5 hour (average) cycle time assumed by JDN.
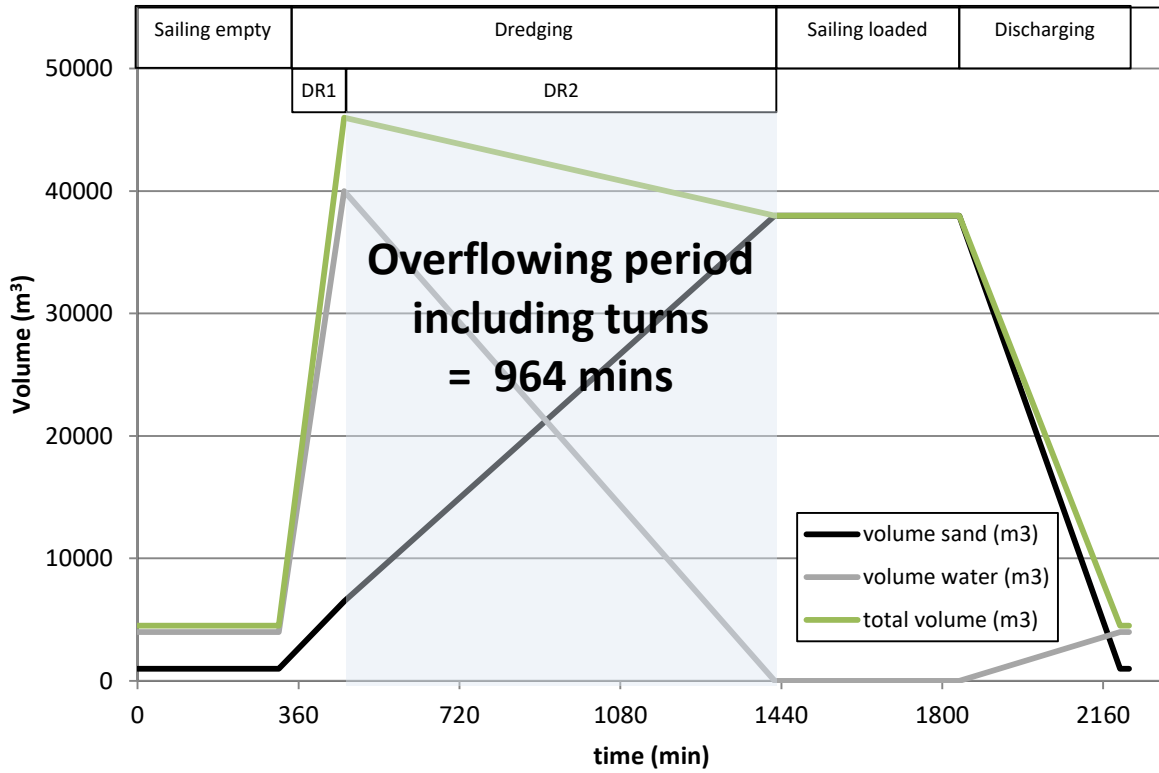
Figure 2.5: TSHD hopper loading graph – volumes

*Source:    modified from JDN (2015)*

# 3. Processes associated with dispersion of sediment plumes resulting from dredging

## 3.1. Introduction

Dredging by trailing suction hopper dredger can lead to the release of sediment into the water column, resulting in an increase in turbidity and sediment deposition away from the dredging area. These processes leading to this release of sediment, and the subsequent behaviour of the plume once it is released, need to be reflected where relevant in the modelling process, and are described below.

As described in Section 2.5, dredging activities by TSHD involves the collection and pumping of sediment and water from the seabed into a hopper on board the TSHD. The hopper is continually filled with the pumped water and sediment slurry and the water and the finer sediment fractions overflow over a central weir and discharge through the hull. The coarser fractions (and a proportion of the finer fractions) are retained in the hopper.

## 3.2. Release of fine sediment into the surrounding waters

### 3.2.1. Near-field mixing of the overflow plume

**The dynamic plume**

Sediment released through the overflow is initially released with momentum in a water-sediment mixture through the hull of the dredger. The water-sediment mixture is denser than water and so the mixture moves downwards as a jet because of its initial momentum and then it accelerates downwards because of gravity.

As the mixture moves downwards it entrains surrounding water, which dilutes the plume and slows its motion. The mixing of the plume is analogous to the mixing of a dense jet in crossflow (albeit complicated by the fact that the release of the plume is initially moving because of the motion of the dredger).

In shallow waters it is typical for the dense jet, sometimes referred to as a "dynamic plume" to impact onto the bed. In the present case, however, the depth of water (around 200 m) means that the dynamic plume does not reach the bed but mixes within the surface 50 m (approximately) and then forms a "passive" plume which is advected by currents and mixes according to the ambient turbulence and current gradients (Fischer et al, 1979), with particles also settling downwards through gravity.

The dynamic and passive plume phases are both represented within the plume dispersion modelling (see Section 5).

**The surface plume**

As silt-laden water flows into the overflow weir, it then falls (inside the outlet pipe) in the form of an annular jet which impacts on the water surface inside the outlet pipe (which is at the same level as the local sea level). This impact of the jet on the water inside the pipe causes air bubbles to be trapped which are transported downwards and ejected via the hull along with the water and fine sediment. The presence of bubbles in the overflow discharge increases the buoyancy of the discharge and causes part of the discharge to remain within the vicinity of the dredger hull, after which the upward-directed current flow at the aft of the dredger, together with the mixing effect of the propeller jets, brings this plume to the surface. The extent of the surface plume is complex as it is subject to 3-phase interaction (water, sediment and bubbles), propeller

turbulence, the geometry of the ship and motion of the flow around the dredger hull (Decrop et al, 2015).  In general, the standard rule of thumb in deeper water is that 5-15 % of the overflow discharge forms the surface plume (Spearman et al, 2011).  In shallower water, especially where the effects of propellers and flow underneath the keel can affect the near-bed, this proportion rises (de Wit, 2015).

The surface plume is represented within the plume dispersion modelling (see Section 5) and for the purposes of this report it is assumed (conservatively) that 15 % of the overflow discharge forms this surface plume as described in Section 8.3.

**The Environmental Valve**

The TSHD Cristóbal Colón has the ability to remove air bubbles from the overflow discharge through use of the so called "environmental valve".  The effect of the valve is to dramatically reduce the extent and concentration of the surface plume by ensuring that more of the overflow discharge descends downwards as part of the dynamic plume described above. The valve partially blocks the overflow outlet pipe causing the water level in this pipe to rise, preventing the formation of the annular jet, and thus preventing bubble formation.  The environmental valve can be seen as a mitigation option for reducing the effect of the plume within the surface 20-30 m, but it does not reduce the overall discharge of sediment into the water column as a whole.

The effect of the use of the environmental valve on the dispersion of the plume is examined in Section 10.

## 3.2.2.   Disturbance by the draghead

The release of sediment into the surrounding waters by phosphate mining is dominated by the overflow plume.  However, there will, in addition, be a much smaller release of sediment into the water column as a result of disturbance by the draghead.  This proportion is influenced by the size of the draghead, the speed of the draghead across the ground and the sediment type.  Based on the measurements of draghead plumes carried out for the TASS project HR Wallingford and Dredging Research Ltd. undertook a number of measurements of draghead plumes for different sediments and different dredger speeds for the TSHD Cornelia (HR Wallingford and Dredging Research, 2004).

For a single similarly-size draghead moving at similar speeds to those expected in the present study the 2004 experiments indicate that the release of silty sand with about 20 % fines would be in the region of 1 kg/s.  This is similar to results of measurements from similar experiments for the TASS project, undertaken at Rotterdam undertaken by Deltares (2008), albeit for slightly larger dragheads.  The value of 1 kg/s has been used in this study in a sensitivity test to demonstrate that the effect of the draghead is not significant to the overall impact of the dredging.  The results of the sensitivity test (not shown) indicated that increases in suspended sediment concentration resulting from the draghead were less than 1 mg/l and confined to within a few hundred metres of the dredging and to the bottom 10 m of the water column.  As a result, any effects of the draghead will be confined to the dredging area which is the conclusion in the EIA (Steffani, 2012).

### 3.2.3. Settling of particles in the plume

The sediment released into the water column as a result of dredging by TSHD can be a mixture of different sediment fractions, depending on the nature of the sediment type and the characteristics of the TSHD. However, as discussed in Section 4.3, for the present phosphate mining off the coast of Namibia the vast majority of the release of sediment will be fine sediment (less than 63 µm in diameter).

The *in situ* fine sediment has a range of fractions of size, but most of this fine sediment in the fine sediment size range is below 20 µm in diameter (i.e. a mixture of clay, fine silt and medium silt). When settling individually in still freshwater particles in these size ranges have a settling velocity of 0.2 mm/s or less – even 100 times less in the case of clay particles (Soulsby, 1997). However, when released in an initially dense plume in seawater, these particles flocculate (aggregate together) because of electrostatic forces and the presence of extra-cellular polymeric substances (EPS) present in the water column (Manning and Dyer, 2007; Manning et al, 2013, Parsons et al, 2016; Decho and Guierrex, 2017) and because of bacteria (Zhang et al, 2018; Wheatland et al, 2019).

Measurements of the settling velocity of fine sediment released from TSHD have shown that typically the settling velocity of the flocs formed by the fine sediment in dredging plumes is around 1-2 mm/s with only a small percentage of the mass being significantly less than this (Smith and Friedrichs, 2011). For this reason the setting velocity used in this study is 1 mm/s.

### 3.2.4. Effects of the passive plume

Once sediment released from the dredger has formed a passive plume, it will be dispersed by the action of currents and will mix with the surrounding waters, becoming more diluted over time. Importantly, though individual sediment particles, or flocs of particles, may stay in suspension over a long period of time, the longevity of individual particles is not relevant to understanding the environmental effects of the plume (Spearman, 2015). The environmental effects of the sediment plume depend on whether the plume takes the suspended sediment concentrations, and any resulting deposition, outside of the range for which the local species are adapted. The chemical composition of the plume and deposition is a further consideration that may apply in some circumstances.

In the original EIA (NMP, 2012a), the threshold for increases in suspended sediment concentration below which it was expected that there would be no environmental impact, defined as chronic effects on marine biota, was taken as exceedance of 20 mg/l for 72 hours duration. This was based on assessments from diamond mining in Namibia waters (EMBECOM, 2004). Since the time of the original EIA, the consensus amongst environmental scientists in Namibia and South Africa is that 20 mg/l may be an over-estimate of the threshold for which impact can be considered to be negligible for the whole range of species encountered in Namibian waters. Later work by Smit et al (2008) for a range of marine species of in Norwegian deep sea waters has shown that a lower value of 7.6 mg/l for negligible impact, defined as the concentration at which no more than 5 % of taxa may be compromised, is more appropriate (Lwandle, 2020). Similarly to the EMBECOM (2004) determination, there is an inherent exposure duration in this threshold, as it was derived from standard toxicity tests that measured organisms responses over 72 or 96 hour exposures.

Although the natural concentrations of heavy metals exceed the sediment quality guidelines for the region, the Verification Studies indicated they do not represent a toxicity risk in this phase either *in situ* or following physical disturbance (NMP, 2014b, Section C2.1). The verification work therefore concluded that the impacts associated with the sediment plume are mainly related to its physical properties.

On this basis, heavy metal contamination of the sediment plume has been disregarded in this study and any impact on marine species in the water column has been taken in this study as insignificant when the predicted increases in suspended sediment concentrations above background fall below the value of 7.6 mg/l. Note that this value relates to both benthic and pelagic species.

The evidence available suggests that the natural variation in suspended sediments near the bed (ignoring episodic high turbidity events) is around 15-20 mg/l and it can be considered that local marine species will be adapted to these conditions. Therefore for near bed conditions it can be assumed that the threshold of 7.6 mg/l is conservative. At mid-depth and the surface, however, the natural variation in suspended sediment is less. The variation in background suspended sediment concentrations is further discussed in Section 4.3.1.

# 4. Description of the physical environment

## 4.1. Regional context

### 4.1.1. Currents

The surface currents in the region are dominated by the Benguela current (see Figure 4.1).  The surface current is driven north by the dominating southern wind.  The Coriolis Effect causes the surface flow to be angled offshore.  There is also an undercurrent travelling towards the South Pole which is angled towards the coast by Coriolis resulting in strong upwelling in coastal waters shallower than about 200 m.
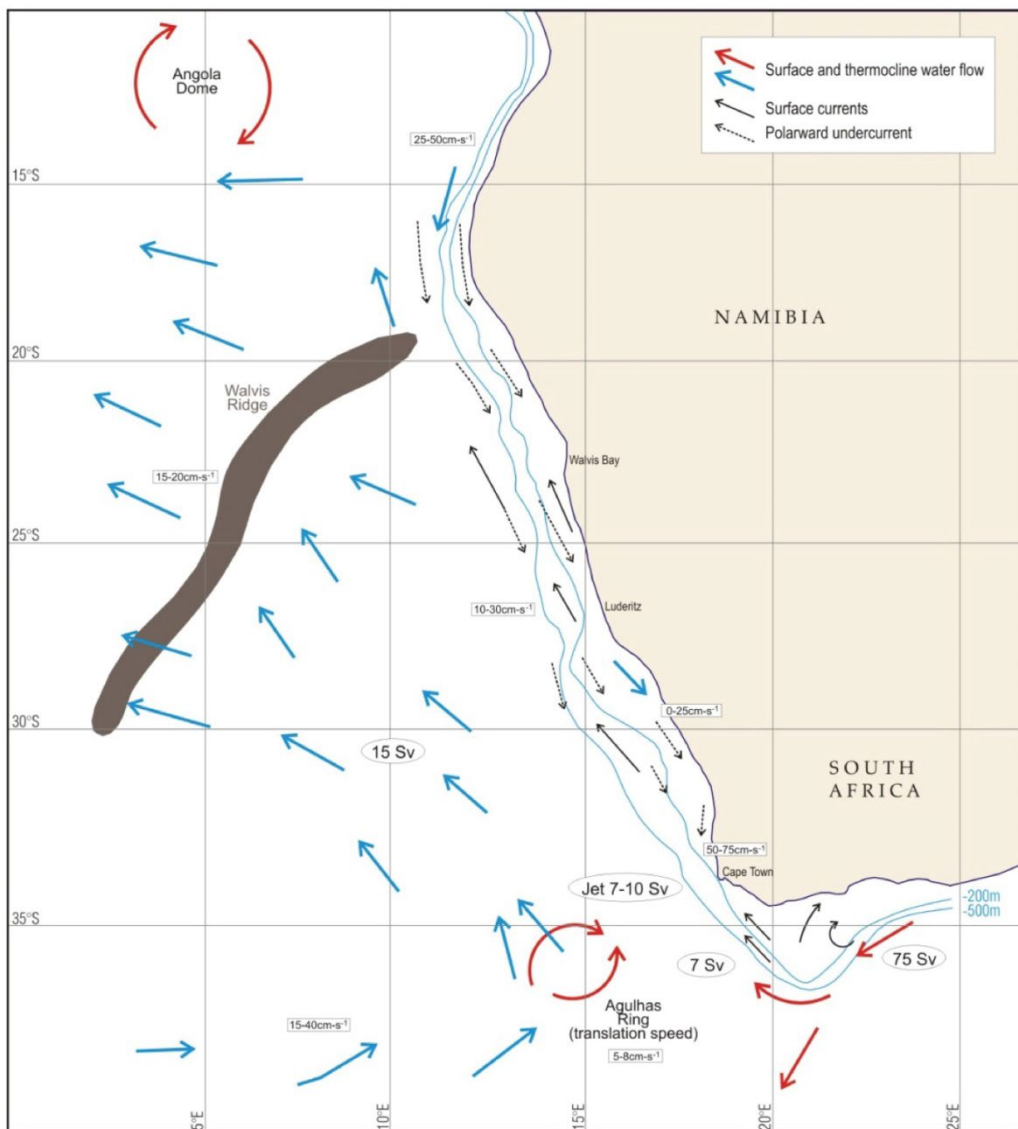


Figure 4.1: Ocean currents on coast of Namibia (Benguela current)

*Source:    NMP (2014a) Part 2*

An oceanographic survey undertaken on behalf of NMP of through-depth currents for two 45 day periods in June-September 2013 in the ML, found that the tidal current was fairly weak, see Figure 4.2. This figure shows the currents at 50 m depth in about 200 m depth of water and the tidal current is a maximum of about 0.1 m/s while the maximum observed current is about 0.4 m/s. The observed tidal current shows a dominant diurnal tendency, a feature of the Namibian coast which has been observed by some researchers (e.g. Simpson et al 2002). However, some researchers have instead observed slight dominance of the semi-diurnal tidal forcing (e.g. Monteiro et al, 2005) or even strong semi-diurnal dominance (Lass et al, 2005).
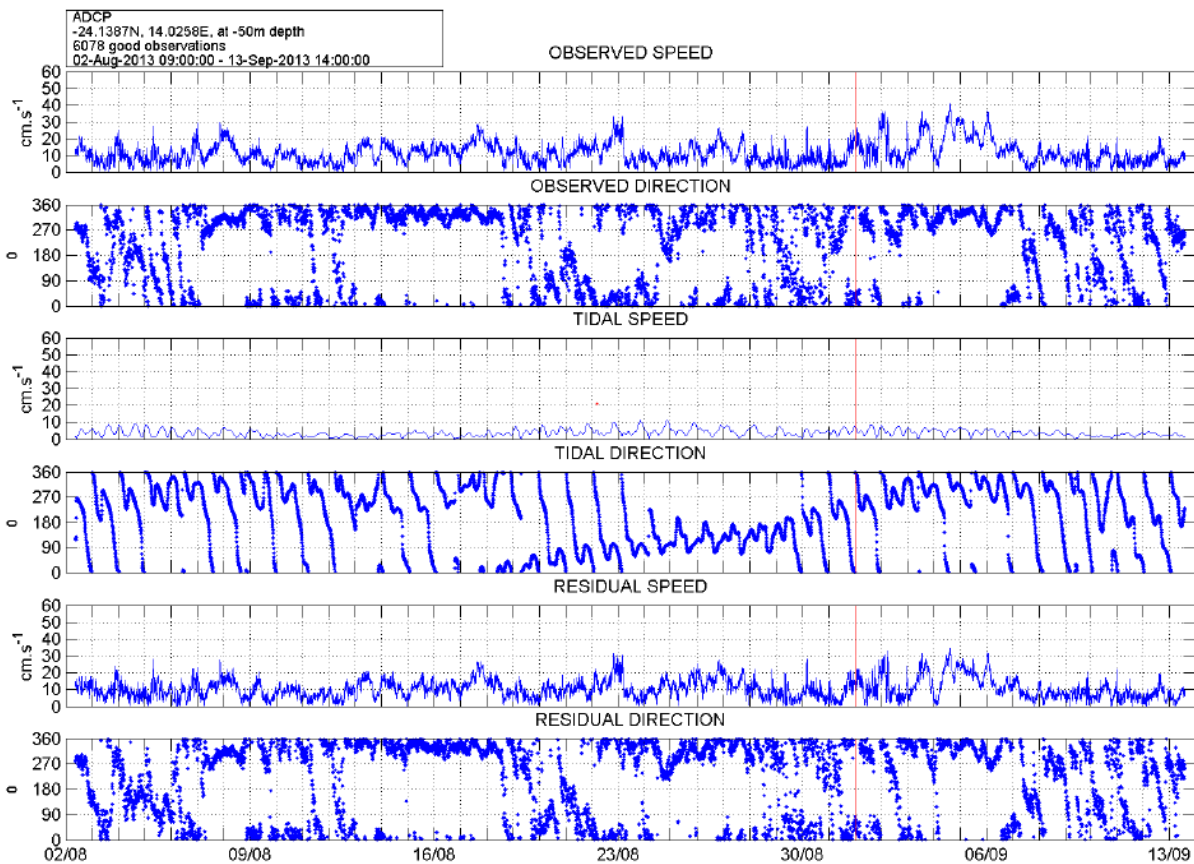


Figure 4.2: Observed current at 50m during austral winter

*Source:    NMP (2014b)*

The residual current (obtained by subtracting the tidal current) at this depth tends to be mostly towards NW or N with maximum about 0.3 m/s while the weak tidal current has a greater tendency to rotate around the compass. The tidal current strength is found to be generally similar through depth except near the surface where it is rather stronger.

## 4.1.2.    Waves

The predominant waves on the Namibian coastal shelf come from a narrow directional band between S and SSW. The wave conditions are relatively stable throughout the year and are dominated by swell, the average significant wave height is around 2 m. For 5-10 % of the year significant wave heights are greater than 4 m (NMP, 2012b), with wave periods of up to 16 seconds.

Waves have not been included in the modelling owing to the large water depth. It is unlikely that dredging will be undertaken in wave heights of the size necessary to significantly change the behaviour of the plume and it is also unlikely, except in very extreme conditions, that there will be any resuspension of sediment on the bed. This is because deposition of fine sediment will make the bed "smooth" and prone to less turbulence (Soulsby, 1997; Whitehouse et al, 2000).

## 4.1.3.  Winds

Wind data for the area has been obtained from ERA5 (Hersbach et al, 2016). ERA5 is a climate reanalysis dataset, generated using Copernicus Climate Change Service information. ERA5 gives an estimate of historical atmospheric activity based on numerical models combined with observations. The name ERA refers to 'ECMWF ReAnalysis', with ERA5 being the fifth major global reanalysis produced by ECMWF (after FGGE, ERA-15, ERA-40, ERA-Interim), and ECMWF being the European Centre for Medium-Range Weather Forecasts.

Data processing for ERA5 is carried out by ECMWF, using ECMWF's Earth System model IFS, cycle 41r2. ERA5 provides high quality medium-high resolution estimates of atmospheric and surface wave parameters, with a horizontal resolution 31 km, 137 vertical levels and data archived hourly. ERA5 is currently available from 1979 to mid-2019, and will extend from 1950 to present when complete. ERA5 is being developed through the Copernicus Climate Change Service (C3S).

Wind roses have been generated based on a long hourly time series of hourly ERA5 data, from 1979 to mid-2019, at 24°S 14°E. Figure 4.3 shows a wind rose based on all the data. 12 direction sectors are represented, showing the direction from which the wind blows. The length of the bars shows the frequency of flow in each direction sector. Wind speed is indicated by the colour shading. A strong dominance of wind direction from the south is seen, with 70% of winds coming from the south sector.

Wind roses are also shown based on data for each month separately, in Figure 4.4 (for January), Figure 4.5 (February), Figure 4.6 (March), Figure 4.7 (April), Figure 4.8 (May), Figure 4.9 (June), Figure 4.10 (July), Figure 4.11 (August), Figure 4.12 (September), Figure 4.13 (October), Figure 4.14 (November) and Figure 4.15 (December). All the monthly figures use the same layout and colourscale as the annual wind rose Figure 4.3. The monthly roses show that the dominant wind sector is from the south in all months of the year. During the austral (southern hemisphere) winter months, in May, June, July and August, there in a relative increase in winds coming from the sector centred on 150°N.
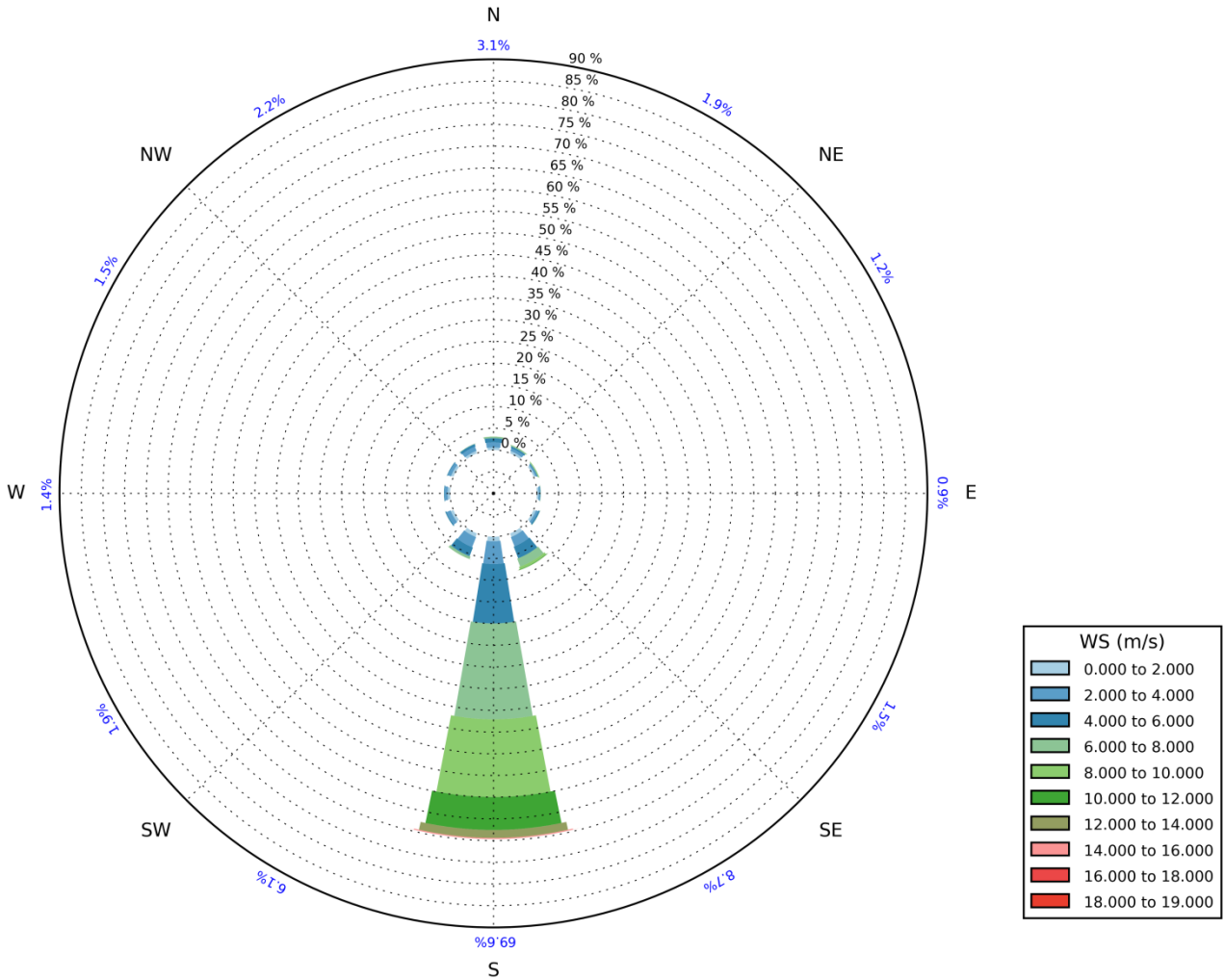
Figure 4.3: Wind rose at 24°S 14°E: all data from 1979 to mid-2019

*Source:    Generated using ERA5 data from Copernicus Climate Change Service information (2019)*
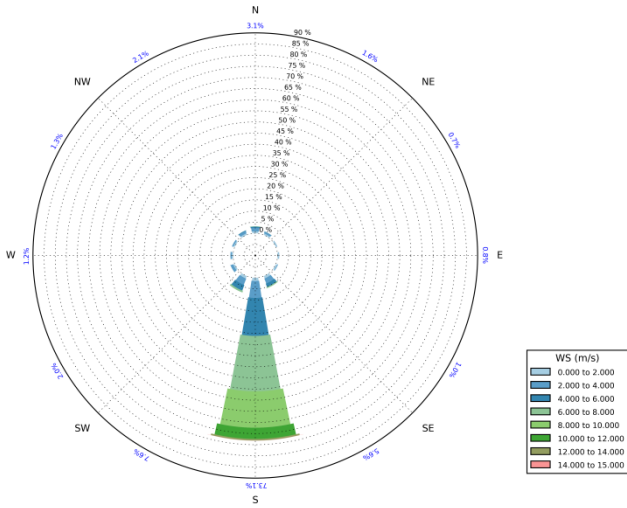
Figure 4.4: January wind rose at 24°S 14°E
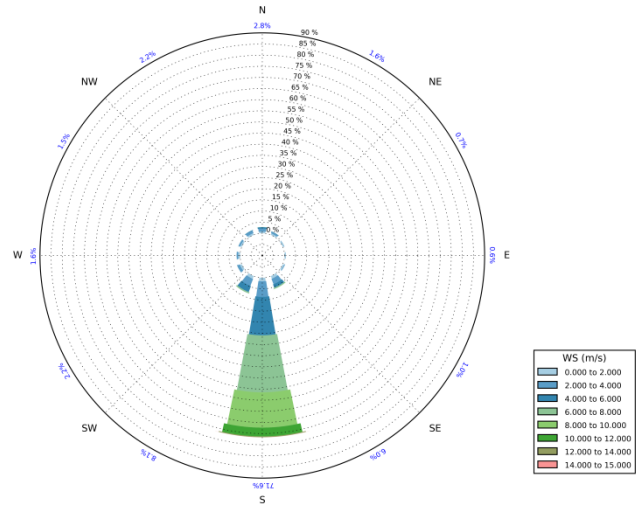


Figure 4.5: February wind rose at 24°S 14°E
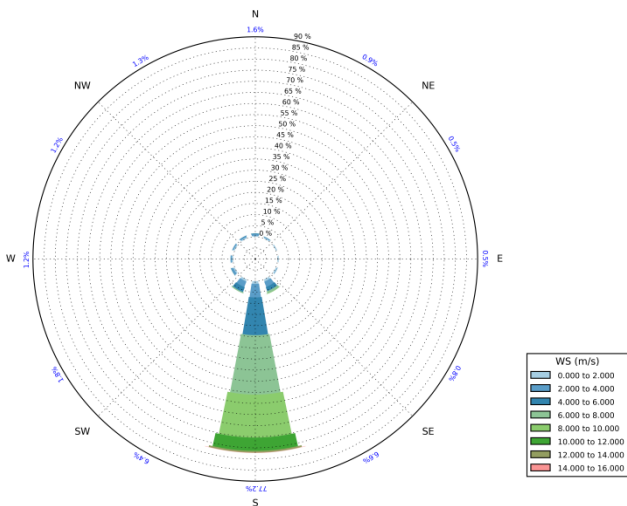


Figure 4.6: March wind rose at 24°S 14°E
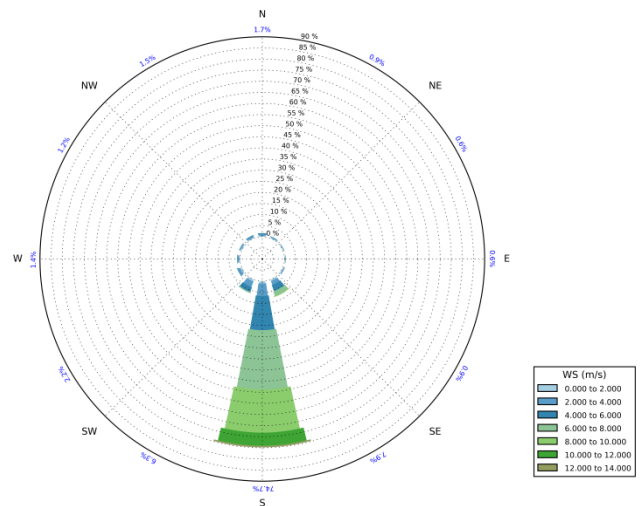


Figure 4.7: April wind rose at 24°S 14°E
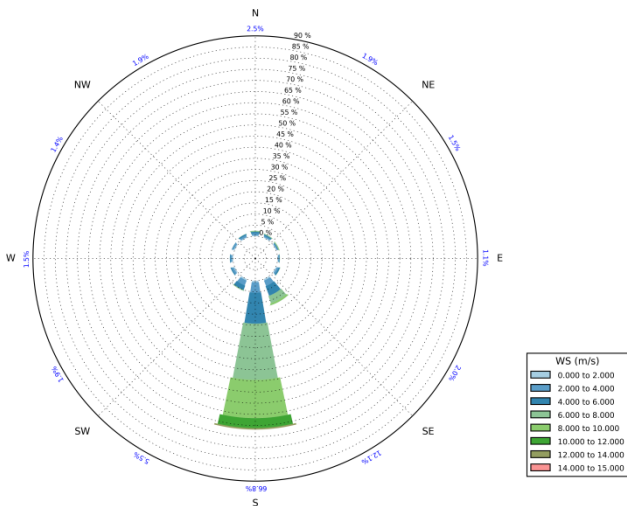


Figure 4.8: May wind rose at 24°S 14°E
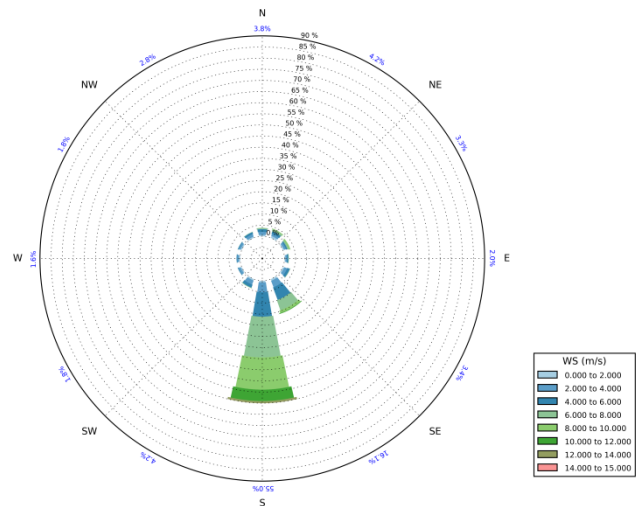


Figure 4.9: June wind rose at 24°S 14°E
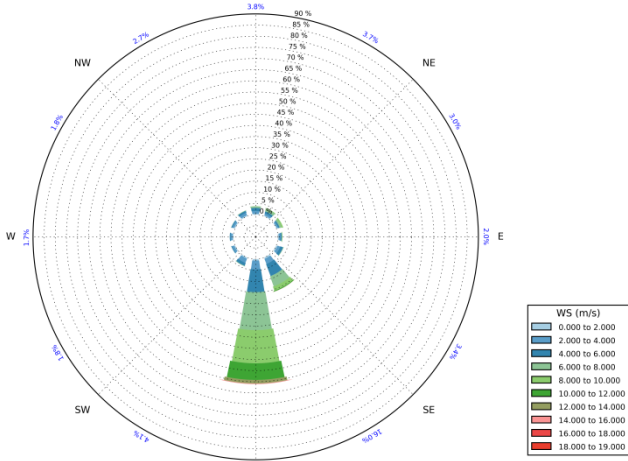
Figure 4.10: July wind rose at 24°S 14°E
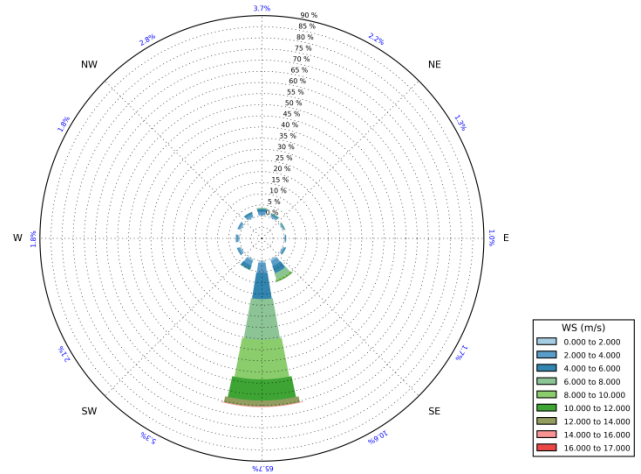


Figure 4.11: August wind rose at 24°S 14°E
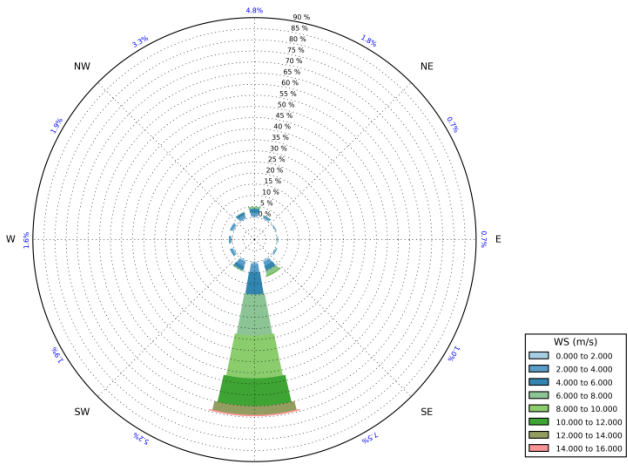


Figure 4.12: September wind rose at 24°S 14°E
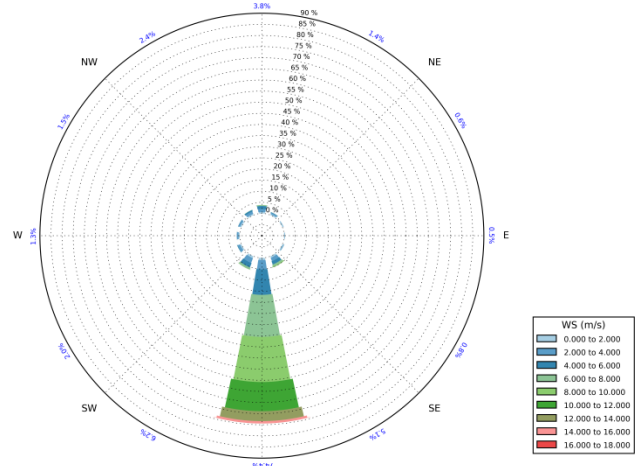


Figure 4.13: October wind rose at 24°S 14°E
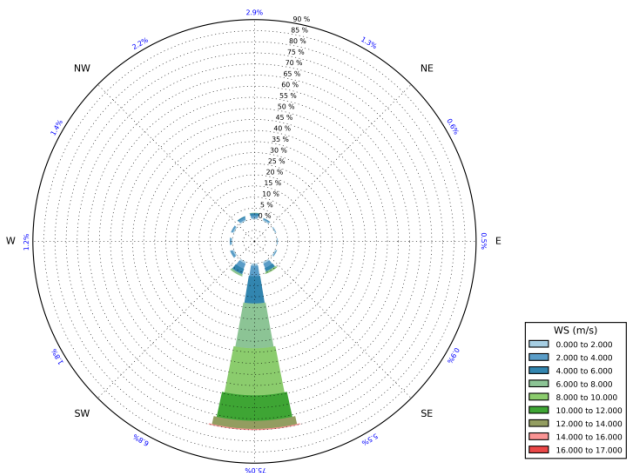


Figure 4.14: November wind rose at 24°S 14°E
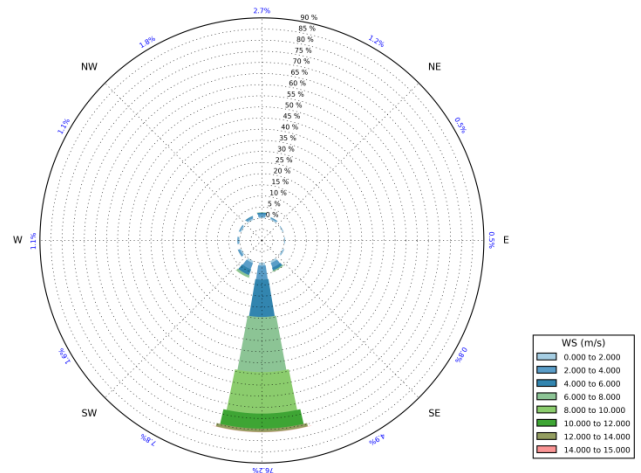


Figure 4.15: December wind rose at 24°S 14°E

## 4.2. Project site details

### 4.2.1. Introduction

The original Environmental Impact Assessment and Environmental Management Plan (EMP) was submitted to the Environmental Commissioner in April 2012 (NMP, 2012a). The 2012 EMP committed NMP to undertake a package of verification studies prior to the commencement of dredging.

The subsequent Verification Programme included various specialist studies that were completed during 2013 and 2014, prior to award of the ECC, providing evidence in support of the original impact assessments contained in the 2012 EIA, with specific focus of the assessment of the primary target dredge site SP-1 (NMP, 2014).

The Verification Programme entailed updated surveys and assessments in the following areas:

- Water Column and Sedimentary Environment;
- Fisheries and Biodiversity;
- Geophysics and Geophysical Habitat Mapping.

This information, especially the water column and sediment sampling under the Verification Programme, has informed the understanding of the project area described below.

### 4.2.2. Currents

As part of the Verification Programme, a detailed 90 day current survey was carried out in June-September 2013 (Austral winter period) in approximately 200 m of water. An upward looking Acoustic Doppler Current Profiler (ADCP) covered the top 100 m of the water column and two aquadopp acoustic profilers were deployed at about 150 m and near bed thus providing an essentially complete profile (NMP, 2014b).

As stated above, the tidal component was found to be small and dominated by diurnal variation. The current is strongest and N or NW bound near the surface and in the bottom half of the water column more S or SE currents were measured. This is consistent with there being upwelling in the waters shallower than about 200 m.

There was no equivalent survey carried out during the Austral summer period. However the following comment from NMP (2014a, *Appendix C2.1 Water Column and Sediments*) suggests that there will be stronger poleward near-bed flows in later summer:

*"Monteiro (in litt) raises the caveat that his conclusions are based on conditions measured at the proposed mining site in winter and may be different especially in late summer when dissolved oxygen advection into the area (ventilation) may be reduced due to the dominance of poleward flows of SACW from the Angola region."*

### 4.2.3. Seawater temperature

Seawater temperatures were collected at various times during the 90 day Austral winter survey period.

During the first 45 day period the mean temperature was 12.31 ºC at 97 m depth, 11.77 ºC at 148 m and 11.20 ºC at 193 m. During the second period it was 11.72 ºC at 93 m, 11.23 ºC at 142 m and 10.94 ºC at 188 m.

During late June a number of Conductivity Temperature and Depth (CTD) downcasts were made through the whole water depth of 200 m and the resulting temperature profiles are shown in Figure 4.16. In most (but not all) of the profiles there is a thermocline occurring between 15 m and 30 m below the surface. Below 50 m the temperature decreases approximately linearly with depth.
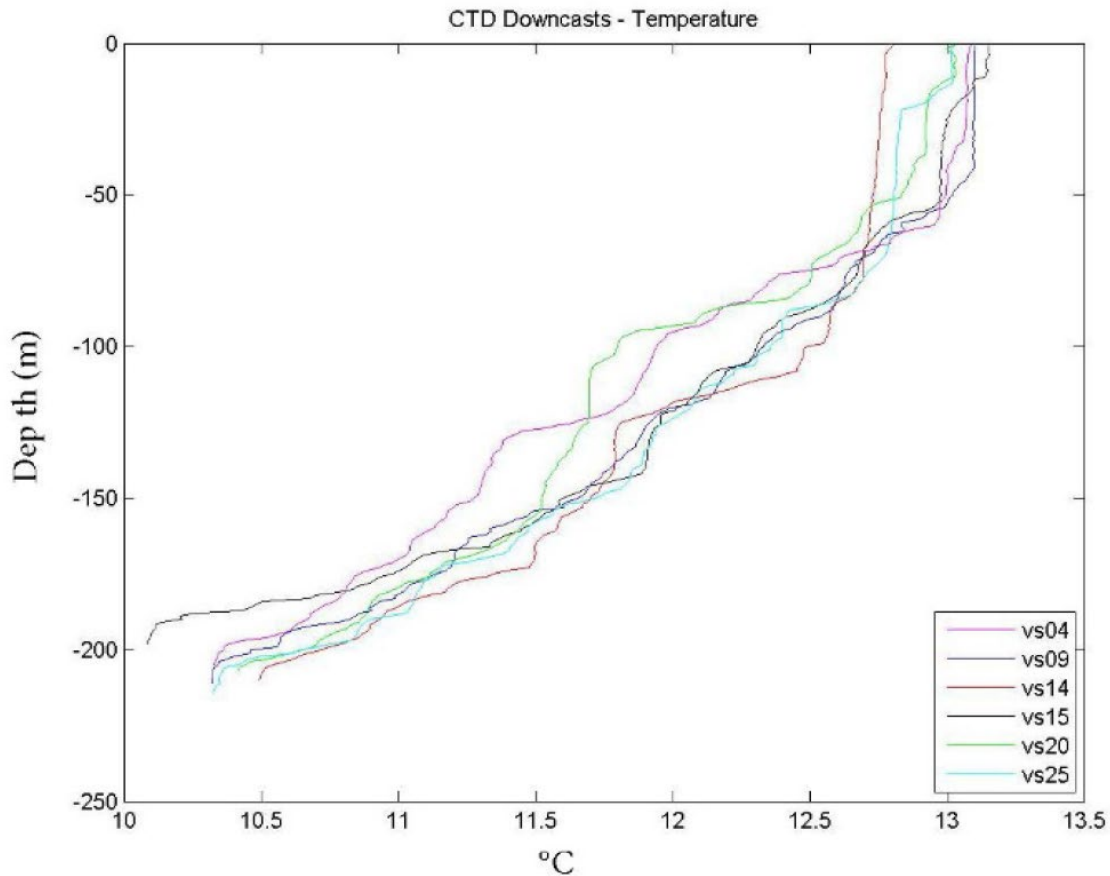


Figure 4.16: Temperature profiles 26-30 June 2013

*Source:    NMP (2014a) Section C2.1*

## 4.2.4.    Salinity

The measured salinities show slightly higher salinity near the surface resulting from evaporation (NMP, 2014b). Since the salinity variation is quite low it is not considered important for flow or dispersion modelling.

# 4.3.  Sediments

## 4.3.1.    Suspended sediment concentrations

As part of the Verification Survey, turbidity was measured between 8 June and 13 September 2013 using an RBR CTD fitted with a turbidity sensor (NMP, 2014b, *Sandpiper Project Section C2 Water Column and Sedimentary Environment*). In all 86 days of turbidity data were collected at the survey location, at a depth of 187-192 m below sea level (which is estimated to be around 5-10 m above the seabed).

The measured turbidity data is presented in Figure 4.17.  The data shows several episodic high-turbidity events of between a few hours and 24 hours which rise to peaks in turbidity between 350 NTU and 1,300 NTU (Nephelometric Turbidity Units).  Similar turbidity events were observed by Monteiro et al. (2005) suggesting that turbidity currents are episodically generated further inshore and pass through the proposed mining area to deeper waters.  However, some of the observed events occur during periods when currents are aligned in a north or south direction, suggesting that other causes, such as trawling, may be responsible.
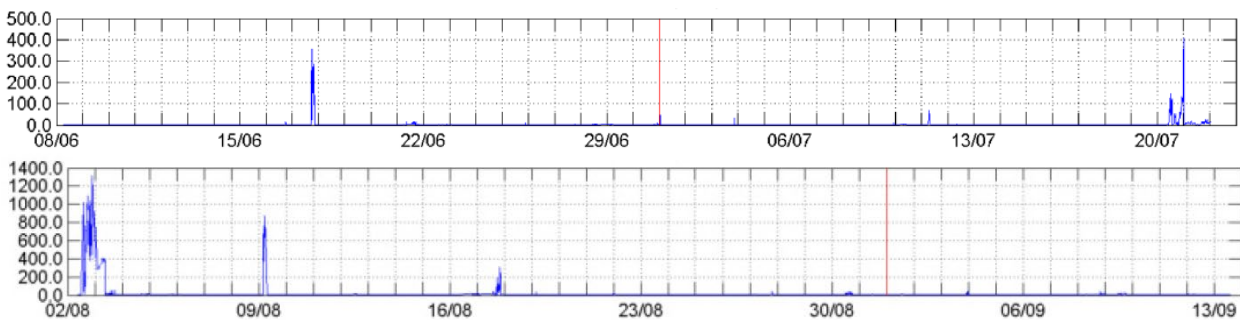


Figure 4.17: Measured turbidity 5-10 m from the seabed over the period 8 June to 13 September 2013

*Source:    NMP (2014a) Section C2.1*

The extent to which these high turbidity events occur regularly throughout the site is important when considering  the potential impacts of dredging on ecology.  As discussed below for lower and more frequently experienced suspended sediment concentrations, if marine species have adapted to be tolerant to these high turbidity events then they will also be tolerant of the much lower concentration increases arising from plumes.  However, the extent of these high turbidity events is at present unknown.  For this reason, a conservative approach has been taken in this report whereby it is assumed that the high turbidity events are localised and unrepresentative of typical suspended sediment concentrations.

The same data, but with the high turbidity events removed, is shown in Figure 4.18.  This data shows that turbidity varies between 0 NTU and 20 NTU.  A summary of the statistics is provided in Table 4.1.
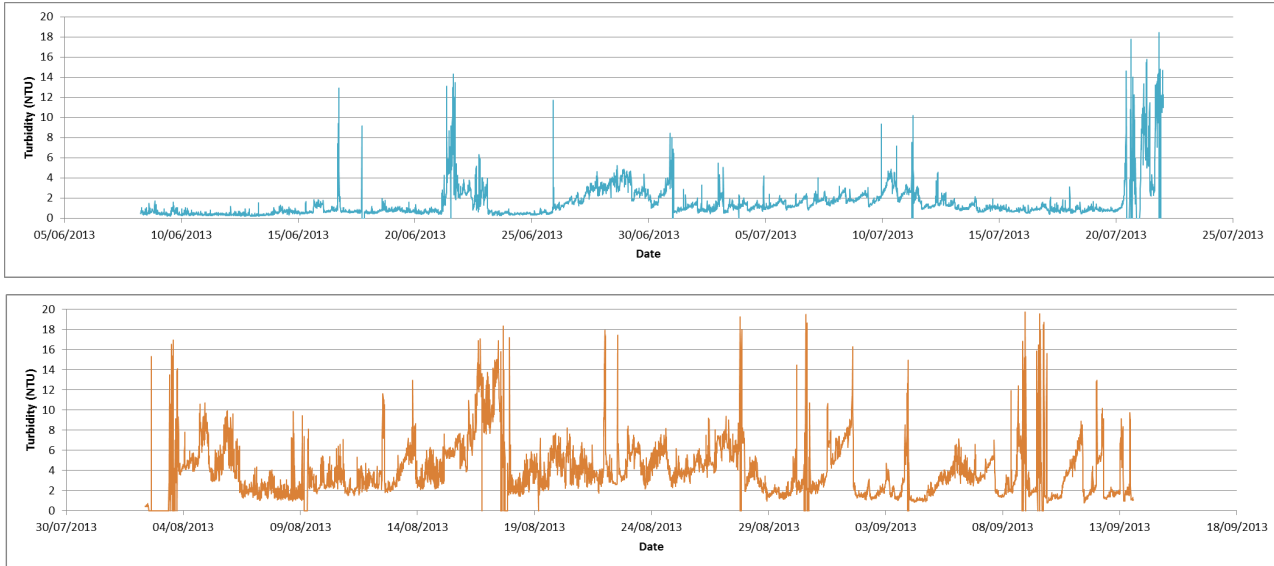
Figure 4.18: Measured turbidity 5 m above the bed over the periods (top) 8 March to 22 July and (bottom) 3 August to 13 September 2013

*Source:    NMP (2014a) Section C2.1 (modified)*

Table 4.1: Summary of measured near-bed turbidity

| Statistic | Turbidity (NTU) |
|-----------|-----------------|
| Median | 1.9 |
| 5%-tile | 0.4 |
| 95%-tile | 7.5 |
| Maximum | 19.7 |

The summary of statistics in Table 4.1 indicates that (ignoring the high turbidity events) there is regularly experienced natural variation of background turbidity of more than 7 NTU (0.4 to 7.5 NTU).  At present there is no site-specific data from the proposed mining site for the conversion of Optical Back Scatter (OBS) measurements (in NTU) to suspended sediment concentrations (in mg/l).  The experience of HR Wallingford is that 1 NTU can be equivalent to anything from 1 to 5 mg/l although typically 1 NTU = 2-3 mg/l.  For the near-bed environment use of a typical conversion between NTU and mg/l  suggests that the typical background variation in suspended sediment concentration is around 15-20 mg/l.

Additional evidence from vertical profiling (NMP, 2014b, *Sandpiper Project Section C2 Water Column and Sedimentary Environment*) suggests that the turbidity in the middle of the water column is considerably less than that at the bed, although the surface is slightly higher owing to the capture of wind-blown dust particles from the mainland on the sea surface.  This is a recognised phenomenon at the Namibian coastline (Dansie et al., 2017).  It is assumed that the typical range of natural turbidity is an order of magnitude less for the mid-depth and for surface turbidity compared to the near-bed turbidity.

The natural typical range of suspended sediment concentration is an important consideration in evaluation of dredging operations (assuming that chemical contamination is not a consideration). Any marine species living in the local environment is likely to be adapted to be tolerant of this natural variation (and potentially, tolerance of larger concentrations) and therefore changes in suspended sediment concentration which fall within this range do not change the background environment, and hence unlikely to represent an impact.

Further information on the sensitivity of species to changes in suspended sediment concentration can be gained from laboratory experiments. This modelling study has used the results of a comprehensive study of mining tailings on a spectrum of marine species (Smit et al., 2008). This work identified a threshold of increase in suspended sediment concentration of 7.6 mg/l, below which impact was negligible across a range of species including filter-feeding zooplankton, molluscs, crustacea, algae and fish. This is considered an appropriate threshold to adopt in this study, taking into account the depth-varying variability in suspended sediment concentrations (Lwandle, 2020).
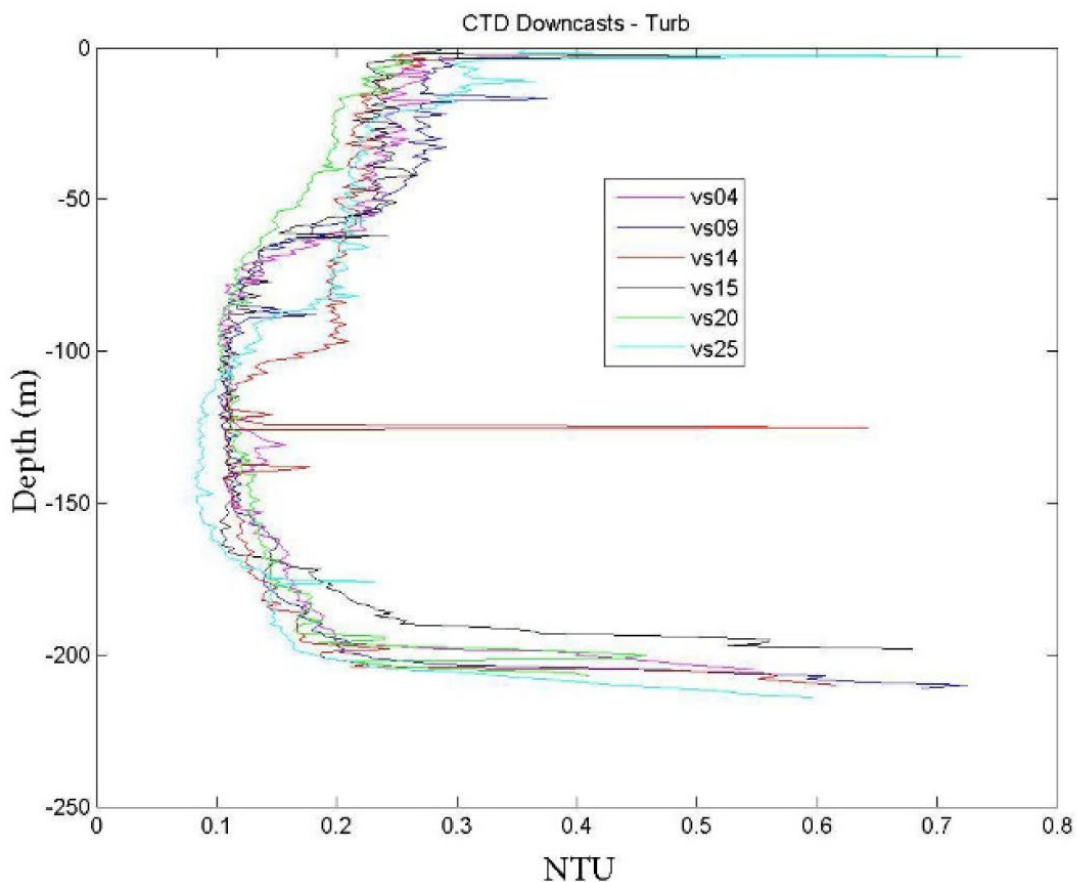


Figure 4.19: Measured turbidity from CTD downcasts

*Source: NMP (2014a) Section C2.1*

### 4.3.2. Natural settling rates of sediment

Sedimentation rates in the inner shelf mud belt off Namibia calculated using radiocarbon ages of planktonic foraminifera have been reported to reach values in excess of 0.5 mm/year, while on the outer slope sites sedimentation rates of 0.05-0.17 mm/year have been found (Mollenhauer et al., 2007).  These measured natural fluxes are more than 2 orders of magnitude smaller than the deposition flux from dredging discussed in Section 9.3.

### 4.3.3. Surface seabed sediment

As part of the Verification Studies (2014a), NMP carried out a grab sample survey of surface sediments in the dredging area, and including sites east and west of the dredging area found that the surface seabed sediment in the dredging area was very silty sand, varying from 28 % to 46 % silt, the remaining being sand (see Figure 4.20).  The clay content was found to be less than 3 %.  The median particle size (D50) for this surface sediment, including reference sites north and south of the area, was found to vary between 75 µm and 155 µm, representing very fine and fine sand, respectively.  Some of the samples highlighted the presence of shell, although shell was not accounted for in the analysis of particle size distribution.
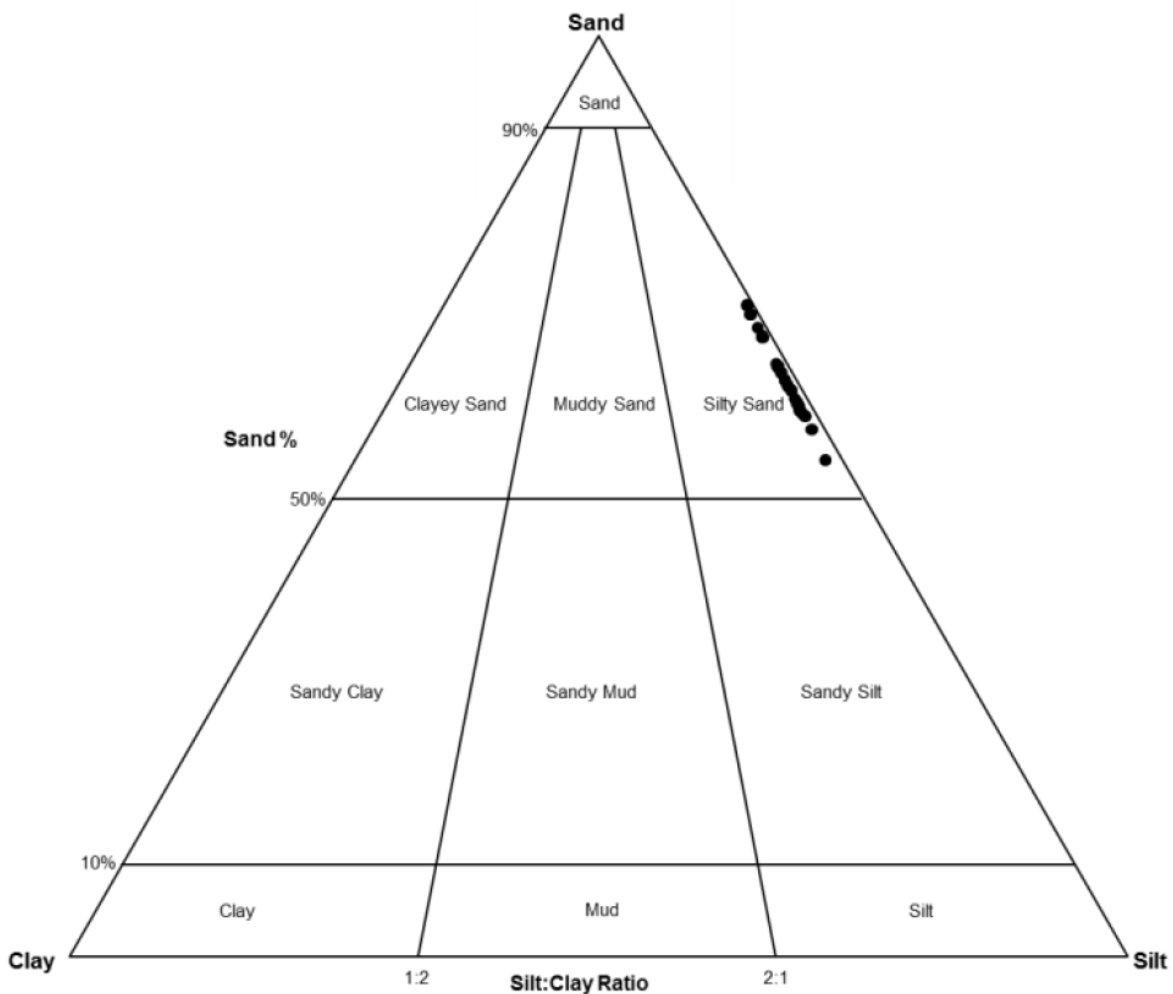


Figure 4.20: Ternary diagram showing a surficial sediment classification of collected Day grab samples

*Source:    NMP (2014a) Section C2.1*

The wider distribution of surface sediment types is shown in Figure 4.21.  At water depths of less than 150 m, high sedimentation of organic matter forms a diatom layer, creating a "mud-belt".  Between this mud belt and 300-400 m water depth, the bed is characterised by sandy sediment while further offshore the bed becomes increasingly muddy (Steffani, 2012).
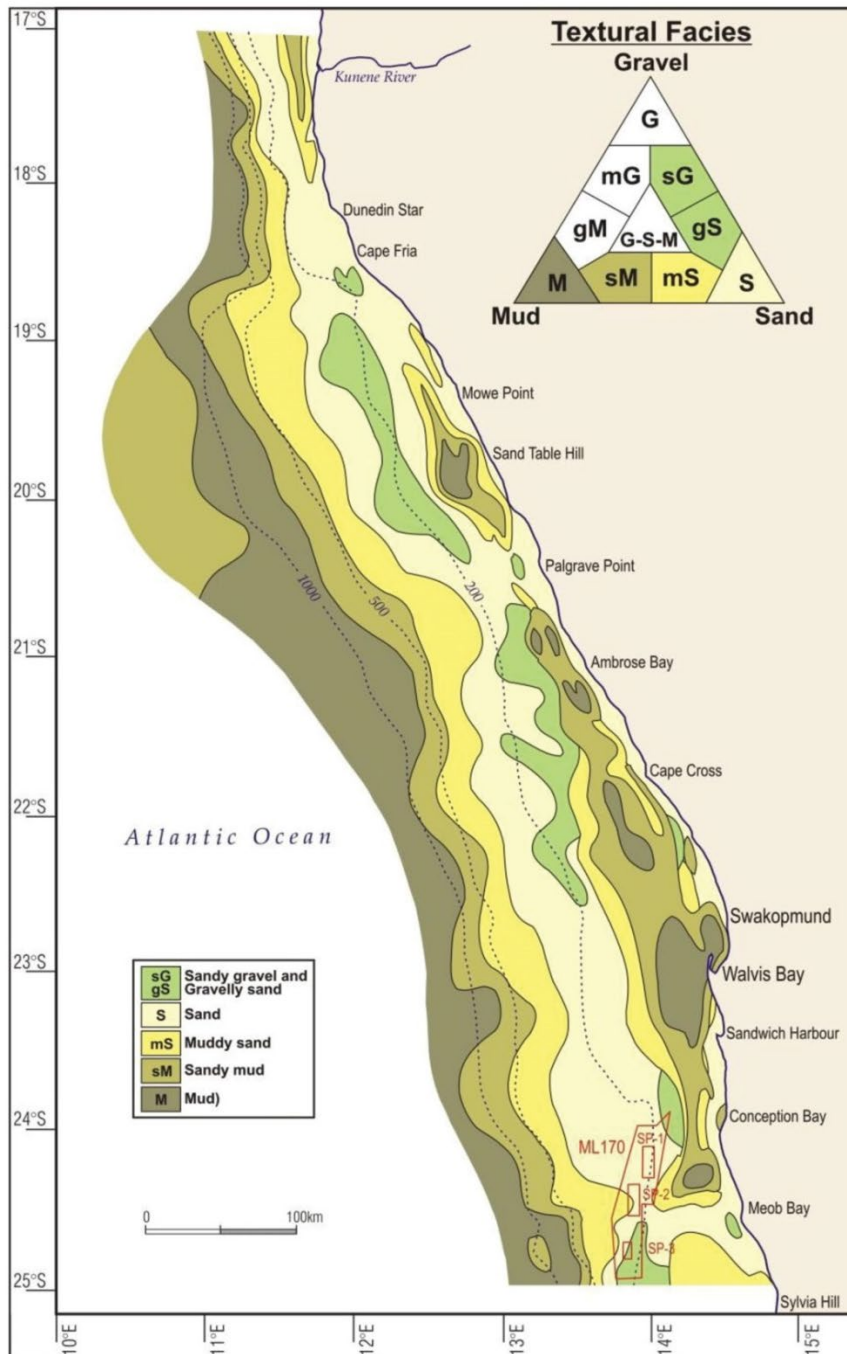


Figure 4.21: Surface sediments on the Inner and Outer Namibian Shelf, showing the proximity to the ML 170 Licence Area, the SP-1 candidate dredging area and earlier candidate dredging areas SP-2 and SP-3

*Source:    Marine Benthic Specialist Study, Steffani (2012)*

### 4.3.4. Sediment sizes associated with the sub-surface Phosphate resource

The sub-surface seabed sediment (which includes Phosphate) comprises three layers, the particle size distributions of which are presented in Figure 4.22. The three layers can be broadly described in terms of their particle size as follows:

- Layer 1: The surface layer. Medium sand with less than 10 % fines and around 20 % gravel or shell.
- Layer 2: The surface middle layer and the bulk of the resource. Medium sand with around 20 % fines and around 10 % gravel.
- Layer 3: Not part of the resource but lying directly underneath the resource. Extremely plastic footwall clays.

When dredging occurs, it is assumed that Layer 1 and Layer 2 will be dredged along with a small proportion of Layer 3. There is no incentive for Layer 3 to be dredged as it does not form part of the resource, but it is assumed that a small amount may be removed during the dredging of the layers above. Table 4.2 shows the relative proportions of each layer in the dredging volume, based upon the sampling (Bateman, 2011a). On the basis of this information, Layers 1, 2 and 3 represent 21 %, 76 % and 3 % of the mass of sediment (and phosphate) that will be dredged. An average or "composite" particle size distribution has been used for the purpose of the modelling in this report, based on two core samples LA and LB as shown in Figure 4.22 (Bateman, 2011b).
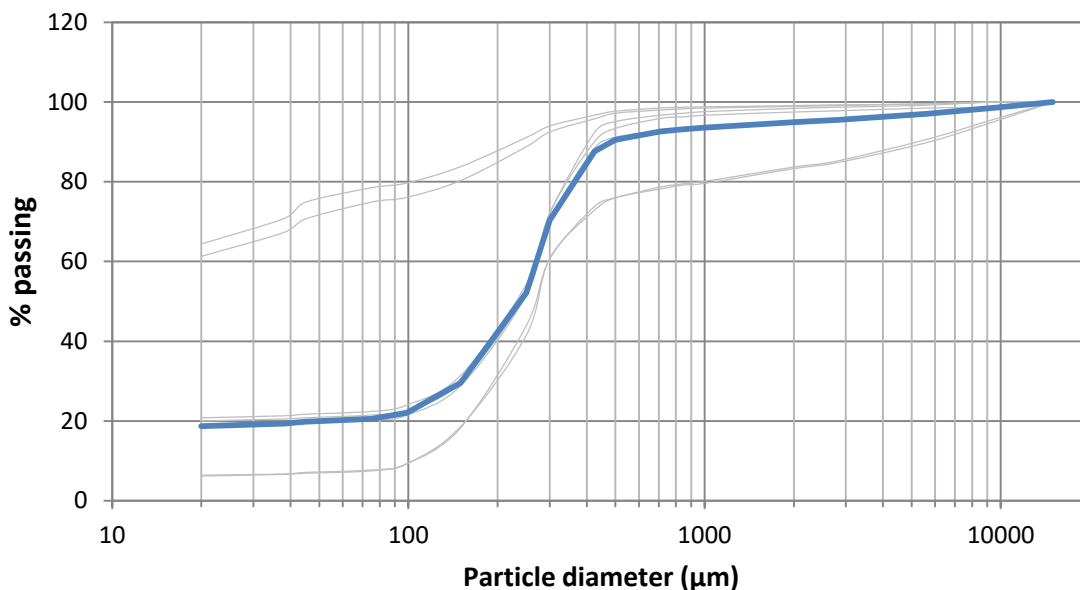


Figure 4.22: Particle size distribution of resource showing the representative or composite PSD used for the study

*Source: Bateman (2011b)*

Table 4.2: Characteristics of resource layers

| Layer | Thickness (m) | Proportion of dry mass (%) |
|---|---|---|
| L1 | 0.5 | 21 |
| L2 | 2 | 76 |
| L3 | 0.1 | 3 |

*Source:    Bateman (2011a)*

### 4.3.5.    Re-suspension of sediment

The Validation document (NMP, 2014b, Section C2.1 *Water Column and Sediments*) estimated the potential for re-suspension of sediment based on measurements by Monteiro (2005) at the Outer Shelf in 400 m water depth.  The conclusion was that the bottom shear stress generated by near-bed currents would be sufficient to prevent the settling of fine sediment.  This conclusion was also drawn by the Marine Benthic Specialist Study (Steffani, 2012) based on the distribution of surface sediment types – specifically that there are muddier substrates inshore and offshore of the proposed dredging area (See Figure 4.21) implying that currents are faster and able to prevent the deposition of muddy sediments in the region of the 200 m depth contour where dredging is proposed to occur.  This is a natural conclusion, but assumes that the nature of the fine particulate material in the area is similar to that of the fine sediment which will be released from the dredger, and that the magnitude of the natural background sediment fluxes and the dredging fluxes are of a similar order.

The nature of the background suspended sediment (disregarding the high turbidity events) is of low concentration and detrital (NMP, 2014b, Section C2.1) and it has been inferred that the levels of turbulence in this area are sufficient to prevent deposition of this primarily organic material.  However, the nature of the high turbidity events described in Section 4.3.1 is poorly understood.  These events could be created by release of hydrogen sulphide from the mud belt (NMP, 2014b, Section C2.1) or from local trawling activity (which can cause plumes to the observed high turbidity events, e.g. Clarke et al, 2016).

The composition of plumes originating from the mud belt might be expected to be detrital, and hence of low settling velocity, which would explain why plumes of sediment concentration of several hundred mg/l do not settle over the (greater than 50 km) distance between the site and the mud belt.  However, if the high turbidity events seen at the site do originate in the mud belt and are composed of sediment which is similar to that which will be released by the dredging, then the lack of fine sediment at the site would suggest that the levels of turbulence are indeed able to prevent the material settling from dredge plumes, especially as the annual flux of sediment through the site would be of a similar order.

On the other hand, if the observed high turbidity events arise because of local trawling, the plumes are likely to be mainly composed of surface detritus and the flux through the site arising from these plumes can be shown to be an order of magnitude less than that resulting from the proposed dredging.  On this basis, the absence of fine sediment at the site at present could not be used as basis for concluding that the dredging site will remain free of fine sediment under the dredging scenario.

In addition, it is possible that extreme currents (and/or waves) will result in some reworking of the deposited sediment.  The measured currents (see Section 6.3) only represent around 2 months of the year and it is possible that larger scale ocean gyres, upwelling fronts or extreme weather events give rise to greater levels of turbulence than observed during this time period.

The detailed modelling undertaken in this study, based on the calibration of the flow model to the 3 month period of observed data and using representative thresholds of erosion and representative settling behaviours of disturbed sediment, indicates that there is little or no resuspension of overflowed sediment arising from the observed currents at the dredging site. Essentially the observed near-bed currents at the site (see Figure 6.6, Figure 6.12 and Figure 6.16), under the low-friction turbulent conditions (e.g. Soulsby, 1997; Whitehouse et al, 2000) which will result from deposition of fine sediment caused by the dredging, will be insufficient to re-suspend, or to prevent, deposition of sediment.

On balance the model prediction that the low levels of turbulence, arising from the observed currents and waves at the site, will be insufficient to prevent deposition of fine sediment, appears correct. However, the presence of high turbidity events (whether natural or anthropogenic), which do not appear to result in deposition of fine sediment at the site, give rise to some uncertainty about this conclusion.

This matter is discussed further in Section 11.

### 4.3.6. Heavy metal contaminants

As reported in the Verification studies, NMP (2014a, C2.1 *Water Column and Sediments*), there are two possible pathways by which heavy metals may impact on marine species: through direct exposure and through ingestion. However, the Verification Studies concluded that neither of these pathways would lead to an increase heavy metal contamination:

■ While surficial and subsurface sediments in the dredging area support relatively high concentrations of the heavy metals (arsenic, cadmium, chromium, copper and nickel) the bioavailability of these heavy metals is largely negligible, as established by elutriation tests. The low release of the metals into the dissolved phase indicates that although their natural concentrations exceeded the sediment quality guidelines for the region they do not represent a toxicity risk in this phase either in situ or following physical disturbance.

■ The alternative toxicity pathway of the heavy metals is via complexing with organic particles and then ingestion by deposit and filter feeders. However, as regards *demersal fish*, transfer of heavy metal contaminants is generally attenuated at the primary consumer level (dominated by copepods) with low transfer efficiencies to fish. As regards *benthic species*, the Verification studies concluded that the proposed mining operations in the survey area are not expected to increase exposures of benthic fauna to heavy metals over and above that which occurs naturally in the region and hence the risk of any bio-accumulation is low.

As a result of these findings, the contamination of heavy metals is not considered further in this study.

## 4.4. Sensitive receptors

Potentially sensitive receptors have been identified during previous EIA studies (NMP, 2014b). These and other receptors have been raised as concerns by both EIA reviewers and project stakeholders (Newell and Muhapi, 2018). The potentially sensitive receptors identified by others and included within this report for presentation alongside the plume modelling results include:

■ Fish Spawning Areas and trawling protected juvenile zones;

■ Hake and Monk commercial fishing grounds;

■ Mariculture and Saltworks Operations water intake.

This report has not set out to justify the selection of these receptors, and has not validated if these are the main or best receptors to be included for further analysis. The list of receptors has been put forward by project stakeholders as requiring additional consideration. The location of these features, including where the data have been obtained from are described below.

### 4.4.1.    Fish Spawning Areas

For the purpose of the analysis within this report, fish spawning areas have been taken to be all areas of shelf that are shallower than 200 m (Gordoa et al, 2006). The original EIA also indicated that fish spawning is generally confined to water depths less than this (NMP, 2012a).

The 200 m boundary is used as a fishing limit by Law within Namibian waters, restricting bottom trawling in areas shallower than 200 m.

### 4.4.2.    Hake and Monk commercial fishing grounds

For consistency with the original assessment and verification programme, mapping data for the locations of historical hake and monk fishing activity from the original EA (NMP, 2012) have been used in this report – see Figure 4.23.

Other reports have noted that there is evidence that Cape hake and monkfish do live in the Mining Licence Area but that they make up only a small proportion of the overall commercial stock of those target species in Namibian waters (NMP, 2014d).  The catch data in (Figure 4.23) indicates that there has been no commercial fishing within the proposed dredging area itself.

The locations of hake and monkfish commercial grounds are also available from the Benguela Current Commission (BCC), run by the Ministry of Fisheries and Marine Resources in Namibia. The Commission have collated a wide range of data from all industries including fishing which is available on the BCC interactive data portal site (http://www.benguelacc.org/index.php/en/marisma). Reference can also be made to qualitative information on the hake fishery resource and the present understanding of hake behaviour and the social and ecological factors affecting fishing activity, leading to inaccuracies in the current assessment of resource abundance (Paterson and Kainge, 2014).
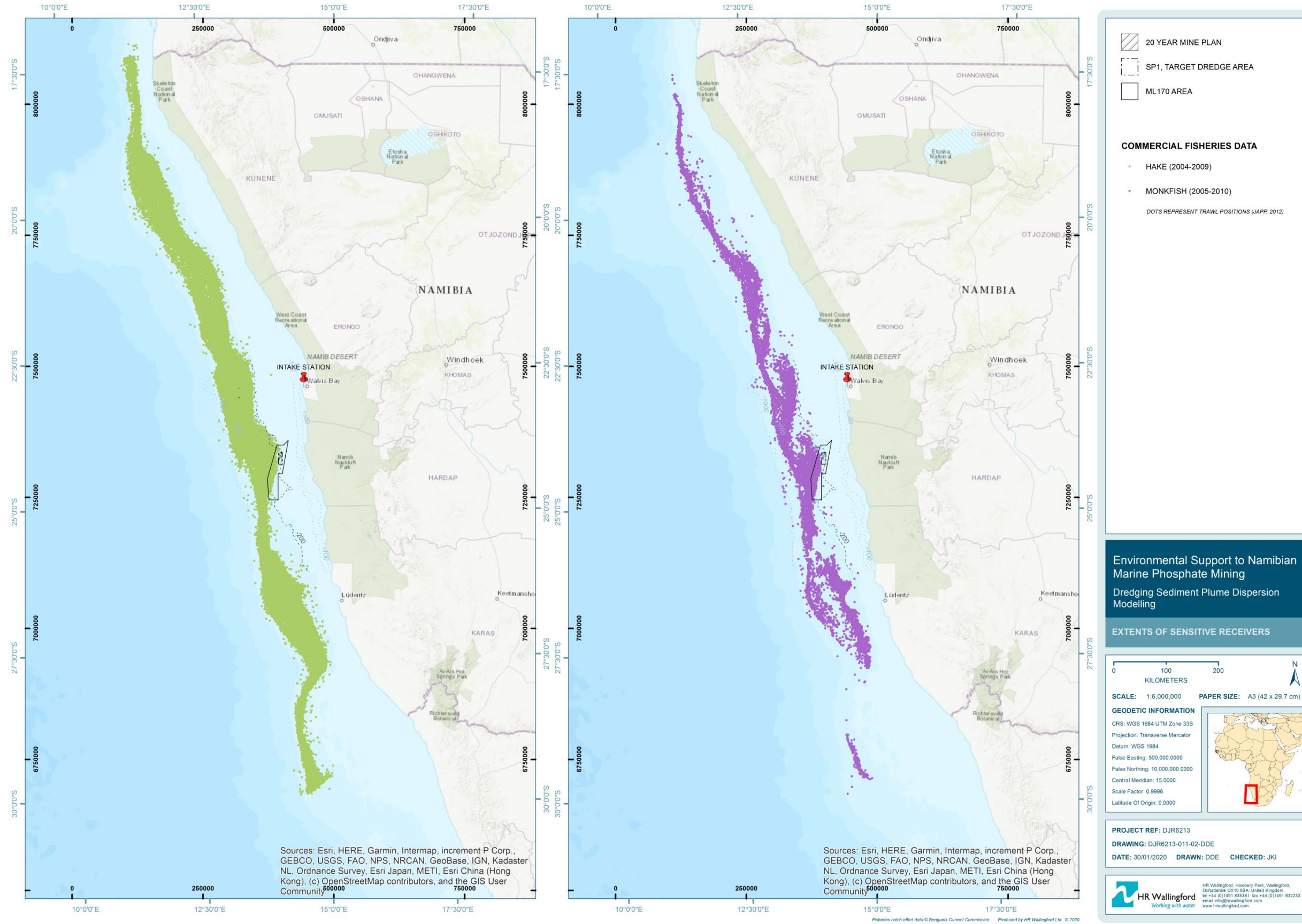
Figure 4.23: Commercial Fishing Areas for Hake and Monkfish

### 4.4.3.  Mariculture and Saltworks Operations water intake

The location of the water intake for the saltworks operation in Walvis Bay is shown in Figure 4.24 below. The location of the intake for the purpose of the analysis is taken as: 22°57'53.33"S, 14°26'5.95"E.



Figure 4.24: Location of Walvis Bay Salt Refiners
*Source:    Google Earth, SIO, NOAA, U.S.Navy, NGA, GEBCO (2019)*

# 5. Overview of modelling approach

## 5.1. Background

Dispersion of sediment plumes is one of the most sensitive aspects of new marine mining proposals. Regulators and stakeholders typically require comprehensive examination of the scale and extent of water column and sedimentation effects. These are important issues for the Sandpiper project.

Factors including the complexity of ocean currents, the exploitation of important commercial fisheries in the region, and the concerns over interactions of the Sandpiper project with sediment plumes. These factors have been borne in mind in developing the modelling approach. The assessment studies must be of sufficient quality to stand the test of detailed examination by regulators/ stakeholders.

The approach has also been informed by ongoing discussion with NMP on the data already available to support the proposed work, and the phasing of work. This led towards an approach that employs ocean models coupled with a local 3D model to represent the processes that will affect sediment plume.

## 5.2. Outline of approach

In order to reassure stakeholders of the robustness of the assessment, and given the quality of data available, a sophisticated numerical modelling approach has been adopted. This involves the development of a local 3D flow model (driven with boundary conditions from an ocean model) to reproduce the detail of the 3D ocean and tidal currents in the vicinity of the mining. The key stages of the project are outlined below.

### 5.2.1. Inception

This stage involved review of the available data and confirmation of the modelling approach. Previous studies and the governing legislation were sourced from NMP and critically reviewed for information relevant to the study. Information on comparable projects and research were accessed from HR Wallingford's own library of resources.

Review was undertaken of the relevant datasets including meteorological and hydrodynamic data (wind, water level, and currents), sediment data (seabed sediment, suspended sediment concentration) and water quality data (salinity, temperature, suspended solids).

### 5.2.2. 3D flows

The foundation of the modelling process is a robust understanding of the 3D flow field. In this case, the model is driven by a global ocean model (Mercator) which was found to be the most accurate of the available hindcasts for the purposes of the study.

The Mercator ocean model hindcasts was used as boundary conditions for changes in mean sea level, currents, salinity and temperature to a TELEMAC-3D (www.opentelemac.org) local model of the area of interest. Tidal boundary conditions were imposed using TPXO global tidal model predictions. The TELEMAC-3D model was validated against the available oceanographic observations. The effect of wind stress on surface flows was derived from ERA-Interim global model re-analysis data.

### 5.2.3.  Sediment release

The sediment analysis undertaken by JDN was used as the based for the release of sediment from the overflow and hence as the source terms for the plume dispersion modelling.

### 5.2.4.  Sediment Plume modelling

The sediment plume modelling was undertaken using the SEDPLUME-RW plume dispersion code to predict the temporal and spatial distribution of changes in suspended sediment concentration, and of sediment deposition, arising from the proposed mining.  SEDPLUME-RW is a lagrangian dispersion model, representing the plume dispersion through predicting the movement of large numbers of representative particles.  This lagrangian approach means that the model is not susceptible to numerical diffusion (i.e. artificially induced mixing).  The dispersion model used hydrodynamic input from the detailed local TELEMAC-3D model.

It is important to note that all predictions in this study of the extent of suspended sediment and deposition, represent increases above background levels. These background conditions are described in Section 4.3.

# 6. Derivation of current flows in study area

## 6.1. Introduction

A 3-dimensional numerical model has been set up, to reproduce hydrodynamic conditions at the site. The model is based on the open source solver TELEMAC-3D (*www.opentelemac.org*). TELEMAC-3D solves the complete 3D Navier Stokes equations with non-hydrostatic pressure.

This chapter describes the building of the numerical model for this site, and extensive work carried out to attain model calibration. Results are then presented from the calibrated model, for three periods:

- Calibration period (45 days in June-July 2013, during austral winter);
- Validation period (45 days in August-September 2013, during austral winter);
- Austral summer period (March 2013).

## 6.2. Model set-up

### 6.2.1. Geometry

TELEMAC uses a completely flexible mesh of triangular elements, to ensure accuracy with computational efficiency. The model mesh was built in the local UTM coordinate system: UTM Zone 33S [WGS84]. The domain covers around 25,000 km$^2$, stretching from 7200000 mN to 7400000 mN, and from the coast to 340000 mE offshore. The domain is shown with Google Earth aerial imagery in Figure 6.1. The model coastline is defined by the CMap global chart database. The finest resolution of the mesh is 200m in the area of interest, and the coarsest resolution is 5 km at the model's open boundary. The mesh consists of almost 10,000 nodes, connected by almost 20,000 triangular elements, over the model domain.

A number of sources of bathymetric data were combined to define the model bathymetry. The data were resolved to the same vertical datum (relative to mean sea level (MSL)), and combined by selecting the most highly spatially-resolved dataset available for each part of the model domain. Bathymetric data files supplied by the client which were used in setting up the model are listed below (in order of preferential use):

1. Resblocks_bathy.xlsx (finest spatial resolution at the site);
2. 1m_sp1_bathy.shp;
3. gridded_bathy_1.shp;
4. bathymetric contours.shp (large scale regional contours).

In areas where the received data gave sparse coverage, the data were supplemented with bathymetry extracted from the CMap global chart database.
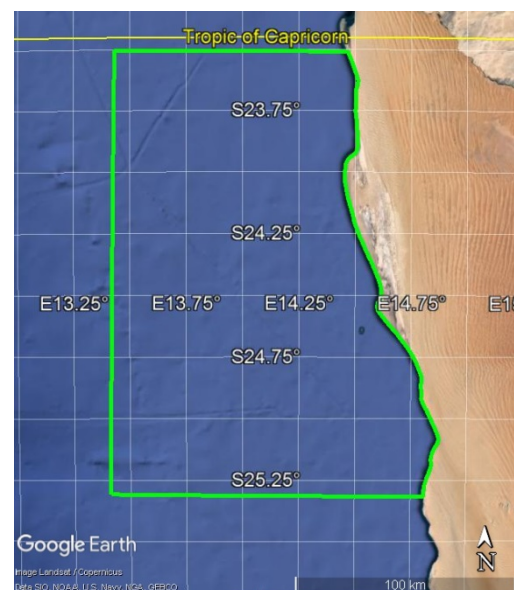


Figure 6.1: Model domain overlaid on Google Earth

*Source:    Google Earth, SIO, NOAA, U.S Navy, NGA, GEBCO (2019)*

The combined bathymetric data was then interpolated onto the nodes of the mesh. Figure 6.2 shows the model mesh and interpolated bathymetry over the model domain. Figure 6.3 zooms in on the finely resolved area. The location of the current meter MP1 (401016mE 7330084mN) is shown in Figure 6.3.
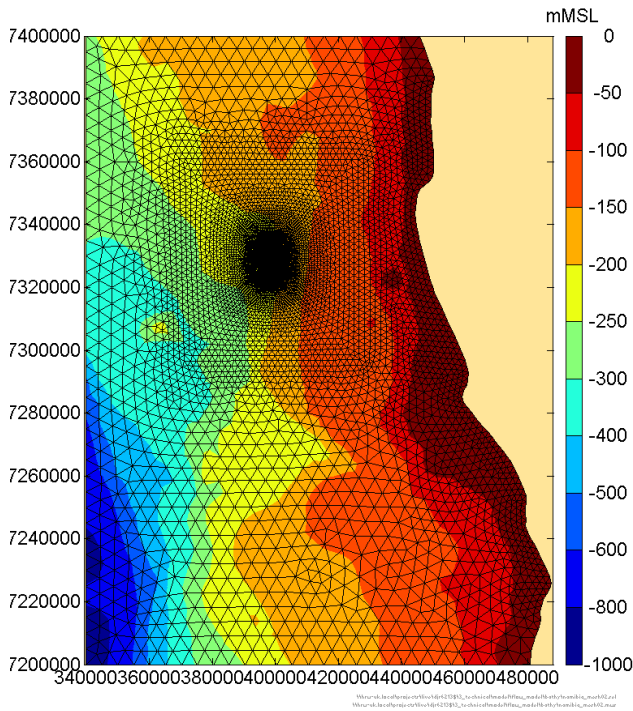


Figure 6.2: TELEMAC-3D model mesh and bathymetry
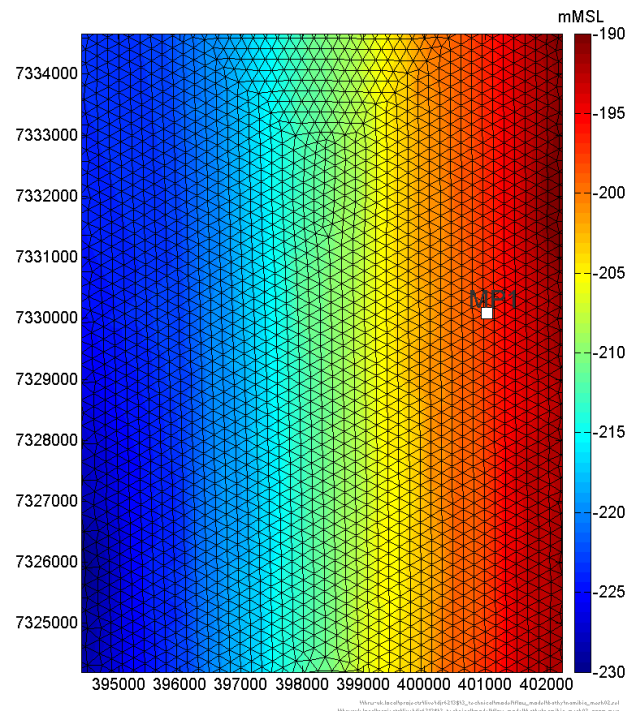


Figure 6.3: TELEMAC-3D model mesh and bathymetry in area of fine resolution

The model consists of 13 quasi-horizontal planes. The planes are distributed unequally through the water column, with more resolution near the surface and bed. A combination of fixed elevation and sigma planes is used. A sigma plane is defined as a proportion of the water depth, thus the elevation of a sigma plane varies over the model domain. The sigma plane's prescribed proportional elevation is applied between the non-sigma planes above and below. The planes are distributed as shown in Table 6.1.

Table 6.1: Vertical distribution of model planes at MP1 (the observation location)

| Plane number | Definition | Elevation at location of MP1 |
|---|---|---|
| 13 | Surface (elevation varies in time and space) | Time-varying |
| 12 | Fixed elevation at -2 mMSL | -2 mMSL |
| 11 | Fixed elevation at -5 mMSL | -5 mMSL |
| 10 | Fixed elevation at -10 mMSL | -10 mMSL |
| 9 | Sigma plane 95% | -19 mMSL |
| 8 | Sigma plane 90% | -29 mMSL |
| 7 | Sigma plane 85% | -38 mMSL |
| 6 | Sigma plane 75% | -57 mMSL |
| 5 | Sigma plane 50% | -104 mMSL |
| 4 | Sigma plane 25% | -150 mMSL |
| 3 | Sigma plane 10% | -179 mMSL |
| 2 | Sigma plane 5% | -188 mMSL |
| 1 | Bed | -197 mMSL |

## 6.2.2.  Boundary conditions

The selection of boundaries conditions is of great importance to the quality of the model outputs, and various configurations were tested as part of the model calibration procedure.  As the hydrodynamics here are driven by local and regional wind- and density-driven flows, as well as tides, the boundary conditions adopted are complex.  The configuration ultimately selected is described here.

**Open sea boundary conditions**

Water level, temperature and salinity are prescribed at the model's open boundaries.

**Water level**

The imposed water level is calculated by combining tidal water levels with variations in mean water levels (which correspond with ocean currents).

The source for tidal levels is the TPXO global tidal dataset (OSU, 2008).  The TPXO dataset is based on a best-fit of tidal levels measured along remote sensing tracks from the TOPEX/POSEIDON satellite project in operation since 2002, to which a harmonic analysis is applied to produce complex amplitudes of earth-relative sea-surface elevation. The TPXO dataset provides eight primary harmonic constituents (M2, S2, N2, K2, K1, O1, P1, Q1), two long period harmonic constituents (Mf, Mm) and three non-linear harmonic constituents (M4, MS4, MN4), on a 1440x721, 1/4 degree global grid resolution.

Each new version of the TPXO dataset increases the quality and the number of harmonic constituents, since it assimilates longer satellite time histories and a finer coverage of the earth surface. These constituents are by definition clean of atmospheric and surge variations, as these variations would not be part of the astronomical periods against which the tidal harmonics are being predicted.  From the TPXO constituent dataset, TELEMAC synthesises tidal water levels at any location (by spatial interpolation), at any time.

The source for time-varying mean water levels is Mercator's Global Ocean Physics Reanalysis.  The data is made available by E.U. Copernicus Marine Service Information and CMEMS.  The product used is GLOBAL_REANALYSIS_PHY_001_030.  This product is a CMEMS global ocean eddy-resolving (1/12° horizontal resolution and 50 vertical levels) reanalysis covering the altimetry era 1993-2018. It is based largely on the current real-time global forecasting CMEMS system.  The model component is the NEMO platform driven at the surface by ECMWF ERA-Interim reanalysis.  Observations are assimilated by means of a reduced-order Kalman filter.  Along track altimeter data (Sea Level Anomaly), satellite Sea Surface Temperature, Sea Ice Concentration and in situ temperature and salinity vertical profiles are jointly assimilated.

A 3D-VAR scheme provides a correction for the slowly-evolving large-scale biases in temperature and salinity.  This product includes daily and monthly mean files of temperature, salinity, currents, sea level, mixed layer depth and ice parameters from the top to the bottom.  The global ocean output files are displayed on a standard regular grid at 1/12° (approximatively 8 km) and on 50 standard levels.  Daily average water levels were extracted at the locations of the TELEMAC model boundary nodes (by spatial interpolation), then interpolated temporally to each model timestep.

For each boundary node of the TELEMAC model, at each model timestep, the TPXO tidal water level and Mercator mean water level were summed and imposed.

**Temperature and salinity**

Temperature and salinity are also extracted from the Mercator Global Ocean Physics Reanalysis.  Temperature and salinity are applied at the TELEMAC model boundary as time-varying, three-dimensional fields (interpolated vertically and horizontally from the Mercator model nodes).  These tracer values were imposed at the boundary when velocities are directed into the model domain.

The TELEMAC model was initialised with 3D fields of temperature and salinity interpolated from the Mercator Global Ocean Physics Reanalysis.  The initial condition is otherwise a flat water level (at MSL), with zero velocities.

**Velocity**

Velocities are not imposed at the model boundary, but freely calculated by the TELEMAC model, subject to a soft boundary condition.

**Atmospheric boundary conditions**

Wind is a local driver for hydrodynamic flow.  Spatially varying winds were applied at the model surface.  The source of wind data is ERA5.  ERA5 is described in Section 4.1.3.  The winds are applied in the TELEMAC-3D model with a drag force formulation described by Wu (1982).

Since density is an important driver for hydrodynamic flow, atmosphere-ocean heat exchange must be considered in the model.  TELEMAC-3D's water quality module, WAQTEL, was coupled to the hydrodynamic module.  Time-varying data was extracted from ERA5: wind velocity, air pressure, air temperature, relative humidity cloud cover, and downward radiation flux.  These were applied in the TELEMAC model to allow calculation of surface heat fluxes.

## 6.3. Model calibration (austral winter)

The period selected for model calibration was the first surveyed period: 45 days from 8th June 00:00 to 23rd June 00:00 2013. One additional day of spin up was included; the model was initialised on 7th June 2013 00:00. The model time zone is UTC.

The calibration process is the tuning of the model schemes, parameters and definitions, to enable the model to most accurate reproduce reality. For this model, "reality" is represented by the observed currents at MP1. The target of the model calibration procedure was to reproduce the observed currents as closely as possible, within computational and time limits of the project. Modelled currents were compared at the five levels shown in the NMP EIA verification study (NMP, 2014c), namely: three levels from the ADCP, representing the mid- and upper water column, and the two AQDs, representing the lower water column.

During the calibration procedure, many aspects of the model were tested. The settings which gave the optimal calibration, within computation time limits, were selected. These aspects tested and selected are listed below.

**Boundary conditions**

■ Two tidal databases were tested at the model boundary: TPXO and FES2014. TPXO is described in Section 6.2.2 above. FES2014 (Lyard et al 2016, Carrere et al 2016) is an alternative global tidal database produced by Noveltis, Legos and CLS (and distributed by Aviso+, with support from Cnes www.aviso.altimetry.fr)". FES2014 was developed based on improvements to FES2004 (Lyard et al, 2006). For the present study, TPXO tidal boundary conditions gave a better model calibration than FES2014.

■ For oceanic boundary conditions, the global HYCOM model was originally applied as time-varying water levels at the boundary. A comparison with an alternative global model – Mercator – gave results closer to the observed currents, thus Mercator was selected instead of HYCOM.

■ The modelled currents were found to be sensitive to the variation of density (defined by temperature and salinity), thus the Mercator chosen and applied in the model.

■ Increased complexity of atmospheric conditions, including spatially-varying winds, and surface heat exchange was introduced by coupling with WAQTEL.

■ The strength of the soft boundary setting was tested and optimised. The water depth was adjusted by $\alpha \, |u_{norm}| \, u_{norm} \, / \, 2g$ (where $\alpha$ is a user-prescribed coefficient, $u_{norm}$ is the component of the velocity normal to the boundary, and $g$ is gravity). This was to stabilise the model and avoid excessive current speeds at the boundary. A value of $\alpha = 0.5$ was adopted.

**Mesh resolution**

■ Different horizontal mesh resolutions and definitions were tested. Resolution ranging from 200 m to 5,000 m as described in Section 6.2 was ultimately used.

■ Different vertical plane placements were tested. The definition in Table 6.1 above was adopted.

**Timestep**

■ The model timestep used was 10 seconds.

**Friction**

■ The Nikuradse scheme for bed friction was used. Different friction coefficients were tested; 0.001 m gave the best calibration.

**Vertical turbulence**

- The mixing length model for vertical turbulence was selected, after also testing the GOTM (General Ocean Turbulence Model) scheme.

- Three mixing length models were tested: Nezu & Nakagawa, Quetin, and Tsanis.  Tsanis (1989) was selected.

- Damping functions defined by Munk & Anderson and Viollet were tested.  A modified Munk & Anderson function (with an increased sensitivity to the Richardson number) was selected.

From the optimised (calibrated) model output, time histories of currents through the water column were extracted.  They are compared against the observed currents in the following figures. Figure 6.4 compares the modelled currents with observations from the ADCP in the upper water column, near the surface, and at around 50m water depth.  Figure 6.5 compares the modelled currents with observations from the ADCP at mid-depth (~100m water depth), and AQD1 in the lower water column (~150m water depth).  Figure 6.6 shows the near-bed currents from the model and AQD2.  The exact elevations of the model plane and observations are given in each plot.

In each figure, model results on the plane closest to the depth of the observations are shown.  The model result is shown in red, and the observations are shown in blue.  Current speeds are plotted against the left axis.  Current directions (°N towards which the current flows) are plotted against the right axis.

Wind speeds and directions during the model run (at the location of MP1) are shown in Figure 6.7.  Wind speeds are plotted against the left axis.  Wind directions (°N from which the wind blows) are plotted against the right axis.

Figure 6.4, Figure 6.5 and Figure 6.6 show that the model is in broad agreement with many of the features of the observed currents.  The magnitude of the velocities is of the same order in the model and observations.  Periods of faster flow for periods of a few days centred on 15th-16th June and 20th-21st July (corresponding with the fastest wind speeds during the period) are seen in model and observations.  The magnitude of near-bed modelled currents (Figure 6.6) is generally lower than the observations, although there is doubt about the quality of the observed data from AQD2 (as discussed in Section 4.2.1 above).

The directions of the observed currents have a varied pattern during the campaign: during some periods the direction is sustained over several days; at other times the current direction shows tidal rotation.  The current flows in different directions through the water column.  This complex pattern of flow direction has been captured by the model, which shows the observed temporal differences and vertical shear.

A snapshot of velocity vectors is shown in Figure 6.8.  The snapshot is extracted from the model at 16th June 00:00. The red vectors show the modelled current field at 5 m below the surface; the black vectors show the modelled currents at 5m above the bed.  The vectors have been gridded with 1,000 m spacing for clarity.  The blue shaded background shows the model bathymetry, and a white square shows the location of MP1.  At this time, the flow field is directed generally northward, with near-surface currents towards NNW, and near-bed currents towards NNE.

A second snapshot is extracted from the model at 2nd July 2013 00:00, and is shown in Figure 6.9.  At this time, the 3D current field is markedly different to Figure 6.8.  The near-surface flow is directed offshore, while near-bed flow shows a complex pattern with a significant southward component.  (Note that the velocity scale has been increased in Figure 6.9 compared to Figure 6.8, for visibility).  Different directions are seen for modelled near-surface and near-bed flows.

The hydrodynamic model is considered calibrated sufficiently for the purposes of supporting the plume model. The same set up can now be used to model other periods, by forcing the model with initial conditions and boundary conditions from other periods. The next period modelled is described in Section 6.4.
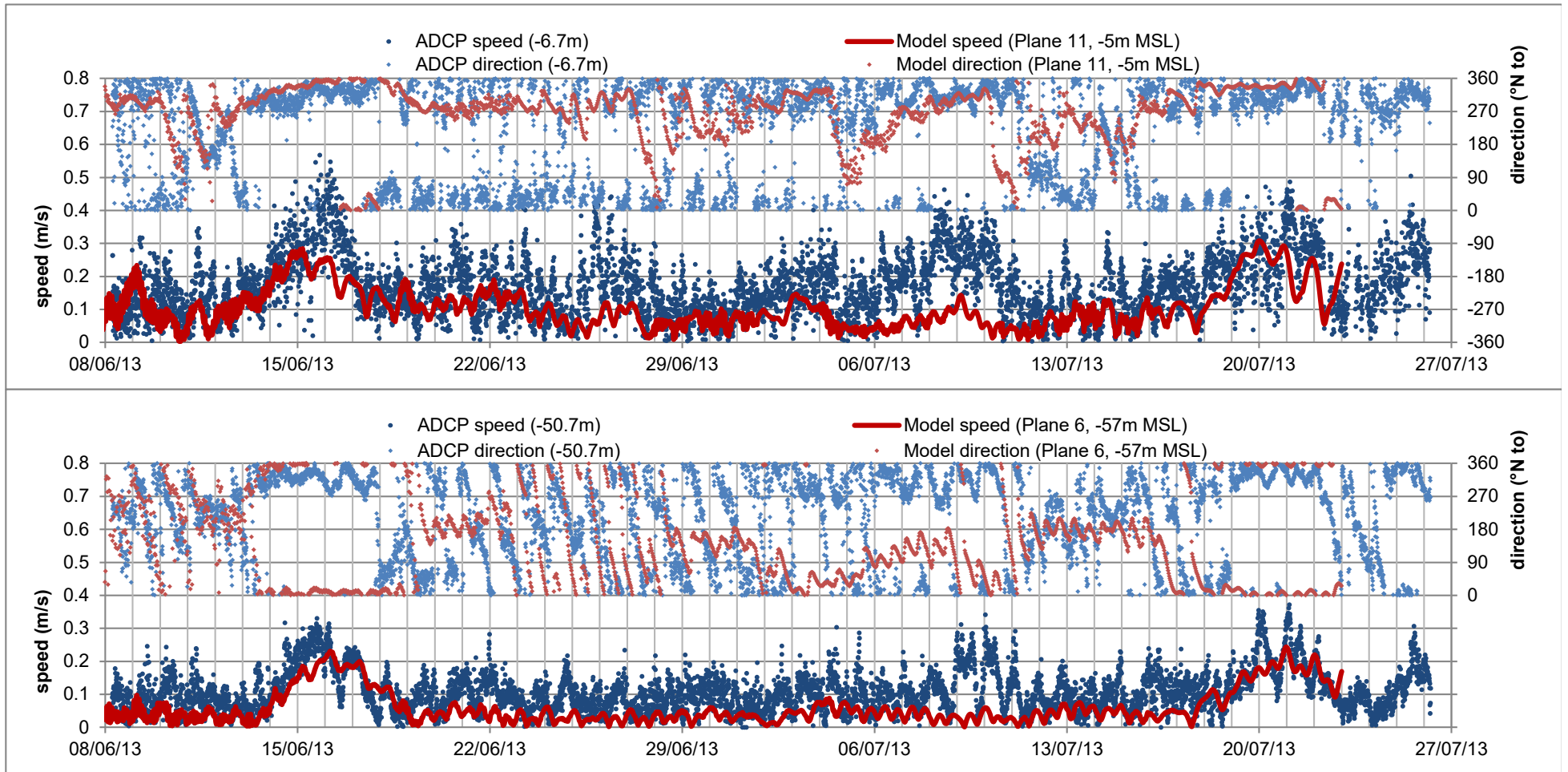
Figure 6.4: Calibration period observed (ADCP) and modelled currents at MP1 location: upper water column

Figure 6.5: Calibration period observed (ADCP and AQD1) and modelled currents at MP1 location: mid-lower water column

Figure 6.6: Calibration period observed (AQD2) and modelled currents at MP1 location: near-bed
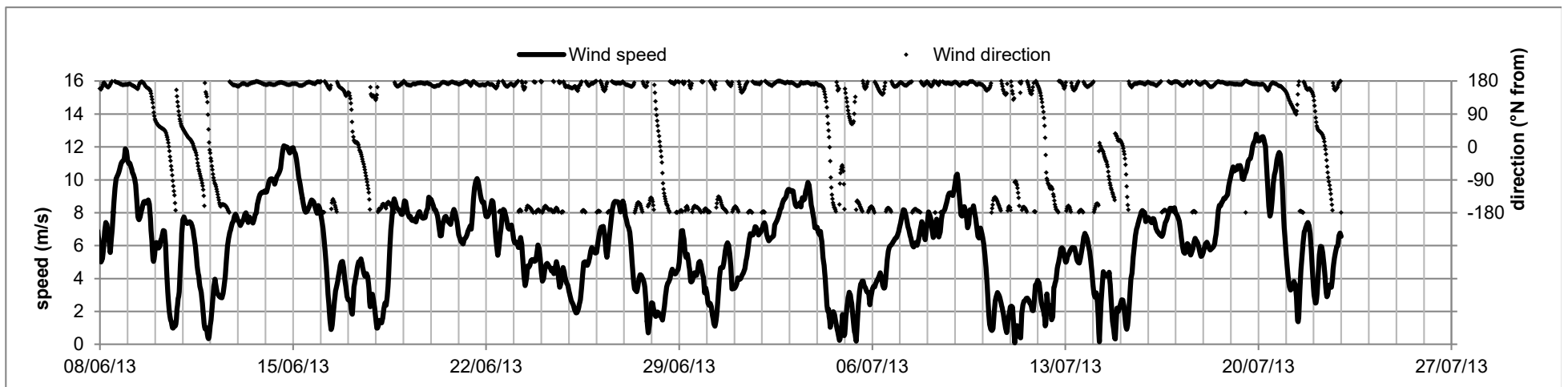


Figure 6.7: Wind speed and direction at MP1 during calibration period

*Source:     ERA5: Copernicus Climate Change Service information (2019)*
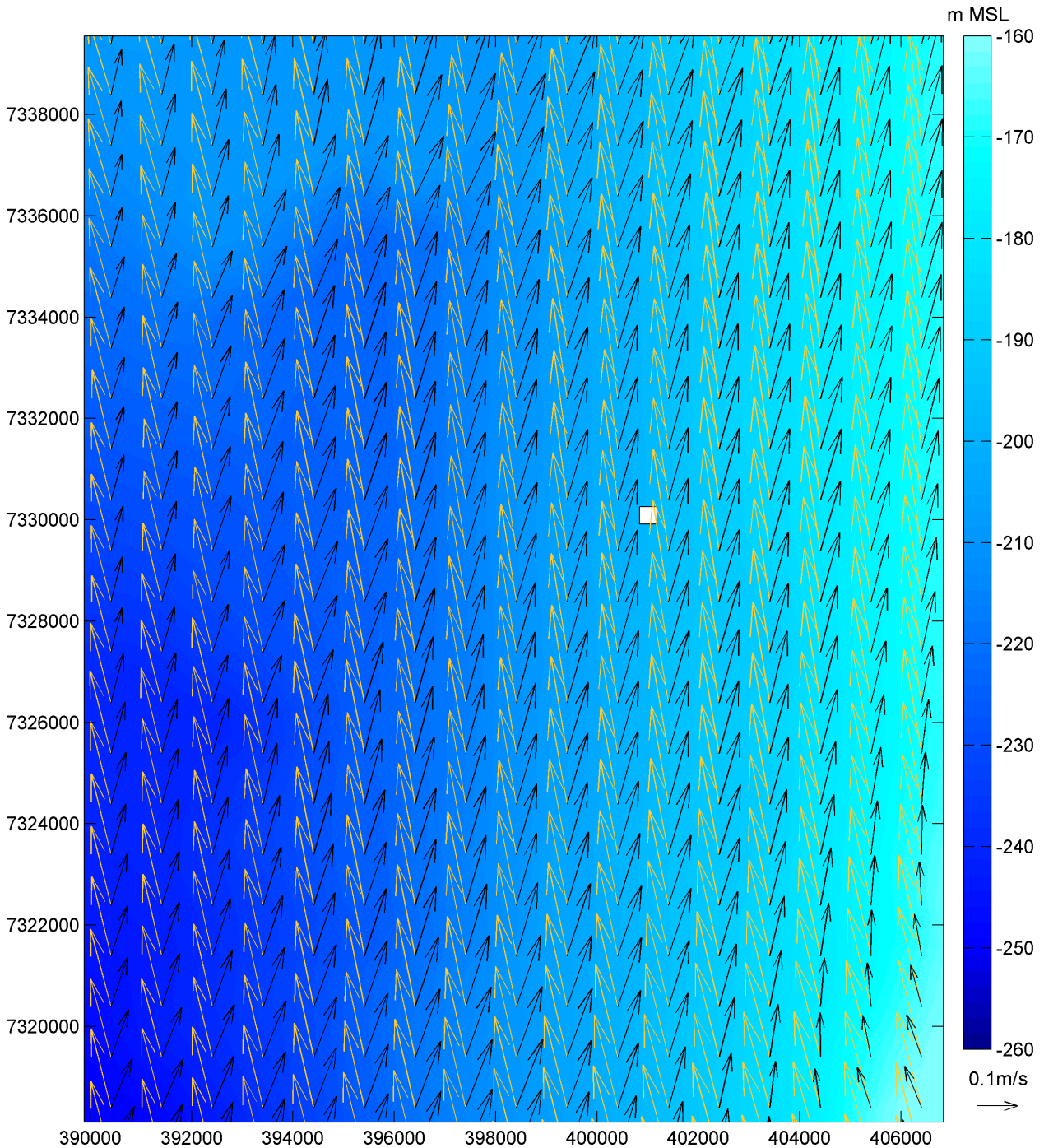
**Figure 6.8: TELEMAC-3D flow field at 16th June 2013 00:00**

*Velocity vectors at 5m below surface (gold) and 5m above bed (black)*
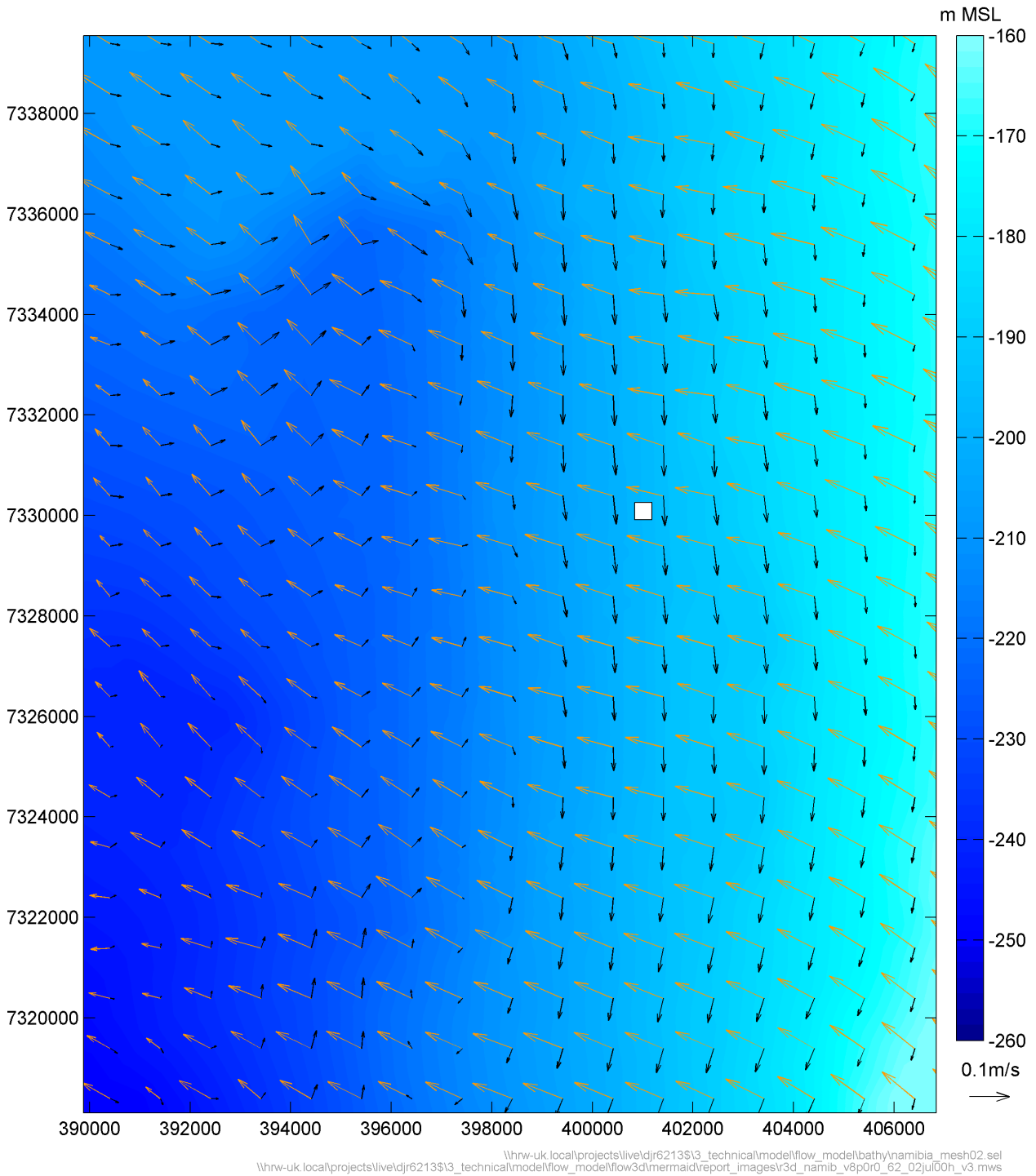
Figure 6.9: TELEMAC-3D flow field at 2nd July 2013 00:00

*Velocity vectors at 5m below surface (gold) and 5m above bed (black)*

## 6.4. Model validation (austral winter)

Observations of current were available at the same location, MP1, for a second period.  The calibrated model was run for this second period to confirm that it satisfactorily reproduces reality.  The validation run is from 1st August 2013 00:00 (including one day spin-up), for 44 days, until 14th September 2013 00:00.  Initial conditions and boundary conditions were extracted/generated from TPXO, Mercator and ERA5 for this period.  The model set up is otherwise the same as the calibrated model.

The modelled currents at MP1 location are compared against the observations by ADCP, AQD1 and AQD2. Figure 6.10 compares the modelled currents with observations from the ADCP in the upper water column, near the surface, and at around 50m water depth.  Figure 6.11 compares the modelled currents with observations from the ADCP at mid-depth (~100m water depth), and AQD1 in the lower water column (~150m water depth).  Figure 6.12 shows the near-bed currents from the model and AQD2.  The exact elevations of the model plane and observations are given in each plot.

For the AQD2 observations in Figure 6.12, the figure uses a reproduction of Figure 27 from NMP (2014b) corrected based on two-beam analysis.  That figure is aligned and overlaid with the model result.  Wind speeds and direction during the model run (at the location of MP1) are shown in Figure 6.13.

Similar to the observations (Figure 4.19), the model predicts a clear thermocline occurring around 20-30 m below surface (not shown), with a near linear variation with depth below 50 m water depth.

The model broadly captures the range of conditions observed sufficiently for the purposes of supporting the plume model.  The observed and modelled current magnitudes are of the same order.  The temporal variation and vertical shear (flow in different directions through the water column) of observed currents are captured in the model.
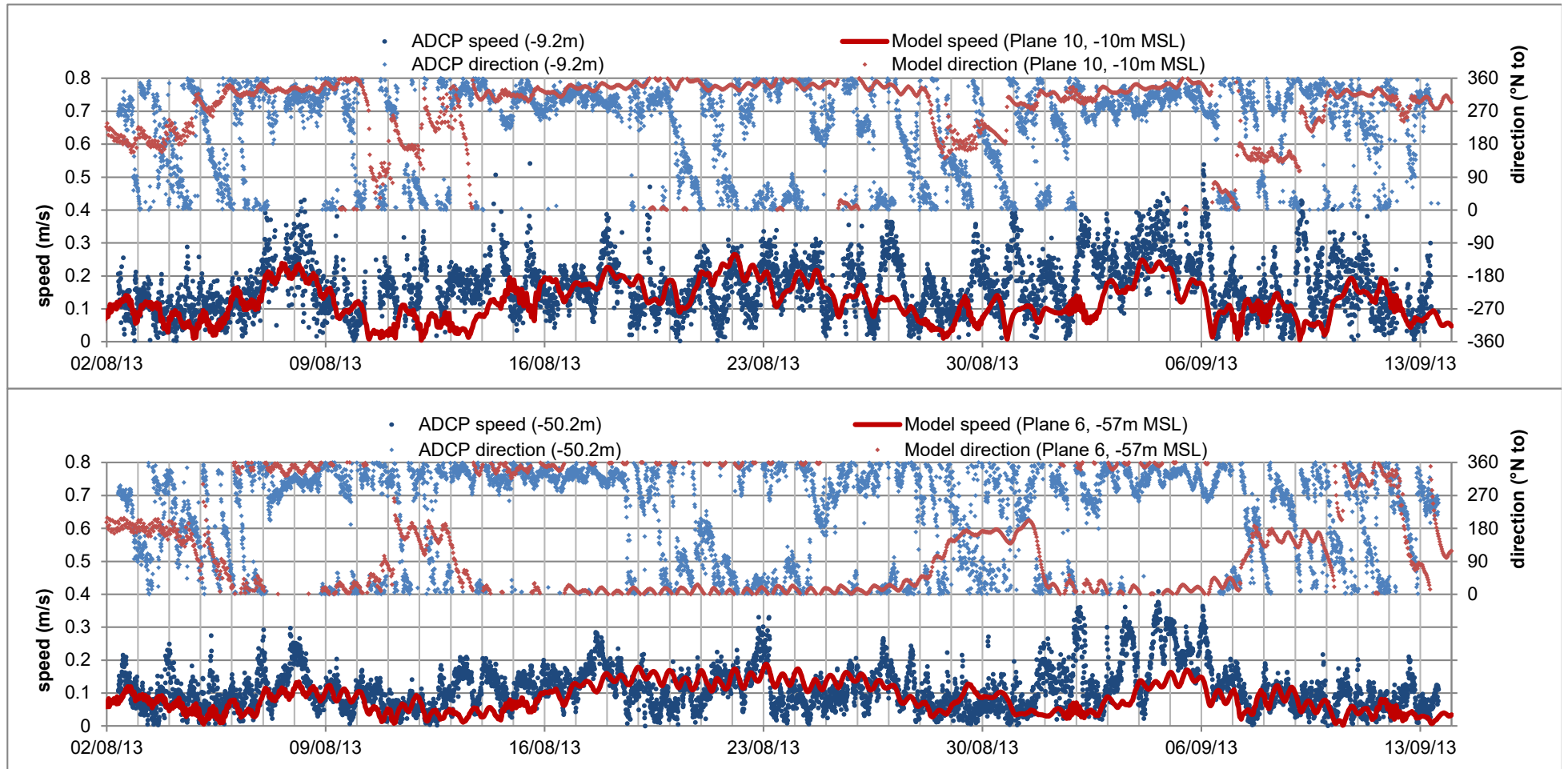
Figure 6.10: Validation period observed (ADCP) and modelled currents at MP1 location: upper water column

HR Wallingford
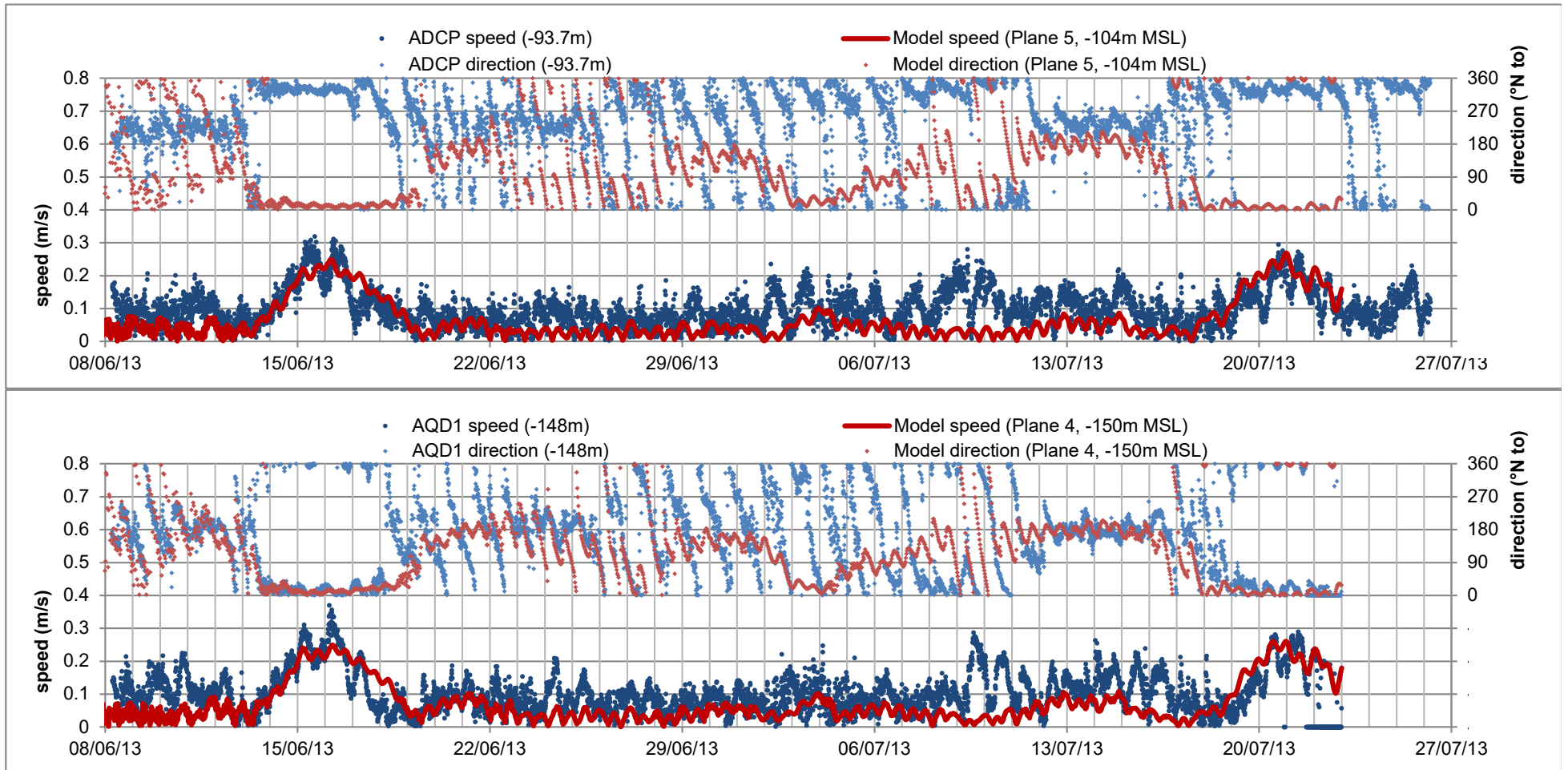*Working with water*
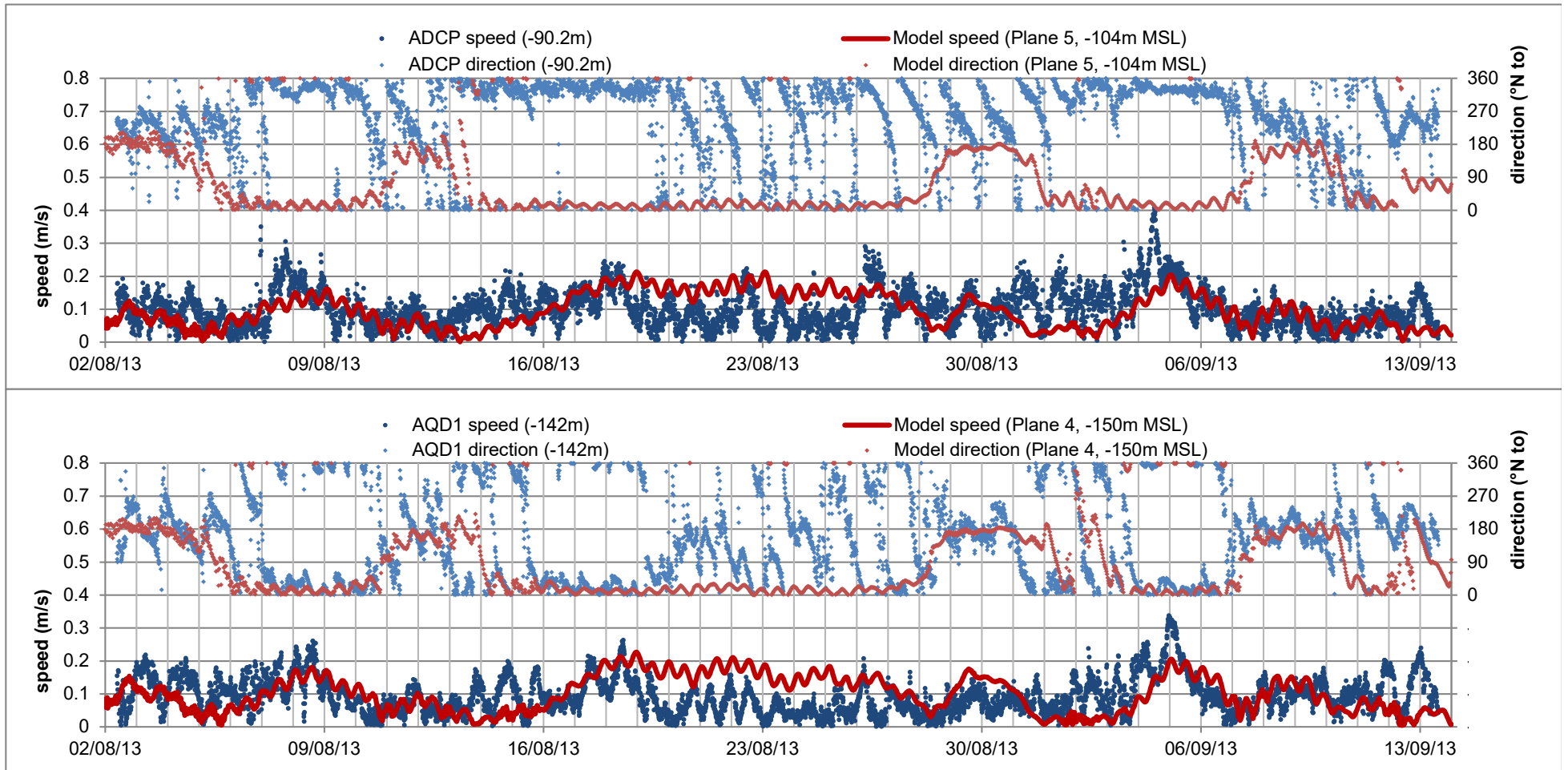


Figure 6.11: Validation period observed (ADCP and AQD1) and modelled currents at MP1 location: mid-lower water column
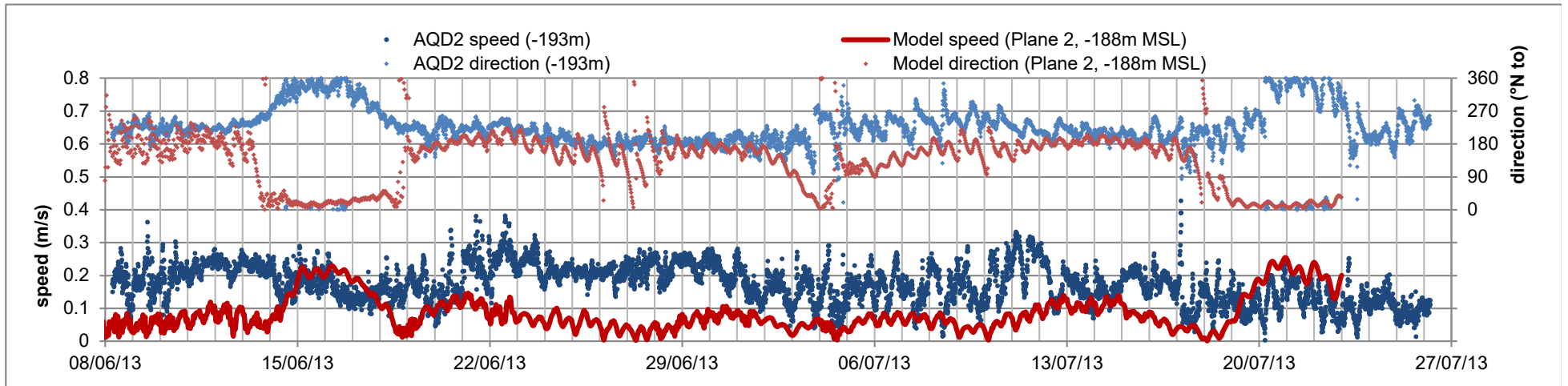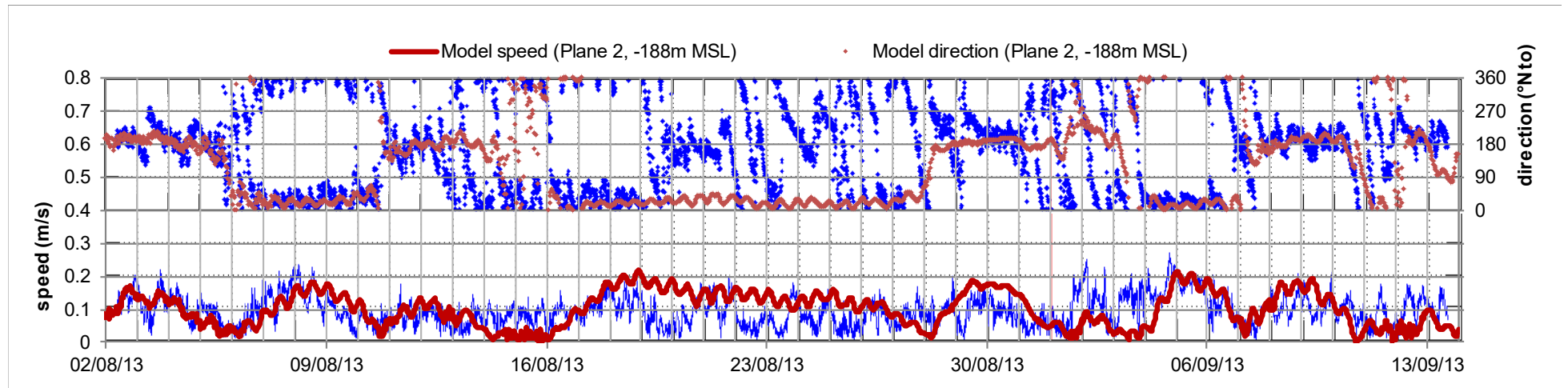
Figure 6.12: Validation period observed (AQD2) and modelled currents at MP1 location: near-bed

*Source:  AQD2 data shown in this figure (in blue) is reproduced from NMP (2014b) (Figure 27 p244/530), observations made at -188m depth, and corrected based on two-beam analysis.  The figure is aligned and overlaid with the model result.*



Figure 6.13: Wind speed and direction at MP1 during validation period

*Source:  ERA5: Copernicus Climate Change Service information (2019)*

## 6.5.  Austral summer period

An austral summer period model run was also modelled for the purposes of this report.  Summer 2013 was selected.  On inspection of water temperatures in the Mercator model, the warmest month was March, hence this month was selected for the model run.  Including a one-day spin up, the model run started 28th February 2013 00:00 and ran for 32 days until 1st April 2013 00:00.

Model results are presented as the same time series output as the austral winter runs above, although there are no observations to compare the model against.  Figure 6.14 shows the modelled currents in the upper water column.  Figure 6.15 shows modelled currents at mid-depth and in the lower water column. Figure 6.16 shows the near-bed currents from the model.  Near bed currents are shown to flow southwards throughout the duration of the model run.

Wind speeds and direction during the model run (at the location of MP1) are shown in Figure 6.17.

For the summer conditions the model predicts a more prominent thermocline (than for winter conditions) owing to the sun's warming effect at the sea surface (not shown).  The model predicts a 2 °C reduction in temperature over the 50 m water depth at the surface.

Figure 6.14: Austral summer period modelled currents at MP1 location: upper water column

Figure 6.15: Austral summer period modelled currents at MP1 location: mid-lower water column

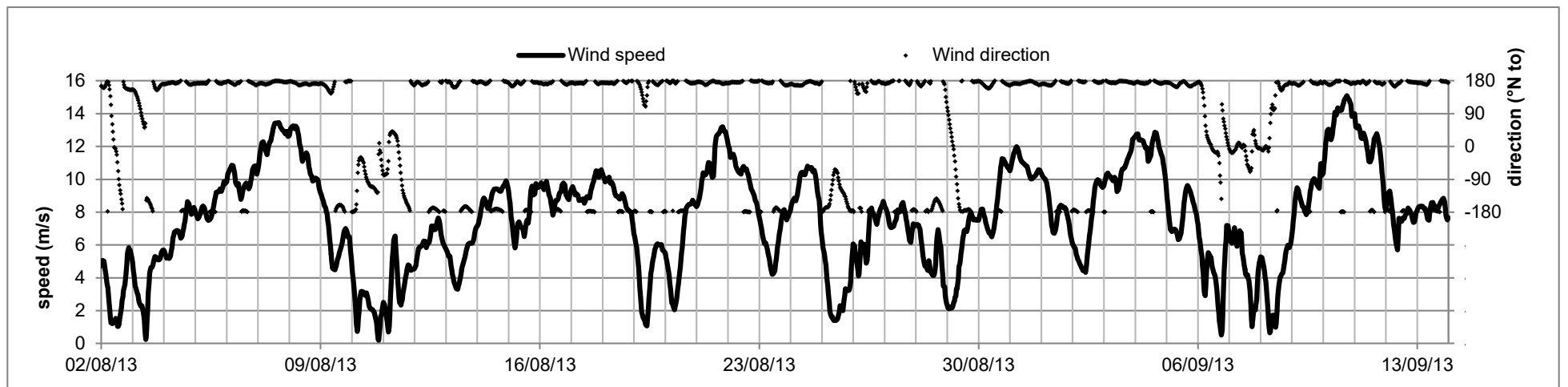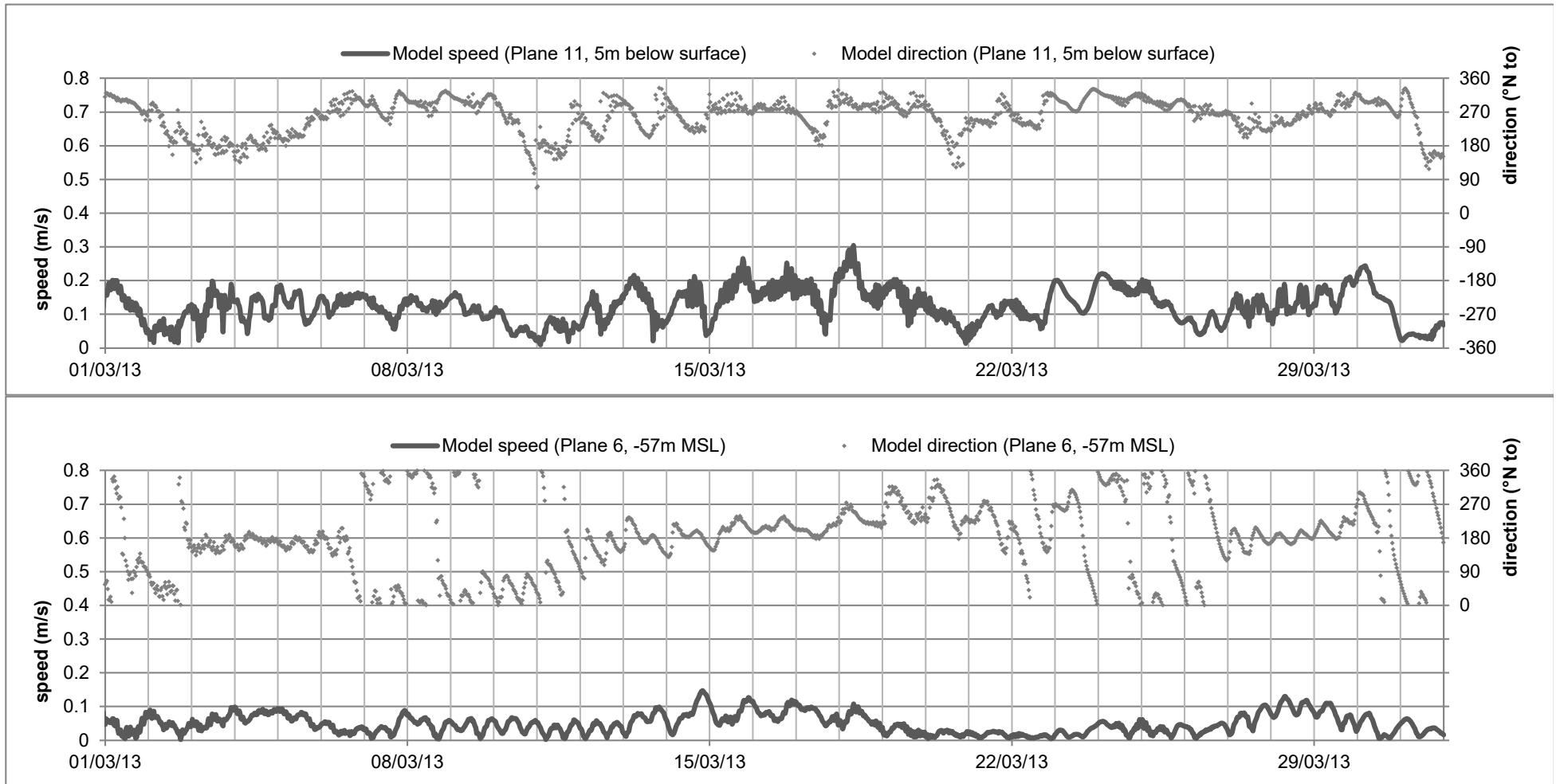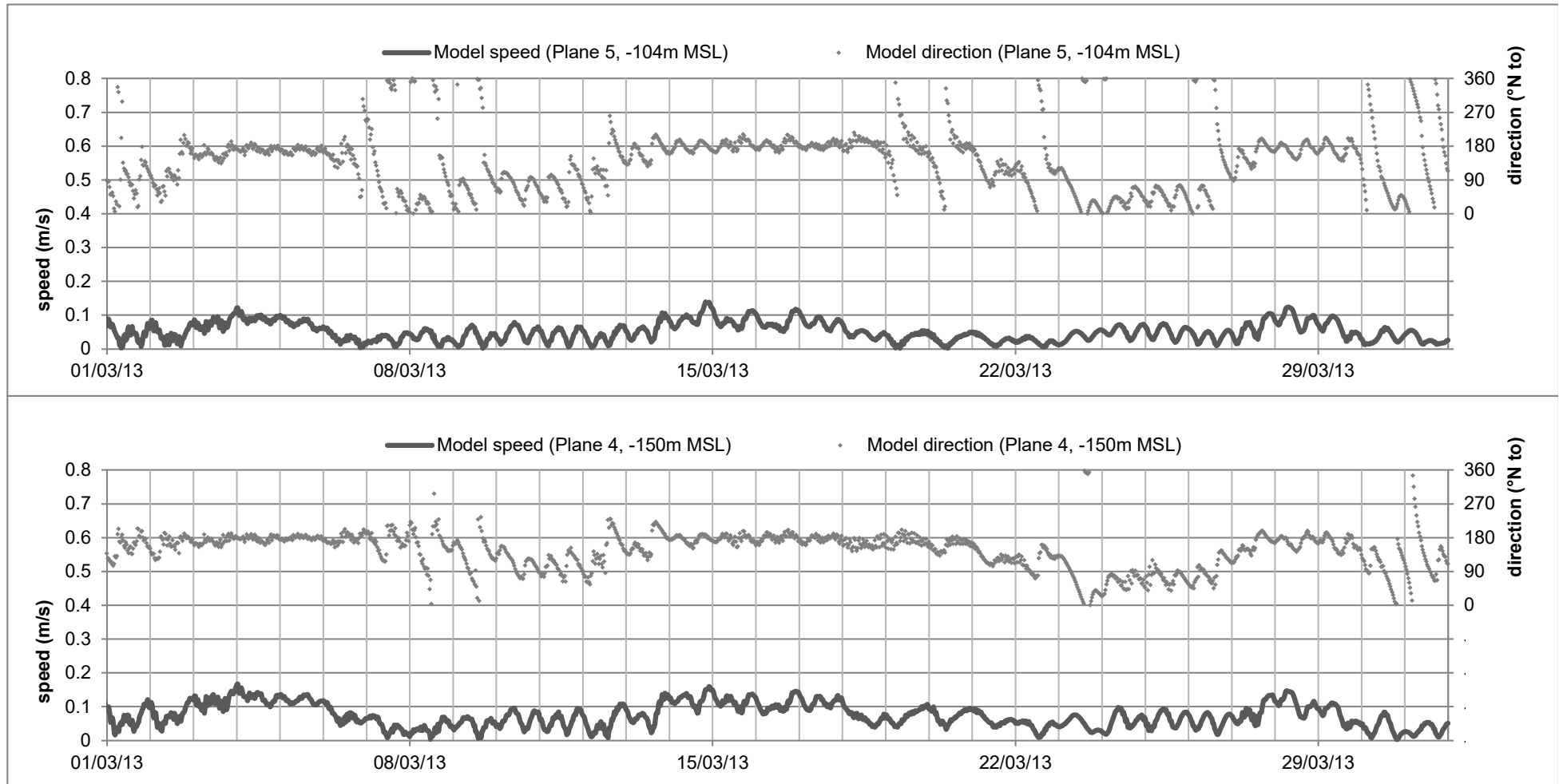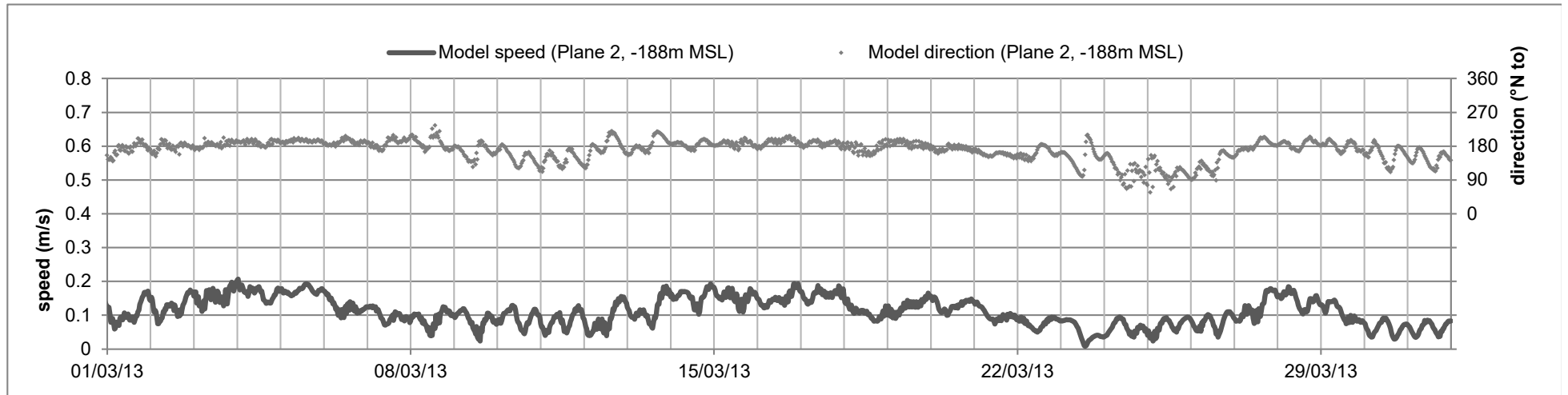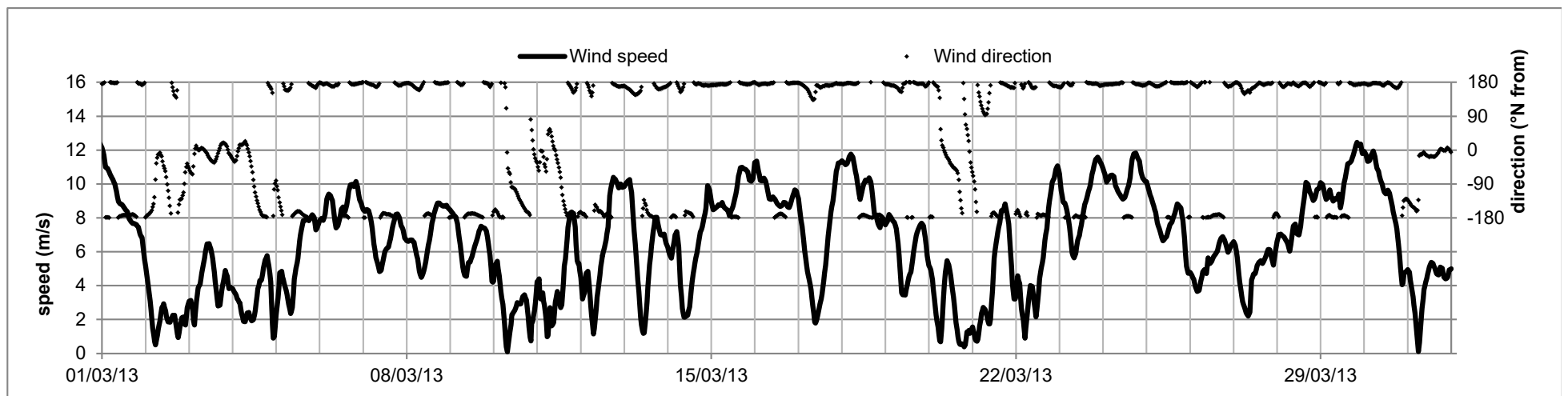Figure 6.16: Austral summer period modelled currents at MP1 location: near-bed



Figure 6.17: Wind speed and direction at MP1 during austral summer period

*Source: ERA5: Copernicus Climate Change Service information (2019)*

## 6.6. Representativeness of periods modelled

The periods selected for sediment modelling are June 2013 (for austral winter) and March 2013 (for austral summer). Given their intended use for understanding long-term plume dispersion, it is important to be satisfied that these periods are representative of the flow conditions.

To address how representative these periods are, ten years of modelled currents have been downloaded from Mercator's Global Ocean Physics Reanalysis GLOBAL_REANALYSIS_PHY_001_030. Time series have been extracted at the Mercator model node at 14°E 24.2°S – the closest Mercator node to MP1. Daily average current speed and direction, over the 10 years between 2008 and 2017 (inclusive) are plotted here. Figure 6.18 shows Mercator currents at 5m below the surface, Figure 6.19 shows Mercator currents at 109m below the surface. Speeds (in m/s) are plotted as coloured lines (one colour per year) against the left vertical axis. Directions (°N towards which the current flows) are plotted at coloured dots (one colour per year) against the right vertical axis. These long term current time histories represent the main seasonal cycles and variability in the ocean at this location.

Mercator currents at 5m below the surface (Figure 6.18) show considerable variability through each year shown. The current directions reveal a seasonal pattern, with a dominance of flow toward NW to N for much of the year. As austral winter progresses, this dominant direction becomes more eastward until March/April. Modelled current speeds are generally less than 0.3m/s, with several events with stronger flow spanning a few days duration (as seen in the observations, for example 15th-16th June 2013 and 20th-21st July 2013).

Mercator currents at 109m below the surface (Figure 6.19) show some different features. The preferred directions of flow at this mid-depth elevation are either towards the south or towards the north. Some seasonal variation in direction is apparent: during austral winter months June-October there are more occurrences of northward flow; during austral summer January-March, southward flow is more common. Current speeds (which are daily averages) are again always less than 0.3m/s, with periods of faster flow which last for a few days at a time.

It is thus inferred that March is a representative month for austral summer flows, and June is a representative month for austral winter flows.

The year modelled, 2013, is plotted in dark green in Figure 6.18 and Figure 6.19, and highlighted using a thicker line for speed, and larger symbol for direction. 2013 is seen to be a typical year, in keeping with the general seasonal variability described above.

A Benguela Niño event is known to have occurred between November 2010 and April 2011 with sea surface temperature off the coast of Angola and Namibia several degrees warmer than seasonally normal (Rouault et al., 2018). There is little evidence for impact of this event on Mercator currents in Figure 6.18 or Figure 6.19. Analysis of Mercator temperatures would be required to determine whether the Benguela Niño event was successfully simulated in the Mercator model, and further study could assess its impact on the current field in the area of interest.
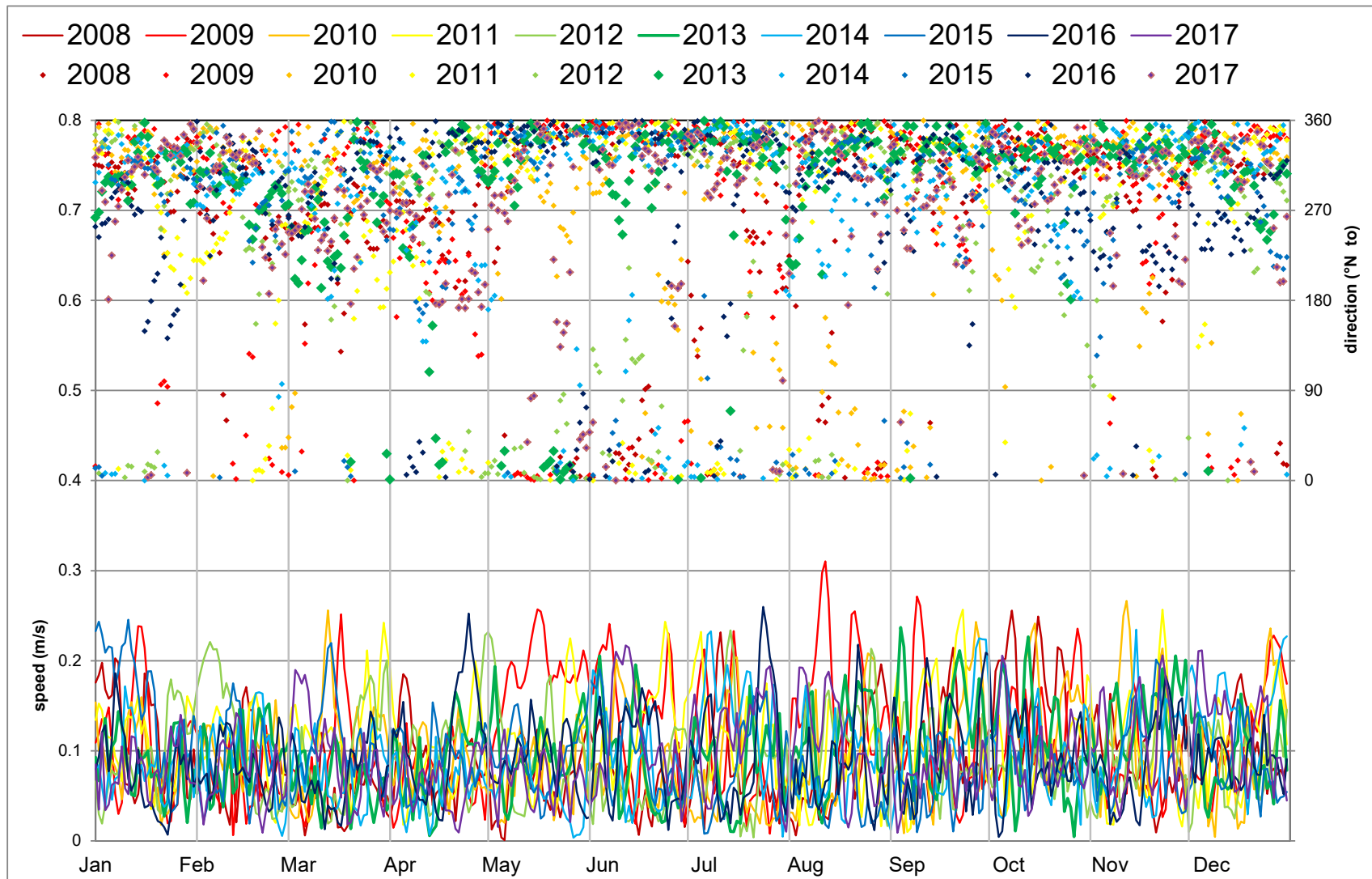
Figure 6.18: Ten years of Mercator model currents at 5 m below the surface at 14°E 24.2°S

*Source:    Mercator GLOBAL_REANALYSIS_PHY_001_030*
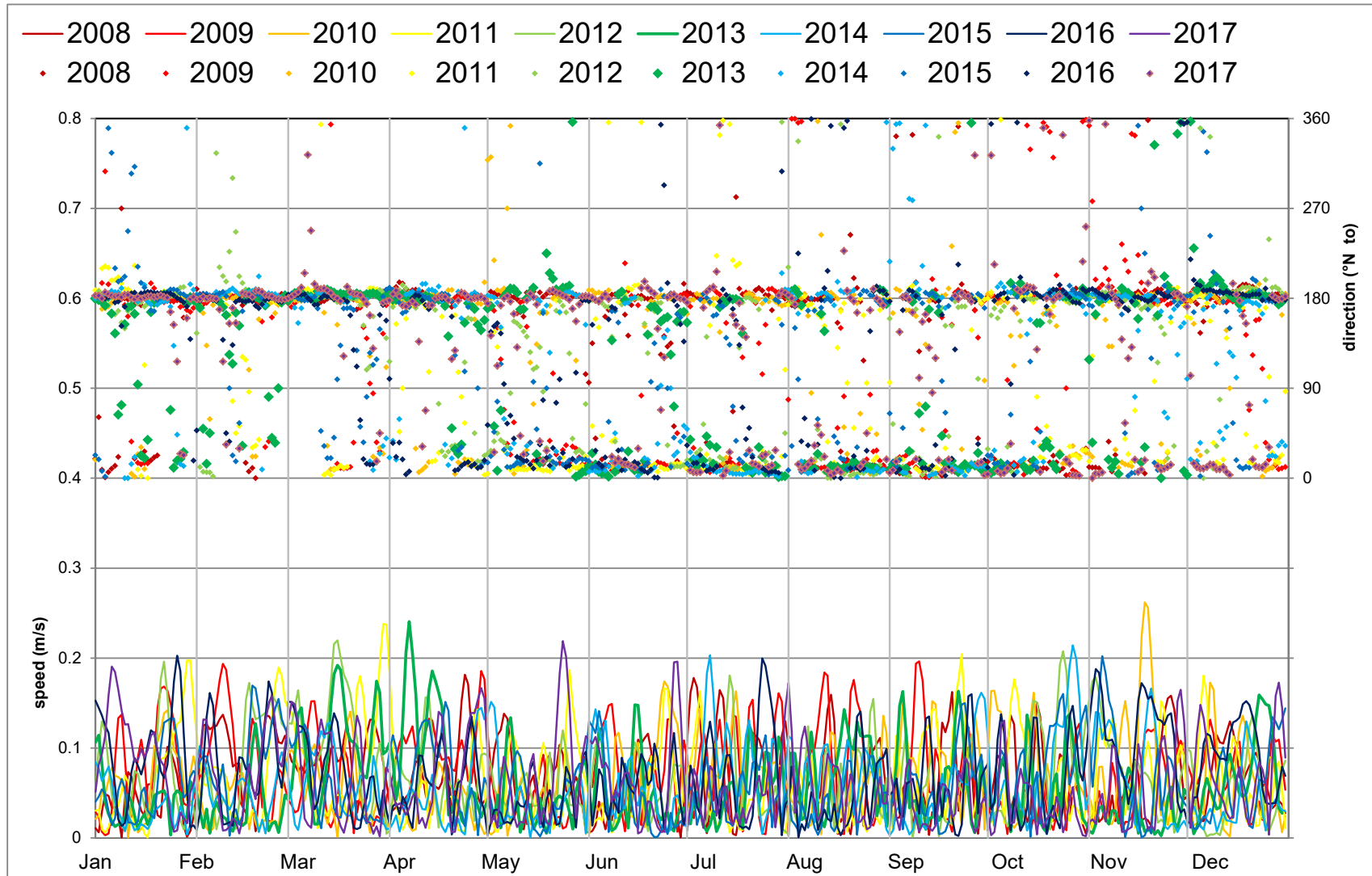
Figure 6.19: Ten years of Mercator model currents at 109 m below the surface at 14°E 24.2°S

*Source:    Mercator GLOBAL_REANALYSIS_PHY_001_030*

# 7. Estimation of the rates of release of sediment from the dredging activities into the surrounding waters

## 7.1. Overflow sediment source term calculations

The following overflow sediment source term calculations are based on the information provided by JDN. These are used in the sediment plume modelling.  The calculation assumes that <u>all</u> the fine sediment entering the dredger hopper will be expelled as overflow.  In practice some fine sediment will be trapped within the pore spaces of the coarser sand-sized particles of the resource, and some additional fine sediment will settle, reducing the discharge of fine sediment in the overflow.  This conservative approach allows the modelling to be representative of different operational strategies by the dredging contractor, as different strategies will result in different amounts of fine sediment retained in/discharged from the hopper.

**Dredged slurry velocity calculation**

■ JDN input data:

- Slurry flow rate = 6.65 $m^3$/s
- Slurry density = 1.15 $t/m^3$
- Number of suction pipes = 1 no
- Suction pipe diameter = 1,300 mm = 1.3 m.

■ Calculation output:

- Dredged slurry velocity = 6.65 / (1 * ¼ * $\pi$ *$1.3^2$ ) = 5.0 m/s.

**Total dredged slurry pumped for full hopper load**

■ JDN input data:

- Slurry flow rate = 6.65 $m^3$/second
- Slurry in suction pipe:
  – Volume = 7 $m^3$ (i.e. equivalent volume when 1 $m^3$ of in-situ bed material at bulk density 1.9 $t/m^3$ is slurrified to a bulk density of 1.15 $t/m^3$)
  – Mass <90 $\mu$m = 0.28 t / m³ situ
  – Mass >90 $\mu$m = 1.08 t /m³ situ
  – Hopper loading duration (including turning) = 798 minutes (see Table 2.3) = 47,879 s

■ Calculation output:

- Slurry solids content = (0.28 + 1.08) / 7 = 0.194 tds/$m^3$
- Hopper loading rate dry solids = 0.194 * 6.65 = 1.292 tds/s
- Total dredged slurry pumped for full hopper load = 1.292 * 47,879 = 61,860 tds.

**Solids mass in fully loaded hopper**

■ JDN input data:

- Net hopper load (i.e. full load, not including rest load) = 54,285 tds.

**Overflow sediment source term**

■ Input data from above calculations:

- Total dredged slurry pumped for full hopper load = 61,860 tds
- Net hopper load (i.e. full load, not including rest load) = 54,285 tds
- Number of dredging cycles per week = 2.87 (see Section 2.5).

- Calculation output:
  - Solids discharged through hopper overflow = 61,860 – 54,285 = 7,575 tds
  - Overflow duration whilst loading the hopper with dredged material = 684 minutes
  - Overflow sediment source term = (7,575 * 1,000) / (684 * 60) = 185 kg/s
  - Cycle time = 58.5 hours (including maintenance and downtime).

A broad estimate of the amount of fine sediment likely to be retained in the hopper is provided by assuming a porosity of 40 % in the settled coarser material in the hopper and assuming that the fine sediment concentration within these pores is equal to the incoming fine sediment concentration. This gives a mass of trapped fine sediment within the hopper as 37,750 m$^3$ x 40 kg/m$^3$ x 40 % (where 40 kg/m$^3$ is the fine sediment concentration entering the hopper). Averaged over the 684 minutes of overflow discharge, this equates to a reduction in the average fine sediment discharge rate from 185 kg/s to 170 kg/s. However, the value of 185 kg/s has been used for the plume dispersion modelling.

## 7.2. Summary of predicted releases from the dredging activity

The below overflow sediment source term has been calculated based on the information provided by JDN and the assumptions stated in Section 2.4. The specific information used and full step-by-step calculations are provided in Section 7.1.

- Average time of dredging cycle (including maintenance and downtime) = 58.5 hours.
- Initial loading period without overflowing (including a turn) = 142 minutes.
- Overflow duration whilst loading the hopper with dredged material (not including turning) = 684 minutes.
- During the period of overflowing there are an additional 10 turns of 28 minutes when overflow ceases.
- **Average overflow sediment source term during loading = 185 kg/s.**

# 8. Plume dispersion modelling

## 8.1. The SEDPLUME-RW plume dispersion model

Modelling of the plume was reproduced using the SEDPLUME-RW 3D lagrangian dispersion model (Mead. 2004). The SEDPLUME-RW models has been used on more than 100 plume studies world-wide which incorporates a near-field integral plume model (Spearman et al., 2003, 2007) based on the formulation by Lee and Cheung (1990) to reproduce the rapid initial mixing caused by the plume jet following release. In the far-field phase turbulent mixing is reproduced through randomly moving particles by small amounts based on the eddy diffusivity, although the main mixing effect is the large-scale shear dispersion caused by spatial gradients in current speed (Fischer et al., 1979). Details of the SEDPLUME-RW model are provided in Appendix A.

The SEDPLUME-RW model used the TELEMAC-3D predictions of current and turbulent mixing to advect the and disperse the plume, predicting mean concentration increases over the layers that fall between the TELEMAC-3D model planes (see Table 6.1) giving 12 layers in all.

The sediment plume simulations were run on a 66 km by 32 km domain with 200 m resolution and a 30 second time step using approximately 11.8 million particles. The near-field sub-model was run with a 0.01 second time step and was used to calculate the mixing over the first 100 seconds of plume release on each time-step of the far-field model.

It is important to note that all predictions in this study of the extent of suspended sediment and deposition, represent increases above background levels. These background conditions are described in Section 4.3.

## 8.2. Scenarios modelled by the plume dispersion model

In all 10 dredging scenarios were modelled using the SEDPLUME-RW dispersion model.

The first 8 of these scenarios consisted of a single dredger, dredging in each corner of the SP-1 (20 year) mining area (see Figure 8.1), for Austral Winter (June/July) and Austral Summer (March) conditions. The purpose of these scenarios is to establish the suspended sediment footprint (and the nature of changes in suspended sediment concentrations within this footprint) and hence (when combined with the deposition footprint), the Zone of Influence of the plume.

The suspended sediment footprint is defined as the area within which there are predicted increases above background of more than 7.6 mg/l at any time over the predicted dredging operations or where there are mean concentration increases above background of more than 1 mg/l. In practice, however, the results of this study indicate that the area over which there are peak concentration exceedances above background of more than 7.6 mg/l is larger than the area over which mean concentration increases exceed 1 mg/l and so it is the peak concentration increases which define the suspended sediment footprint. Within this footprint there are physical changes to suspended sediment concentration above the levels which could immediately be associated with negligible impact. Whether such changes could potentially cause significant adverse impact will depend on the precise magnitude of the changes and the nature and distribution of the ecological receptors present in the suspended sediment footprint area. Outside of this suspended sediment footprint the predicted changes in suspended sediment concentration will cause negligible impact.

For these runs the simulated dredging consisted of 19 cycles for the Austral Winter (June/ July) simulations and 13 cycles for the Austral Summer (March) run which was shorter.
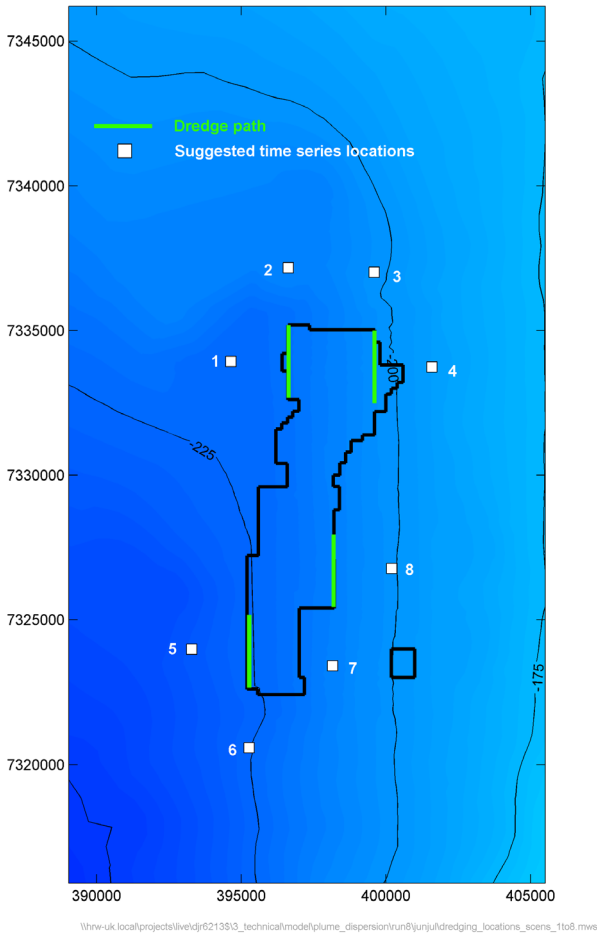
Figure 8.1: Location of dredging for Scenarios 1-8     Figure 8.2: Location of dredging for Scenarios 9 &10
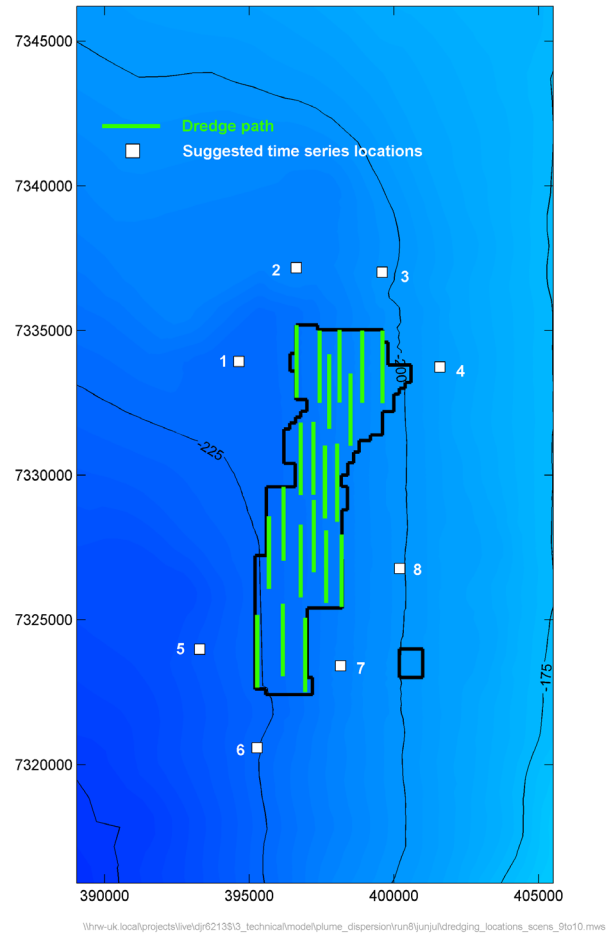
The remaining two scenarios (9 and 10) are designed to give a representative estimate of the distribution of fine sediment over the course of the 20 year mining period. For these runs the dredging is distributed evenly over the 20 year mining plan area. The distribution is slightly different for the Austral Winter (June / July) and Austral Summer (March) runs because the SEDTRAIL-RW run was shorter for the austral summer run (Figure 8.2).

## 8.3. Predicted near field mixing of the various plume releases

The dynamic plume model predicts that over a period of 100 seconds the major part (estimated to be 85 %) of the sediment discharged as overflow will descend in the form of a dynamic plume to a (centroid) depth of 30-40 m depending on the strength of the ambient currents. Over this period the plume mixes over a depth of around 30 m, resulting in sediment concentrations of 300-400 mg/l.

As discussed in Section 3.2.1 the presence of bubbles in the overflow discharge increases the buoyancy of the discharge which causes part of the overflow discharge (estimated to be 15 %) to create a surface plume. This surface plume is assumed to be distributed over the top 20 m of the water column.

These two source terms are illustrated in Figure 8.3.
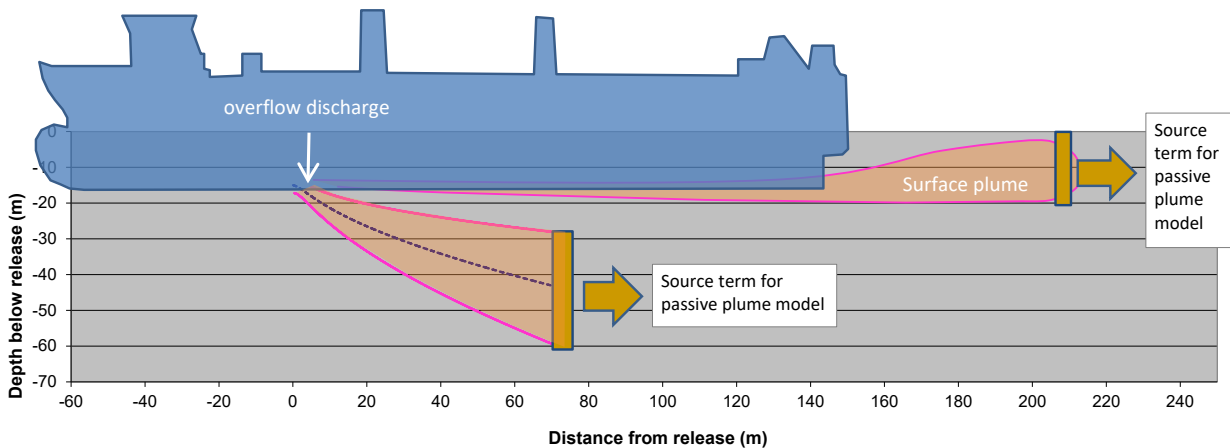


Figure 8.3: Summary of the source terms used for the plume simulations

The extent of the surface plume can be mitigated through use of the Environmental Valve. The valve removes (the vast majority) of air bubbles from the overflow discharge and this results in a larger proportion of the overflow discharge forming part of the dynamic plume. The modelling in this report shows that because the dynamic plume represents the vast majority of the overflow discharge and spreads over much of the surface 50 m water depth, the effect of the environmental valve does not in any significant manner change the results of the modelling as summarised in this report. This matter is further discussed in Section 10.

## 8.4. Sediment parameters used by the far-field plume dispersion model

The sediment parameters used in the SEDPLUME-RW model are shown in Table 8.1.

Table 8.1: Sediment parameter settings

| Parameter | Value |
|---|---|
| Critical shear stress for deposition | 0.1 N/m$^2$ |
| Critical shear stress for erosion | 0.2 N/m$^2$ |
| Erosion constant $M_e$ $[\frac{\delta m}{\delta t} = M_e(\tau_e - \tau)]$ | 0.002 kg N$^{-1}$m$^{-2}$s$^{-1}$ |
| Settling velocity of fine sediment | 1 mm/s |
| Dry sediment density of deposited fine sediment | 500 kg/m$^3$ |

# 9. Sediment plume modelling results

## 9.1. Introduction

The results of the modelling are summarised on this section but the results for all of the simulations are shown in Appendix B and C. In all cases, the predictions of the extent of suspended sediment and deposition, represent increases above background levels.

**The results in this section and in Appendix B are presented in the following forms:**

■ **Contour plots of maximum (peak) predicted increase in depth-averaged suspended sediment concentration above background.** The suspended sediment concentrations over the top 40-50 m, mid-depth 90-110 m and bottom 40-50 m of the water column have been averaged over these depths to produce "top", "mid-depth" and "bottom" concentrations. These maximum concentration plots show the maximum values of top, mid-depth and bottom concentrations at each point in the model at any time, so are not indicative of the concentration distributions at any specific instant. The actual sediment plume at any instant covers a smaller area than these envelopes imply.

All peak concentration plots are plotted with the lowest concentrations above background shown being 7.6 mg/l in accordance with the work of Smit et al (2008) on acute (a few days or less) impacts (See Section 3.2.4 and Lwandle, 2020).

■ **Contour plots of mean predicted increase in depth-averaged suspended sediment concentration above background.** These mean plots of depth-averaged suspended sediment concentration (averaged over the top 40-50 m, mid-depth 90-110 m and bottom 40-50 m of the water column) take into account the duration of increases in concentration as well as their magnitude; as such they are more reliable than the maximum concentration plots for representing the typical increase in suspended sediment concentration experienced at any location. However, the mean concentration increase plots will not highlight short-lived, high magnitude increases in suspended sediment concentration.

All mean concentration plots are plotted with the lowest concentration increases shown being 1 mg/l. This is because the mean concentration increases relate to 45 and 32 day periods and are chronic (long-term) impacts rather than the acute (short-term) impacts considered by Smit et al, 2008 and Lwandle, 2020. A level of 1 mg/l is considered to be an appropriate threshold for this purpose, as it represents the typical variation in suspended sediment concentration in the middle and upper layers (though the typical variation in suspended sediment concentration is much higher near the bed and here 1 mg/l is more conservative).

■ **Contour plots of predicted sediment deposition at the end of each modelled scenario (of 45 or 32 days) above background.**

■ **Contour plots of predicted sediment deposition at the end of the 20 year period modelled scenario above background.** These plots are also shown with the lowest deposition being 5 mm. Given the long period over which this deposition will occur, deposition of less than 5 mm was considered to be of negligible impact.

**Appendix C provides:**

■ **Time series of predicted increases in suspended sediment concentration above background**. These plots provide context to the peak and mean concentration plots showing how the predicted peaks in concentration above background represent a relatively small proportion of time.

## 9.2. Zone of influence of dredging plumes

### 9.2.1. Overview

The Zone of Influence (ZoI, see Section 1.5) is shown in Figure 9.1. The ZoI is a combination of the suspended sediment footprint resulting from acute increases above background in suspended sediment concentration above 7.6 mg/l anywhere in the water column (calculated on the basis of dredging scenarios 1 to 8), and the deposition footprint arising from deposition of fine sediment of more than 5 mm over the 20 year period of mining (calculated on the basis of dredging scenarios 9 and 10).

It should be noted that the ZoI does not imply that there will be an actual ecological impact within this area. The ZoI identifies that there are physical changes to suspended sediment concentration and to the seabed substrate above the levels which could immediately be associated with negligible impact. Whether such changes could potentially cause significant adverse impact will depend on the precise nature of the changes and the nature and distribution of the ecological receptors present in the ZoI. The physical changes within the ZoI are considered in more detail below. The nature of any consequent ecological impact on marine species on the ZoI will be identified in other reports prepared for NMP. Outside of the ZoI there is no meaningful change expected to the suspended sediment regime or to the seabed substrate resulting from the proposed dredging and impacts on ecology from these physical changes can be considered to be negligible.

### 9.2.2. Zone of Influence at the regional scale

Figure 9.2 and Figure 9.3 show that the ZoI covers a small area compared to the shelf fishing area of the Namibian shelf region. The figures also show that there is a very small overlap between the commercial fishing area and the ZoI. The ZoI extends over an area 513 km$^2$ outside the 20 year mining plan area and up to 11 km$^2$ outside of the ML 170 Licence Area. Any extension of the ZoI outside of the ML 170 is inshore of the 200 m contour.

The figures show that the ZoI is well separated from the coast and does not affect the sensitive region of Walvis Bay.

### 9.2.3. Zone of Influence at the local scale

Figure 9.4 shows the ZoI superimposed on the Hake and Monkfish fishing areas derived from the 2012 EIA (NMP, 2012) at local scale. The figures show that the ZoI will extend up to 25 km north, 9 km east, 17 km south and 3 km west of the 20 year mining plan area in SP-1. The figures also show that the ZoI only just intersects with the fishery areas, with 3 hake catch locations (out of a total of 63,351 recorded locations) and 1 monkfish catch location being recorded within the ZoI (out of a total of 22,208 locations).

The figures also show that the ZoI extends into waters with depths shallower than 200 m water depth. The ZoI extends 288 km$^2$ into this area.
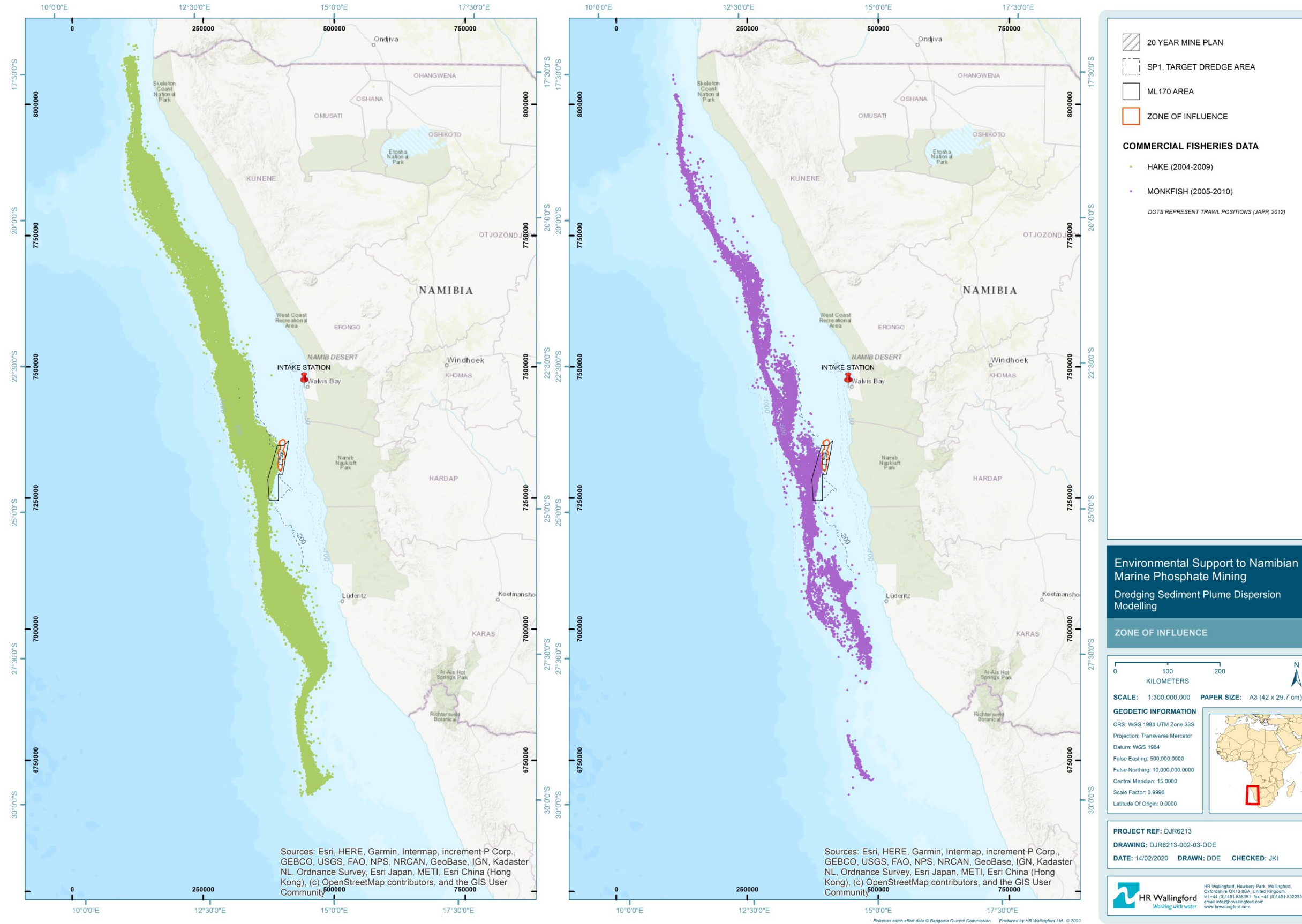
Figure 9.1: Zone of Influence (ZoI), SP-1 and ML 170 areas with Hake and Monkfish commercial fishing areas (at shelf scale)

Figure 9.2: Zone of Influence (ZoI), SP-1 and ML 170 areas with historic Hake catches (at regional scale)
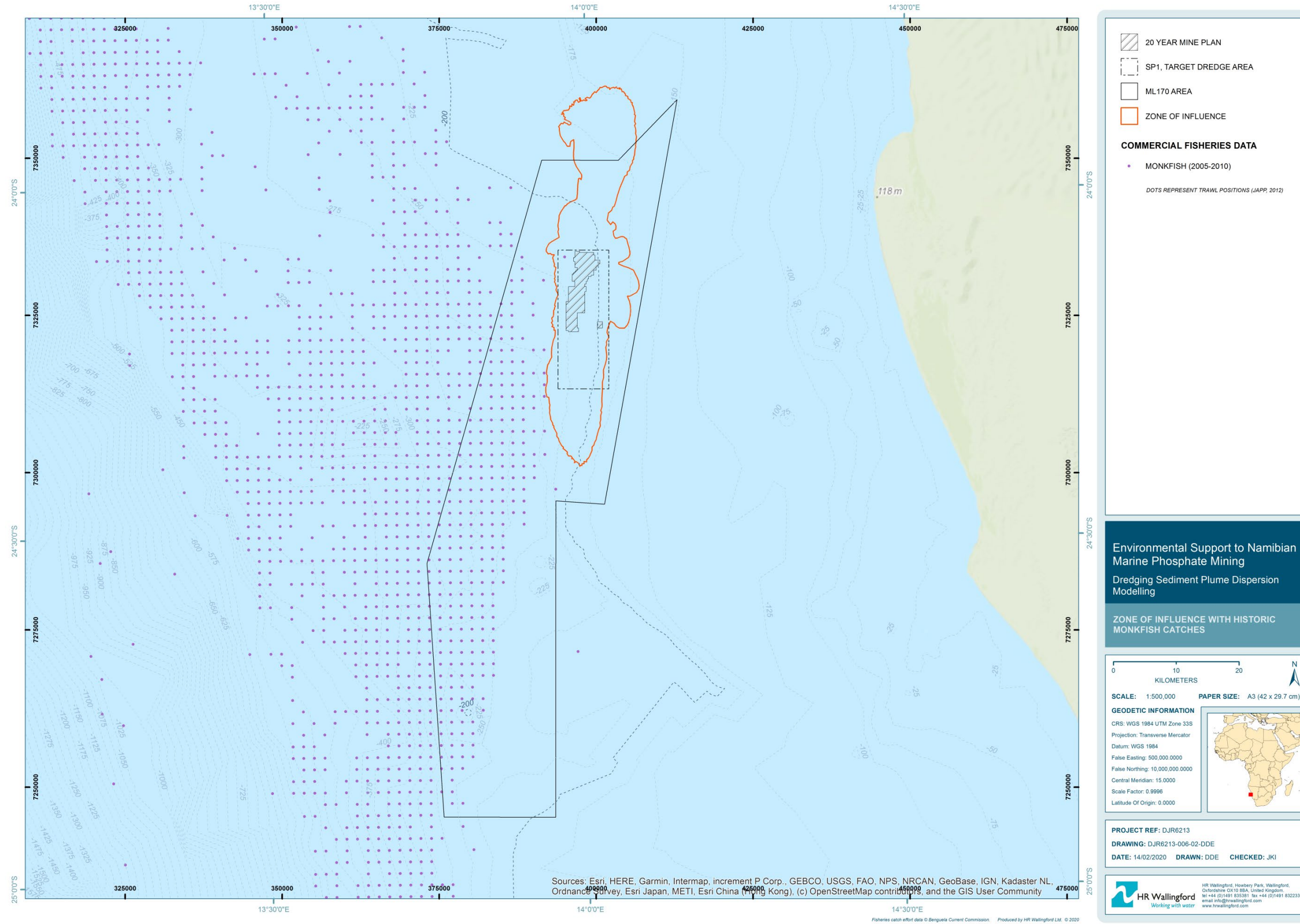
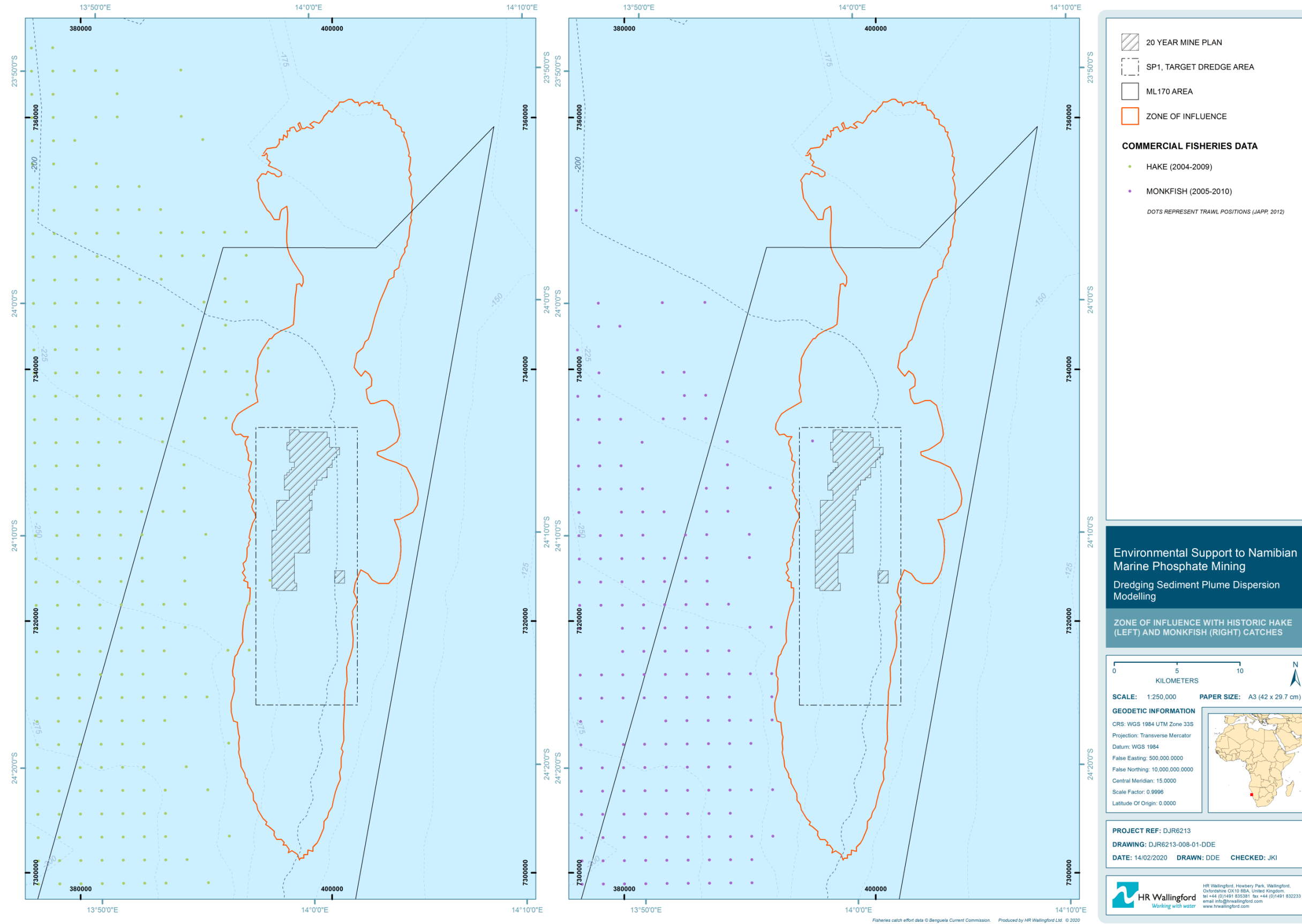Figure 9.3: Zone of Influence (ZoI), SP-1 and ML 170 areas with historic Monkfish catches (at regional scale)

Figure 9.4: Zone of Influence (ZoI), SP-1 and ML 170 areas with historic Hake and Monkfish catches (at local scale)

### 9.2.4. Comparison of the Zone of Influence and the extent of the sediment plume at any given moment

It must be emphasised that the ZoI represents the area within which non-negligible changes in suspended sediment and/or deposition above background are predicted to occur *at any time* within the proposed 20 year period of mining. However, at any given moment within the 20 years, the plume represents a much smaller area than the ZoI, as exemplified in Figure 9.5. The figure shows representative snapshots of the near-surface (Top), Mid-depth, and near-bed (Bottom) plumes at different times in a typical dredging cycle (the plumes at lower levels in the water column occur later than the surface plume and the plume does not exist at all depths of the water column at the same time). The figure shows that each of these plumes typically cover an area of 1-5 km$^2$ while the ZoI represents an area of 546 km$^2$. The typical extent of the plume is therefore less than 1 % of the ZoI area at any given time.
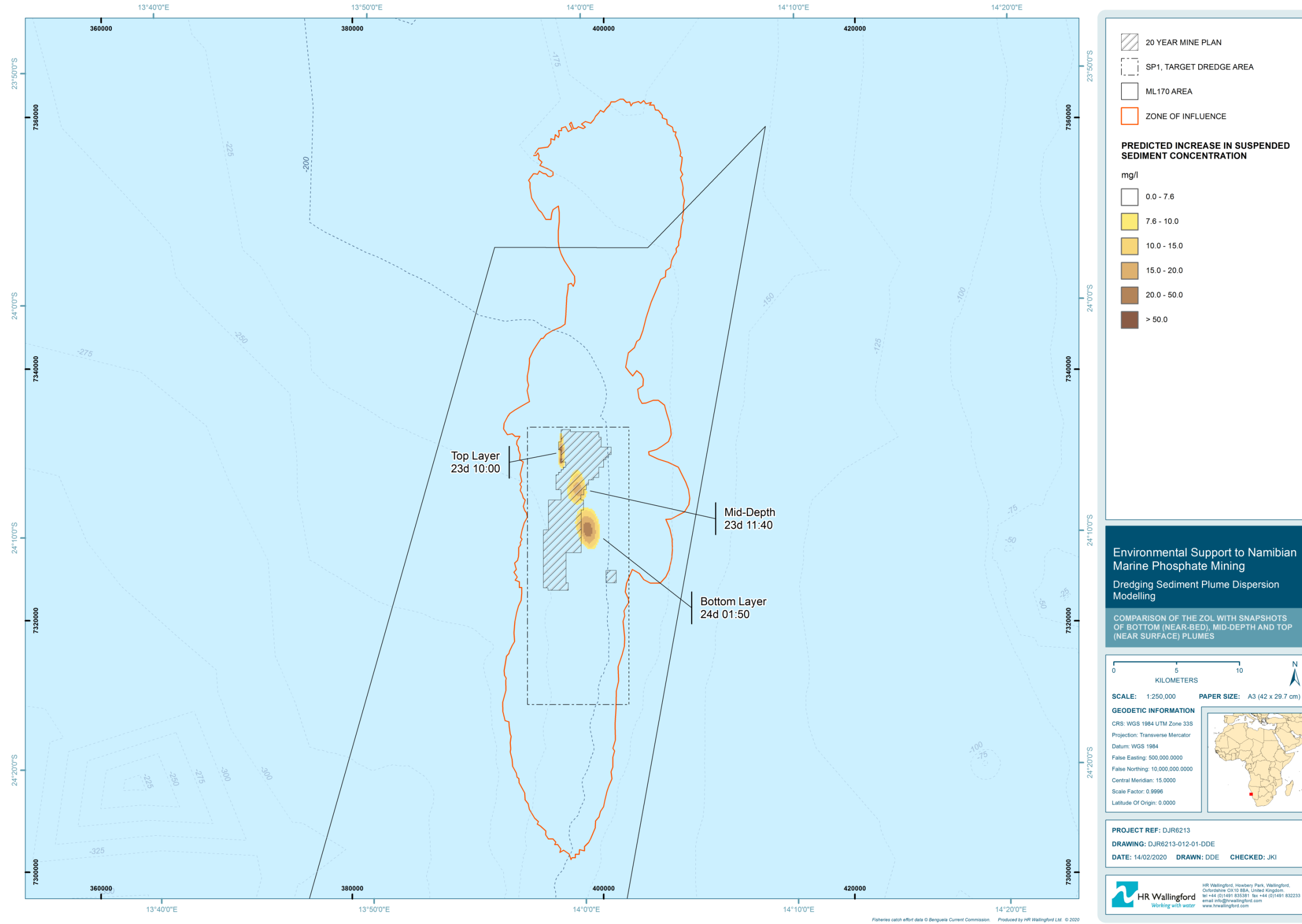
Figure 9.5: Comparison of the ZoI with snapshots of Bottom (near-bed), Mid-depth and Top (near-surface) plumes from one cycle of the dredging operation starting on day 23 of the Scenario 1 simulation (at local scale)

### 9.2.5. General description of vertical plume behaviour during a dredging cycle

The ZoI figures presented above do not provide an indication of the general behaviour and vertical progress of the sediment plume through the water column. Taking the results plume dispersion modelling presented in Appendix B as a whole the behaviour of the plume over an individual dredging cycle is summarised in Figure 9.6 and below.
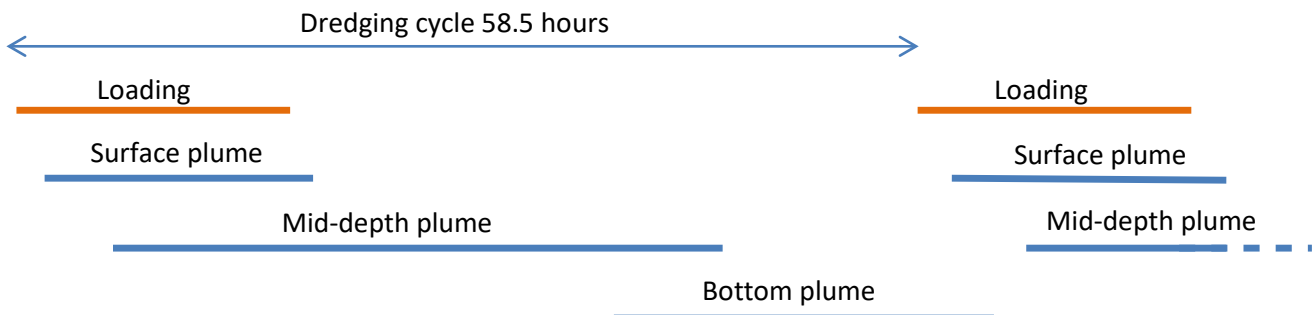


Figure 9.6: Illustrative summary of plume behaviour on each dredging cycle

- Loading takes 18 hours;
- The surface plume (defined by sediment concentration increases above background of greater than 7.6 mg/l) is present for up to 3 hours following cessation of dredging;
- The mid-depth plume is present for 25-30 hours following cessation of dredging;
- The bottom plume is present for 17.5-30 hours but appears 20 or so hours after dredging ceases;
- The next period of loading starts and the surface plume becomes apparent before the bottom plume disappears;
- There is therefore no time when there is no plume present, either at the surface or mid-depth or bottom of the water column;
- Plumes are present (to some extent) in the bottom / mid-depth / surface for (on average) 41 % / 73 % / 34 % of the time, respectively; and,
- Deposition over an individual cycle (58.5 hours) is predicted to be 0.3 mm or less.

## 9.3. Extent and rate of fine sediment deposition

### 9.3.1. The potential for smothering

Appendix B shows the fine sediment deposition above background resulting from all of the modelled scenarios. With the exception of Scenario 9 (dredging in the SE in Austral winter), where deposition is predicted to be up to 12 mm over the 42 day period modelled (13 mg/cm$^2$/day or less), the predicted deposition is 6 mm or less over the 30-42 day period modelled (9 mg/cm$^2$/day or less). These rates indicate annual deposition of less than 9 cm/year and that the vast majority of the deposition over the course of the proposed dredging will settle at a rate which is less than 10 mg/cm$^2$/day – i.e. less than the rate which is

normally considered as being the threshold for adverse impact for the most sensitive sessile species like coral (PIANC, 2010).  The EIA (Steffani, 2012) did not identify any benthic species with this level of sensitivity.  This indicates that that there is little or no risk of a smothering effect from the dredging.

## 9.3.2.    The potential for change in substrate type

Figure 9.7 shows the predicted deposition above background that will occur over the 20 year period of dredging.  The predicted deposition more or less covers the same area as the ZoI discussed in Section 9.2 and the thickness of predicted deposition varies up to 0.7 m within the 20 year mining area and up to 0.7 m outside of this area, with an average depth of deposition of 0.07 m of deposition over the whole of the deposition footprint.  Depending on the thickness of deposition, and the extent to which bioturbation can occur, the predicted fine sediment deposition has the capacity to change the surface substrate from a silty sand to silt.  As stated in Section 4.3.5 this study has found no evidence that significant resuspension of fine sediment will occur and so the predicted deposition is likely to remain indefinitely as shown in Figure 9.7.

Bioturbation is the reworking of the surface sediments by animal activity such as burrowing, ingestion, and defecation of sediment.  As the dredging occurs, both deposition and bioturbation will occur gradually and it can be assumed that over time the top layer of the current (predominantly sandy) seabed and mixed by bioturbation will be mixed with the fine sediment depositing as a result of dredging.  In places where deposition of fine sediment is small compared to the depth of bioturbation, then the deposited fine sediment will be mixed into the surface layer of the underlying sandy sediment, causing an increase in silt content but otherwise not affecting the nature of the substrate.  In places where deposition of fine sediment is large, or comparable with the depth of bioturbation then it is likely that the substrate will change from a primarily sandy sediment to a primarily silty sediment.

Mollenhauer et al. (2007) reported that, based on radionuclide 210Pb dating, the typical depth of mixing caused by bioturbation on the Namibian shelf is around 0.1 m, although in the EIA studies Steffani (2012) noted that benthic infauna burrow up to 0.2 m into the surface sediment.  The Verification Programme for the site also found larger macrobenthos taxa present, that agitate and mix surficial sediments.  These include taxa such as Diopatra sp (polychaete worms) and Callianassa sp (burrowing shrimps) that are understood do so to >0.1 m depth.  It can therefore be deduced from this that the top 0.1 m of the surface sediment is generally well-mixed but that the extent of mixing reduces over the underlying 0.1-0.2 m depth, becoming minimal at a depth of 0.2 m.

To derive an approximate threshold for a change in substrate from silty sand to silt, the difference in dry density (i.e. sediment mass concentration) between depositing fine sediment (estimated as 500 kg/m$^3$ for the purposes of this report) and the existing bed (1,350 kg/m$^3$; JDN, 2013), and also the fine sediment already present in the existing bed, can be taken into consideration.  On this basis it is estimated that thicknesses of deposition arising from dredging of a few centimetres or less will be mixed through this 0.1 m layer, causing a minor increase in the silt content of the sand, but not changing the overall nature of the silty sand substrate.  However, larger thicknesses of deposition above background in the region of 0.1 m or more will cause the surface layer to become predominantly silty.

Table 9.1 summarises the predicted area of seabed which will experience more than 0.1 m of deposition above background and so which can be considered as experiencing substrate change.

Table 9.1: Summary of area extent of predicted deposition above background

| | Whole area | Outside of 20 year mining area | | Outside of ML 170 area |
|---|---|---|---|---|
| | | Total | Inshore of -200 m contour | |
| Deposition footprint (> 5 mm depth in 20 years) | 445 km$^2$ | 412 km$^2$ | 237 km$^2$ | 84.5 km$^2$ |
| Deposition footprint (> 0.1 m depth in 20 years) | 185 km$^2$ | 151 km$^2$ | 26 km$^2$ | 10 km$^2$ |

It is noted that none of the recorded Hake catch locations have taken place in an area predicted to experience some deposition.  Only one of the recorded Monkfish catch locations (out of a total of 22,208 recorded locations) has taken place in an area predicted to experience some deposition, though this area is not predicted to experience substrate change from silty sand to silt.

The scale of these predicted effects are underpinned by the assumptions above, about bioturbation levels for example, and so would need to be verified by field monitoring of the dredging activity.
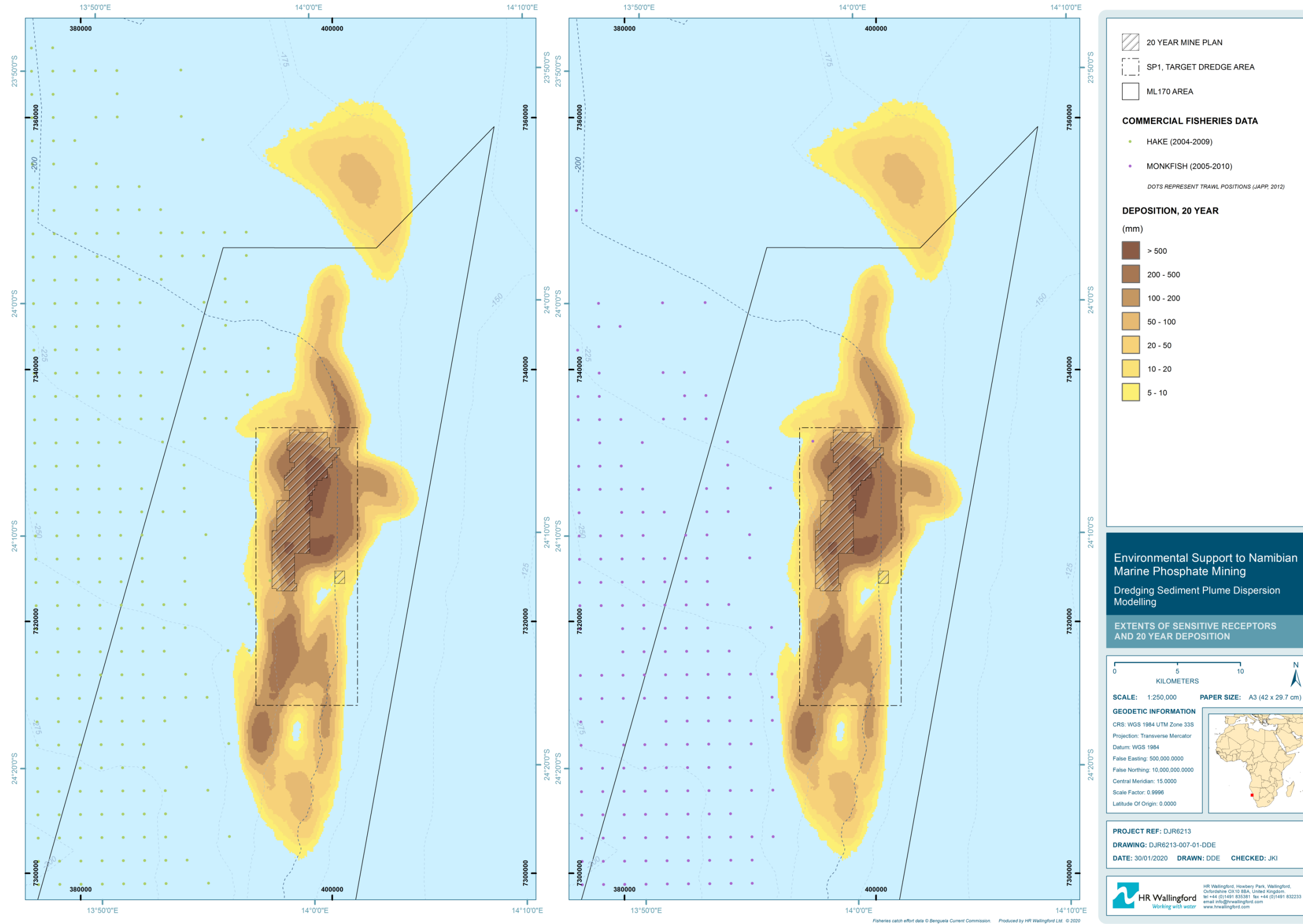
Figure 9.7: Extent of predicted sediment deposition over the 20 year period of mining, along with the historic records of Hake and Monkfish catches (at local scale)

## 9.4. Extent and magnitude of changes in suspended sediment concentration

Appendix B presents the predicted peak and mean concentration increases above background for dredging in different areas of the proposed 20 year mining area, for austral summer and austral winter conditions. The figures show that:

■ The highest peak suspended sediment concentration increases are experienced at the surface but the surface plume is constrained relatively close to the vicinity of the dredging. The extent of peak increases above background in concentration above 7.6 mg/l at mid-depth and near bed plumes is more extensive than at the surface but the predicted concentration increases are less.

■ Except in the close vicinity of the dredging near the surface the predicted peak increases in plume concentration outside of the proposed mining area are less than 50 mg/l. Note that peak concentrations in the immediate vicinity of the dredger (i.e. within 100 m horizontally) will be under-predicted in the model results because resolution of the model output grid is insufficient to resolve the plume at this distance.

■ The largest extent of peak increases above background in concentration above 7.6 mg/l in all cases arises in the lower part of the water column. The extents of the peak concentration increases from each of the simulations varies with the position of the dredging but over the course of the 20 year mining plan, the suspended sediment footprint extends up to 23 km north, 8 km east, 12 km south and 4 km west of the 20 year mining plan area.

■ The magnitude of predicted increases in mean concentration indicate that increases in mean concentration are always predicted to be below 5 mg/l except at the surface within 100 m (horizontally) of the dredging where mean increases of up to 18 mg/l are predicted. Any increases above 1 mg/l are patchy and vary considerably with the position of the dredging.

Appendix C presents time series of predicted increases in suspended sediment concentration above background, at the locations shown in Figure 8.1 and Figure 8.2 (each location being 2 km from the border of the 20 year mining area). The figures show that the surface concentrations above background do not exceed the threshold of 7.6 mg/l while the mid-depth concentrations and near-bed concentrations for 4 % of the time or less. Exceedances above background of the threshold of 7.6 mg/l are predicted to occur for a maximum of 15 hours. This period is no more than 20 % of the exposure durations in standard toxicity tests used to inform the threshold.

# 10. Mitigation through use of the Environmental Valve

## 10.1. Effects on the wider extent and distribution of the sediment plume throughout the water column

Plume dispersion modelling was undertaken to examine the effect of the use of the Environmental Valve on the model results in the form of output used in this report – i.e. the average concentration increases occurring over the bottom 40-50 m, the mid-depth 90-100 m and the surface 40-50 m.  Scenario 1 was repeated, this time including the effects of the Environmental Valve.  The effect of the Environmental Valve was assumed to reduce the discharge of sediment to the surface plume by 80 %, i.e. it was assumed that 3 % of the overflow discharge was captured in the surface plume, compared with 15 % without the use of the valve.  The choice of an 80 % reduction was based on detailed numerical modelling work by Decrop et al (2015).

The results are summarised in Figure D.1 of Appendix D.  Comparison of this figure with Figure B.1 of Appendix B shows that the differences in the predicted plume behaviour is barely perceptible.  On this basis it is concluded that the Environmental Valve will have little effect on the wider extent and distribution of the sediment plume throughout the water column.

## 10.2. Effects on extent and distribution of the sediment plume through the surface 20-30 m

While the Environmental Valve does not affect the wider distribution and vertical behaviour of the plume, it has a significant effect on the amount of the plume which is released into the potentially environmentally more important surface 20-30 m water depth.  Figure D.2 of Appendix D shows the results of the same sensitivity test described above but this time comparing the peak concentrations experienced in the surface 25 m layer with and without the effect of the Environmental Valve.  It can be seen that without the valve the predicted increases in concentration at the surface above background of 7.6 mg/l are predicted to extend up to 1.5 km NW of the dredging. With the Environmental Valve the predicted increases in concentration at the surface are below 7.6 mg/l.

It is concluded that the Environmental Valve could play a significant role in mitigating effects of the dredge plume within the surface 20-30 m of the water column.

# 11. Potential refinements to modelling undertaken

The modelling and analysis described in this report has used the available data and understanding of physical processes on the Namibian shelf. The modelling undertaken has used advanced techniques to reproduce the hydrodynamics and dispersion of sediment plumes arising from dredging. The assessment and the conclusions presented represent the current understanding of the likely behaviour and consequent effects of dredging plumes.

However, the studies have indicated that there are some aspects of the modelling which could require refinement as more, and more detailed data becomes available, and these aspects could potentially have an effect on the behaviour of dredging plumes, as outlined below:

■ **The nature of the observed turbidity events**

The extent to which the observed turbidity events are significant in extent (e.g. caused by advection of hydrogen sulphide from the mud belt) or locally generated (e.g. by trawling), and the nature of the particulate matter in these plumes is important to the understanding of whether depositing fine sediment from the dredging plumes can be re-suspended. If the high turbidity events are extensive and with particulate material of a similar nature to that which will deposit as a result of dredging, then, since the substrate at the site is sandy at present, it becomes more likely that the plumes from dredging will be prevented from depositing. On the other hand, if the high turbidity events are localised and composed of detrital material then they are not representative of the dredging plumes and there is no reason to doubt the deposition predicted by the numerical model in this report.

The extent to which the observed turbidity events are significant in extent or locally generated is important to the understanding of the levels of turbidity which can be tolerated by local ecology. If the local ecology is adapted to the observed high turbidity events, then the much smaller increases in turbidity resulting from dredging are not likely to cause an adverse impact.

■ **Measurements of near bed currents**

The measurements of near bed currents in the second period of measurements had problems with one of the ADCP beams. The measurements were corrected through removing the erroneous beam data and processing the remaining beams. This corrected data compared very well with the model, but it would be useful to provide further confirmation through undertaking further measurements.

■ **The potential effects of extreme weather events and larger scale gyre and upwelling events not captured in the observed data**

The detailed numerical model described in this report has been calibrated and then validated against the observed current magnitude and direction. The resulting validated model predicts that the currents at the site are insufficient to prevent the deposition of fine sediment released into the water column as a result of the proposed dredging. Analysis of the effects of waves suggests that the stirring effect of even the largest waves will be insufficient (alongside the currents) to prevent this deposition. However, the available current measurements are limited to around 3 months of data. It is therefore possible that more extreme events occur from time to time – either as a result of extreme weather events or larger scale ocean gyres or upwelling events – which will result in greater levels of turbulence at the seabed and potentially lead to some resuspension and re-distribution of the deposited material over the longer-term.

■ **Settling velocity**

The plume dispersion outlined in this report has used representative values of settling velocity measured from plumes from trailer suction hopper dredgers, but the values used could be improved by using values based on analysis of fine sediment and seawater taken from the site.

■ **Overflow sediment discharge**

The dispersion modelling undertaken in this report has taken a conservative stance with respect to the predicted rate of discharge of sediment in the dredging overflow.  In practice some sediment will be trapped within the pores of the sand-sized particles settling in the hopper.  The average release rate during loading is therefore likely to be less than the 185 kg/s used in this report and therefore the extent of plumes and the related deposition will be less.  The estimation of the variation in release rate can be improved as the dredger contractor confirms the detail of their methodology for mining.

Collection of additional site data, to specifically address these issues, would facilitate further refinement of the modelling undertaken to date.  It is therefore planned that, following consent, further measurements and analysis will be undertaken. This will provide the additional validation data sets to refine the numerical modelling as necessary and to demonstrate its reliability and accuracy.

# 12.Summary

### Zone of influence (ZoI)

The overall Zone of Influence from this dredging activity for the 20-year period extends over an area of 513 km$^2$ outside of the 20 year mining plan area.  The overall (20-year) ZoI intersects with a very small proportion of the areas identified as important for hake and monkfish trawling.  Within this overall ZoI, 288 km$^2$ extends into waters with depths shallower than the 200 m water depth representing fish habitat where trawling is prohibited.

It must be emphasised that the overall ZoI represents the area within which non-negligible changes in suspended sediment and/or deposition above background are predicted to occur at any time within the proposed 20 year period of mining.  However, at any given moment within the 20 years, the plume represents a much smaller area than the ZoI. For example, the ZoI for a single dredging operation extends up to 5 km$^2$ outside the 20-year mining plan area.

### Sediment deposition

With specific regard to the footprint of sediment deposition over 20-years, the area is similar to (but slightly smaller than) the overall ZoI described above.  Whilst the predicted deposition rates appear unlikely to be sufficiently high to cause an ecological smothering effect, the seabed area experiencing greater than 0.1 m of deposition above background rates is likely to change to a predominantly silty substrate.  It is predicted that 151 km$^2$ of seabed over the 20-year licence period, outside the 20 year mining plan area will experience a change in substrate. The scale of this predicted effect would need to be verified by field monitoring of the dredging activity.

### Suspended sediments

The extents of predicted increases in peak suspended sediment concentration vary with the position of the dredging but, as a whole, the suspended sediment footprint associated with the 20 year mining plan is predicted to extend up to 23 km north, 8 km east, 12 km south and 4 km west of the 20 year mining plan area.  The predicted peak increases in plume concentration outside of the 20 year mining plan area are less than 50 mg/l above background.

Mean increases in suspended sediment concentrations above background are always predicted to be below 5 mg/l, except at the surface within 100 m (horizontally) of the dredging.

Time series analysis at locations sited 2 km from the boundary of the 20 year mining plan area shows that the predicted increase in surface concentrations of suspended sediments above background, outside of the 20 year mining plan area, do not exceed the acute concentration threshold of ecological effects of 7.6 mg/l. The mid-depth concentrations and near-bed concentrations increases above background exceed this threshold for 4 % of the time or less.

### Single dredge cycle

During a single dredging cycle, the plume (defined by sediment concentration increases above background of 7.6 mg/l) is present at the surface for up to 3 hours following cessation of dredging, and in the middle of the water column for 25-30 hours following cessation of dredging.  The bottom plume is present for 17.5-30 hours but appears 20 or so hours after dredging ceases.

Deposition above background over an individual cycle (58.5 hours) is predicted to be 0.3 mm or less and corresponds to a total volume of about 15,000 m$^3$.

### Walvis Bay

There is no indication of the risk of an effect due to dredging within the 20 year mining plan area upon water quality for the salt refining industry intake in Walvis Bay.

### Potential refinements to modelling undertaken

The modelling and analysis described in this report has used the available data and understanding of physical processes on the Namibian shelf. The modelling undertaken has used advanced techniques to reproduce the hydrodynamics and dispersion of sediment plumes arising from dredging. The assessment and the conclusions presented represent the current understanding of the likely behaviour and consequent effects of dredging plumes.

However, the studies have indicated that there are some aspects of the modelling which could potentially require refinement. These aspects include addressing the nature of the observed high turbidity events, the currently available measurements of near bed currents, the contribution of extreme weather or ocean events to long-term deposition, the settling velocity of dredged material released in the overflow and the overflow sediment discharge.

Collection of additional site data, to specifically address these aspects, would facilitate further refinement of the modelling undertaken to date. It is therefore planned that, following consent, further measurements and analysis will be undertaken. This will provide the additional validation data sets to refine the numerical modelling as necessary and to demonstrate its reliability and accuracy.

### Summary information for the sediment plume

Summary information for the sediment plume is provided overleaf in Table 12.1.

Table 12.1: Summary information for sediment plume

| Aspect of plume | | Outside 20 year mining plan area | | | Outside of ML 170 area | At Walvis Bay intakes |
|---|---|---|---|---|---|---|
| | | Total area | Inside fishery area | Inshore of -200 m contour | | |
| Zone of Influence | | 513 km$^2$ | ~10 km$^2$ (Hake) ~3 km$^2$ (Monkfish) | 288 km$^2$ | 11 km$^2$ | None |
| Peak suspended solids above background (20 years' dredging) * | | < 48 mg/l | < 25 mg/l | < 30 mg/l | < 18 mg/l | None |
| Mean suspended solids above background (20 years' dredging) | | < 18 mg/l | < 2 mg/l | < 4 mg/l | < 3 mg/l | None |
| Depth of sediment deposition (20 years' dredging) | | ≤ 0.7 m | 0 m (Hake) ≤ 0.02 m (Monkfish) | ≤ 0.5 m | ≤ 0.08 m Mean 0.02-0.03 m | None |
| Area of sediment deposition (20 years' dredging) | > 5 mm depth | 412 km$^2$ | ~3 km$^2$ | 237 km$^2$ | 84.5 km$^2$ | None |
| | > 0.1 m depth | 151 km$^2$ | 0 km$^2$ | 26 km$^2$ | 10 km$^2$ | None |
| Single dredging operation ZoI, typical area of plume (if present) | | 1-5 km$^2$ | | | | None |
| Sediment deposition (single operation) | Thickness | ≤ 0.3 mm | ≤ 0.3 mm | ≤ 0.3 mm | ≤ 0.3 mm | None |
| | Volume | ~15,000 m$^3$ | Dependent on dredging location | | | None |

Note:     *  Not including immediate (near-field) vicinity of dredger

# 13.References

Bateman, 2011a. Sandpiper, 3 Mtpa Phosphate Project, Bulk Sample 1797B – Size analyses, Report by Bateman Advanced Technologies Ltd., June 2011.

Bateman, 2011b. Testwork report, Characterization of Sandpiper High Grade Marine Phosphate Feed and Phosphate Solubility Results, Report by Bateman Advanced Technologies Ltd., June 2011.

Carrere L., F. Lyard, M. Cancet, A. Guillot, N. Picot, 2016.  FES 2014, a new tidal model - Validation results and perspectives for improvements, presentation to ESA Living Planet Conference, Prague 2016.

Clark, M. R., Althaus, F., Schlacher, T. A., Williams, A., Bowden, D. A., Rowden, A. A., The impacts of deep-sea fisheries on benthic communities: a review, ICES Journal of Marine Science, Volume 73, Issue suppl_1, January 2016, Pages i51–i69, https://doi.org/10.1093/icesjms/fsv123.

Dansie, A., Wiggs, G., Thomas, D., Washington, R., 2017.  Measurements of windblown dust characteristics and ocean fertilization potential: The ephemeral river valleys of Namibia.  Aeolian Research 29 (2017) 30–41.

Decho, A. W. and Gutierrez, T., 2017.  Microbial extracellular polymeric substances (EPSs) in ocean systems, Front. Microbiol. https://doi.org/10.3389/fmicb.2017.00922.

Decrop, B., DE Mulder, T., Torrman, E. and Sas, M, 2015. Numerical simulation of near-field dredging plumes: Efficiency of an environmental valve, Journal of Environmental Engineering, 141(12).

Elfrink, B., Prestedge, G., Rocha, C.B.M. and Juhl, J., 2003. Shoreline evolution due to highly oblique incident waves at Walvis Bay, Namibia.  Coastal Sediments 2003. Accessed 10/01/2020. https://www.dhigroup.com/upload/dhisoftwarearchive/papersanddocs/sediments/cs2003_elfrink_et_al.pdf.

EMBECOM, 2004. Dredging-related re-suspension of sediments: Impacts and guidelines for the marine dredging. Specialist study for the environmental impact report for the pre-feasibility phase of the marine dredging project in Nambdeb's Atlantic 1 Mining Licence Area and in near shore areas off Chameis. 72pp.

Fischer H.B., List E.J., Koh R.C.Y., Imberger J., and Brooks N.H., 1979. Mixing in Inland and Coastal Waters. New York : Academic. 483 pp.

Gordoa, A., Lesch, H., and Rodergas, S. 2006. Bycatch: complementary information for understanding fish behaviour. Namibian Cape hake (M. capensis and M. paradoxus) as a case study.  ICES Journal of Marine Science, 63: 1513-1519.

Hersbach, H., Dee, D., 2016.  ERA5 reanalysis is in production. ECMWF Newsletter No. 147 – Spring 2016.

Inthorn, M., Mohrholz, V., and Matthias, Z., 2006. Nepheloid layer distribution in the Benguela upwelling area offshore Namibia. Deep Sea Research I. 53: 1423.

Lwandle, 2020. NMP Hydrodynamic Modelling: Turbidity threshold justification, 07 April 2020.

Jan De Nul, 2013. Dredging Technology, Sandpiper Phosphate Project, Report PS.NAM-PA-13.002-FJ-A, April 2013.

Jan De Nul, 2015. Reduction of fines content on board Cristobal Colon, Sandpiper Phosphate Project, Report PS.NAM-PA-13.002-FJ-C, July 2015.

Jan De Nul, 2019. JDN vessel specification sheet and email communication between JDN and NMP (provided by Namibian Marine Phosphate (Pty) Ltd (NMP)), December 2019.

Lass, H.U. and Mohrholz V. On the fluctuations and vertical structure of the shelf circulation off Walvis Bay, Namibia, Continental Shelf Research, 25: 1473-1497.

Lee, J. H. W., and Cheung, V., 1990 Generalized lagrangian model for buoyant jets in current, Journal of Environmental Engineering, volume 116, number 6.

Lyard F., L. Carrere, M. Cancet, A. Guillot, N. Picot, -016. FES2014, a new finite elements tidal model for global ocean, in preparation, to be submitted to Ocean Dynamics in 2016.

Lyard, F., F. Lefèvre, T. Letellier and O. Francis., 2006. Modelling the global ocean tides: a modern insight from FES2004, Ocean Dynamics, 56, 394-415, 2006.

Manning, A.J. and Dyer, K.R., 2007. Mass settling flux of fine sediments in Northern European estuaries: measurements and predictions. *Marine Geology*, 245, 107-122, doi:10.1016/j.margeo.2007.07.005.

Manning, A. J., Spearman, J. R., Whitehouse, R. J. S., Pidduck, E. L., Baugh, J. V. and Spencer, K. L., 2-13. Flocculation dynamics of mud:sand mixed suspensions, In: *Sediment Transport Processes and Their Modelling Applications*, Andrew J Manning (ed.), InTech. DOI: 10.5772/3401. (2013).

Mead, C. T., 2004. Realisation of the potential of lagrangian models in aquatic dispersion studies, Proceedings of the 3rd International Conference on Marine Waste Water Disposal and Marine Environment, Catania, Italy, Paper E18. (2004).

Mollenhauer, G. , Inthorn, M. , Vogt, T., Zabel, M., Sinninghe Damsté, J. S., and Eglinton, T. I., 2007. Aging of marine organic matter during cross-shelf lateral transport in the Benguela upwelling system revealed by compound-specific radiocarbon dating , Geochemistry, Geophysics, Geosystems, 8, Q09004. . doi: 10.1029/2007GC001603.

Monteiro, P.M.S., Nelson, G., van dep Plas, A., Mabille, E., Bailey, G.W. and Klingelhoeffer, E., 2005. Internal tide – shelf topography interactions as a forcing factor governing the large-scale distribution and burial fluxes of particulate organic matter (POM) in the Benguela upwelling system, Continental Shelf Research 25: 1864-1876.

Newell, R, and Muhapi, S., 2018. Independent review of written comments by Interested and Affected Parties (I&AP) in respect of an Environmental Impact Assessment (EIA) submitted by Namibia Marine Phosphate (Pty) Ltd for an Environmental Clearance Certificate (ECC). Final Draft, signed. December 2018.

Mathieu Rouault, Serena Illiga, Joke Lübbecke, Rodrigue Anicet Imbol Koungue., 2017. Origin, development and demise of the 2010–2011 Benguela Niño. Journal of Marine Systems, http://dx.doi.org/10.1016/j.jmarsys.2017.07.007.

NMP, 2012a. Namibian Marine Phosphate (Pty) Ltd. Environmental Impact Assessment for the proposed dredging of phosphate enriched sediments from Marine Licence Area No. 170. 30 March 2012. Prepared J Midgley & Associates.

NMP, 2012b. Namibian Marine Phosphate (Pty) Ltd. Sandpipe Phosphate Project, Project Feasibility Report PS-NAM-PA-12.002-FJ-A, March 2012.

NMP, 2014a. Namibian Marine Phosphate (Pty) Ltd. Environmental Verification Report Dredging of Marine Phosphate ML 170. Section D, Appendix 6 – dredging project description.

NMP, 2014b. Namibian Marine Phosphate (Pty) Ltd. Sandpiper Project Verification Programme. Volume 1: Main Report. Namibian Marine Phosphate (Pty) Ltd. Mining Licence Area No 170. November 2014.

NMP, 2014c. Namibian Marine Phosphate (Pty) Ltd. Sandpiper Project Verification Programme. Volume 2: Appendices. Namibian Marine Phosphate (Pty) Ltd. Mining Licence Area No 170. November 2014.

NMP, 2014d.  Namibian Marine Phosphate (Pty) Ltd.  Independent Peer Reviews - Verification Studies, Sandpiper Project.  November 2014.

OSU (2008), OSU Tidal Data Inversion Software and Atlas, Oregon State University, http://volkov.oce.orst.edu/tides/.

Parsons, D.R., Schindler, R.J., Hope, J.A., Malarkey, J., Baas, J.H., Peakall, J., Manning, A.J., Ye, L., Simmons, S., Paterson, D.M., Aspden, R.J., Bass, S.J., Davies, A.G., Lichtman, I.D. and Thorne, P.D., 2016.  The role of biophysical cohesion on subaqueous bed form size, *Geophysical Research Letters*, 43, doi:10.1002/2016GL067667. (2016).

Paterson, B., and P. Kainge. 2014. Rebuilding the Namibian hake fishery: a case for collaboration between scientists and fishermen.  Ecology and Society 19(2):49.

PIANC. 2010. Dredging and port construction around coral reefs, PIANC Report 108.

Simpson, J.H., Hyder, P., Rippeth T.P., Lucas, I.M., 2002.  Forced oscillations near the critical latitude for diurnal-inertial resonance, American Meteorological Society, Journal of Physical Oceanography, 32(1): 177-187.

Smith, S.J., and Friedrichs, C.T., 2011. Size and settling velocities of cohesive flocs and suspended sediment plume aggregates in a trailing suction hopper dredge plume, Continental Shelf Research, 31: S50-S63.

Soulsby, R.L., 1997 Dynamics of marine sands, Thomas Telford Publications, London.

Spearman, J., Bray, R. N., and Burt, T. N., 2003. Dynamic representation of trailer dredger source terms in plume dispersion modelling, CEDA Dredging days, November, 2003.

Spearman, J. R., Bray, R. N., Land, J., Burt, T. N., Mead, C. T. and Scott, D.2—7.  Plume dispersion modelling using dynamic representation of trailer dredger source terms, Estuarine and Coastal Fine sediment dynamics, INTERCOH 2003, Proceedings in Marine Science: 8, Elsevier, Amsterdam. (2007).

Spearman, J., 2015.  A review of the physical impacts of sediment dispersion from aggregate dredging, Marine Pollution Bulletin, 94: 260-277.

Spearman, J., De Heer, A. and Aarninkhof , S.G.J. and Van Koningsveld, M., 2011.  Validation of The TASS System For Predicting The Environmental Effects Of Trailing Suction Hopper Dredging,  Terra et Aqua, 125, p14. (2011).

Steffani, N. (2012) Marine Benthic Specialist Study, Appendix 1C, Environmental Impact Assessment Report, Dredging of marine phosphates from ML 170, 2012.

Tsanis, I. 1989. Simulation of wind-induced water currents.  Journal of hydraulic Engineering, Vol. 115, n°8, pp1113-1134, 1989.

Wheatland, J. A. T., Bushby, A. J. and Spencer, K. L., 2019. Quantifying the structure and composition of flocculated suspended particulate matter using focused ion beam nanomatography, *Environ. Sci. Technol*., 51:8917-8925. (2019).

Whitehouse, R.J.S., Soulsby R.L., Roberts W.R. and Mitchener H., 2000, Dynamics of estuarine muds, Thomas Telford Publications, London.

Wu, J., 1982. 'Wind-stress coefficients over the sea surface from breeze to hurricane', J. Geophys. Res. 87 (C12), 9704–9706, 1982.

Zhang, N., Thompson, C.E.L., Townend, I.H., Rankin, K.E., Paterson, D.M. and Manning, A.J., 2018.  Non-destructive 3D Imaging and Quantification of Hydrated Biofilm-Sediment Aggregates Using X‑ray Microcomputed Tomography. *Env. Sci. Tech*., 52, 13306-13313, DOI: 10.1021/acs.est.8b0399. (2018).

# Appendices

# A. SEDPLUME-RW model

## A.1. Description of the SEDPLUME-RW far-field plume dispersion model

### A.1.1. Representation of sediment plume dispersion

In SEDPLUME-RW, the release of suspended sediment is represented as a regular or intermittent discharge of discrete particles. Particles are released throughout a model run to simulate continuous sediment disturbance or for part of the run to simulate sediment disturbance over an interval during the tidal cycle, for instance to represent the resuspension of fine sediment during dredging or mining operations. At specified sites a number of particles are released in each model time-step and, in order to simulate the release of suspended sediment, the total sediment released at each site during a given time interval is divided equally between the released particles. Particles can be released either at the precise coordinates of specified locations, or distributed randomly, centred on the specified release sites (which may move in time). The particles can be released at specific depths or intervals through the water column.

For more complicated cases the SEDPLUME-RW model makes use of an integral buoyant jet model to provide source terms for the far-field dispersion.  This is described in Section 2.

### A.1.2. Large scale advection

SEDPLUME-RW uses TELEMAC flow model results to provide hydrodynamic input.  TELEMAC can be used to model either 2D or 3D currents.  For TELEMAC-3D, as in this study,  the 3D currents are used directly by SEDPLUME-RW.

Each particle is then advected by the local flow conditions. Because the three dimensional structure of the flow is calculated by SEDPLUME-RW, effects such as shear dispersion of plumes are automatically represented.

### A.1.3. Turbulent diffusion

In order to simulate the effects of turbulent eddies on suspended sediment plumes in coastal waters, particles in SEDPLUME-RW are subjected to random displacements in addition to the ordered movements which represent advection by mean currents. The motion of simulated plumes is, therefore, a random walk, being the resultant of ordered and random movements. Provided the lengths of the turbulent displacements are correctly chosen, the random step procedure is analogous to the use of turbulent diffusivity in suspended sediment transport models. This is discussed in more detail below.

(a)      Lateral diffusion

The horizontal random movement of each particle during a time-step of SEDPLUME-RW consists of a displacement derived from the parameters of the simulation. The displacement of the particle in each of the orthogonal horizontal directions is calculated from a Gaussian distribution, with zero mean and a variance

determined from the specified lateral diffusivity. The relationship between the standard deviation of the displacement, the time-step and the diffusivity is defined in Reference 1 as:

$$\frac{\Delta^2}{\Delta t} = 2D \tag{3}$$

where:

D        = standard deviation of the turbulent lateral displacement (m)

$\Delta t$        = time-step (s)

$\Delta$        = lateral diffusivity ($m^2 s^{-1}$).

In a SEDPLUME-RW simulation, a lateral diffusivity is specified, which the model reduces to a turbulent displacement using Equation (3). No directional bias is required for the turbulent movements, as the effects of shear diffusion are effectively included through the calculated depth structure in the mean current profile.

(b)        Vertical diffusion

Whilst lateral movements associated with turbulent eddies are satisfactorily represented by the specification of a constant diffusivity, vertical turbulent motions can vary significantly horizontally and over the water depth, so that vertical diffusivities must be computed from the characteristics of the flow field, rather than specified as constants. In SEDPLUME-RW it is possible to use the vertical diffusion computed by the TELEMAC model, as in this study, or instead to use the mixing length approach of Nezu and Nakagawa (Reference 2) with modification for vertical density gradients based upon the methodologies of Munk and Andersen (Reference 3) or Toorman (Reference 4).

The value of the computed vertical diffusivity is calculated at each particle position, then a vertical turbulent displacement is derived for each particle from its $K_z$ value using an equation analogous to (3) for the lateral turbulent displacement.

(c)        Drift velocities

A particle undergoes a random walk as follows:

$$x^n = x^{n-1} + A(x^{n-1}, t^{n-1})\Delta t + B(x^{n-1}, t^{n-1})\sqrt{\Delta t}\ \xi^n \tag{4}$$

where $x^n$ is the position of the particle at time $t^n$, A is the advection velocity at timestep n-1 and B is a matrix giving the diffusivity. $\xi$ is a vector of three random numbers, each drawn from a normal distribution with unit variance and zero mean. In the case of SEDPLUME-RW, B is diagonal, with the first two entries equal to $\sqrt{(2D)}$ (as introduced in the previous section) and the third diagonal entry being equal to the local value of $\sqrt{(2K_z)}$.

The movement of a particle undergoing a random walk as described in equation (4) can be described by the Fokker-Planck equation in the limit of a very large number of particles and a very short timestep, where we introduce subscripts *i,j* and *k* running over the three coordinate directions:

$$\frac{\partial f}{\partial t} + \frac{\partial}{\partial x_i}(A_i f) = \frac{\partial^2}{\partial x_i \partial x_j}\left(\frac{1}{2} B_{ik} B_{jk} f\right) \tag{5}$$

The probability density function $f(x,t|x_0,t_0)$ is the probability of a particle which starts at position $x_0$ at time $t_0$ being at position $x$ at time t.

Equation (5) can be compared with the advection-diffusion equation for the concentration of a pollutant, *c*:

$$\frac{\partial c}{\partial t} + \frac{\partial}{\partial x_i}(u_i c) = \frac{\partial}{\partial x_i}\left(K_{ik}\frac{\partial}{\partial x_k}c\right) \qquad (6)$$

where $K_{ik}$ is the eddy diffusion matrix, diagonal in our case but not necessarily so. Thus identifying *f* with *c*, we can see that the two equations are equivalent provided that we take the advection velocity as:

$$A_i = u_i + \frac{\partial}{\partial x_k}K_{ik} \qquad (7)$$

In the case of SEDPLUME-RW, the diffusivity varies only in the vertical and is constant in the horizontal, so the horizontal advection velocity is simply the flow velocity (assuming that the relatively small effects of changing water depth can be neglected). However, when considering the movement of particles in the vertical it is important to include the gradient of the diffusivity (often referred to as a drift velocity) in the advection step. If this term is omitted then particles tend to accumulate in regions of low diffusivity, which in our case means at the surface and at the bed.

This subject is discussed in considerably more detail in References 5, 6, 7, and 8.

## A.1.4.    Sedimentation processes

(a)    Settling

In SEDPLUME, the settling velocity (ws) of suspended sediment is assumed to be related to the suspended sediment concentration (c) through an equation of the form:

$$w_s = \max\left(w_{\min}, Pc^{Q}\right) \qquad (8)$$

where $w_{\min}$, *P* and *Q* are empirical constants. Having computed a suspended mud concentration field, as described subsequently in this section, a settling velocity can be computed in each output grid cell from Equation (8) and used to derive a downward displacement for each particle during each time-step of a model simulation. This displacement is added vectorially to the other computed ordered and random particle displacements. Note that there is a specified minimum value of ws. This results in settling velocities being constant at low suspended mud concentrations.

(b)    Deposition

SEDPLUME-RW computes bed shear stresses from the input tidal flow fields using the rough turbulent equation, based on a bed roughness length input by the user. Where the computed bed stress, tb, falls below a specified critical value, td, and the water is sufficiently deep, then deposition is assumed to occur. Mud deposition is represented in SEDPLUME by particles approaching the sea bed becoming inactive when tb is below td. Whilst active particles in the water column contribute to the computed suspended mud concentration field, as described subsequently in this appendix, inactive particles contribute to the mud deposit field.

(c)    Erosion

The erosion of mud deposits from the sea bed is represented in SEDPLUME  by inactive particles returning to the water column (becoming active) when $\tau_b$ exceeds a specified erosional shear strength, $\tau_e$. The number of particles which become re-suspended in each cell of the output grid in each time-step of a simulation is determined by the equation:

$$\frac{\partial m_e}{\partial t} = M\left(\tau_b - \tau_e\right) \tag{9}$$

where:

$m_e$ = the mass eroded (kg)

$t$ = time (s)

$M$ = an empirical erosion constant.

### 1.5    Computation of suspended mud concentrations

SEDPLUME-RW computes suspended mud concentrations are computed by summing the mass of mud represented by the particles in each 2D or 3D cell of the output grid, and assuming that the resulting mass is evenly distributed over the cell area.

### 1.6    Computation of mud deposit distributions

SEDPLUME-RW computes mud deposit distributions by summing the mass of mud represented by the inactive particles in each cell of the output grid, and assuming that the resulting mass is evenly distributed over the cell area.

## A.2.    Description of the SEDPLUME-RW near-field plume dispersion module

### A.2.1.    Introduction

The near-field plume module models the near-field mixing that occurs as the negatively buoyant jet of the overflow mixes with the surrounding waters.

### A.2.2.    Near-field mixing

The descent of the dynamic plume is reproduced using a Lagrangian technique whereby a thin disc (which can be thought of as a section of a bent cone) of the released dynamic plume is tracked as it moves under the forces of momentum and negative buoyancy.  The technique has been used for both dredger plume and outfall plume modelling (e.g. References 9, 10 and 11).

Entrainment of ambient water into the plume is modelled using the formulations of Lee and Cheung (Reference 12) and accounts for both shear entrainment (i.e. as occurs in jets and dominates the initial stages of the dynamic descent) and forced entrainment (which dominates in the latter stages of descent and is due to the flow of ambient water into the plume).  The increase in mass due to shear entrainment is given by:

$$\Delta M_s = 2\pi \rho_a b_k h_k E \Delta t \left| V_k - u'_{amb} \cos \phi_k \cos \theta_k \right| \tag{10}$$

where:

$$E = \sqrt{2}\,\frac{\left(0.057 + \dfrac{0.45\sin\phi_k}{F^2}\right)}{\left(1 + 5\,\dfrac{u'_{amb}\cos\phi_k\cos\theta_k}{|V_k - u'_{amb}\cos\phi_k\cos\theta_k|}\right)} \quad \text{with} \quad F = \frac{|V_k - u'_{amb}\cos\phi_k\cos\theta_k|}{\left(g\,\dfrac{\Delta\rho}{\rho}\,b_k\right)^{1/2}} \qquad (11)$$

and where $\Delta M_s$ is the increase in plume mass due to shear entrainment, $F$ is the local densimetric Froude number and is based on Schatzmann (References 12 and 13), $\phi$ is the angle between the plume descent and the horizontal, $\theta_k$ is the angle between the jet descent and the x-axis, $b_k$ is the radius of the dynamic plume element at time step $k$, $h_k$ is the thickness of the dynamic plume element, $\rho$ is the density of the plume, $V_k$ is the speed of the dynamic plume element, $\rho_a$ is the density of the ambient sea water, $\Delta\rho$ is the difference in density between the plume and the ambient water, $\Delta t$ is the time step, and u'$_{amb}$ is the current speed (in the coordinate system moving with the dredger) of the ambient fluid. The formula suits a wide range of flows and gives the correct buoyancy for a pure jet (no buoyancy just momentum) and a pure plume (no initial momentum, just a density difference) (Reference 11).

Lee and Cheung (Reference 11) also derived an equation for forced entrainment arising in a three dimensional trajectory. The resulting entrainment is as follows:

$$\Delta M_k = \rho_a u'_{amb}\, h_k b_k \left[ 2\sqrt{\sin^2\phi_k + \sin^2\theta_k - (\sin\phi_k\,\sin\theta_k)^2} + \pi\,\frac{\Delta b_k}{\Delta s_k}\cos\phi_k\,\cos\theta_k \right. \qquad (12)$$

$$\left. + \frac{\pi}{2}\,b_k\,\frac{(\cos\phi_k\cos\theta_k - \cos\phi_{k-1}\cos\theta_{k-1})}{\Delta s_k} \right]\Delta t$$

where $\Delta M_k$ is the increase in plume mass due to forced entrainment, $s_k$ is the distance travelled by dynamic plume in timestep $_k$, and $\Delta b_k$ is the change in plume radius, $b_k$–$b_{k-1}$ .

There are three different contributions to forced entrainment which are all significant at different times suggesting that none of these terms can be neglected. The first term represents the forced entrainment due to the projected area of the crossflow while the second and third terms represent corrections due to the growth of the plume radius and the curvature of the trajectory (References 11 and 14). The near-field descent phase is terminated either when the plume impinges on the bed, when the dynamic plume becomes sufficiently diffuse that it becomes a passive plume, or after a time set by the user.

# A.3.  References

1.  H B Fischer, E J List, R C Y Koh, J Imberger and N H Brooks, 1979. Mixing in Inland and Coastal Waters. New York : Academic. 483 pp.

2.  Nezu, I., and Nakagawa, H., Turbulence in open-channel flows, IAHR Monograph Series, Balkema, 1993.

3.  Munk W H and Andersen E A (1948) Notes on a theory of the thermocline, J. Marine Research, 3(1): 276-295.

4.  Toorman E A (2000) Parameterisation of turbulence damping in sediment-laden flows, Report HYD/ET/00/COSINUS3, Hydraulics Laboratory, Katholieke Univeriteit Leuven.

5.  A S Monin and A m Yaglom. "Statistical Fluid Mechanics". MIT Press, Cambridge, Massachusetts, 1971.

6.  A F B Tompson and L W Gelhar. "Numerical simulation of solute transport in three-dimensional randomly heterogeneous porous media". Water Resources Research, Vol 26 pp2541-2562, October 1990.

7.  K N Dimou and E Adams. "A random-walk particle tracking model for well-mixed estuaries and coastal waters". Estuarine, Coastal and Shelf Science, Vol 37, pp99-110, 1993.

8.  B J Legg and M R Raupach. "Markov-chain simulation of particle dispersion in inhomogeneous flows: the mean drift velocity induced in a gradient in Eulerian velocity variance". Boundary Layer Meteorology Vol 24, pp3-13, 1982.

9.  Koh R C Y and Chang Y C , 1973, Mathematical model for barged ocean disposal of waste, Technical Series EPA 660/2-73-029, US Environment Protection Agency, Washington D.C.

10. Brandsma M G and Divoky D J, 1976, Development of models for prediction of short-term fate of dredged material discharged in the estuarine environment, Contract Report D-76-5, US Army Engineer Waterways Experiment Station, Vicksburg, MS, prepared by Tetra Tech, Inc., Pasadena, CA.

11. Lee J H W and Cheung V, 1990, Generalized lagrangian model for buoyant jets in current, Journal of Environmental Engineering, volume 116, number 6.

12. Schatzmann M, 1979, Calculation of submerged thermal plumes discharged into air and water flows, Proceedings of the 18th IAHR Congress, International Association for Hydraulic Research, Delft, 4, pp379-385.

13. Schatzmann , 1981, Mathematical modelling of submerged discharges into coastal waters, Proceedings of the 19th IAHR Congress, International Association for Hydraulic Research, Delft, 3, pp239-246.

14. Frick W E, 1984, Non-empirical closure of the plume equations, Atmospheric Environment, Volume 18, Number 4, 653-662.

# B. Plume dispersion model results

Table B.1: Summary of figures in Appendix B

Note: all increases shown are above background.

| Figure | Austral Summer | Austral Winter | Peak SSC | Mean SSC | Deposition | North West | North East | South West | South East | Evenly 20 year |
|---|---|---|---|---|---|---|---|---|---|---|
| B.1 | | ✓ | ✓ | | | ✓ | | | | |
| B.2 | | ✓ | | ✓ | | ✓ | | | | |
| B.3 | | ✓ | | | ✓ | ✓ | | | | |
| B.4 | | ✓ | ✓ | | | | | ✓ | | |
| B.5 | | ✓ | | ✓ | | | | ✓ | | |
| B.6 | | ✓ | | | ✓ | | | ✓ | | |
| B.7 | | ✓ | ✓ | | | | | | ✓ | |
| B.8 | | ✓ | | ✓ | | | | | ✓ | |
| B.9 | | ✓ | | | ✓ | | | | ✓ | |
| B.10 | | ✓ | ✓ | | | | | | ✓ | |
| B.11 | | ✓ | | ✓ | | | | | ✓ | |
| B.12 | | ✓ | | | ✓ | | | | ✓ | |
| B.13 | ✓ | | ✓ | | | ✓ | | | | |
| B.14 | ✓ | | | ✓ | | ✓ | | | | |
| B.15 | ✓ | | | | ✓ | ✓ | | | | |
| B.16 | ✓ | | ✓ | | | | | ✓ | | |
| B.17 | ✓ | | | ✓ | | | | ✓ | | |
| B.18 | ✓ | | | | ✓ | | | ✓ | | |
| B.19 | ✓ | | ✓ | | | | | | ✓ | |
| B.20 | ✓ | | | ✓ | | | | | ✓ | |
| B.21 | ✓ | | | | ✓ | | | | ✓ | |
| B.22 | ✓ | | ✓ | | | | | | ✓ | |
| B.23 | ✓ | | | ✓ | | | | | ✓ | |
| B.24 | ✓ | | | | ✓ | | | | ✓ | |
| B.25 | | ✓ | ✓ | | | | | | | ✓ |
| B.26 | | ✓ | | ✓ | | | | | | ✓ |
| B.27 | | ✓ | | | ✓ | | | | | ✓ |
| B.28 | ✓ | | ✓ | | | | | | | ✓ |
| B.29 | ✓ | | | ✓ | | | | | | ✓ |
| B.30 | ✓ | | | | ✓ | | | | | ✓ |

## B.1.   Scenario 1: Austral Winter run, dredging in NW of 20 year mining plan area
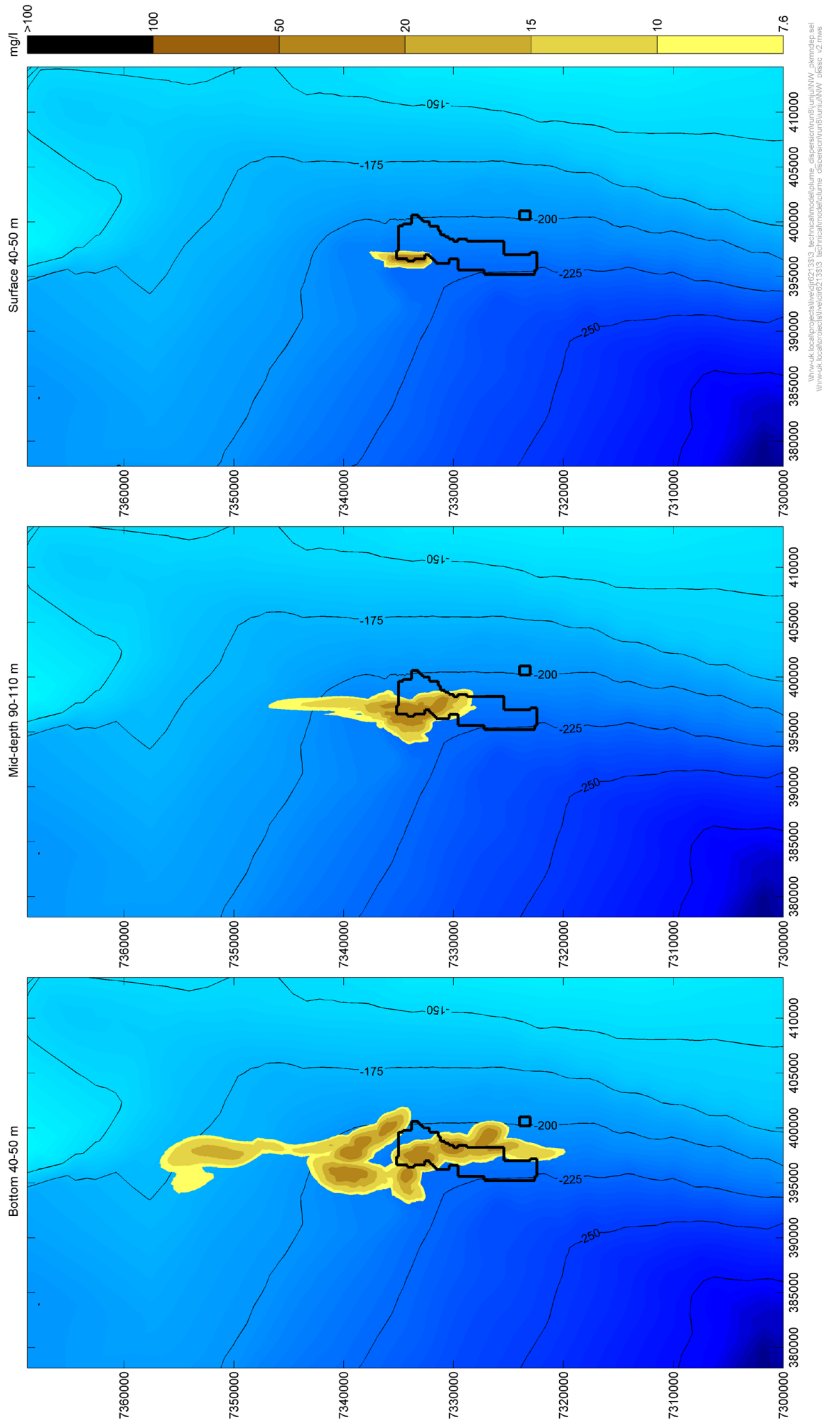


Figure B.1: Peak predicted increases of suspended sediment concentration at the Bottom (left), Middle (middle) and Top (right) of the water column, Scenario 1: Austral Winter run, dredging in NW of 20 year mining plan area
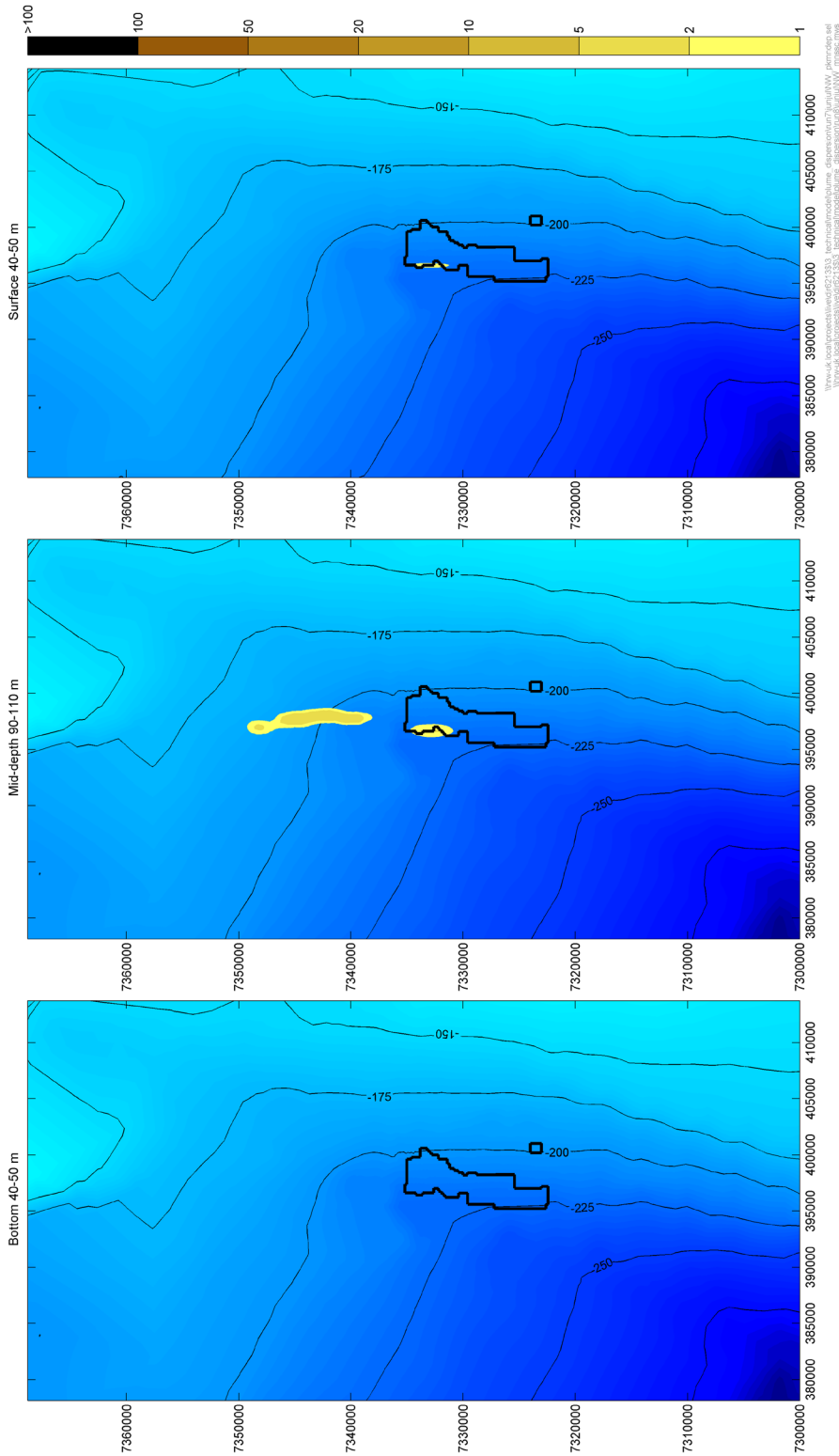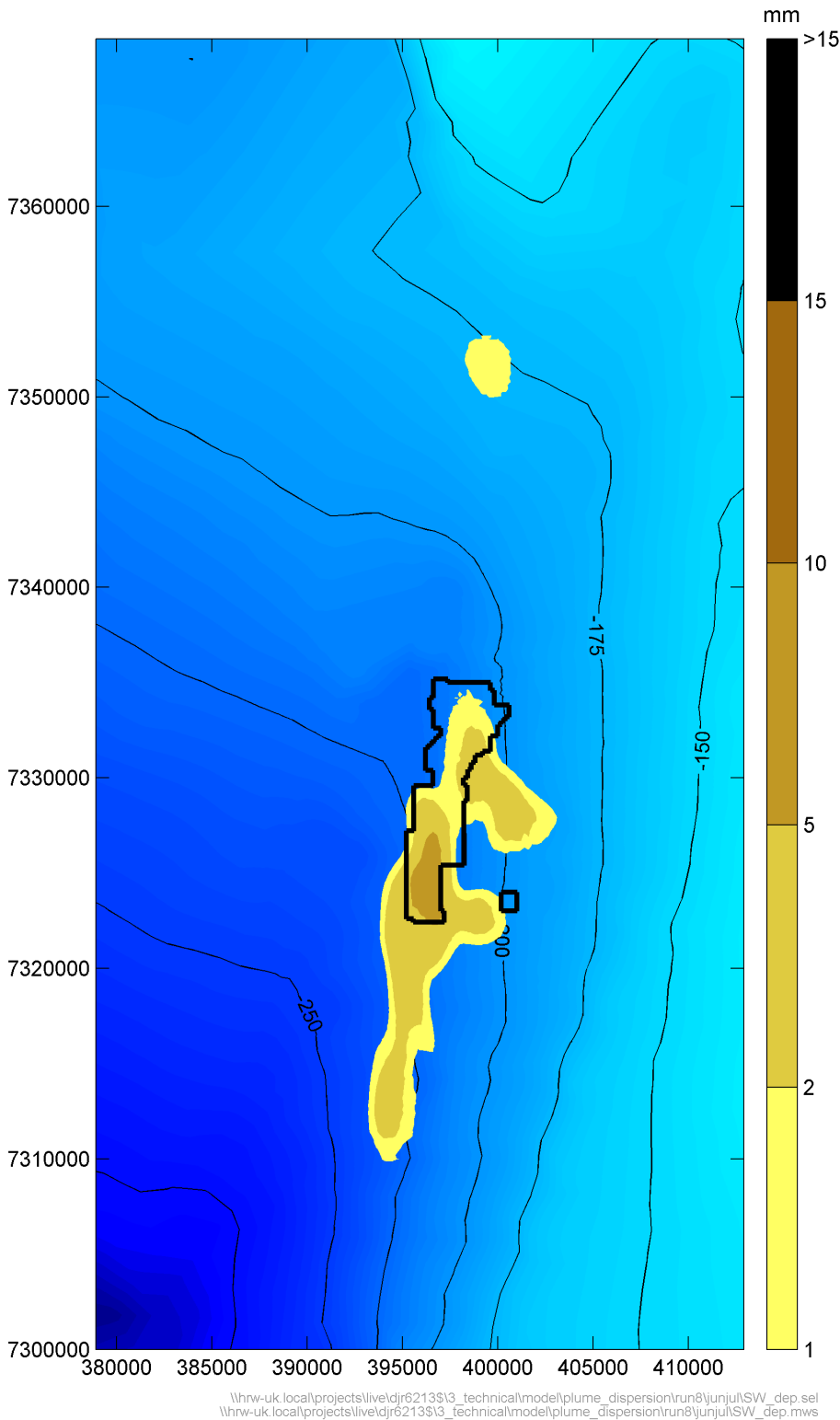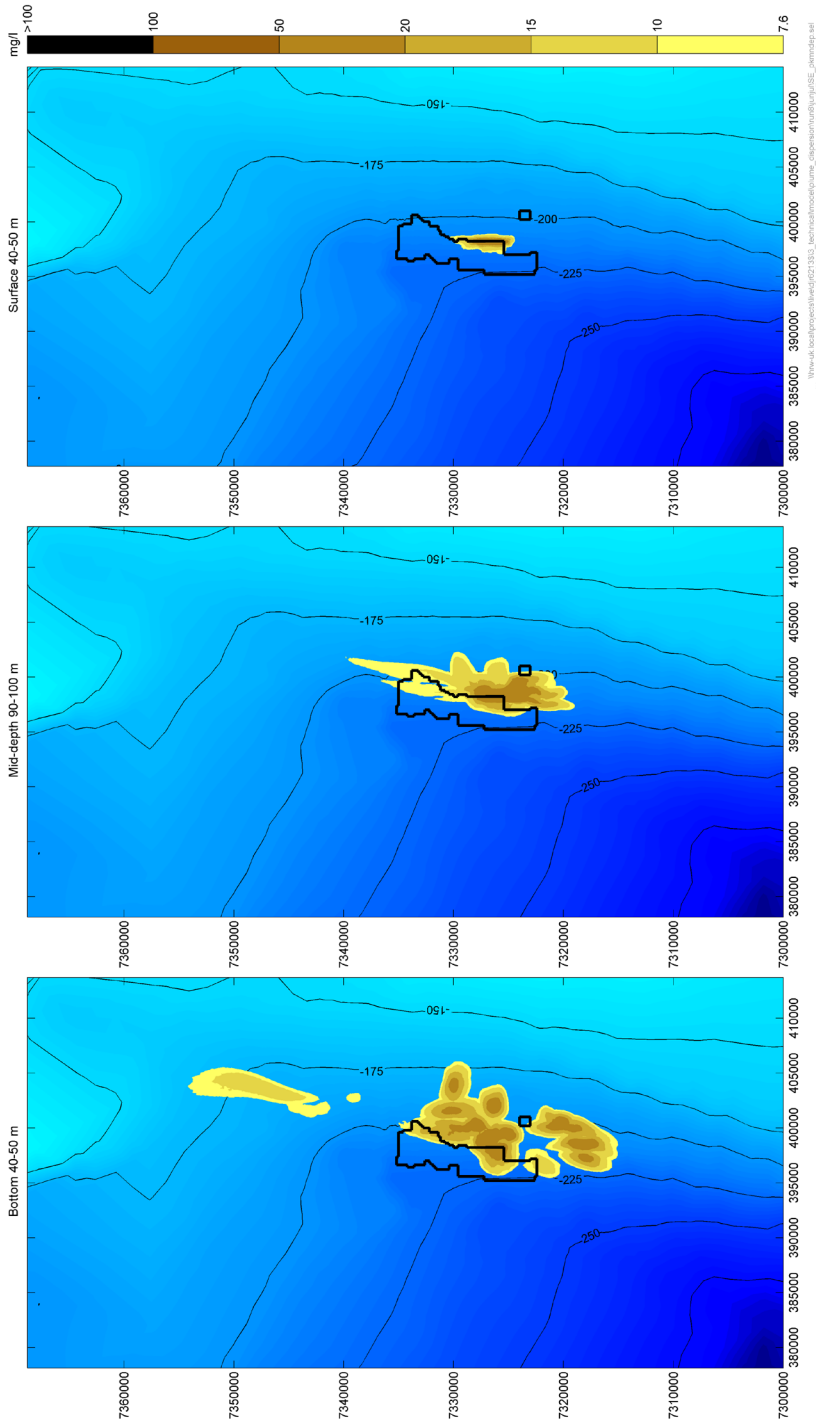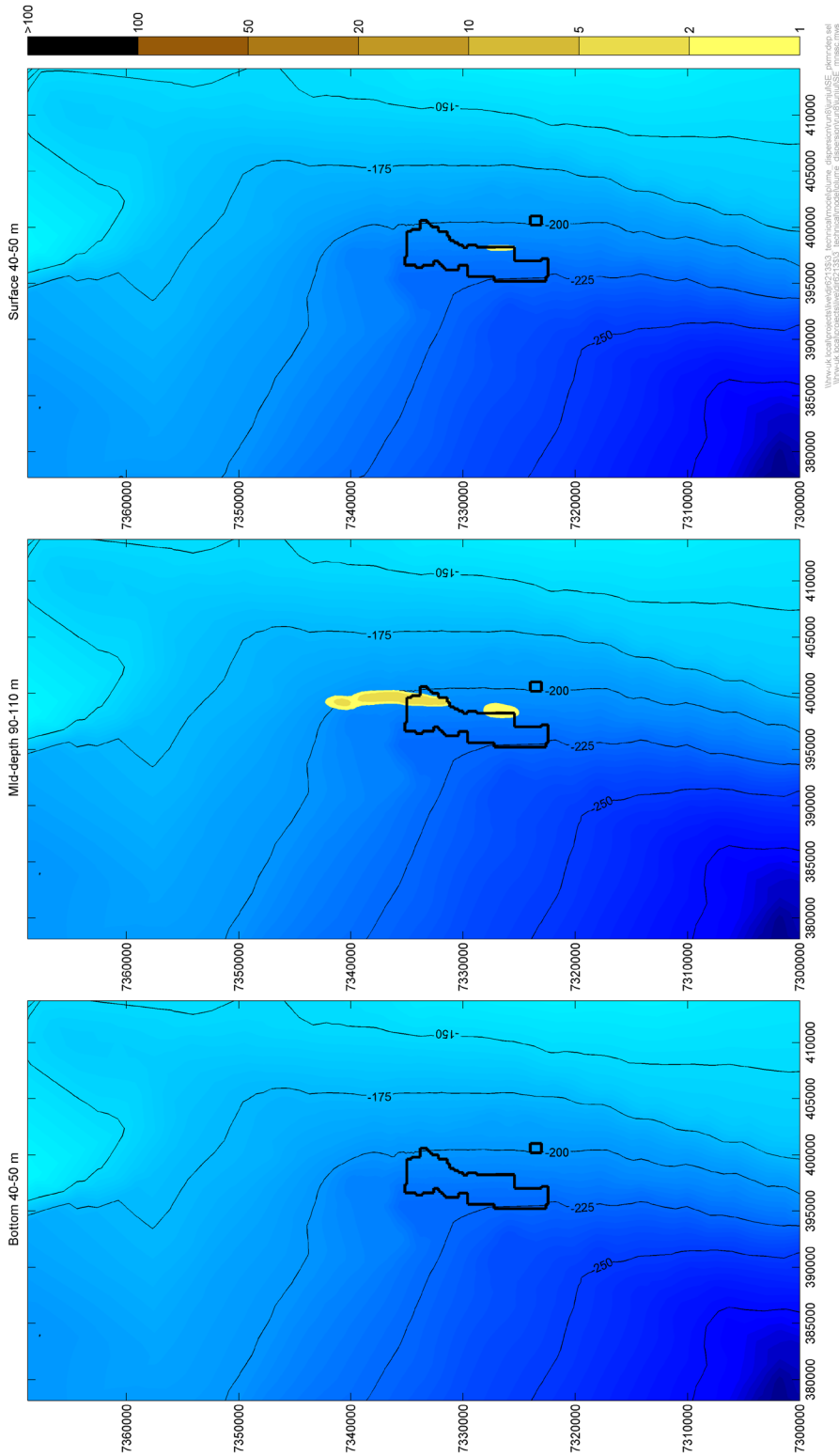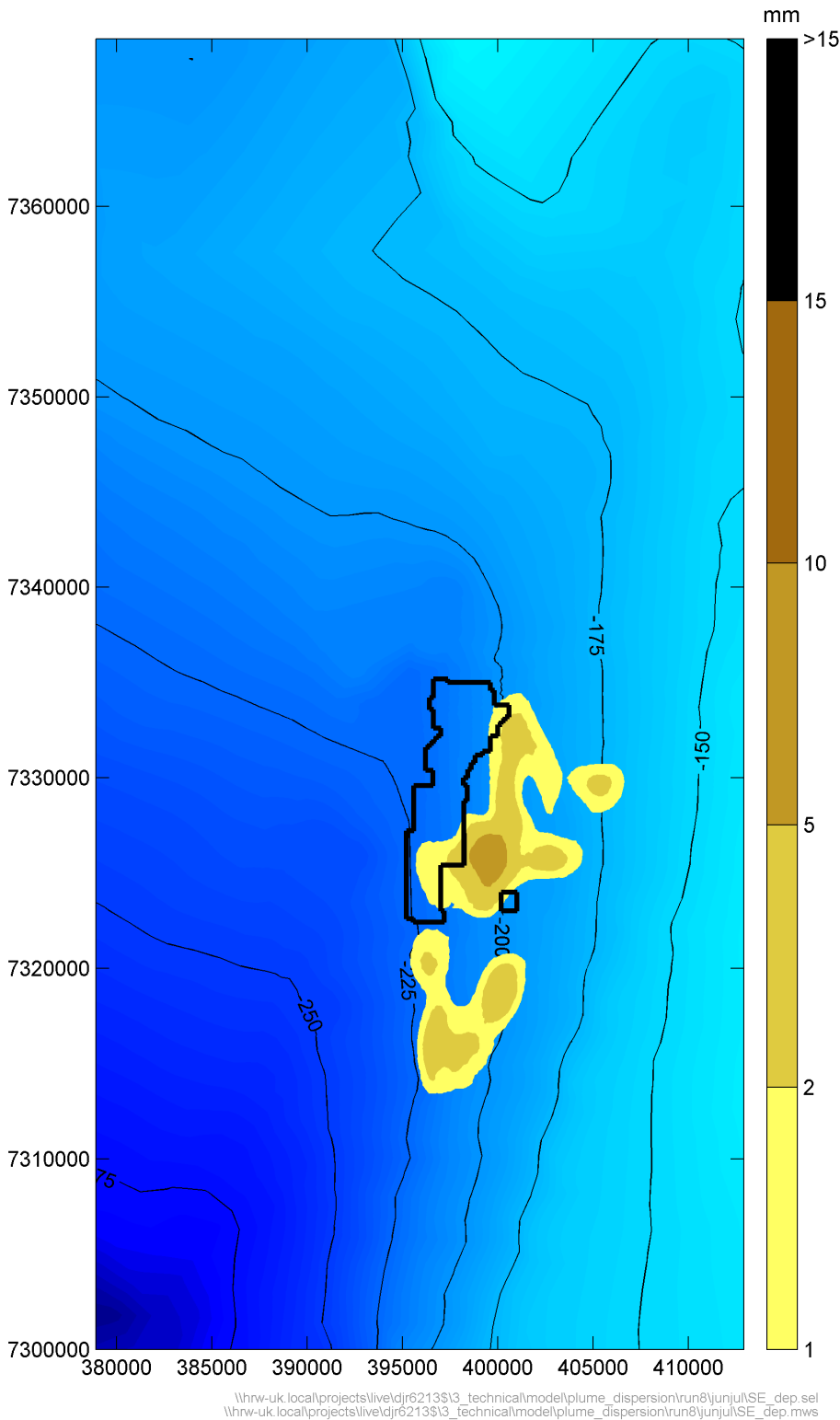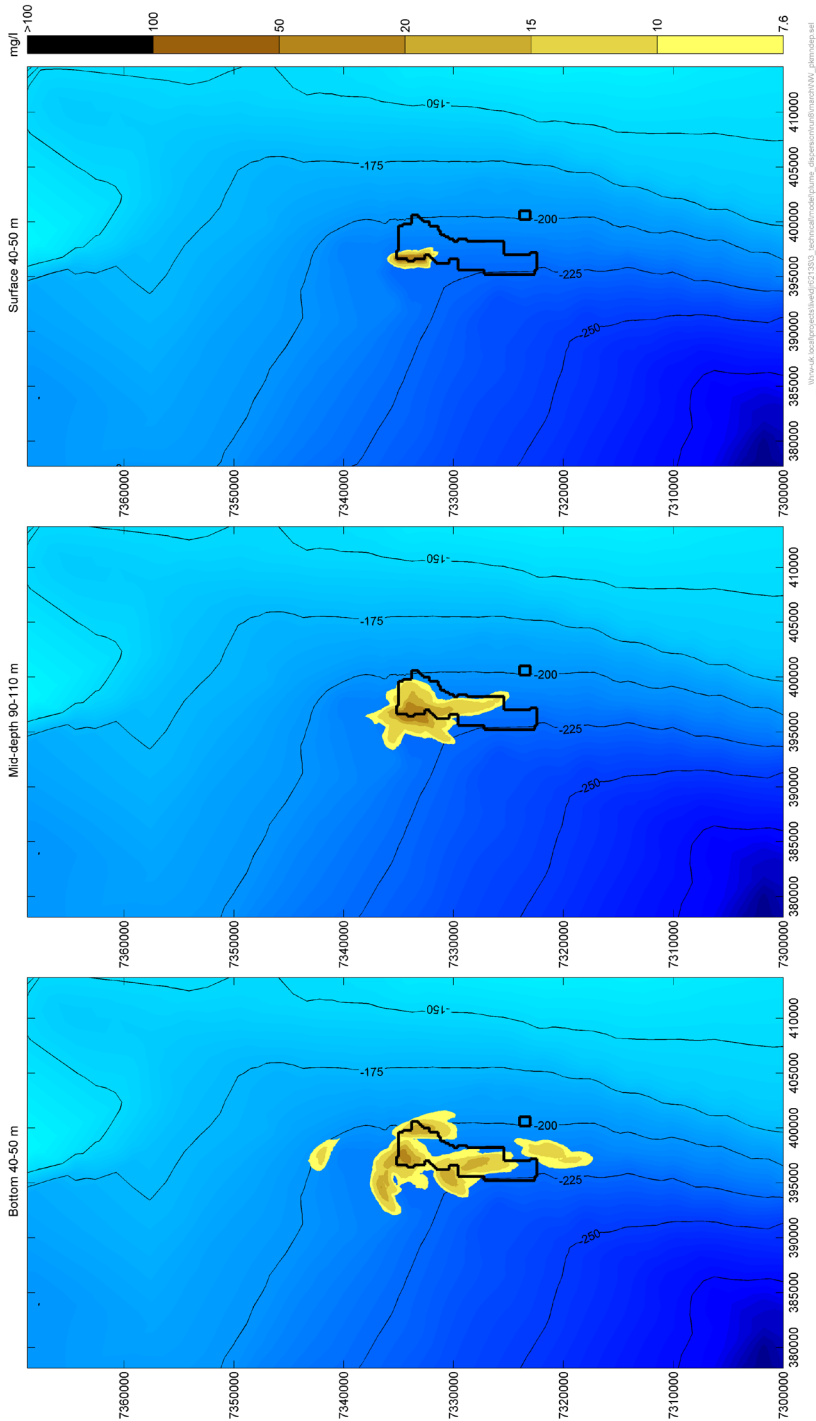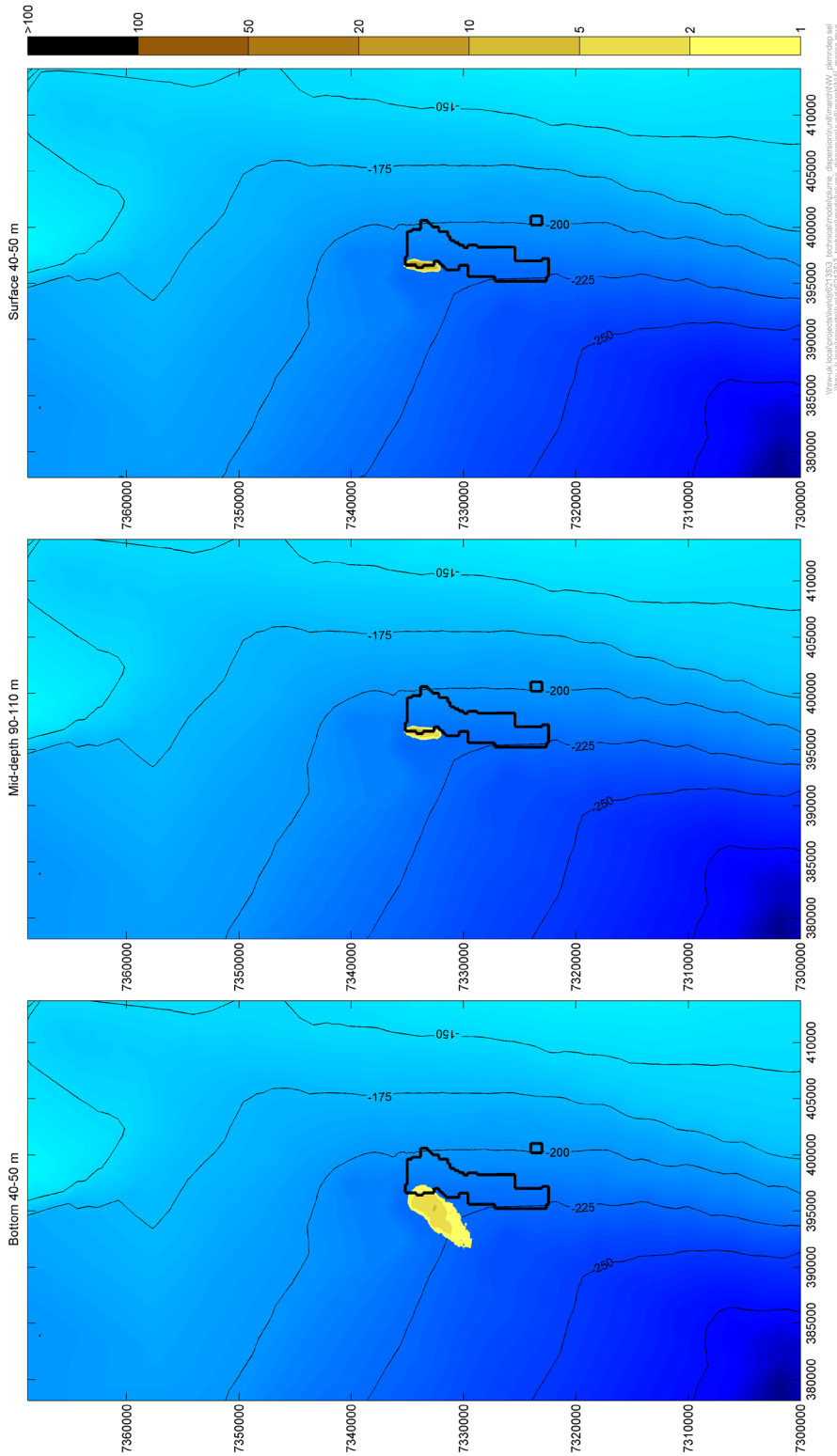
Figure B.2: Mean predicted increases of suspended sediment concentration at the Bottom (left), Middle (middle) and Top (right) of the water column, Scenario 1: Austral Winter run, dredging in NW of 20 year mining plan area
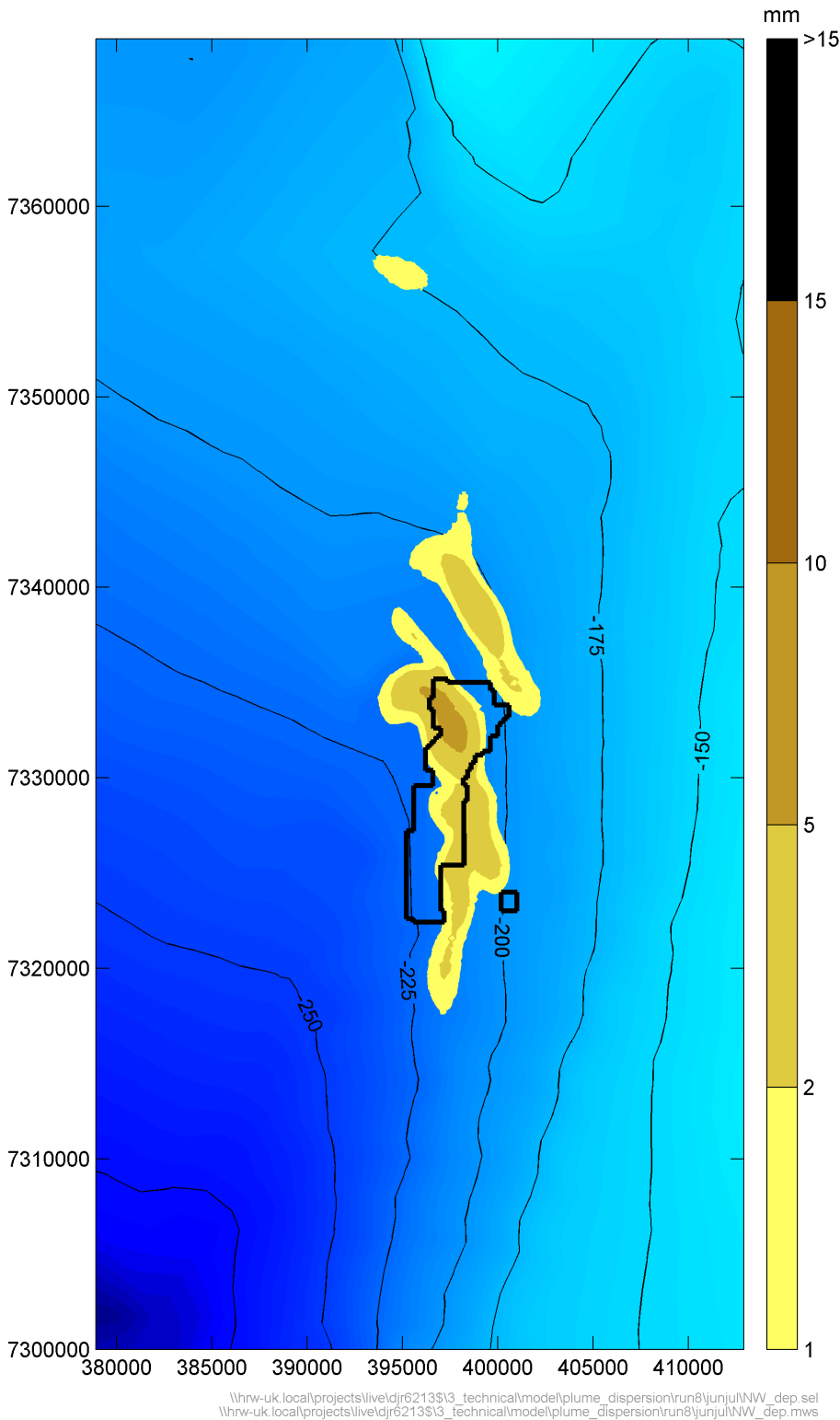
Figure B.3: Predicted sediment deposition after 45 days of dredging, Scenario 1: Austral Winter run, dredging in NW of 20 year mining plan area

## B.2. Scenario 2: Austral Winter run, dredging in NE of 20 year mining plan area
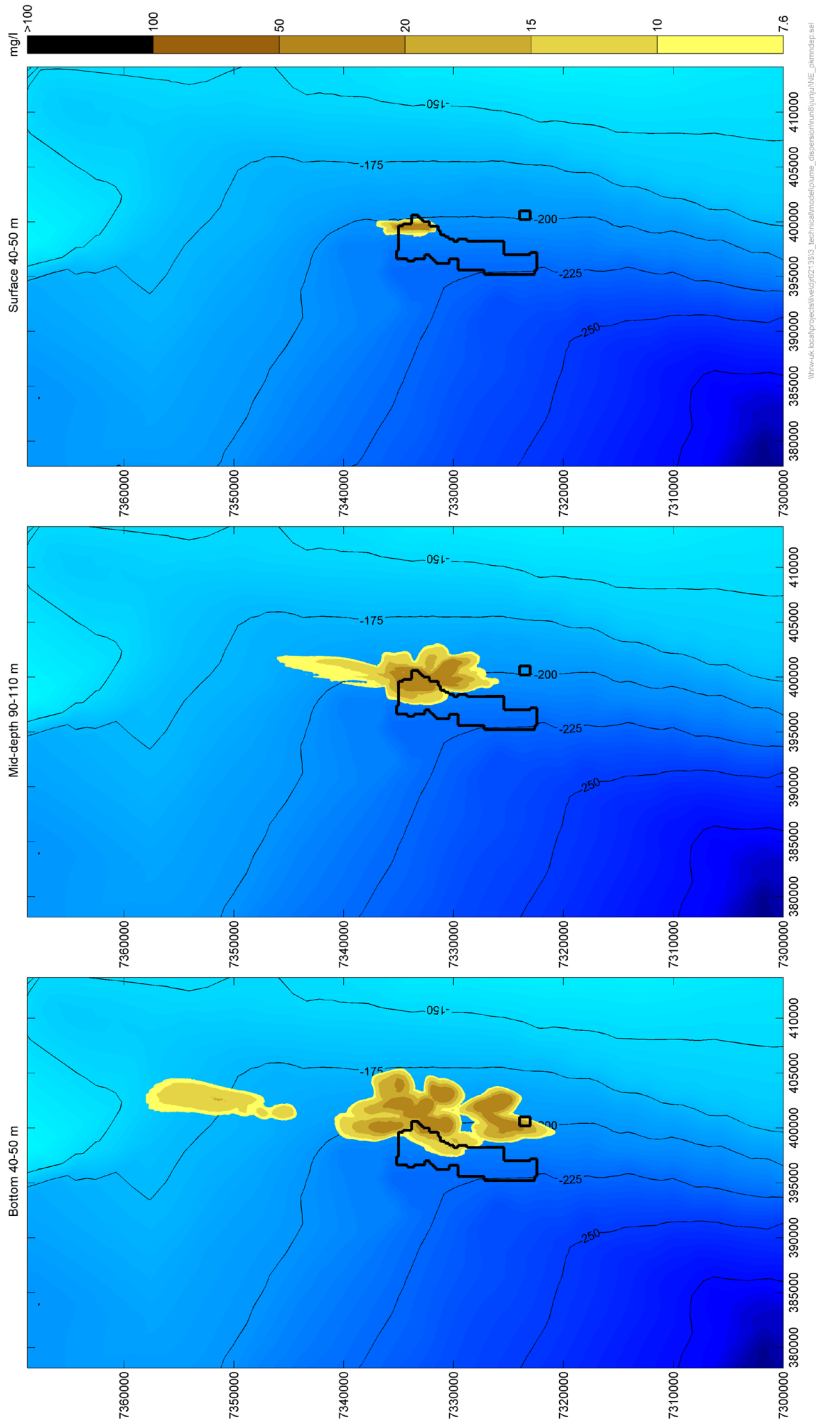


Figure B.4: Peak predicted increases of suspended sediment concentration at the Bottom (left), Middle (middle) and Top (right) of the water column, Scenario 2: Austral Winter run, dredging in NE of 20 year mining plan area
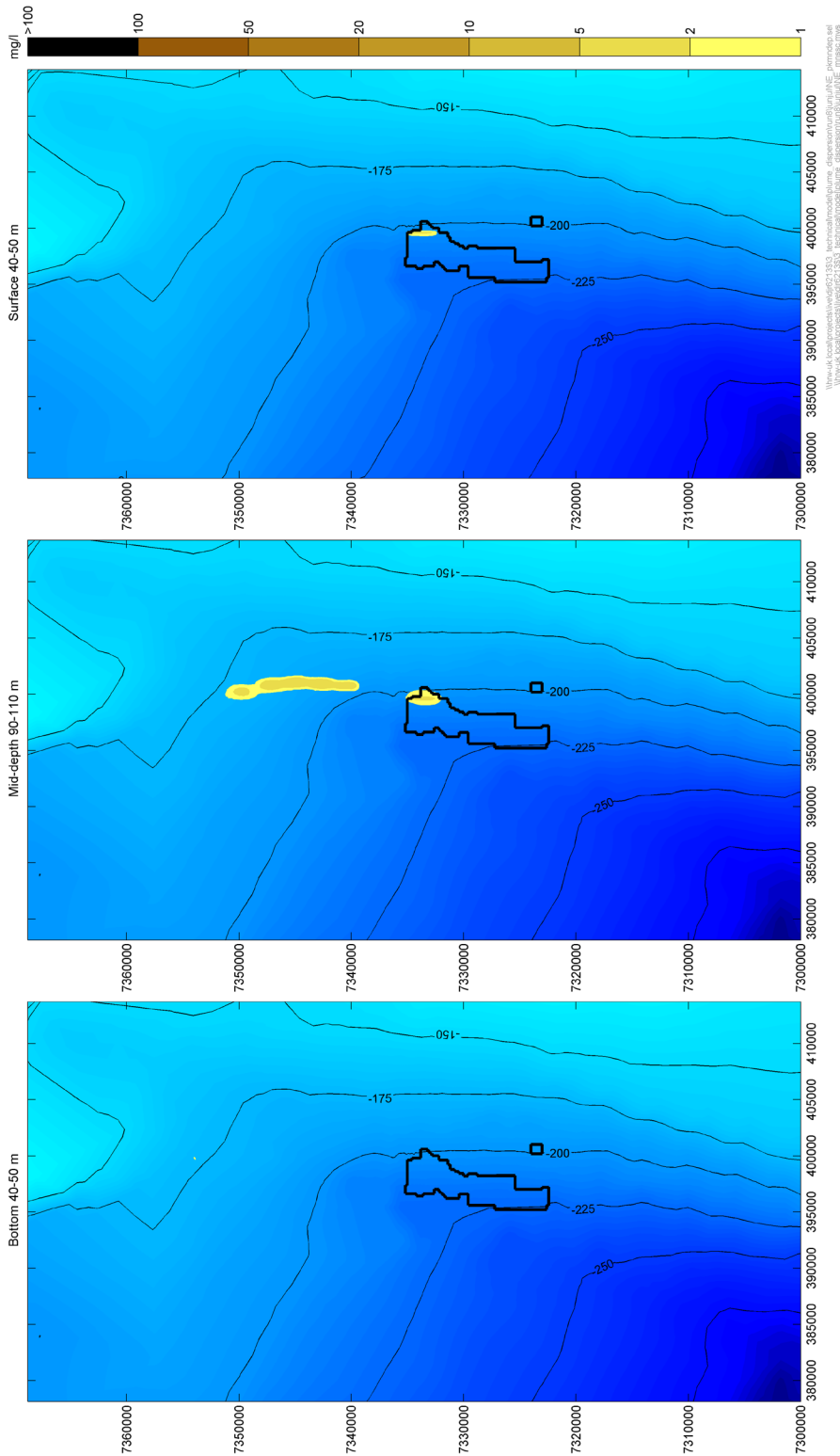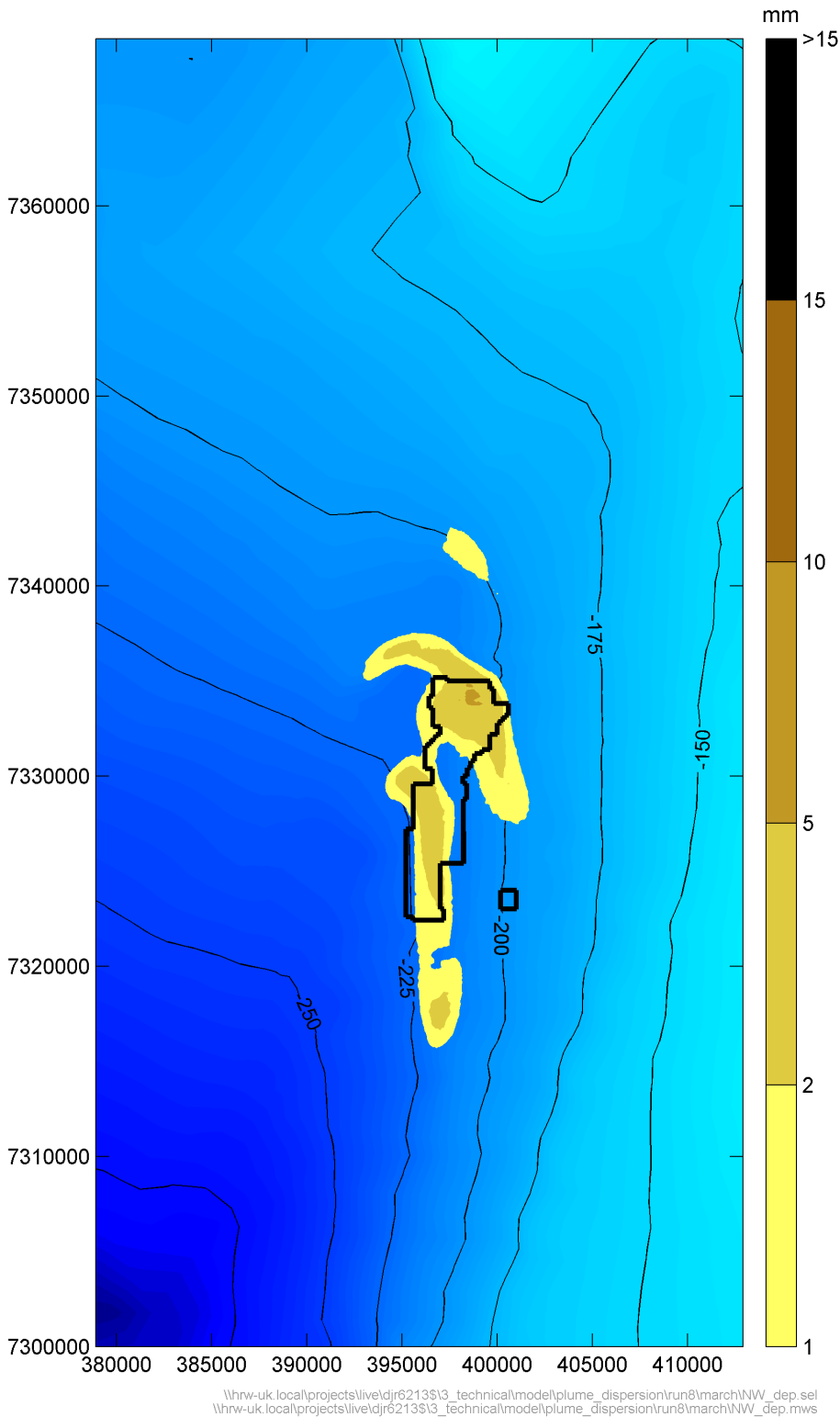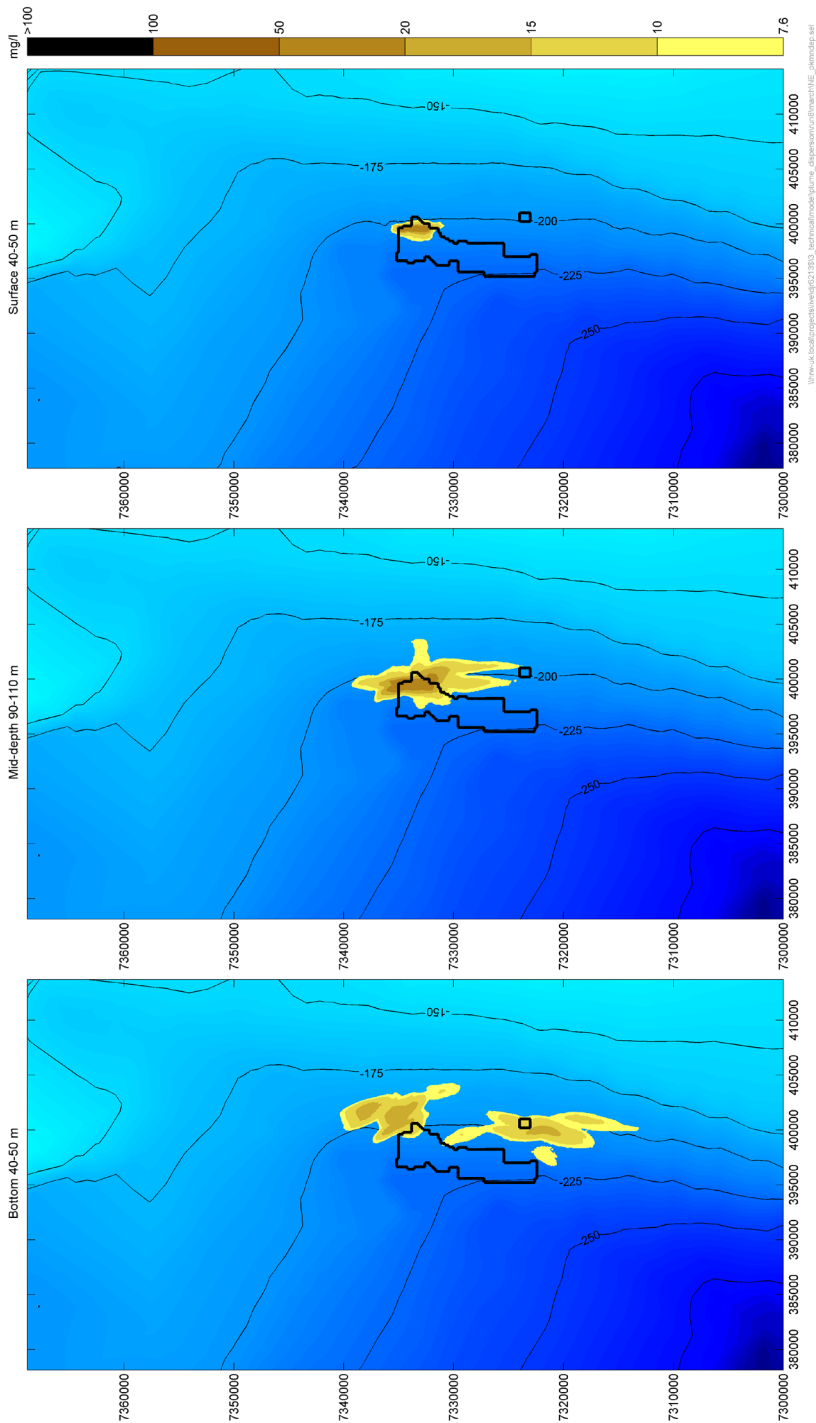
Figure B.5: Mean predicted increases of suspended sediment concentration at the Bottom (left), Middle (middle) and Top (right) of the water column, Scenario 2: Austral Winter run, dredging in NE of 20 year mining plan area
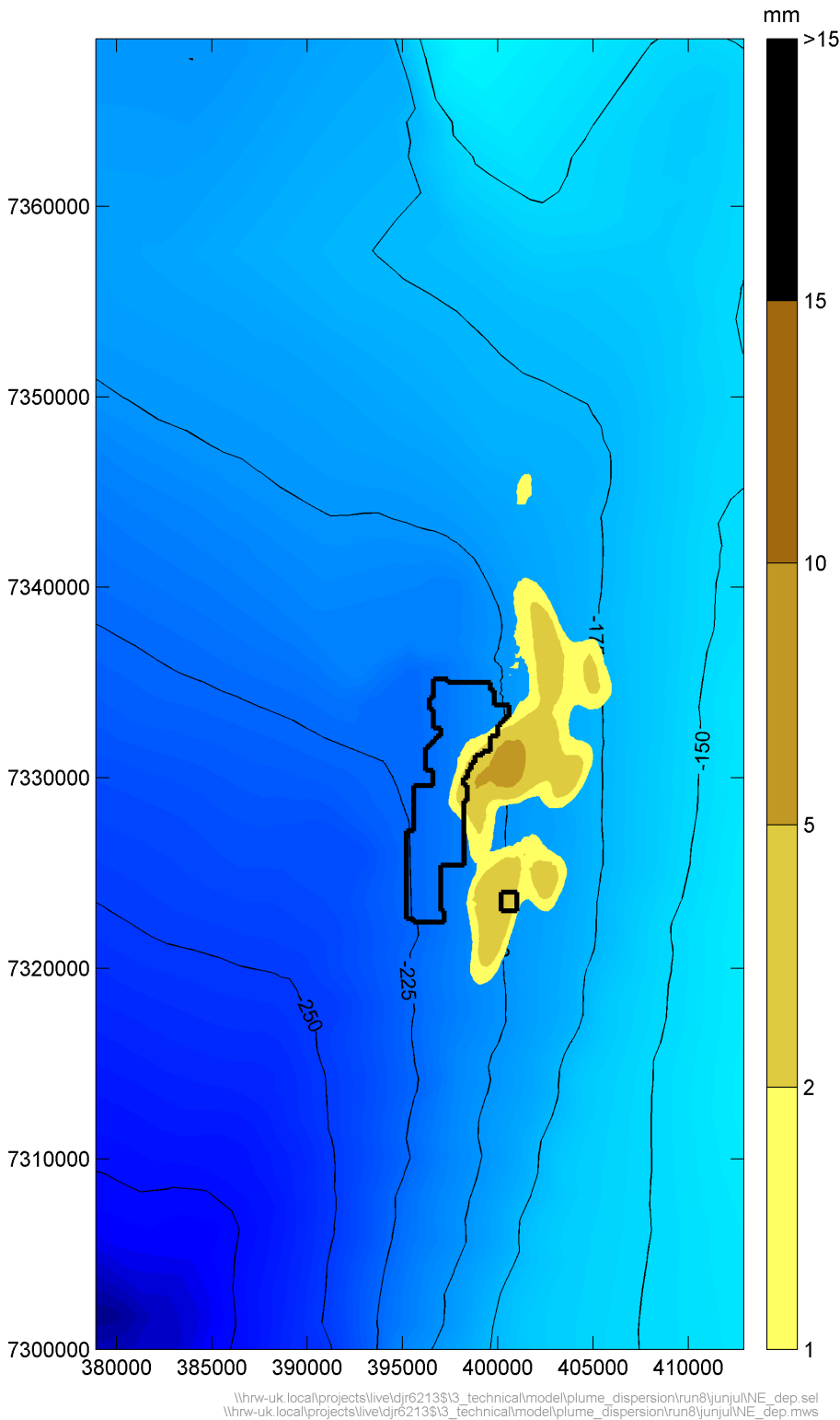
Figure B.6: Predicted sediment deposition after 45 days of dredging, Scenario 2: Austral Winter run, dredging in NE of 20 year mining plan area

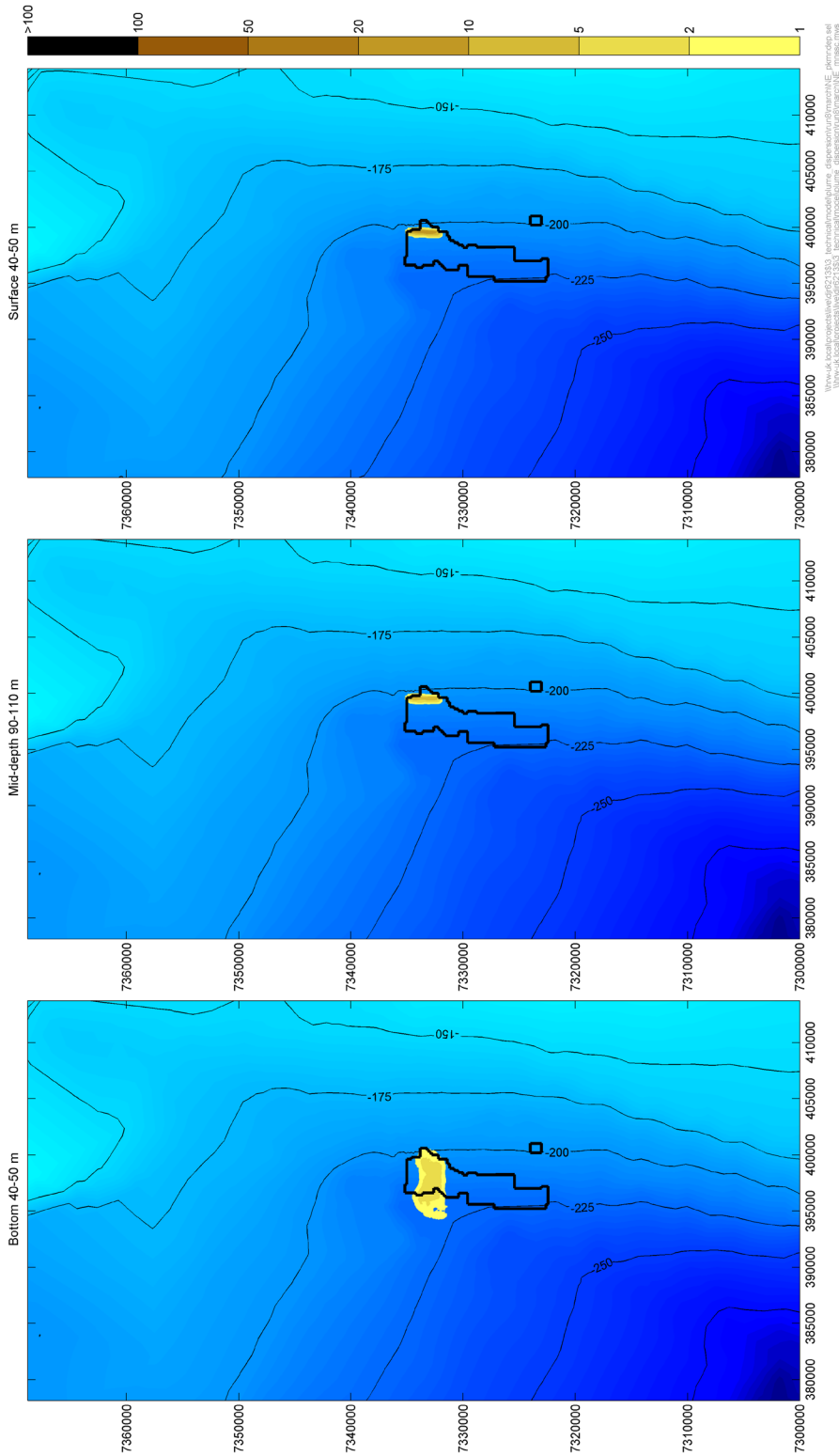## B.3. Scenario 3: Austral Winter run, dredging in SW of 20 year mining plan area
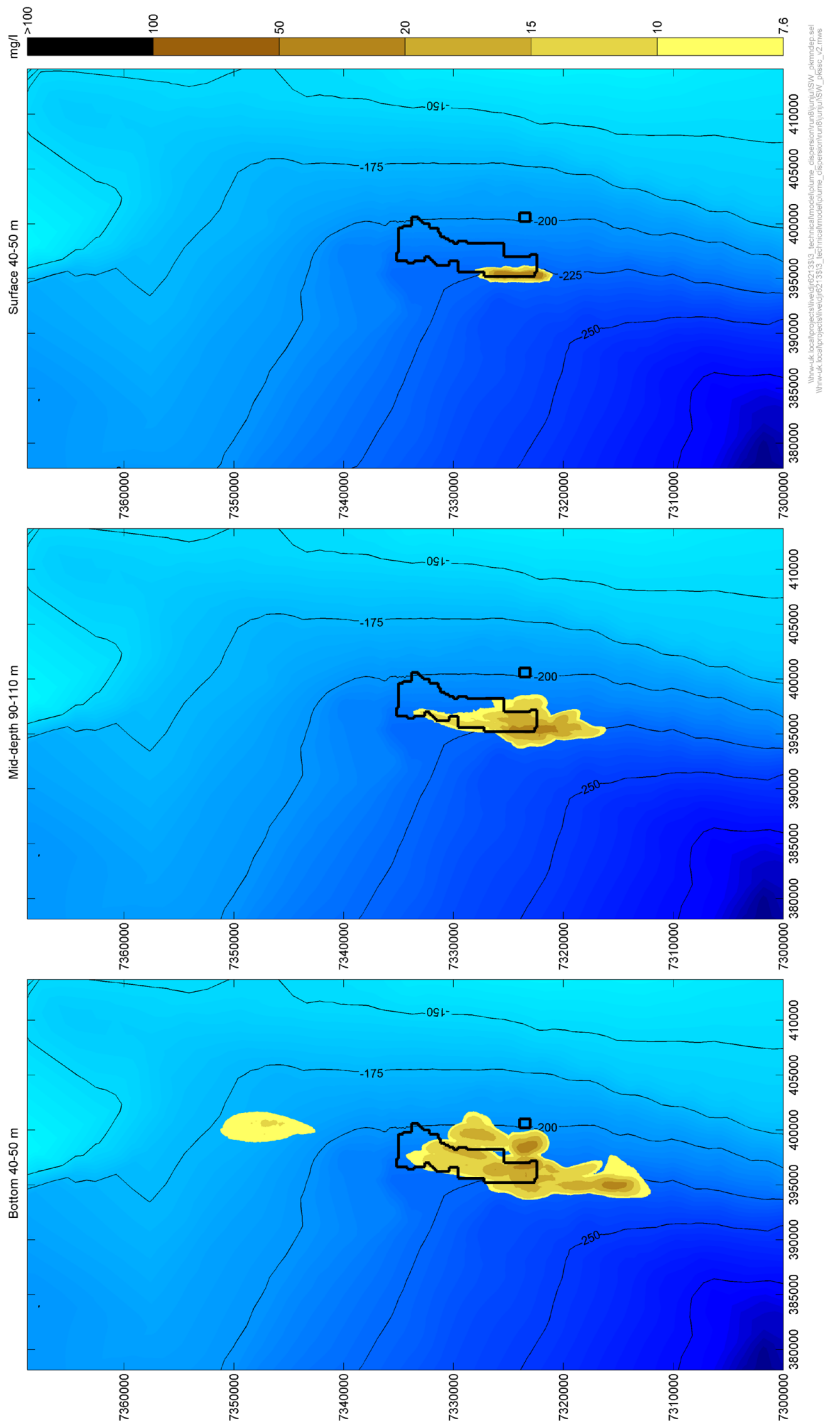


Figure B.7: Peak predicted increases of suspended sediment concentration at the Bottom (left), Middle (middle) and Top (right) of the water column, Scenario 3: Austral Winter run, dredging in SW of 20 year mining plan area
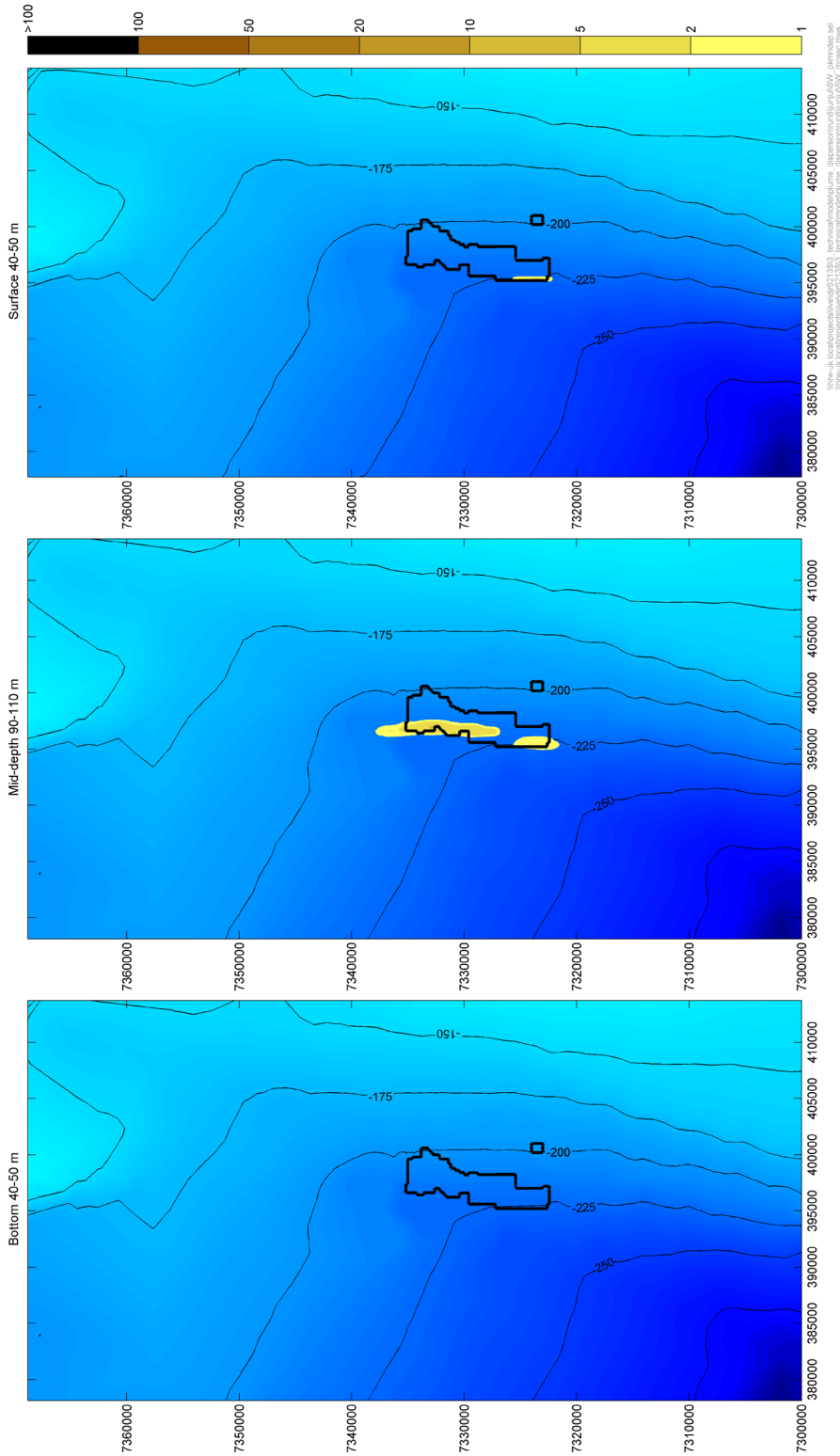
Figure B.8: Mean predicted increases of suspended sediment concentration at the Bottom (left), Middle (middle) and Top (right) of the water column, Scenario 2: Austral Winter run, dredging in NE of 20 year mining plan area

\\hrw-uk.local\projects\live\djr6213$\3_technical\model\plume_dispersion\run8\junjul\SW_dep.sel
\\hrw-uk.local\projects\live\djr6213$\3_technical\model\plume_dispersion\run8\junjul\SW_dep.mws

Figure B.9: Predicted sediment deposition after 45 days of dredging, Scenario 3: Austral Winter run, dredging in SW of 20 year mining plan area

## B.4. Scenario 4: Austral Winter run, dredging in SE of 20 year mining plan area
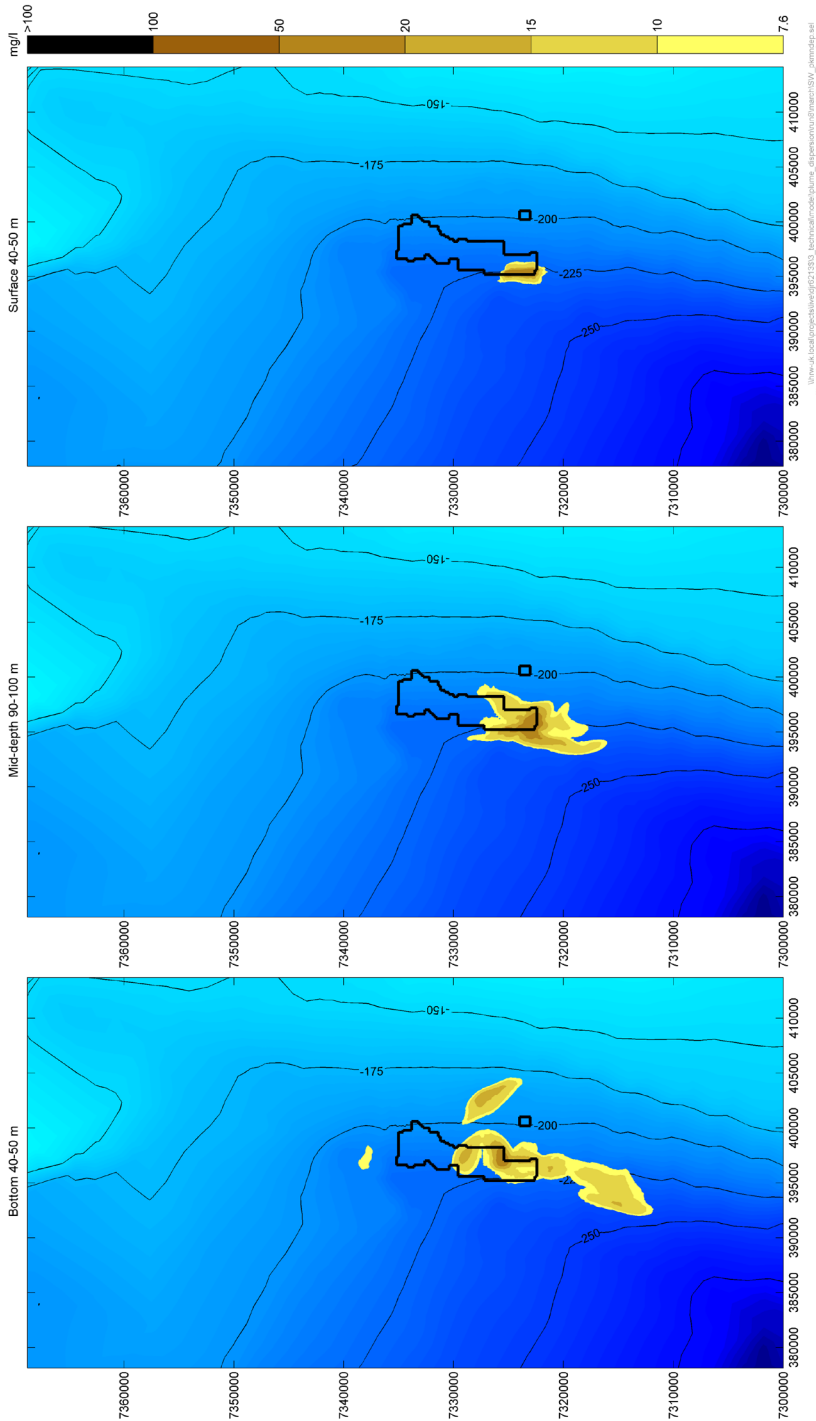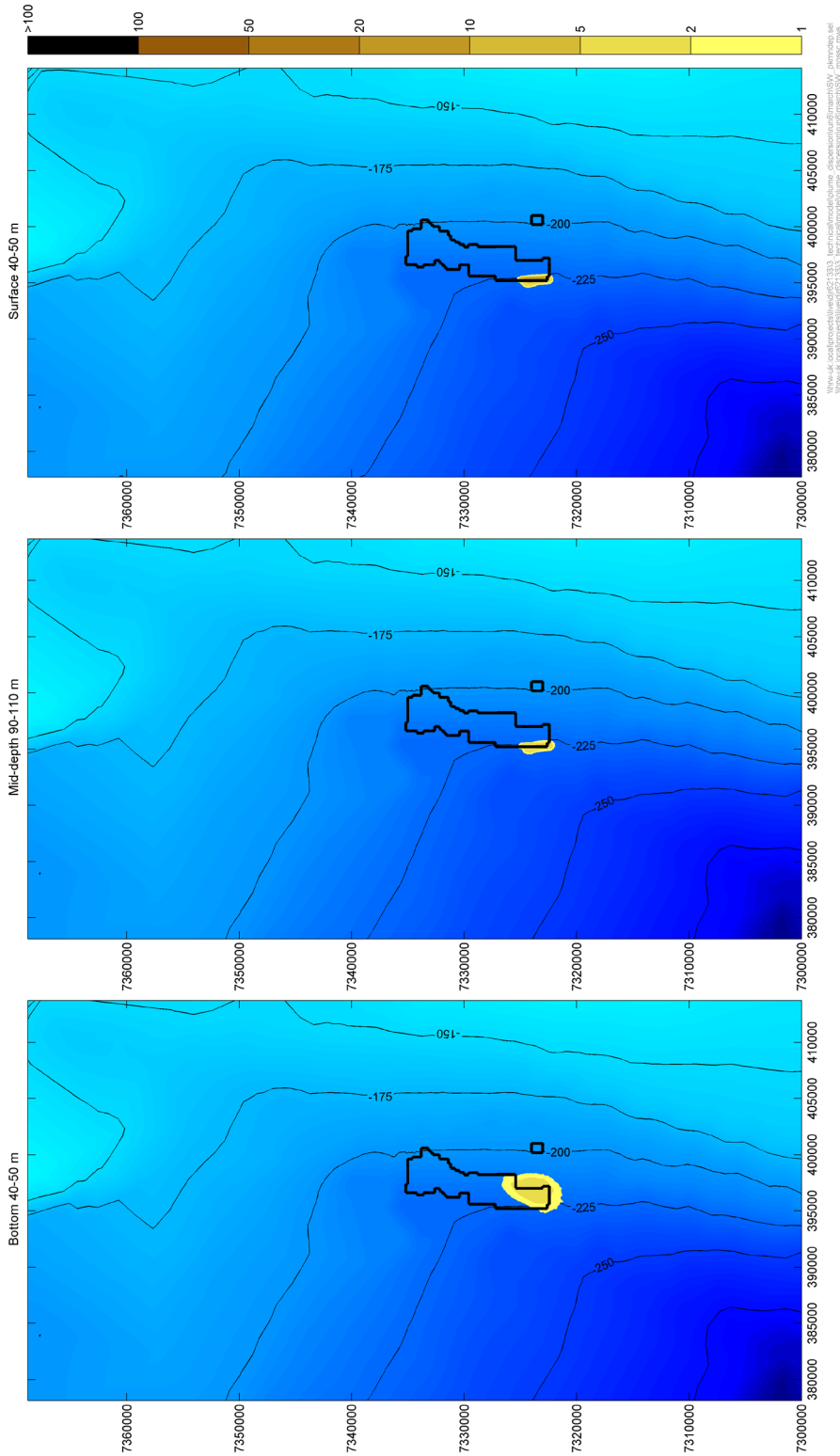


Figure B.10: Peak predicted increases of suspended sediment concentration at the Bottom (left), Middle (middle) and Top (right) of the water column, Scenario 4: Austral Winter run, dredging in SE of 20 year mining plan area

Figure B.11: Mean predicted increases of suspended sediment concentration at the Bottom (left), Middle (middle) and Top (right) of the water column, Scenario 4: Austral Winter run, dredging in SE of 20 year mining plan area
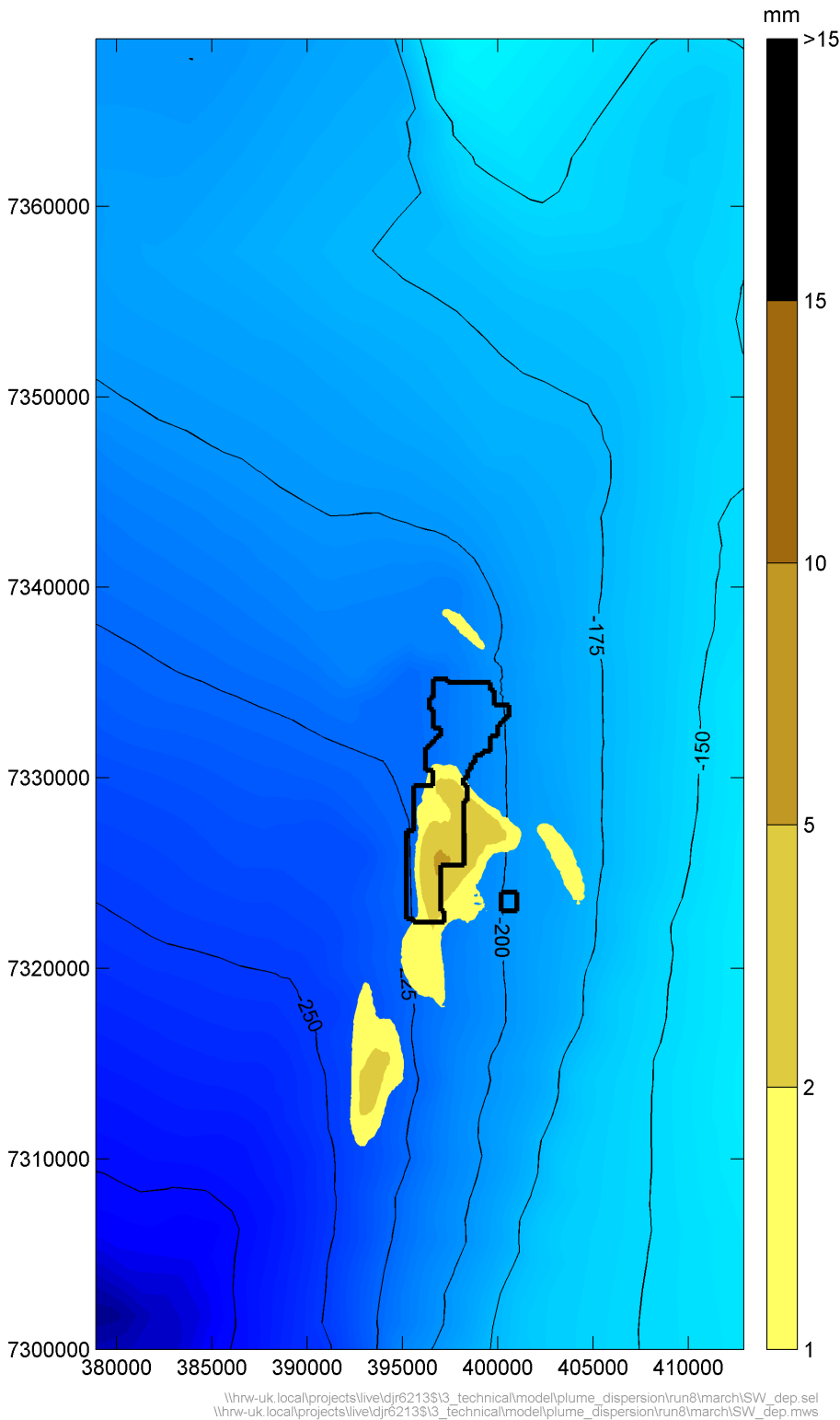
Figure B.12: Predicted sediment deposition after 45 days of dredging, Scenario 4: Austral Winter run, dredging in SE of 20 year mining plan area

## B.5. Scenario 5: Austral Summer run, dredging in NW of 20 year mining plan area
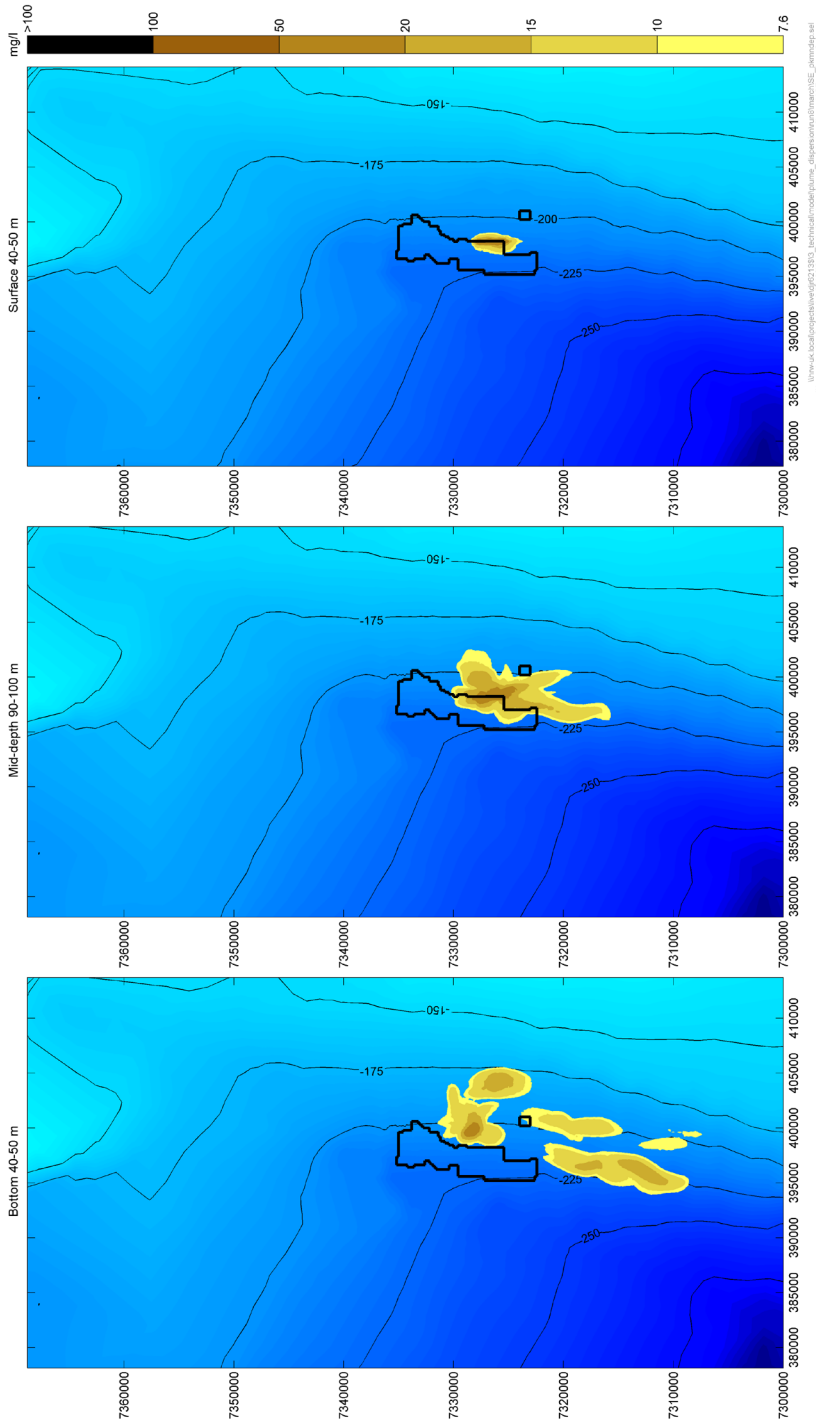
Figure B.13: Peak predicted increases of suspended sediment concentration at the Bottom (left), Middle (middle) and Top (right) of the water column, Scenario 5: Austral Summer run, dredging in NW of 20 year mining plan area
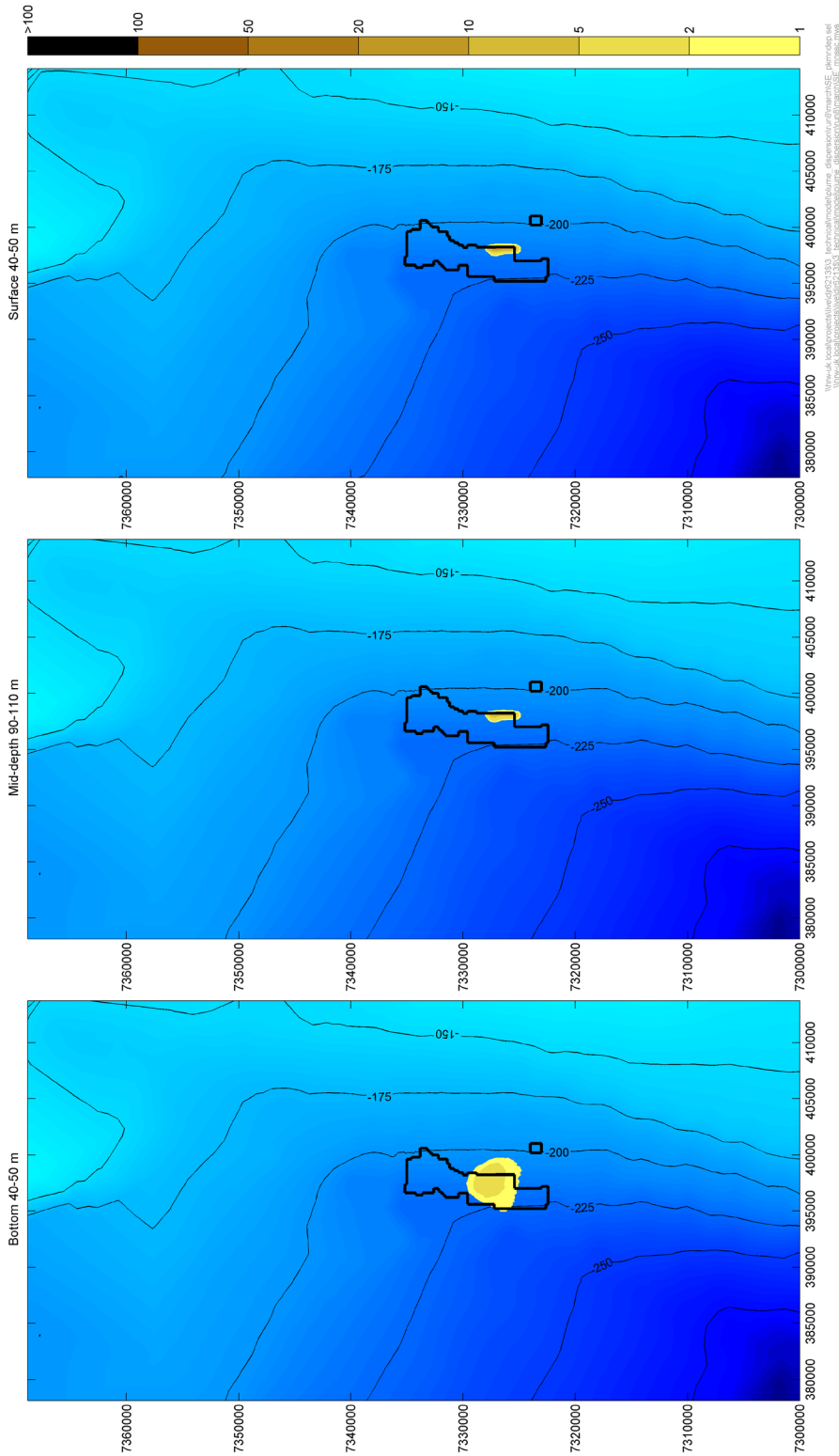
Figure B.14: Mean predicted increases of suspended sediment concentration at the Bottom (left), Middle (middle) and Top (right) of the water column, Scenario 5: Austral Summer run, dredging in NW of 20 year mining plan area

Figure B.15: Predicted sediment deposition after 32 days of dredging, Scenario 5: Austral Summer run, dredging in NW of 20 year mining plan area

## B.6. Scenario 6: Austral Summer run, dredging in NE of 20 year mining plan area



Figure B.16: Peak predicted increases of suspended sediment concentration at the Bottom (left), Middle (middle) and Top (right) of the water column, Scenario 6: Austral Summer run, dredging in NE of 20 year mining plan area
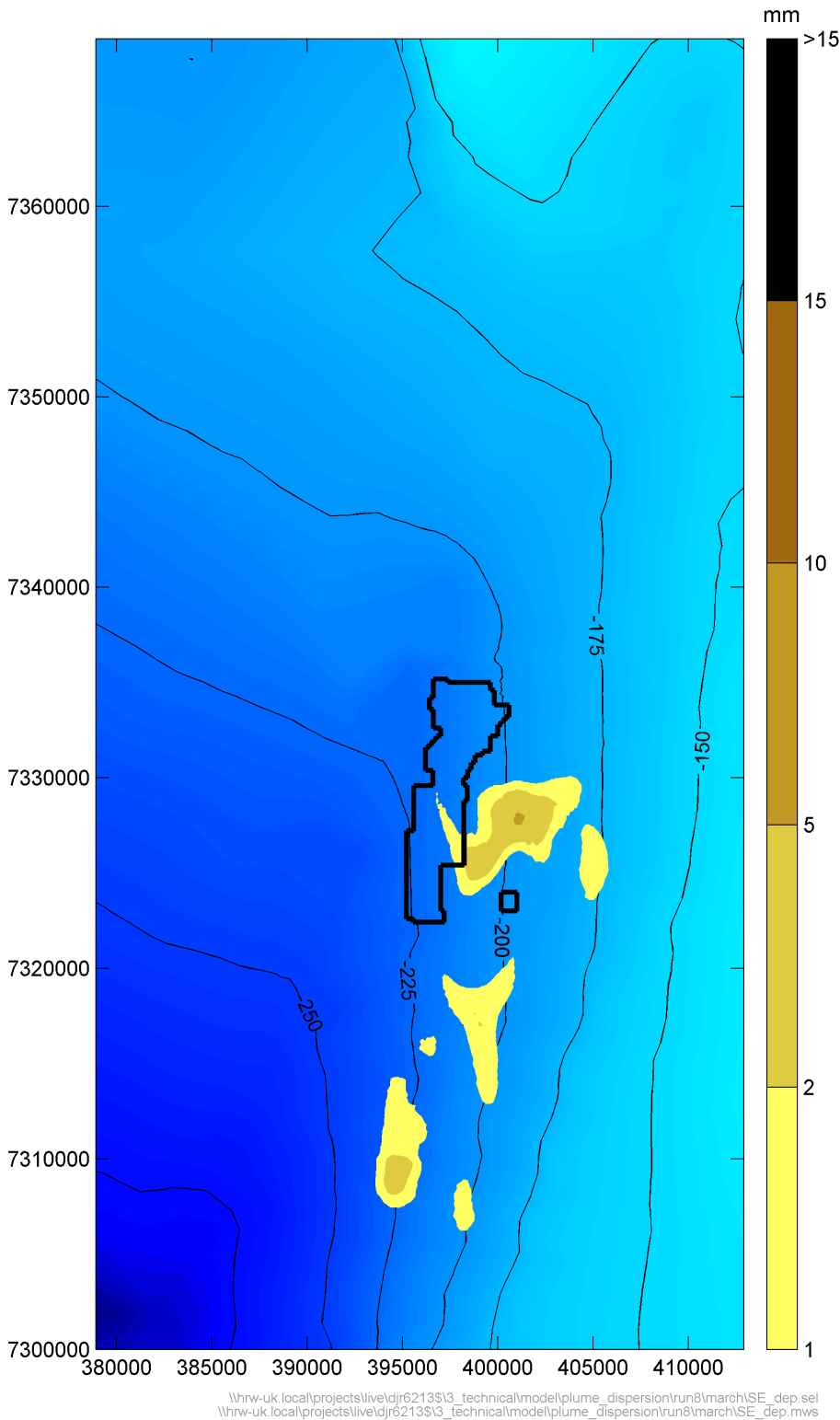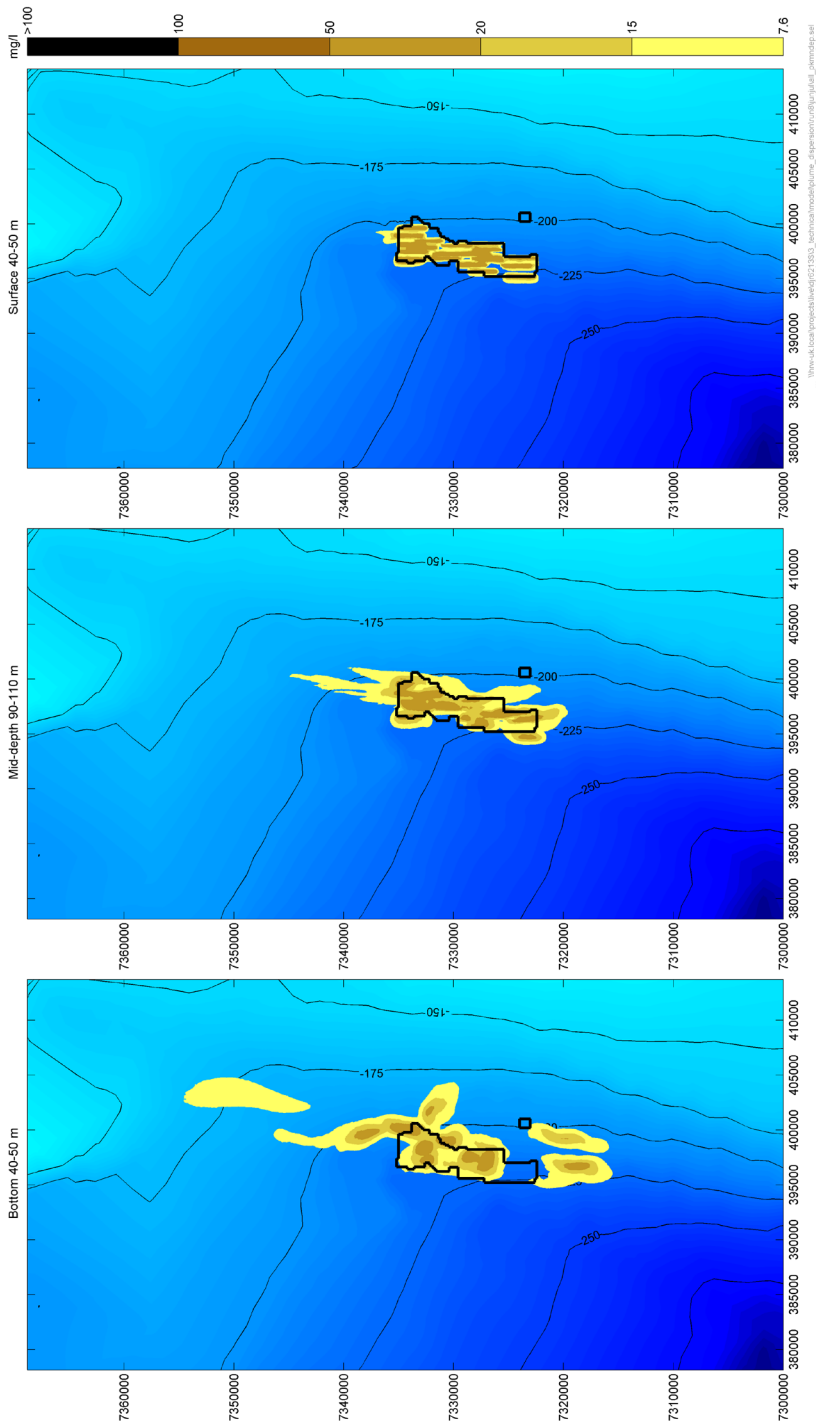
Figure B.17: Mean predicted increases of suspended sediment concentration at the Bottom (left), Middle (middle) and Top (right) of the water column, Scenario 6: Austral Summer run, dredging in NE of 20 year mining plan area
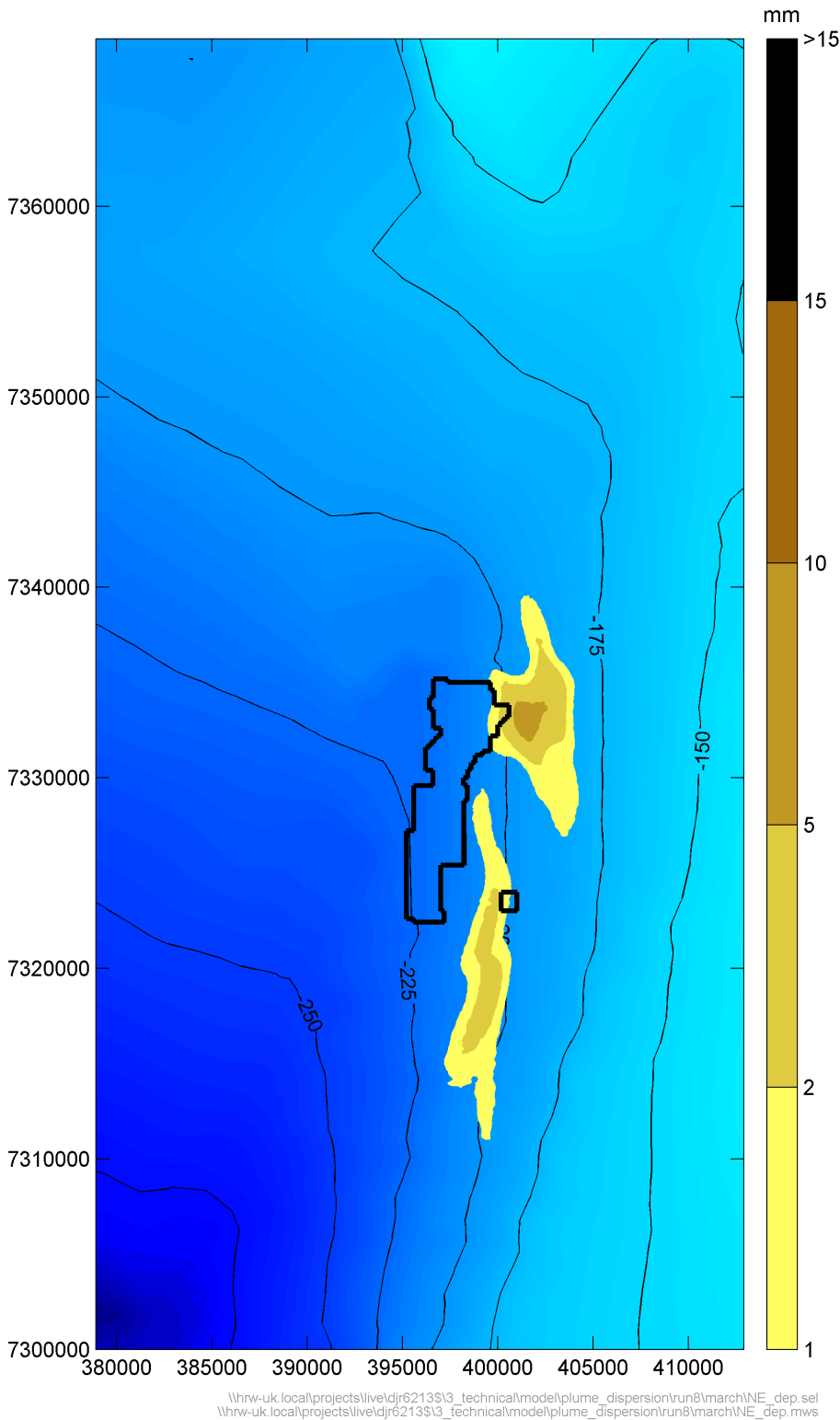
Figure B.18: Predicted sediment deposition after 32 days of dredging, Scenario 6: Austral Summer run, dredging in NE of 20 year mining plan area

## B.7.   Scenario 7: Austral Summer run, dredging in SW of 20 year mining plan area
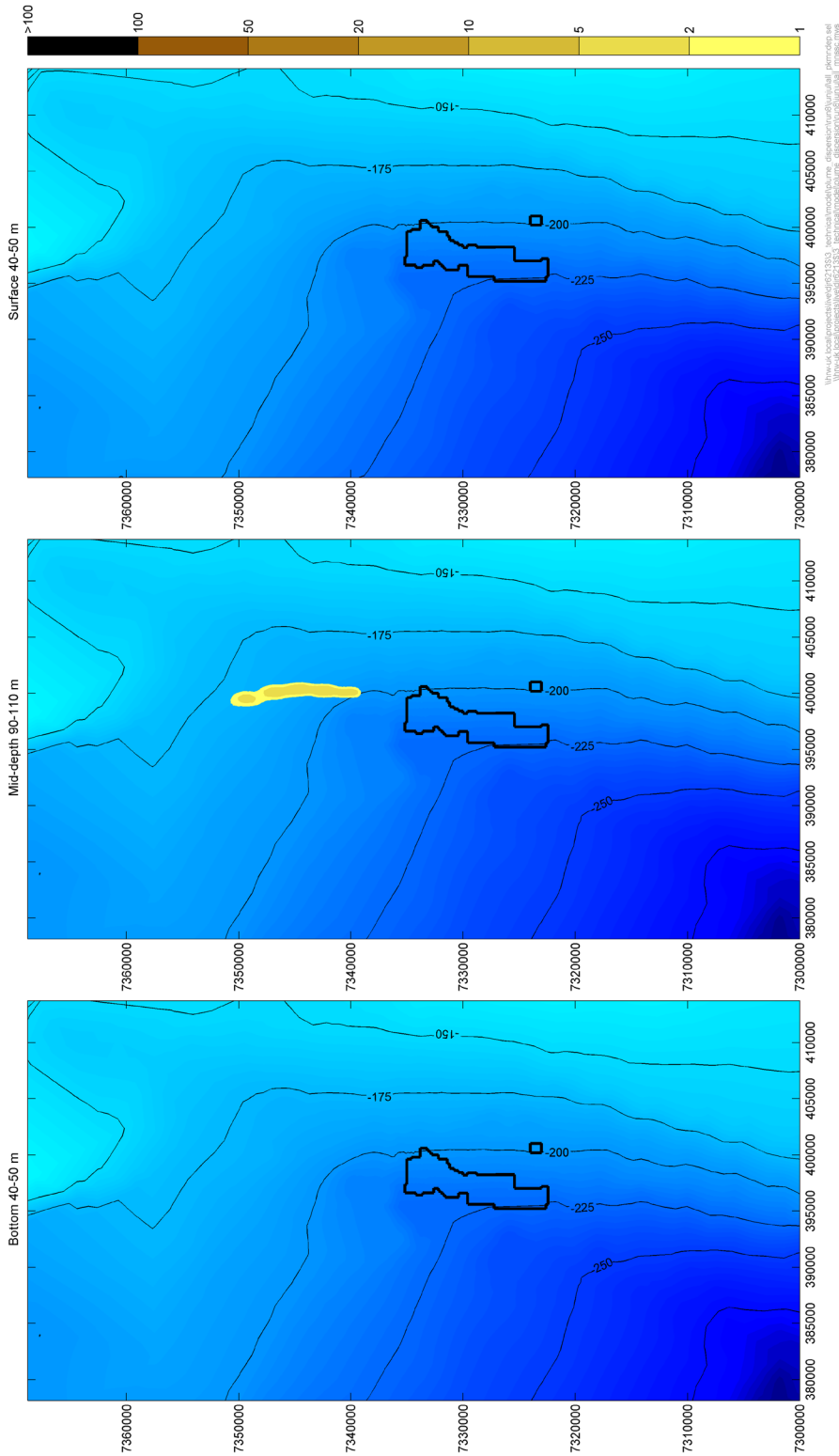


Figure B.19: Peak predicted increases of suspended sediment concentration at the Bottom (left), Middle (middle) and Top (right) of the water column, Scenario 7: Austral Summer run, dredging in SW of 20 year mining plan area

Figure B.20: Mean predicted increases of suspended sediment concentration at the Bottom (left), Middle (middle) and Top (right) of the water column, Scenario 7: Austral Summer run, dredging in SW of 20 year mining plan area

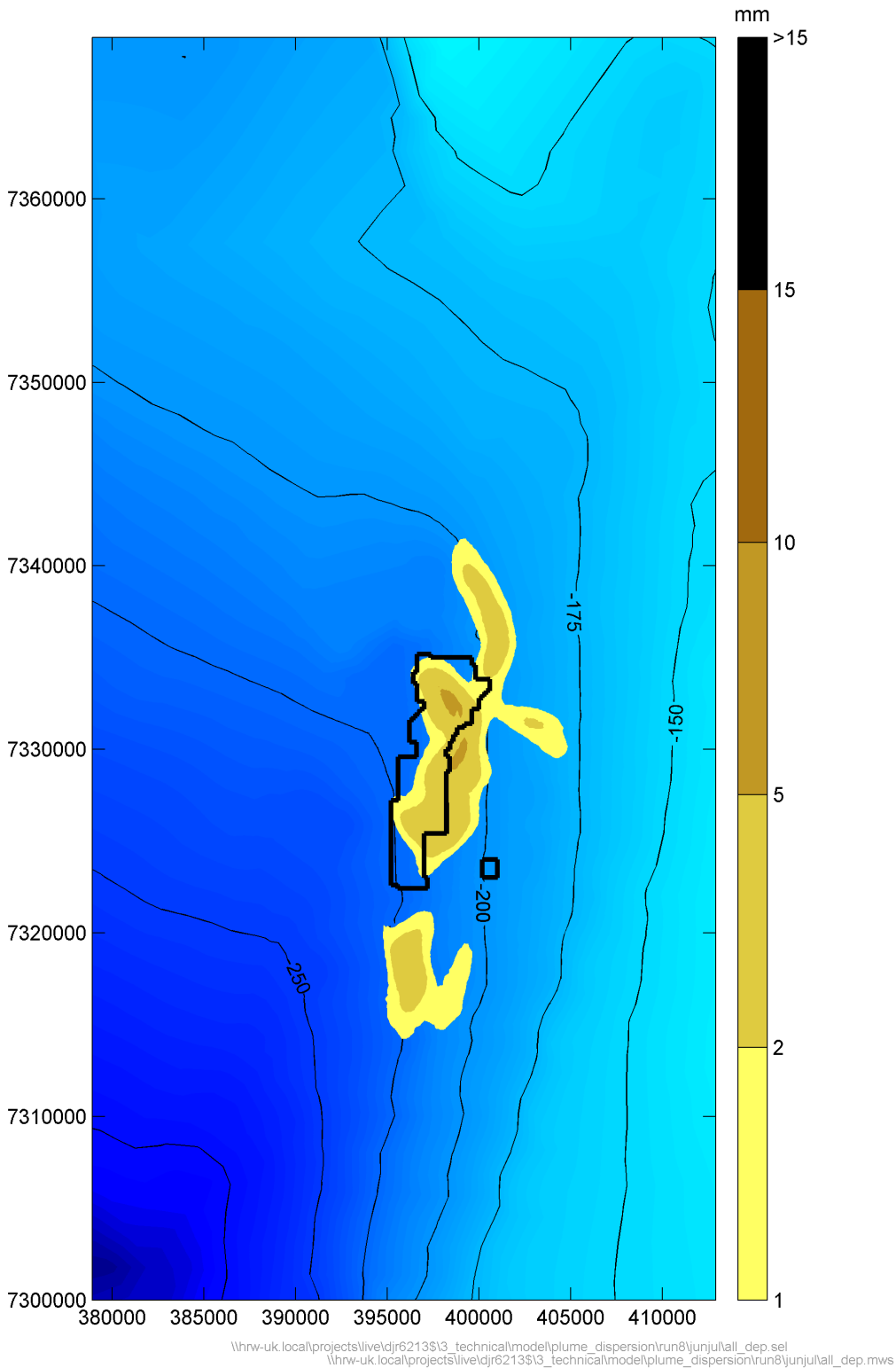Figure B.21: Predicted sediment deposition after 32 days of dredging, Scenario 7: Austral Summer run, dredging in SW of 20 year mining plan area

## B.8. Scenario 8: Austral Summer run, dredging in SE of 20 year mining plan area
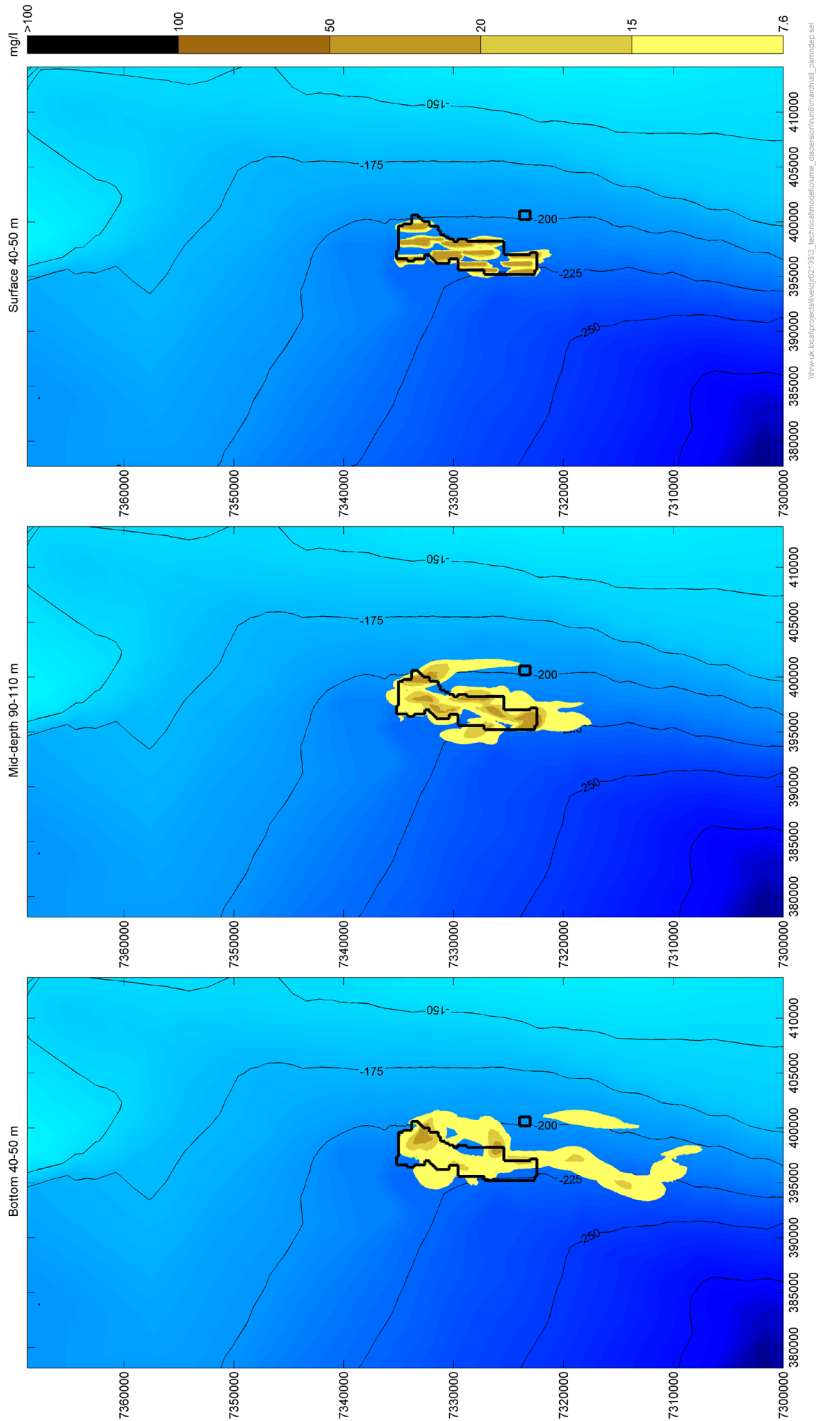


Figure B.22: Peak predicted increases of suspended sediment concentration at the Bottom (left), Middle (middle) and Top (right) of the water column, Scenario 8: Austral Summer run, dredging in SE of 20 year mining plan area
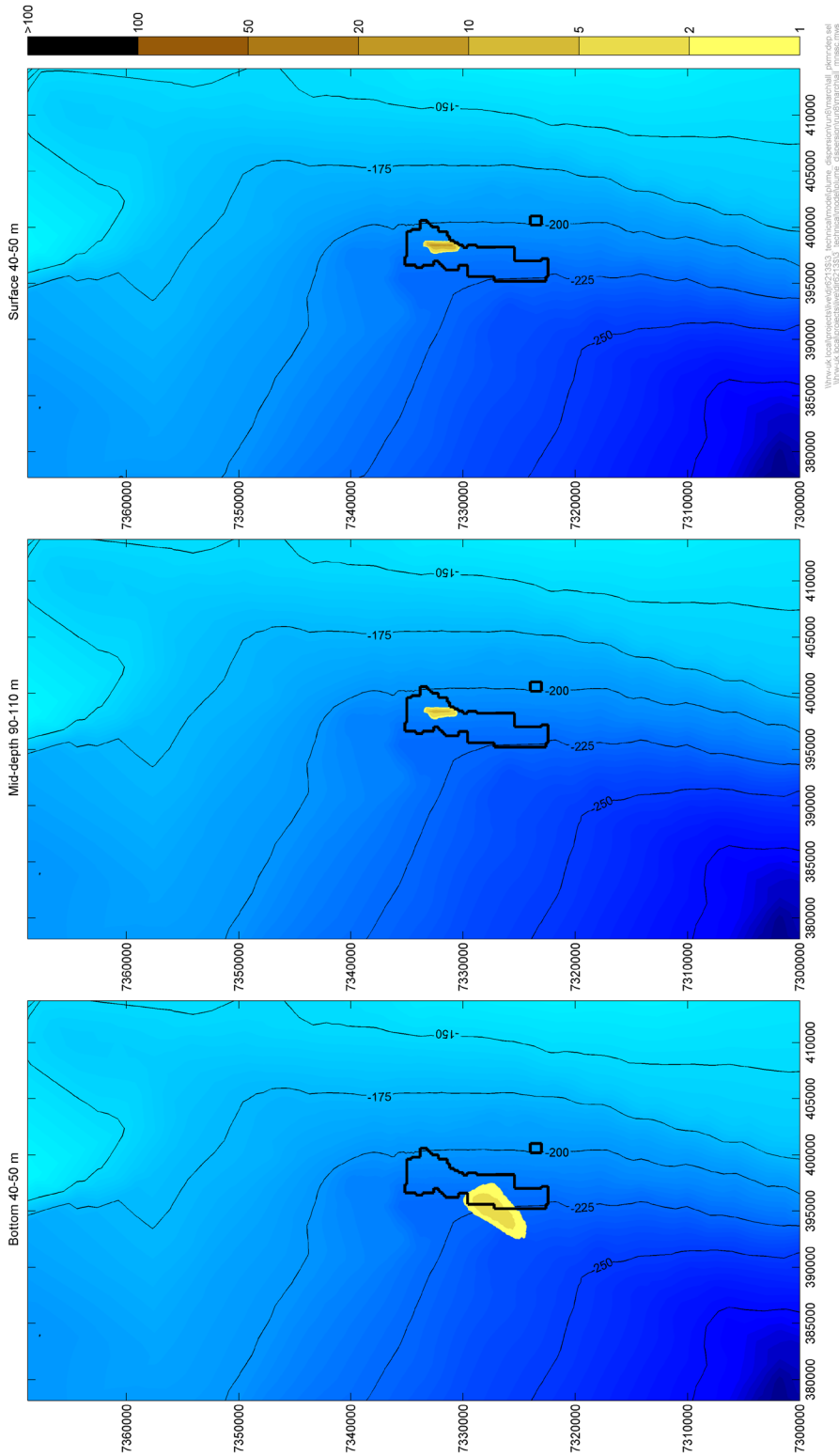
Figure B.23: Mean predicted increases of suspended sediment concentration at the Bottom (left), Middle (middle) and Top (right) of the water column, Scenario 8: Austral Summer run, dredging in SE of 20 year mining plan area

Figure B.24: Predicted sediment deposition after 32 days of dredging, Scenario 4: Austral Summer run, dredging in SE of 20 year mining plan area

## B.9.   Scenario 9: Austral Winter run, dredging distributed throughout 20 year mining plan area



Figure B.25: Peak predicted increases of suspended sediment concentration at the Bottom (left), Middle (middle) and Top (right) of the water column, Scenario 9: Austral Winter run, dredging distributed evenly over the 20 year mining plan area

Figure B.26: Mean predicted increases of suspended sediment concentration at the Bottom (left), Middle (middle) and Top (right) of the water column, Scenario 9: Austral Winter run, dredging distributed evenly over the 20 year mining plan area

Figure B.27: Predicted sediment deposition after 45 days of dredging, Scenario 9: Austral Winter run, dredging distributed evenly over the 20 year mining plan area

## B.10. Scenario 10: Austral Summer run, dredging distributed evenly throughout 20 year mining plan area



Figure B.28: Peak predicted increases of suspended sediment concentration at the Bottom (left), Middle (middle) and Top (right) of the water column, Scenario 10: Austral Summer run, dredging distributed evenly over the 20 year mining plan area

Figure B.29: Mean predicted increases of suspended sediment concentration at the Bottom (left), Middle (middle) and Top (right) of the water column, Scenario 10: Austral Summer run, dredging distributed evenly over the 20 year mining plan area
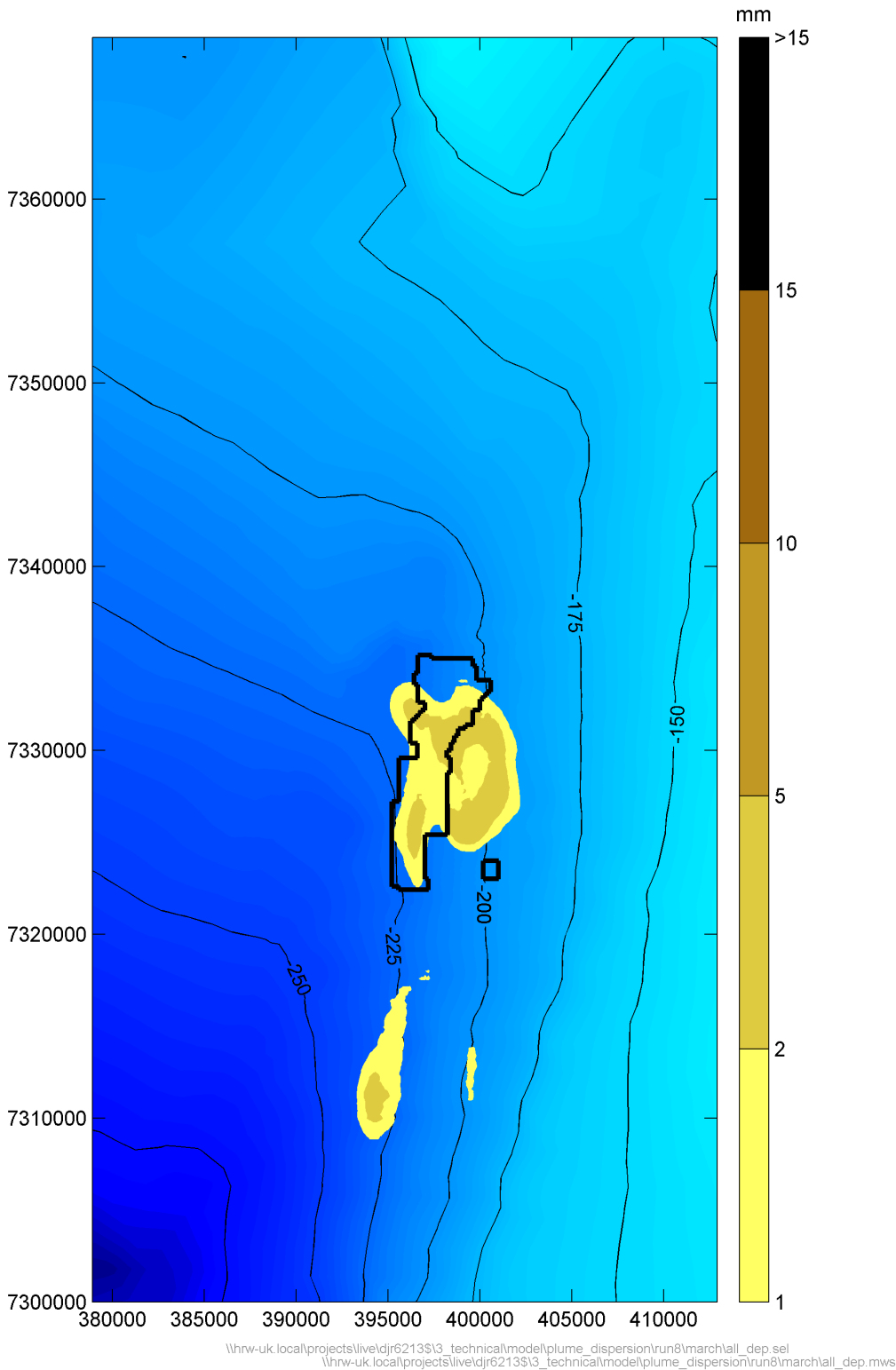
Figure B.30: Predicted sediment deposition after 32 days of dredging, Scenario 10: Austral Summer run, dredging distributed evenly over the 20 year mining plan area

# C. Time series of predicted changes in suspended sediment concentration (above background)

For locations of time series outputs see Figure 8.1 and Figure 8.2 of the main report text.

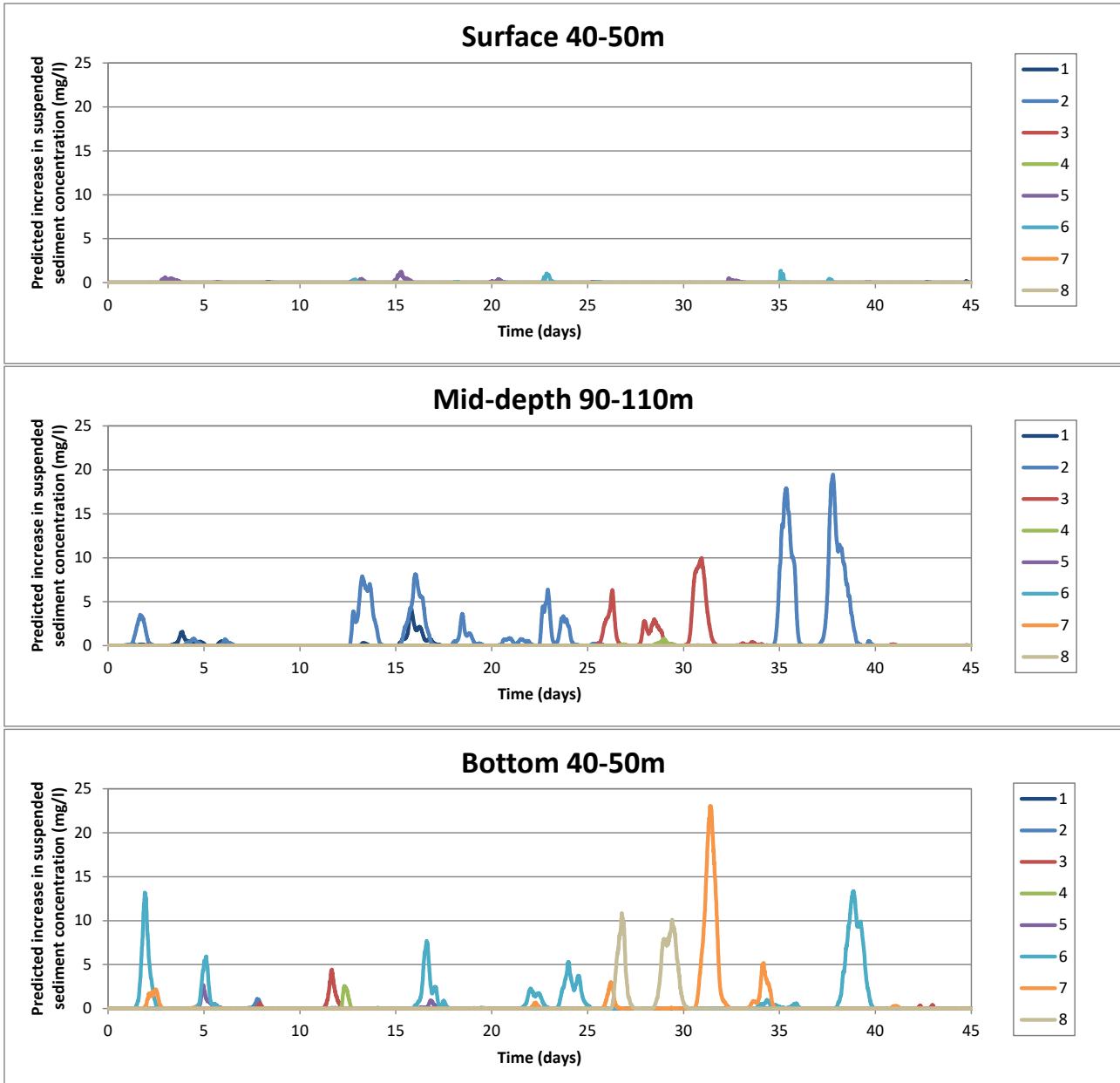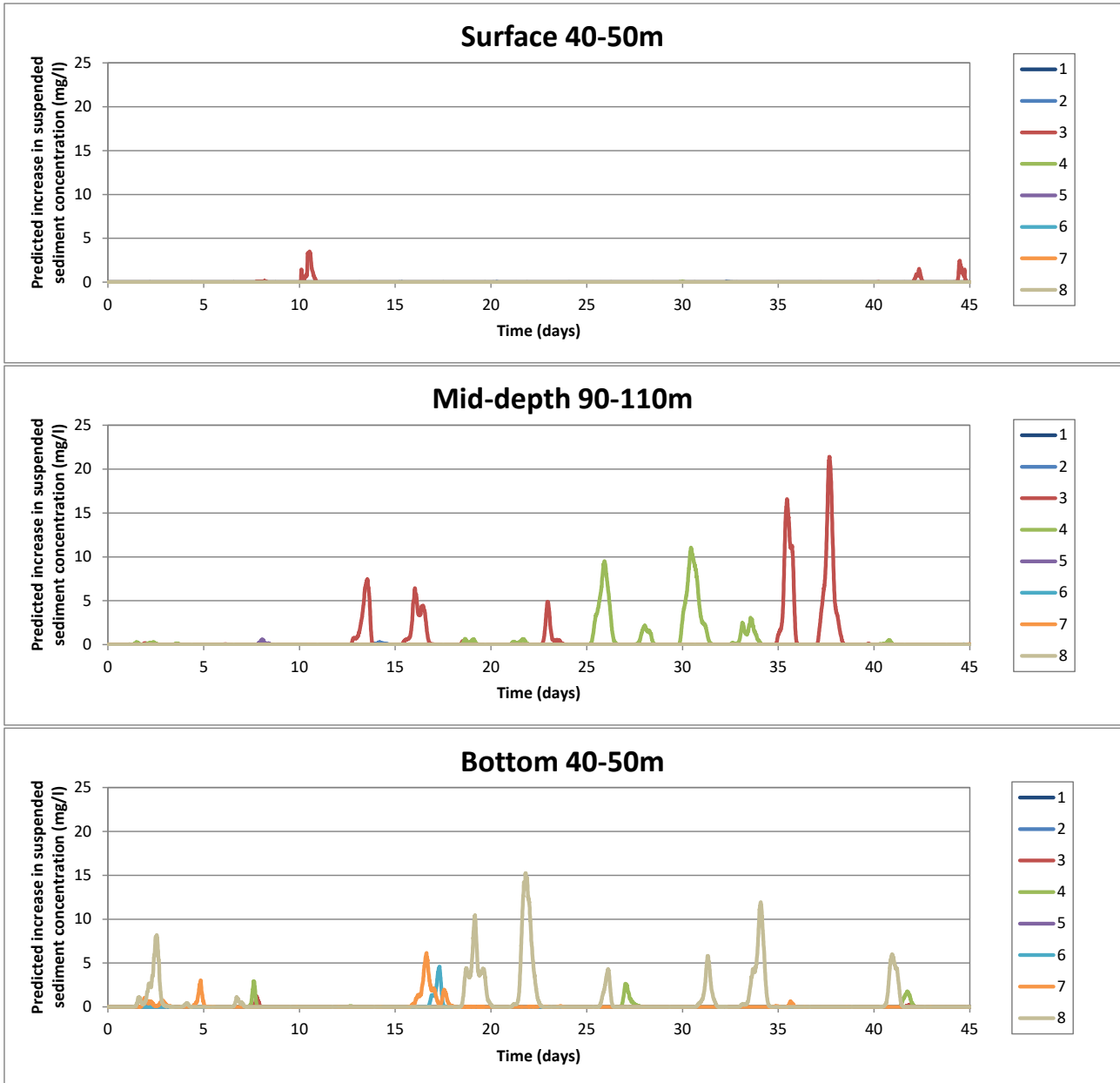## C.1. Scenario 1: Austral Winter run, dredging in NW of 20 year mining area
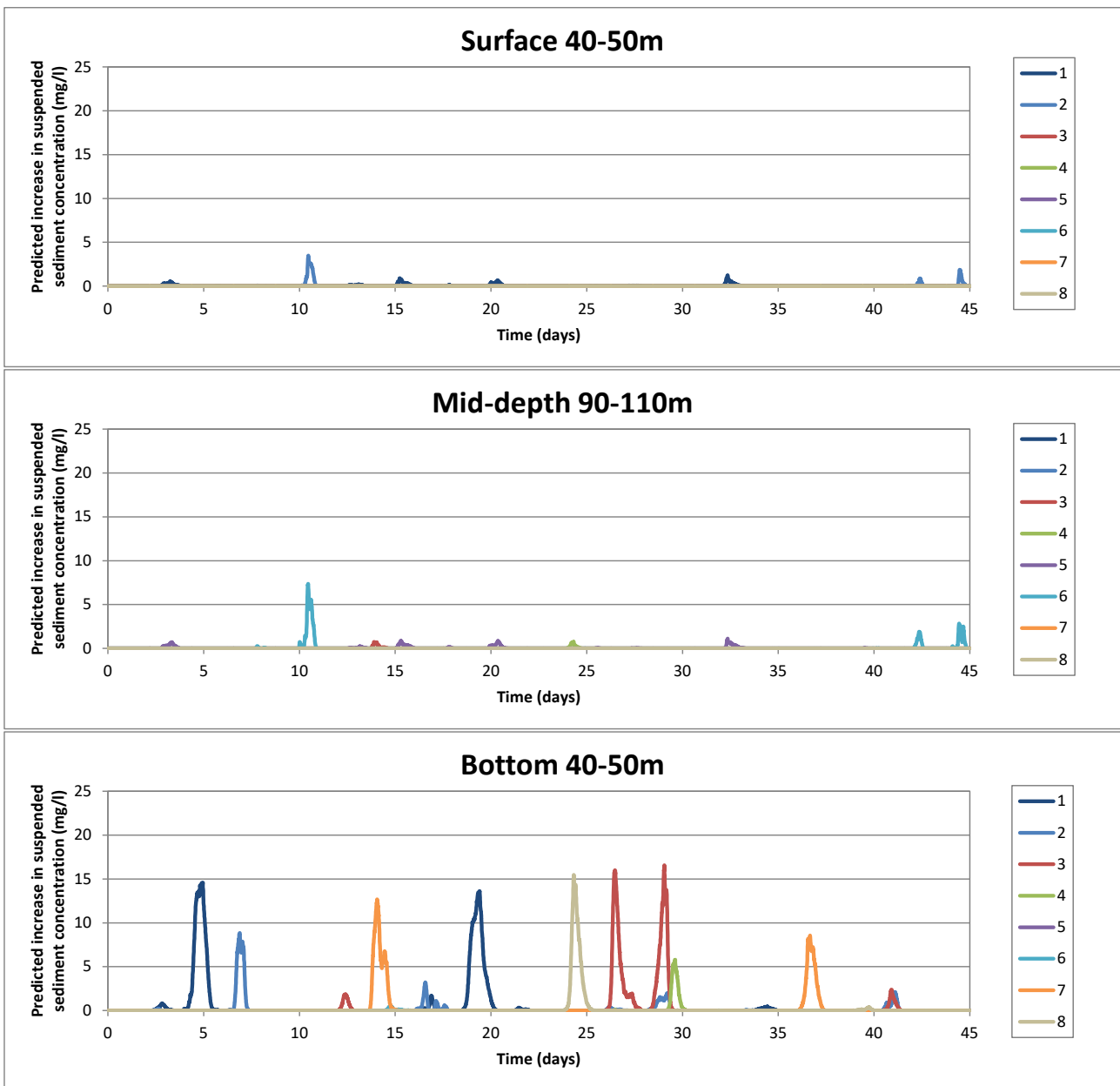


Figure C.1: Time series of predicted increases in suspended sediment concentration at locations shown in Figure 8.1 of main text, Scenario 1: Austral Winter run, dredging in NW of 20 year mining area

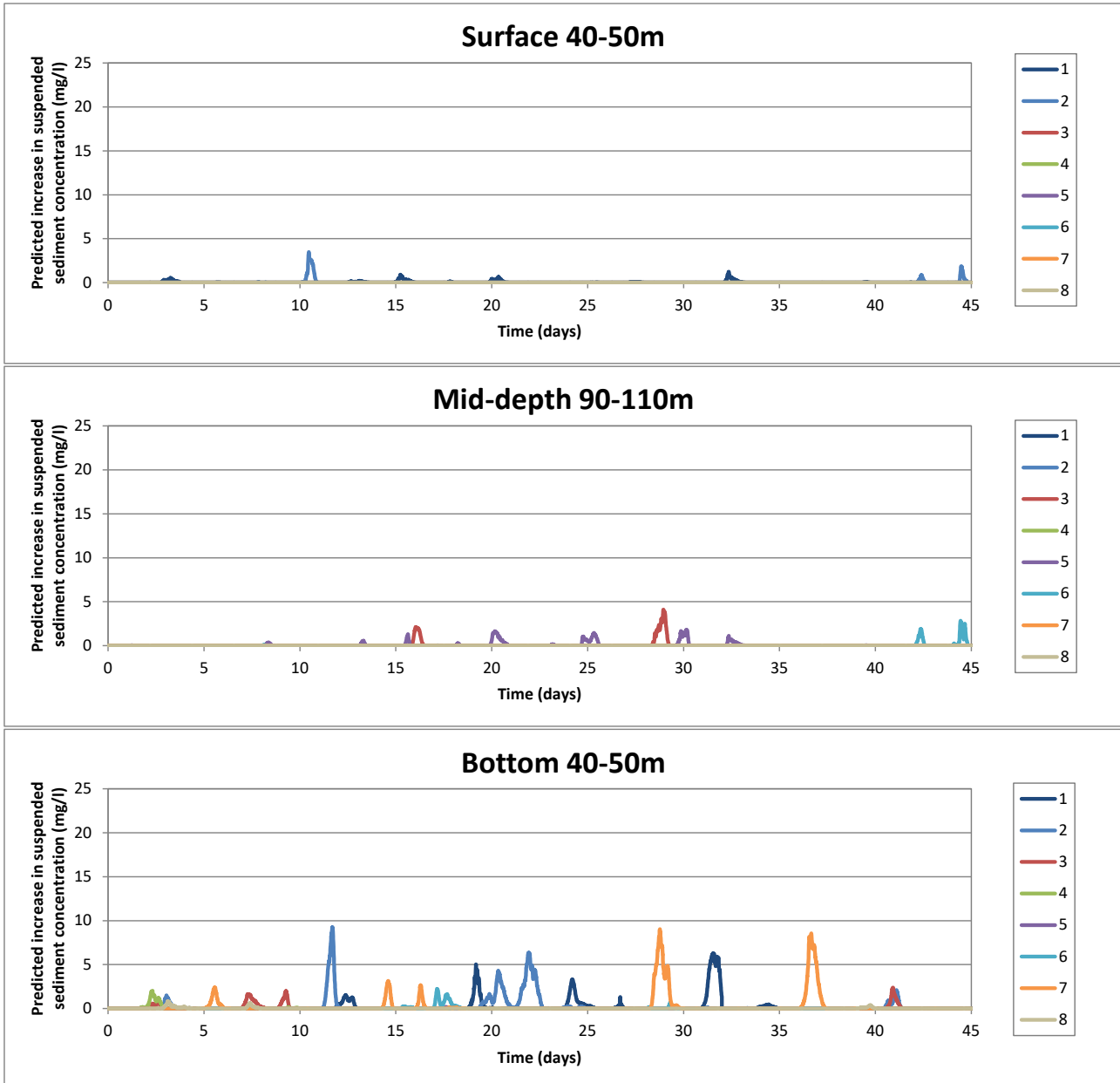## C.2. Scenario 2: Austral Winter run, dredging in NE of 20 year mining area
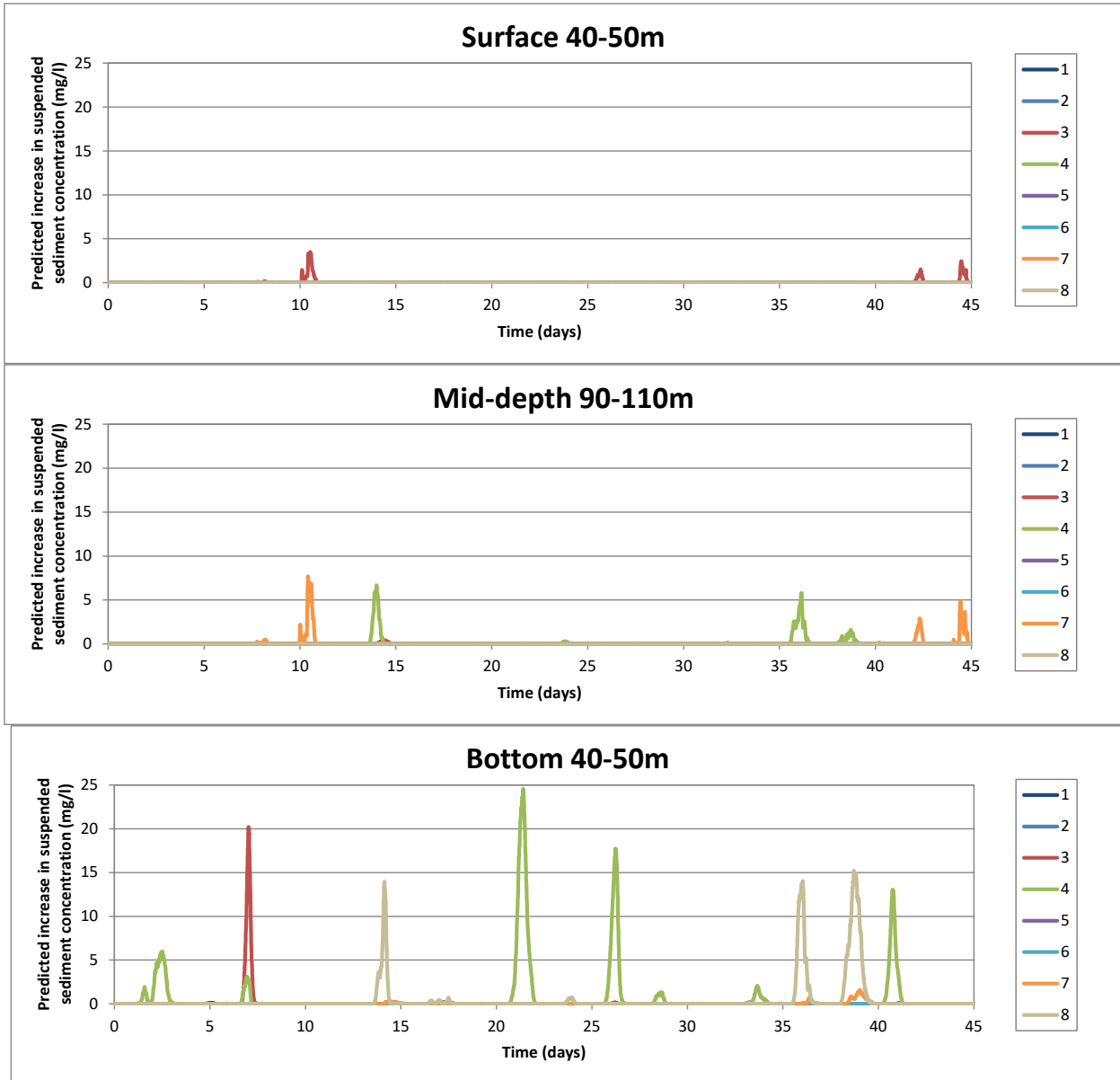


Figure C.2: Time series of predicted increases in suspended sediment concentration at locations shown in Figure 8.1 of main text, Scenario 2: Austral Winter run, dredging in NE of 20 year mining area

## C.3.  Scenario 3: Austral Winter run, dredging in SW of 20 year mining area



Figure C.3: Time series of predicted increases in suspended sediment concentration at locations shown in Figure 8.1 of main text, Scenario 3: Austral Winter run, dredging in SW of 20 year mining area

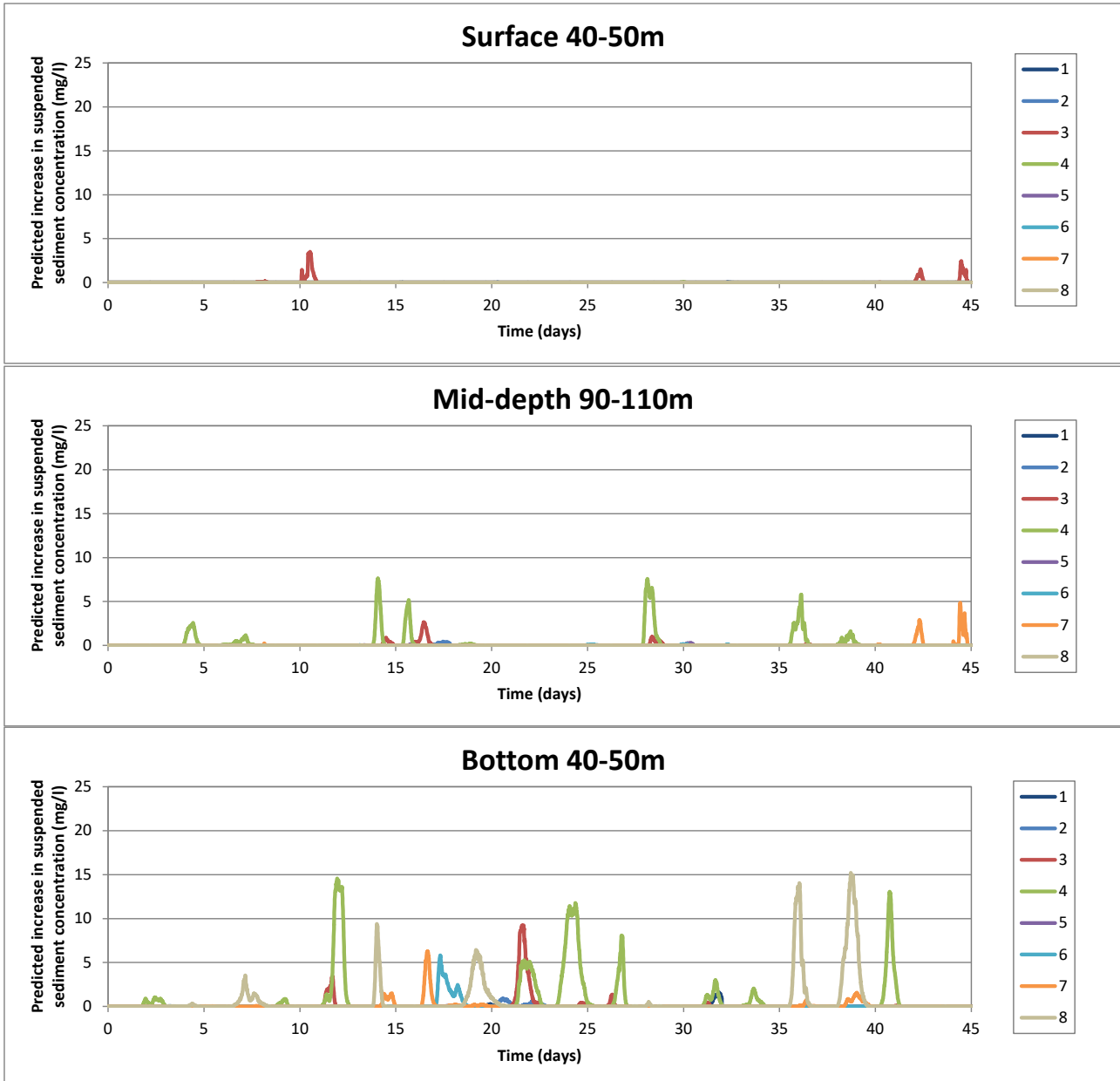## C.4.  Scenario 4: Austral Winter run, dredging in SE of 20 year mining area



Figure C.4: Time series of predicted increases in suspended sediment concentration at locations shown in Figure 8.1 of main text, Scenario 4: Austral Winter run, dredging in SE of 20 year mining area

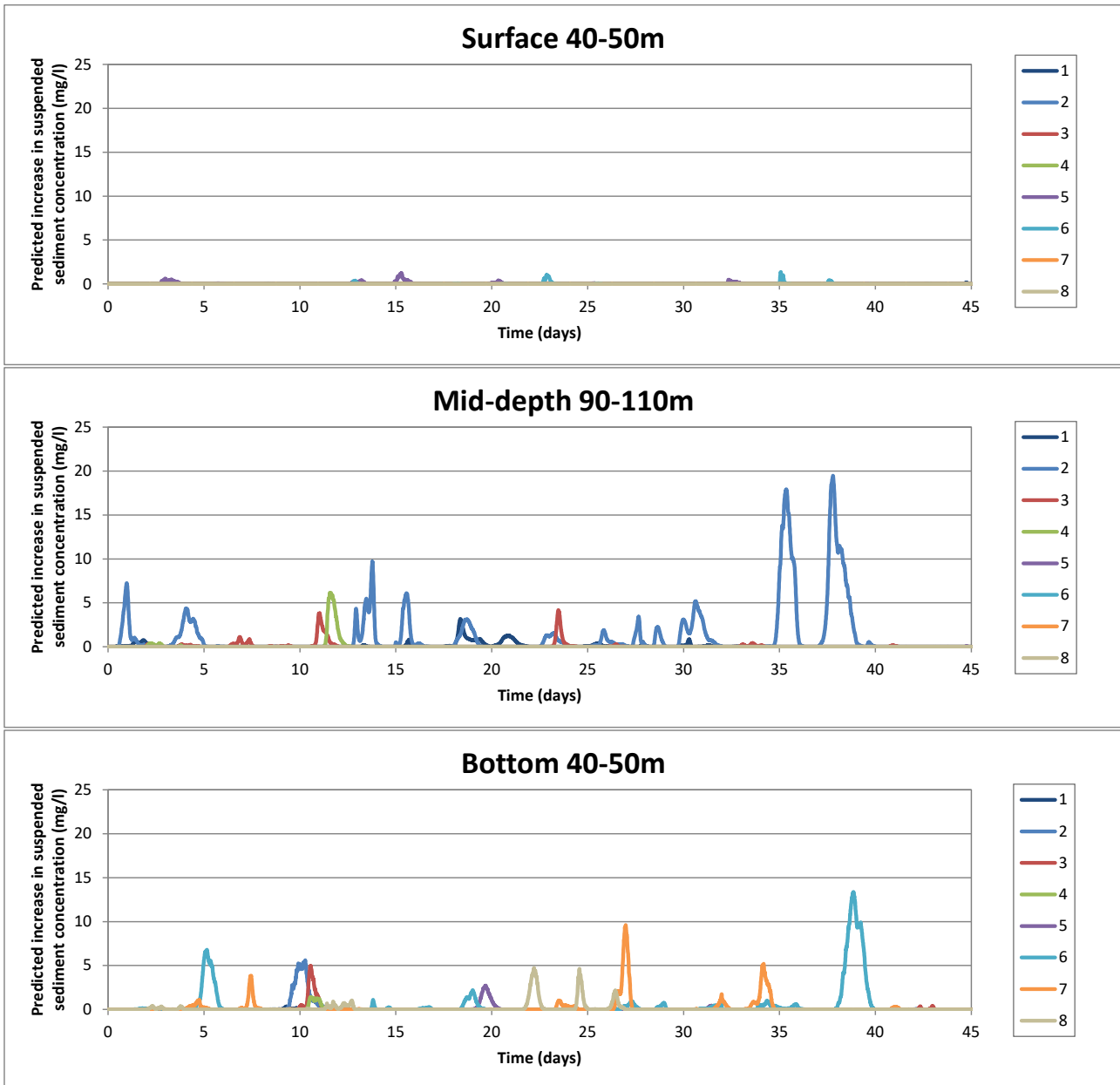## C.5. Scenario 5: Austral Summer run, dredging in NW of 20 year mining area



Figure C.5: Time series of predicted increases in suspended sediment concentration at locations shown in Figure 8.1 of main text, Scenario 5: Austral Summer run, dredging in NW of 20 year mining area

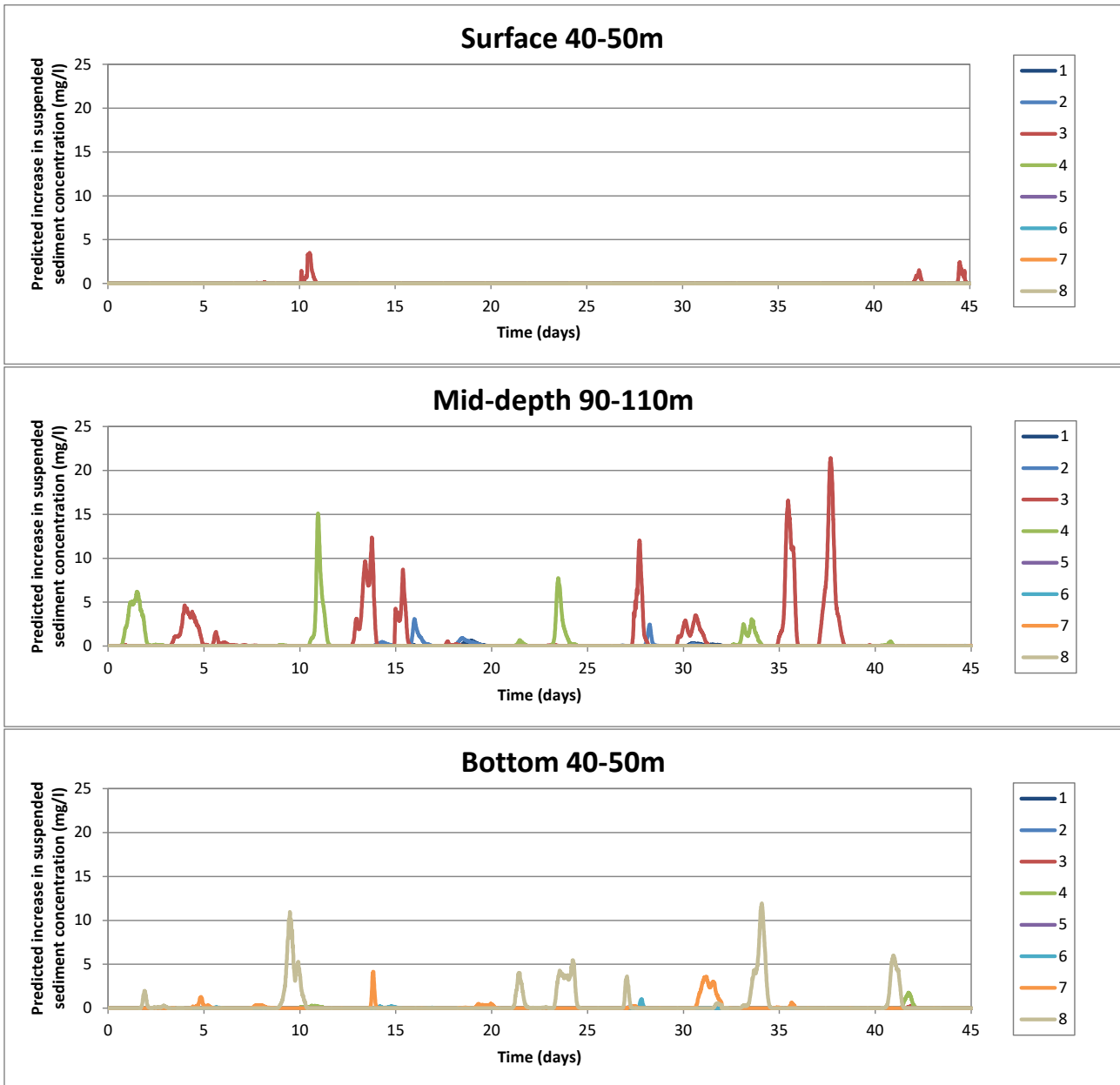## C.6. Scenario 6: Austral Summer run, dredging in NE of 20 year mining area



Figure C.6: Time series of predicted increases in suspended sediment concentration at locations shown in Figure 8.1 of main text, Scenario 6: Austral Summer run, dredging in NE of 20 year mining area

## C.7. Scenario 7: Austral Summer run, dredging in SW of 20 year mining area



Figure C.7: Time series of predicted increases in suspended sediment concentration at locations shown in Figure 8.1 of main text, Scenario 7: Austral Summer run, dredging in SW of 20 year mining area

## C.8. Scenario 8: Austral Summer run, dredging in SE of 20 year mining area



Figure C.8: Time series of predicted increases in suspended sediment concentration at locations shown in Figure 8.1 of main text, Scenario 8: Austral Summer run, dredging in SE of 20 year mining area

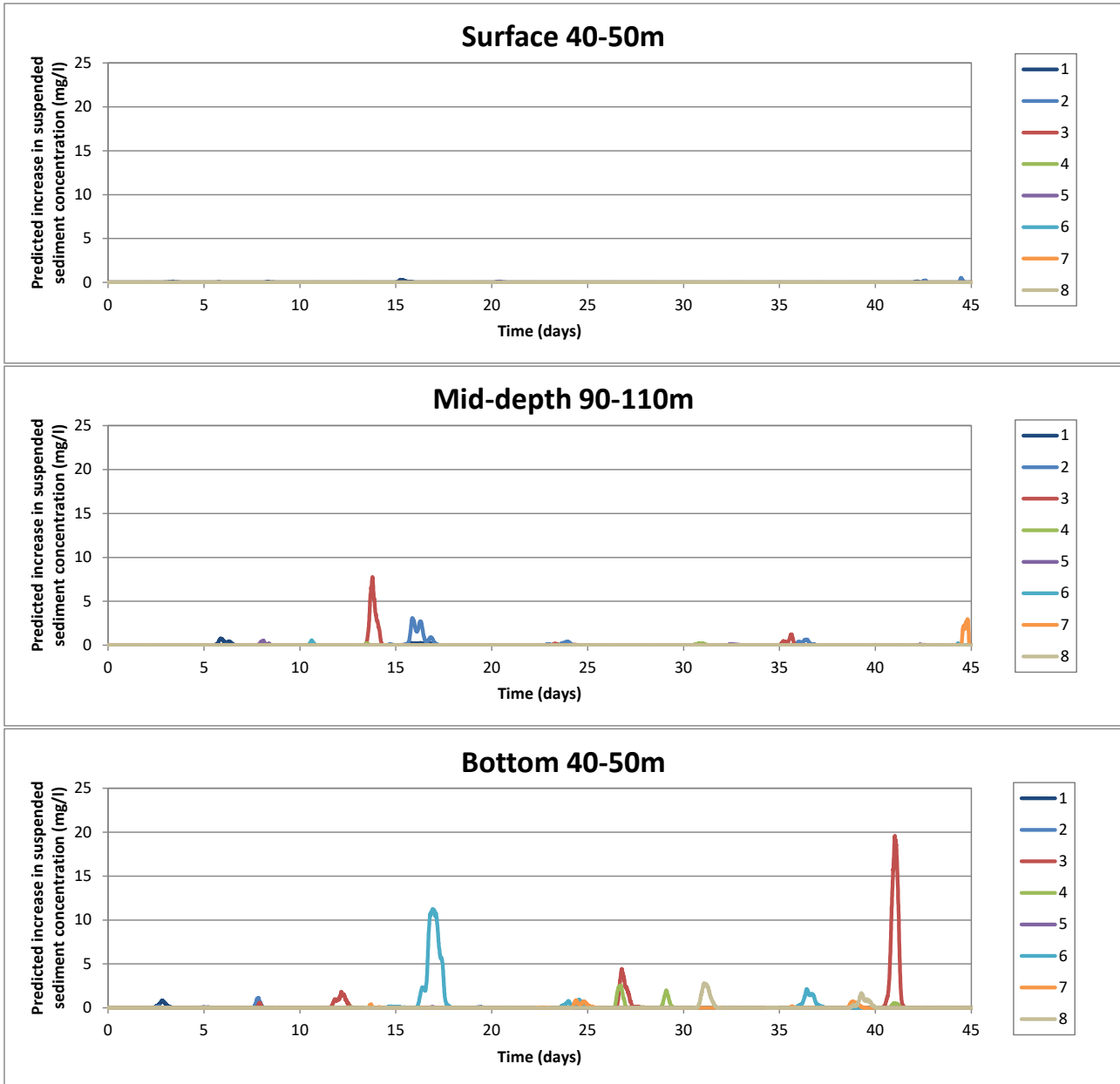## C.9. Scenario 9: Austral Winter run, dredging distributed throughout 20 year mining area



Figure C.9: Time series of predicted increases in suspended sediment concentration at locations shown in Figure 8.2 of main text, Scenario 9: Austral Winter run, dredging distributed throughout 20 year mining area

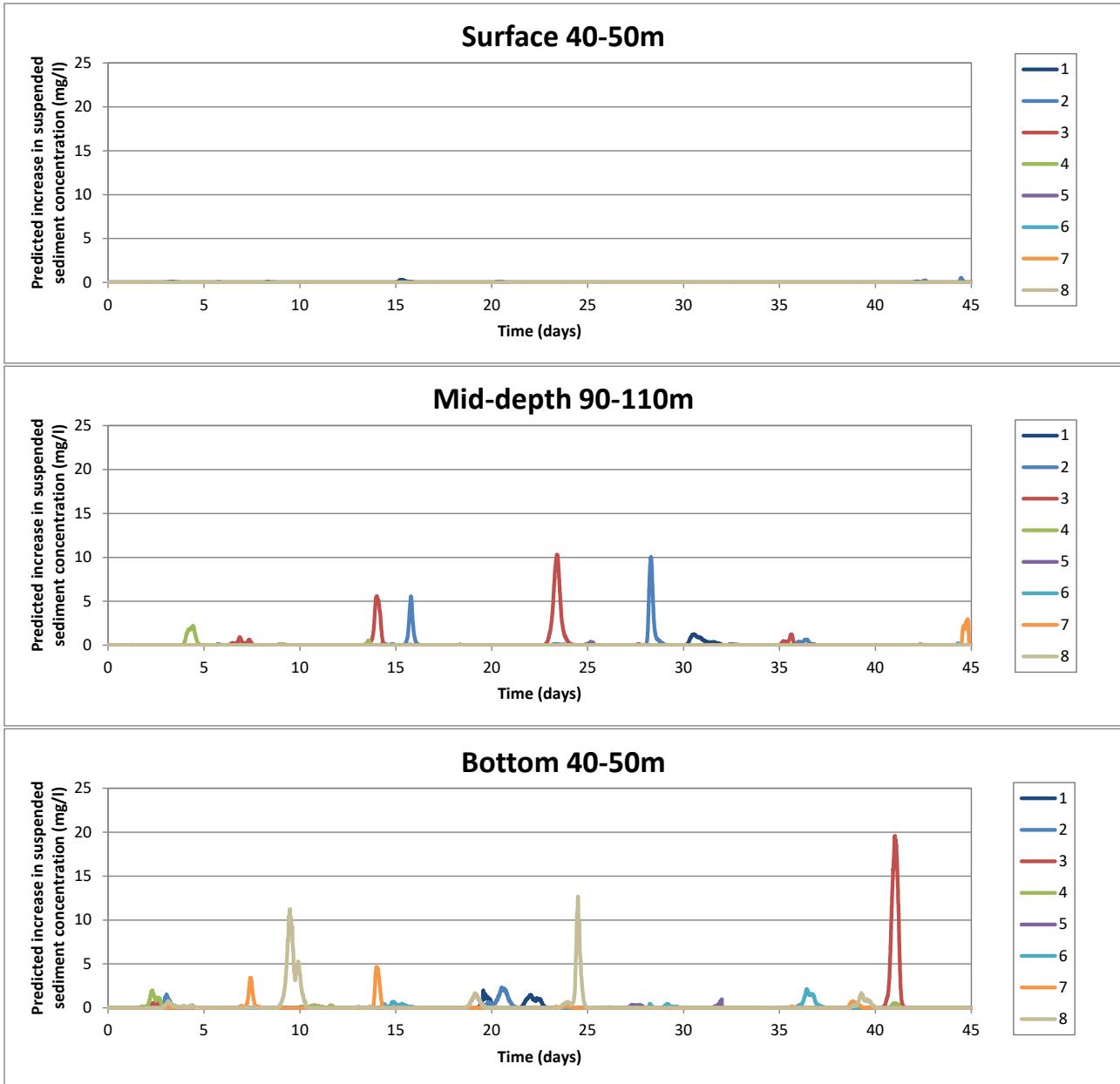## C.10. Scenario 10: Austral Summer run, dredging distributed throughout 20 year mining area



Figure C.10: Time series of predicted increases in suspended sediment concentration at locations shown in Figure 8.2 of main text, Scenario 10: Austral Summer run, dredging distributed throughout 20 year mining area

# D.  Effect of Environmental Valve

Figure D.1 presents the predicted peak concentration increases above background for dredging in the NW of the proposed 20 year mining area (Scenario 1), for Austral winter conditions.  These results are equivalent to those shown in Section B.1 of Appendix B (Figure B.1), except that Figure D.1 includes the effect of the Environmental Valve.  Comparison with Figure B.1 shows there is very little difference in the general wider dispersion of the plume arising from the use of the Environmental Valve.

Figure D.2 shows a comparison, with and without the effect of the Environmental Valve, of the predicted peak concentration above background occurring within the surface 25 m during dredging in the same NW dredging in Austral summer scenario.  The figure shows a surface plume (of more than a 7.6 mg/l increase in sediment concentration) extending up to 1.5 km NW of the dredging without the use of the valve and the absence of a plume (of more than 7.6 mg/l) when the Environmental Valve is used.
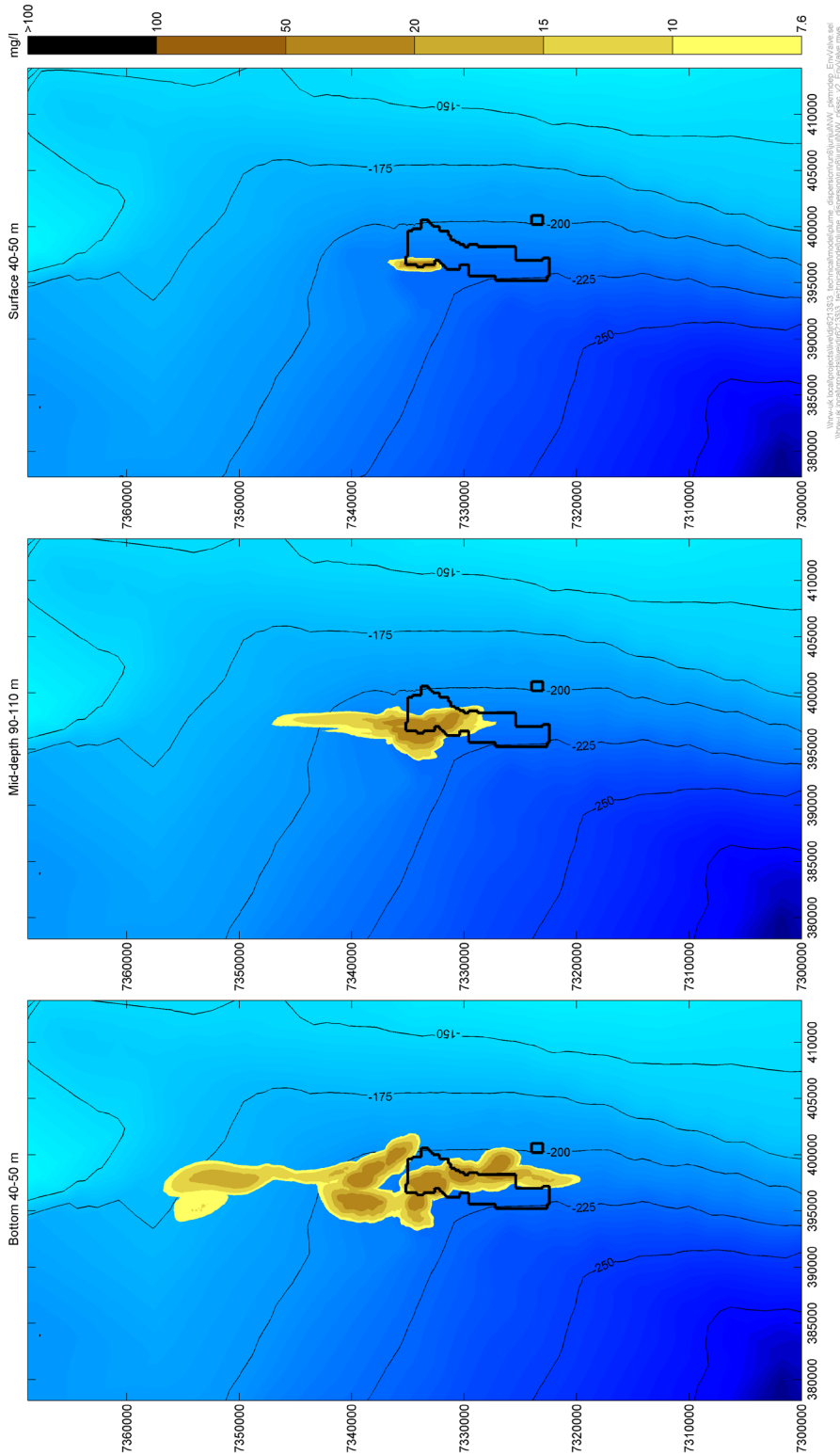
Figure D.1: Peak predicted increases of suspended sediment concentration at the Bottom (left), Middle (middle) and Top (right) of the water column, Scenario 1: Austral Winter run, dredging in NW of 20 year mining plan area, with Environmental Valve
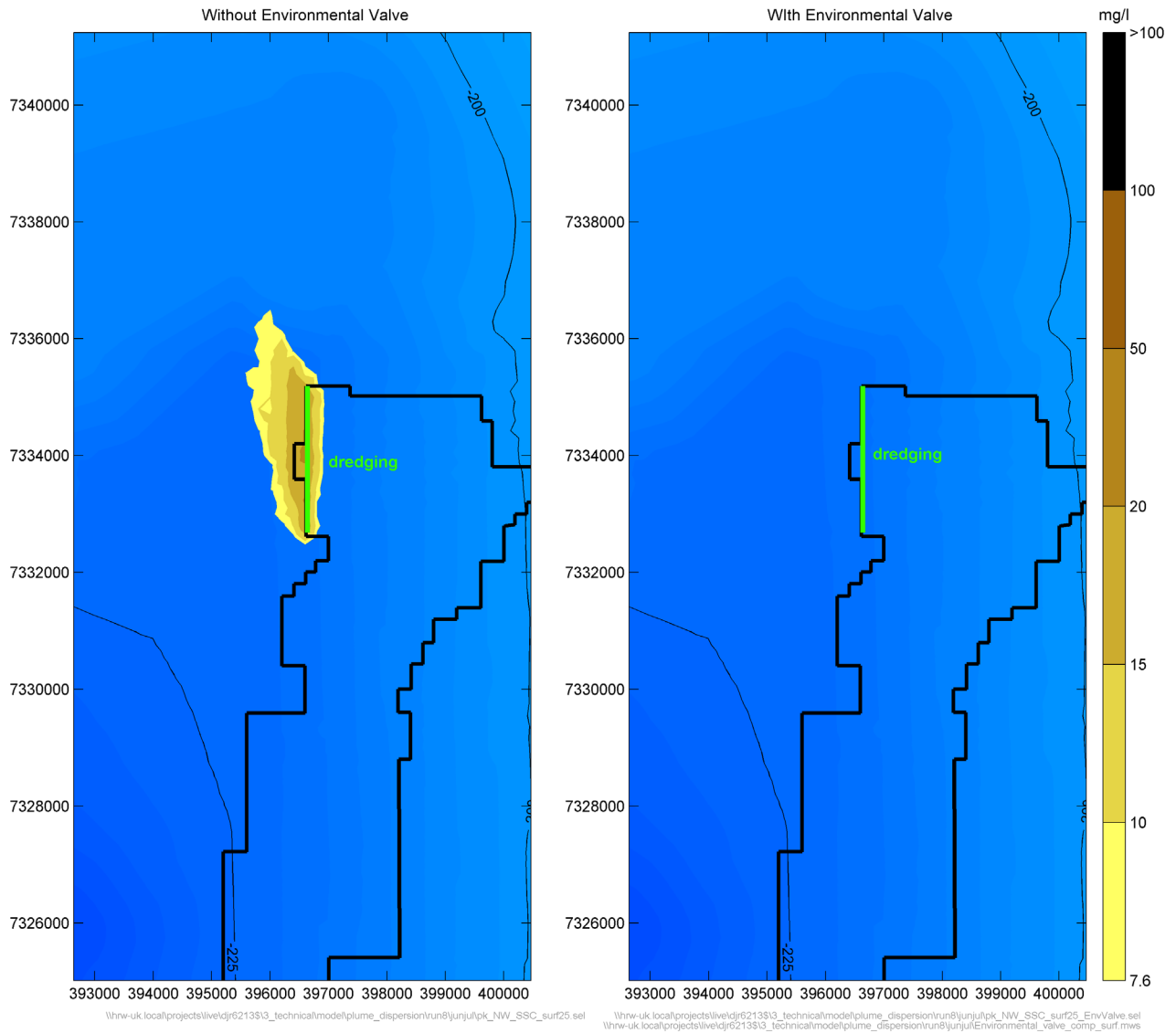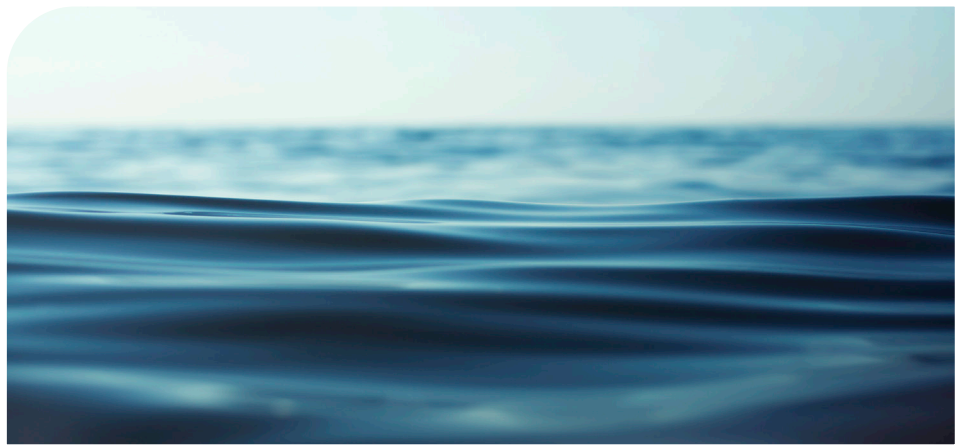
Figure D.2: Peak predicted increases of suspended sediment concentration in the surface 25 m, without (left) and with (right) the use of the Environmental Valve, Scenario 1: Austral Winter run, dredging in NW of 20 year mining area

# HR Wallingford

*Working with water*



HR Wallingford is an independent engineering and environmental hydraulics organisation. We deliver practical solutions to the complex water-related challenges faced by our international clients. A dynamic research programme underpins all that we do and keeps us at the leading edge. Our unique mix of know-how, assets and facilities includes state of the art physical modelling laboratories, a full range of numerical modelling tools and, above all, enthusiastic people with world-renowned skills and expertise.

FS 516431
EMS 558310
OHS 595357